The incorporation and solubility of sulphate, chloride and molybdate anions in borosilicate and aluminosilicate glasses

Shengheng Tan

A thesis submitted to the Department of Materials Science and Engineering at the University of Sheffield in partial fulfilment of requirements for the degree of Doctor of Philosophy

Immobilisation Science Laboratory

Department of Materials Science and Engineering

The University of Sheffield

August 2015

Acknowledgements

First of all, I would like to express my sincere thanks to all of the persons who have helped me throughout my PhD life in the University of Sheffield.

I would like to thank my supervisor Prof. Russell J Hand, without whose precious guidance, advice and inspiration I would not be able to complete my project. I would also like to thank my secondary supervisors Prof. Neil C Hyatt and Dr Michael I Ojovan for their support on my experiments and comments to my work.

Great appreciation is towards staff and students in Immobilisation Science Laboratory (ISL) group for their valuable advice and encouragement during my study. I am also indebted to the technical staff in the Department of Materials Science and Engineering, in particular to Mr Ian Watts and Dr Lisa Holland who have helped me make hundreds of glasses.

Thanks are also given to the University of Sheffield, China Scholarship Council (CSC) and the Department for Business, Innovation and Skills (BIS) in the UK Government for their financial support for my study.

Finally I would like to convey my deepest gratitude and love to my wife, Yishi, who accompanies me through the whole duration of my study and gives me endless support and understanding however hard the PhD study becomes. Deepest gratitude is also to my parents whose dedication throughout my life has always been the most influencing in pushing me forward. Special thanks are given to Prof. Ying Ye from Zhejiang University, China, for his unselfish assistance to my study and life.

Abstract

This thesis investigates the incorporation and solubility behaviour of three anionic species (sulphate, chloride and molybdate) in two different types of glasses (borosilicate and aluminosilicate glasses). These anions can be often found in nuclear waste and their poor solubilities in nuclear waste glasses are a main factor that controls the loading capacity of nuclear waste vitrification. The investigations in this thesis are therefore focused on the compositional dependence of their solubilities in glass, together with the effects of their incorporations on glass structure and properties.

A variety of glass properties have been assessed. Glass densities steadily increased with increasing incorporation of sulphate and molybdate but showed maxima with chloride incorporation. Glass transition temperatures T_g all decreased with initial anionic loadings, whereas further loadings results in either decreased or unchanged T_g depending on anionic species and glass composition. Intense Raman peaks are created due to sulphate and molybdate additions; these characteristic peaks are assigned to the vibrations of SO_4^{2-} and MoO_4^{2-}, respectively. The shift of these peaks with variation of alkaline earth species in glass suggests the association of SO_4^{2-} and MoO_4^{2-} with alkaline earth cations in glass network. The incorporation of chloride does not cause significant changes in the Raman spectra, however.

Based on X-ray diffraction results the visibly homogeneous glasses were completely amorphous while the phase separated glasses contained a number of crystals. There are two mechanisms of phase separation occurring in the glasses with excess sulphate and molybdate: liquid-liquid separation and thereafter crystallisation, which occurs during cooling within glass melts with critical amounts of sulphate or molybdate; or a segregated layer, which occurs if the addition of sulphate or molybdate is too excessive to be completely dissolved in the melt. The crystals formed through the former mechanism are mostly spherical, submicron in size and randomly dispersed. These crystals are more likely to be alkaline earth salts while the segregated layers are essentially sodium salts. The phase separation caused by excess chloride in melt is different. The separated phases in aluminosilicate glasses are all non-chlorine containing and are formed through nucleation and growth during cooling.

Sulphate solubility is observed to steadily increase with the replacement of larger for smaller alkaline earths in borosilicate glasses. Sulphate solubility in aluminosilicate glasses is not achieved as no sulphate can be retained in these compositions. Chloride solubility also increases from MgO-containing to BaO-containing borosilicate glasses like sulphate solubility. However, the retention of chloride in aluminosilicate glasses is selective and sensitive to compositions; barium aluminosilicate glass possesses the highest chloride solubility with the highest chloride retention. In contrast, molybdate solubility increases from BaO-containing to MgO-containing aluminosilicate glasses and from BaO-containing to CaO-containing borosilicate glasses. Molybdate is poorly soluble in magnesium borosilicate glass. Comparison of the behaviour of these three anionic species in glass suggests that the controlling factors for molybdate solubility may be very different from the other two.

Finally three compositional parameters normalised cation field strength (NCFS), electronegativity index (X_R) and cationic size (S_R), which are related to cationic charge and size, but which differ from each other with respect to the contributions of each aspect, are used to express the solubility dependence of each species. Within narrow compositional variations in this study (equimolar substitution among alkaline earths) the above parameters seems to be quite applicable. But the compositional variations in literature glasses are much more complicated and the fittings may not apply. When combined with literature data, the best fitting for sulphate solubility is found with S_R, the index of cationic size, with an increasing exponential relationship between solubility and S_R. For chloride solubility with best fit is obtained with NCFS, the index of cation field strength, with a decreasing exponential relationship between solubility and NCFS. Nevertheless, no convincing correlation for molybdate has been achieved, although X_R, the index of electronegativity of network modifiers, does show a general trend of increasing solubility with linearly decreasing X_R.

Published work

Aspects of the work described in this thesis have been published as follows:

A journal paper entitled "MoO_3 incorporation in magnesium aluminosilicate glasses" by Shengheng Tan, Michael I Ojovan, Neil C Hyatt and Russell J Hand was published in the *Journal of Nuclear Materials* 458 (2015) 335-342.

A conference paper entitled "MoO_3 incorporation in alkaline earth aluminosilicate glasses" by Shengheng Tan, Michael I Ojovan, Neil C Hyatt and Russell J Hand was presented in Symposium EE: Scientific Basis for Nuclear Waste Management XXX VIII in 2014 MRS Fall Meeting in Boston, US, 1-5 December 2014. This paper was published in MRS Proceedings/Volume 1744/2015, labelled as mrsf14-1744-ee05-01.

Table of Contents

List of Figures

List of Tables

1. Introduction

There are some troublesome elements that can be abundant in nuclear wastes but are not readily dissolved in the glass matrices used for vitrification, among which sulphur, chlorine and molybdenum are three examples that are considered in this work. Two glass systems are chosen as the candidate hosts to immobilise the challenging elements: borosilicate and alkaline earth aluminosilicate glasses. The solubility dependence of each element on glass composition is assessed, together with the effects of the incorporation of these elements on glass structure and properties. Afterwards, the similarities and differences among the behaviours of these three elements in glass are compared and summarised. Finally, three compositional parameters, which represent different aspects of the cationic characteristics in glass network, are employed with the aim of establishing some universal dependences for the prediction of solubilities of these elements in glass.

In Chapter 2, the literature review looks into the background and categories of nuclear waste, and then compares advantages and disadvantages of different immobilisation techniques. Vitrification is the primary choice of high level waste immobilisation, but it confronts difficulties in incorporating some troublesome elements such as S, Cl and Mo. The structure of silicate glasses (and with the addition of B_2O_3 or Al_2O_3 to become borosilicate and aluminosilicate glasses, respectively) is then reviewed, coupled with their applications to nuclear waste vitrification. Later, the chemistries of S, Cl and Mo in silicate glass systems are summarised based on previous studies. S, Cl and Mo are all present in nuclear glasses as anions namely SO_4^{2-}, Cl^- and MoO_4^{2-}. The effects of their incorporation on glass structure are however not always consistent among literature, and it is believed that there may be several mechanisms of how these anions are incorporated in glass network dependent on specific glass composition. The solubilities of these anions in glass are also strongly related to the composition features, *e.g.* the ratio of network formers to network modifiers and the different components present in glass. This work focuses on investigating the influence of varying alkaline earth species on the solubility of each of these anions in glass.

Two glass families are chosen as the immobilisation hosts. The borosilicate glass series

are a kind of hybrid arising from an Indian waste glass that is capable of incorporating sulphate and a Russian waste glass that has been investigated for a long time. The proposed borosilicate glass has a nominal molar composition of 20MO-15Na_2O-15B_2O_3-50SiO_2, where M ranges from Mg to Ba. The aluminosilicate glass series originated from earlier studies that showed that calcium aluminosilicate glasses are capable of incorporating abundant Cl^-. The proposed aluminosilicate glass has a nominal molar composition of 45MO-10Al_2O_3-45SiO_2, where M again ranges from Mg to Ba. For each glass composition different levels of SO_3, Cl and MoO_3 are added, respectively, to determine the loading limit and solubility of each of the components.

Chapter 3 describes the detailed procedures of glass production and a variety of characterisation techniques that are used to assess the properties of glasses prepared in this work. The assessments mainly include density measurements, X-ray diffraction, differential thermal analysis, Raman and Fourier transform infrared spectroscopies, scanning electron microscopy, energy dispersive X-ray spectroscopy and transmission electron microscopy.

The results obtained for sulphate incorporation and solubility in borosilicate and aluminosilicate glasses are presented in Chapter 4. The prepared aluminosilicate glasses do not contain sulphate at all and hence only the results obtained with borosilicate glasses are discussed. The discussion covers the factors that are influential to sulphate retention and solubility and the structural changes caused by sulphate incorporation in glass network, as well as the different phase separation mechanisms occurring in the different compositions.

Chapter 5 presents the results obtained for chloride incorporation and solubility in borosilicate and aluminosilicate glasses. The results and discussion in this chapter are also divided into three parts like in Chapter 4, namely the retention and solubility of chloride in glass, the effects of chloride incorporation on glass structure and properties and finally the microstructure of phase separated glasses. It may be mentioned here that the phase separation and structural changes in Cl-containing glasses are distinct from those in SO_3- and MoO_3-containing glasses.

Chapter 6 is about the incorporation and solubility of molybdate in glass. Several complete series of glass compositions, especially those aluminosilicate glasses, have

been prepared with step-by-step increasing molybdate loadings, and the results and discussion in this chapter are more extensive than the previous two chapters. In addition to the common characterisations, high temperature X-ray diffraction studies have been performed on some samples in this chapter to understand the high temperature behaviour of MoO_3-containing glasses. The discussion is divided up in same way as in Chapters 4 and 5.

The similarities and differences among the incorporation of S, Cl and Mo in glass are compared and summarised in Chapter 7. The comparisons include the corrosion of the mullite crucibles by the melts, their retention dependences, their presence in glass, the changes of Raman and FTIR spectra along with increasing loadings, the changes in glass densities, the phase separation occurring in the melts or within glass matrices and the microstructures of phase separated samples. Although all of the three elements are present anionically in the prepared glasses, their influences on glass structure and properties are largely different from each other.

Chapter 8 firstly introduces three compositional parameters which are related to cation field strength, cation electronegativity and cationic size in glass and then explores the correlations between the anionic solubilities and these compositional parameters. For each anion (SO_4^{2-}, Cl^- and MoO_4^{2-}) fittings are carried out within the data in this work and combined with the data from literature. Some models have been established for the universal prediction of anionic solubilities in glass.

Chapter 9 includes the conclusions of this work and some recommendations for future work.

2. Literature Review

2.1. Nuclear waste immobilisation

2.1.1. Nuclear waste

Nuclear energy has constituted an important portion of the world electricity supply since its first civil utilisation in 1950s and currently there are 435 civil nuclear power reactors in operation around the world, with a total net generating capacity of 3.73×10^6 MW (IAEA 2014). This generating capacity also generates a significant volume of nuclear waste, the disposal of which is among the main concerns about the safe use of nuclear power, although its amount is much less than non-nuclear waste from other sources. Nuclear waste can be highly hazardous to humans and the environment and must be disposed of properly. In the UK by 2013, there is 4.3×10^6 m^3 existing nuclear waste with another 1.6×10^5 m^3 nuclear waste scheduled to be produced (NDA 2014). The majority of nuclear waste is produced during the nuclear fuel cycle, comprising the mining, enrichment, transportation, consumption and reprocessing of nuclear fuels, with the remaining issuing from the decommissioning of expired nuclear facilities, military programmes and scientific and medical uses (Wilson 1996, Donald 2010).

Nuclear waste in the UK is subdivided into four categories according to the level of radioactivity (Ojovan and Lee 2005) (see Table 2-1). The radioactivity of very low level waste (VLLW) is so low that it does not require special protection and handling. The low level waste (LLW) and intermediate level waste (ILW) have an activity beyond safety level but do not generate heat that needs to be taken into account in the long-term disposal; however, proper protection from the radioactivity of these wastes is still necessary. High level waste (HLW), which is created in the reprocessing of spent nuclear fuel, is able to emanate persistent and significant radiation and heat. This significantly complicates the treatment and disposal of HLW. Although HLW merely constitutes less than 0.1% of the total volume of nuclear waste, it contains about 95% of the total radioactivity (NDA 2014).

Table 2-1 Categories of nuclear waste in the UK (Ojovan and Lee 2005, Donald 2010).

Category	Definition (Radioactivity and heat generation)
VLLW	$<0.4 \times 10^9$ Bq m^{-3} (β and γ)
LLW	$<4 \times 10^9$ Bq t^{-1} (α); $<12 \times 10^9$ Bq t^{-1} (β and γ)
ILW	$>4 \times 10^9$ Bq t^{-1} (α); $>12 \times 10^9$ Bq t^{-1} (β and γ) <2 kW m^{-3} (heat)
HLW	>2 kW m^{-3} (heat)

2.1.2. Nuclear waste immobilisation

A number of techniques have been proposed and implemented worldwide to treat and dispose of nuclear waste, among which the immobilisation technique is the most acceptable and developed. Immobilisation is a method in which nuclear waste is immobilised in a reliable or inert matrix by incorporation or encapsulation to avert the dispersion of radionuclides to the environment. The paramount parameters in the determination of a suitable matrix for immobilisation are its chemical durability and waste loading capacity. The chemical durability is often characterised by the leaching behaviour of the waste-loaded matrix in aqueous conditions. A suitable matrix usually should have a normalised leaching rate lower than 10^{-5} g cm^{-2} d^{-1} (Ojovan and Lee 2005). Loading capacity is important for a matrix because it relates to the cost and effectiveness of waste immobilisation: a small improvement in waste loading can result in a significant reduction in cost. Other important parameters to be taken into consideration include thermal stability and conductivity, ability to withstand radiation, to form a monolithic wasteform and mechanical properties. In addition, the production technology and the established knowledge of candidate hosts for other uses are also relevant. Consequently, the selection of immobilisation matrix is often a compromise between various aspects and is dependent on the nature of different nuclear waste.

The main matrices so far developed for nuclear waste immobilisation include glass, ceramics, cement and bitumen, each of them having their own range of application depending on the nature of waste needing treatment and the subsequent disposal

requirements. Their definitions and features are detailed below and their advantages and disadvantages in nuclear waste immobilisation are summarised in Table 2-2.

2.1.2.1. Bituminisation

Bitumen is defined as a complex consisting of a variety of high molecular weight hydrocarbons (mainly are asphaltenes, resins and oils) (Ojovan and Lee 2005). Bitumen has been used as a matrix to immobilise LLW and ILW since 1968 (Sobolev *et al.* 2000) and more than 200 000 m^3 radioactive waste is currently immobilised in bitumen (Ojovan and Lee 2005). Generally, bituminisation is realised by embedding nuclear waste into molten bituminous materials and thereby physically encapsulating the radionuclides into a bitumen matrix after cooling.

2.1.2.2. Cementation

Cements aggregate together to form pastes when mixed with water and later become rigid and hardened products by hydration (Bye 1999). Similar to bituminisation, cementation is also a means of physical encapsulation in which the nuclear waste is mixed with cement and water to form a cementitious wasteform encapsulating radionuclides. Most cements used for immobilisation are ordinary Portland cement (OPC) based while some alternative cements have been developed for special requirements (Bart *et al.* 2013). Cementitious materials are more widely used than bitumens for LLW and ILW immobilisation due to some significant advantages over bitumen (Table 2-2).

2.1.2.3. Ceramisation

The technique in which the nuclear waste is chemically incorporated into a ceramic matrix is called ceramisation. It is accomplished by mixing the radionuclides with other raw oxides and then sintering the mixture at high temperatures to form ceramic materials. The idea of ceramisation is triggered by the observation that some natural minerals can contain high radionuclide contents for geological times in nature (Ewing 1999, Ewing *et al.* 2004). The radionuclides can enter crystal lattices either by substitution of original species or by insertion into open channels, depending on radionuclide species and the crystal structure of the matrix. It was first investigated to

immobilise HLW in 1950s (Donald *et al.* 1997) and has been extensively studied so far, although currently there is no industrial scale plant in operation yet (Donald 2010). Polyphase ceramics, *e.g.* Synroc (Ringwood 1979, Ringwood *et al.* 1979), are more commonly used than monophase ceramics for fabrication reasons (Ojovan and Lee 2005).

Table 2-2 Advantages and disadvantages of different immobilisation techniques.

Immobilisation technique	**Advantages**	**Disadvantages**
Bituminisation	Low cost, widely available	Combustible
	Inert in water (Roffey and Norqvist 1991, Gwinner *et al.* 2006, Sercombe *et al.* 2006)	Less stable against radiation and oxidisation
Cementation	Low cost, widely available	Relatively low loading capacity, radionuclides may interact with cement (Ojovan and Lee 2005)
	Good thermal and chemical stability	
	High pH environment to ensure low solubility of radionuclides (Sharp *et al.* 2003)	
	Ability to resist radiation	
	Ability to modify composition	
	Easy and simple processing	
Ceramisation	High loading capacity	Not monolithic
	High ability to withstand radiation	Complex pre-treatment and preparations (Donald 2010)
	High chemical durability	
	Thermal stability	Potentially glassy secondary phases (Ojovan and Lee 2005)
	Natural analogues	
Vitrification	High chemical durability	High cost
	High loading capacity	High requirement in operation
	Ability to withstand radiation	
	Good thermal stability	
	Advanced preparation technology	

2.1.2.4. Vitrification

Vitrification is a process of incorporating nuclear waste into a glassy wasteform. It has been thoroughly investigated and widely applied since 1950s (Ojovan and Lee 2007) and currently it is the first choice of HLW immobilisation. In vitrification, the pre-treated nuclear waste is mixed with glass-forming additives and melted at high temperatures, followed by pouring into steel canisters to form a vitreous monolith after cooling and finally the canisters are to be stored in geological vaults (Ojovan and Lee 2005). According to the way by which the waste is mixed with glass-forming additives (liquid or calcined), the vitrification technique can be divided into two types, namely the one-stage process (in USA and Russia) and the two-stage process (in UK and France) (Ojovan and Lee 2010). Borosilicate glass is the most used matrix for vitrification whilst aluminosilicate and phosphate glass compositions have also been developed for some specific purposes (Ojovan and Lee 2005, Donald 2010).

Vitrification has plenty of advantages (see Table 2-2) which means it is the first choice for HLW immobilisation and a comparable choice for ILW immobilisation (Ojovan and Lee 2005). Nevertheless, some elements which can be often found in HLW are poorly soluble in conventionally used glass compositions (Ojovan and Lee 2005, Ojovan and Lee 2007, Ojovan and Lee 2010). This can cause significant issues when vitrifying HLW enriched in these difficult elements, giving the incentive to seek glass compositions with a higher solubility for them. This thesis is focused on three difficult elements in HLW vitrification: sulphur, chlorine and molybdenum. The similarity among them lies in their presence as negatively charged ions, namely sulphate SO_4^{2-}, chloride Cl^- or molybdate MoO_4^{2-} respectively, and very poor solubility (<1 wt%) (Lutze and Ewing 1988, Ojovan and Lee 2007, Ojovan and Lee 2010). In most cases, they are not major radioactive elements, but they can contain some radionuclides when separating out from glass melt to form secondary phases if they are added in excess. The chemistry of sulphur, chlorine and molybdenum in glass is discussed in Section 2.3.

2.1.2.5. Difficult elements in vitrification

There are two major sources of sulphur in nuclear waste. One is the use of ferrous

sulphamate $Fe(NH_2SO_3)_2$ (Kaushik *et al.* 2006, IAEA 2007, Mishra *et al.* 2008), which functions as a reducing agent to convert Pu^{4+} to Pu^{3+}during the partitioning stage in the reprocessing of nuclear fuels. The other is the consumption of ion exchanger resin which contains sulphur (IAEA 2002, Hamodi and Iqbal 2009, Hamodi 2012). The strongly acidic functional group $-H^+SO_3$ is one of most common groups in the cation exchanger and thus the spent ion exchanger resin is often rich in sulphur. Most of the produced sulphate in nuclear waste is water soluble and as technology advances the majority of sulphate in nuclear waste can be removed by washing from solid waste to waste effluent (Donald *et al.* 1997).

Chloride in nuclear waste is primarily yielded during the pyrochemical reprocessing of nuclear fuel (Metcalfe and Donald 2004, Tomilin *et al.* 2007, Vance *et al.* 2012), which is carried out in mixed alkali chloride eutectic melts aiming to convert uranium and plutonium cations in spent nuclear fuel to metallic species. Consequently, the waste stream generated in this process can contain a large amount of chlorides. The chlorides cannot be simply removed from waste by heating to high temperature because some low melting point radionuclides can be evaporated concomitantly and because of the highly corrosive nature of chlorine gases. Therefore, vitrification may be a more appropriate way for the disposal of chloride bearing nuclear waste.

Molybdenum can be often found at high levels in HLW produced in UK and France (Do Quang *et al.* 2003, Dunnett *et al.* 2012). Unlike sulphur and chlorine, molybdenum is an abundant fission product. The isotopes of molybdenum in nuclear waste include ^{95}Mo, ^{97}Mo, ^{98}Mo, ^{99}Mo and ^{100}Mo (Wilson 1996), all of which are stable except for ^{99}Mo which has a short half-life of 2.75 days. Molybdenum in the spent nuclear fuel from thermal reactors can be both metallic and in oxide form (Volkovicha *et al.* 2003) and can reach 4-8 kg per tonne in the spent fuels prior to reprocessing (Choppin and Khankhasayev 1999). It is dissolved and concentrated in HNO_3 solutions with other fission products, and after evaporation, concentration and blending with additional waste streams, it is present in the waste as precipitates of caesium phosphomolybdate (CPM) and/or zirconium molybdate (ZM) (Jiang *et al.* 2005).

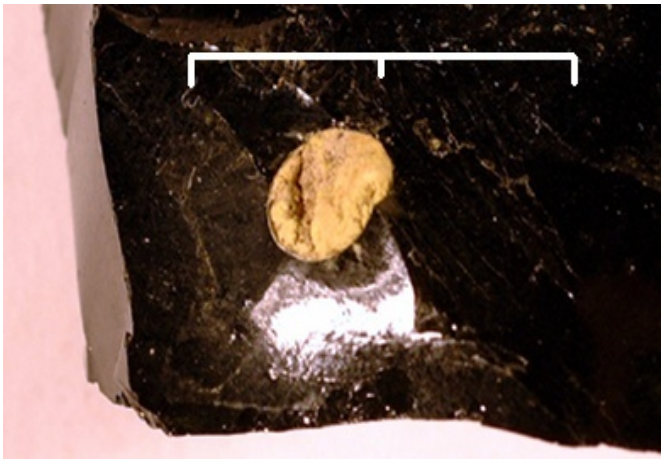

Figure 2-1 Yellow phase in a British Magnox waste simulant glass (Short 2004). The whole scale bar = 2 cm.

The solubility of sulphur, chlorine and molybdenum in the borosilicate glasses used for vitrification is limited. Greater than 1 wt% SO_3 and/or MoO_3 can cause the occurrence of phase separation (Ojovan and Lee 2005). During vitrification, the excess sulphur and/or molybdenum tend to separate out from the melt to form a so-called 'yellow phase' which consists of alkali sulphates, alkali chromates and alkali/alkaline earth molybdates (Short 2004). The molten yellow phase is highly corrosive which can reduce the life of refractories used; the cooled yellow phase is water soluble and able to contain some radionuclides (*e.g.* ^{137}Cs), which could increase the leaching of vitrified radionuclides to the environment if contact with water during long-term geological disposal occurs (Short *et al.* 2005, Taurines and Boizot 2011, Hyatt *et al.* 2012). Chlorine also has a lower than 1 wt% solubility in silicate glasses (Marra *et al.* 1994) and excess chlorine in batch will lead to the formation of a low temperature water soluble salt layer on the melt surface (Siwadamrongpong *et al.* 2004, Schofield 2011). This layer is also detrimental to the vitrification process and should be avoided.

The poor solubility of sulphur, chlorine and molybdenum limits the loading capacity of conventional borosilicate glasses in HLW vitrification. A reasonable approach to enhance the waste loading capacity is to modify the glass compositions whilst maintaining other key properties of glass acceptable. In this thesis, the incorporation behaviours of sulphur, chlorine and molybdenum in two different series of glasses (borosilicate glass and aluminosilicate glass) are investigated in order to understand the compositional dependence of their solubilities in these glass systems.

2.2. Glass matrices

In this thesis two types of glasses are investigated: namely borosilicate and aluminosilicate glasses. Both of them are silicate-based glass systems, whilst they are distinguished by the addition of boron or aluminium as another major network-forming element. Before the discussion about these two glass systems, it is necessary to look into the structure of silicate glass in which SiO_2 is the only network former.

2.2.1. Basic structure of silicate glass

Silicate glasses are typically composed of network formers (SiO_2), network modifiers (*e.g.* Na_2O and CaO) and some intermediates (*e.g.* TiO_2 and Al_2O_3, can be either formers or modifiers depending on glass composition). As a network-forming element, each silicon is strongly covalently bonded by four oxygens to form a SiO_4 tetrahedron. A silicate glass network is built up of SiO_4 tetrahedra, which are connected to each other through bridging oxygens (BO, bonded as Si-O-Si). Network modifying cations enter the glass network, occupy the interstitial space amongst the SiO_4 units and weakly associate with the nearby oxygens from the silicate backbone (Figure 2-2). The addition of network modifiers breaks connections between SiO_4 tetrahedra and causes the formation of non-bridging oxygens (NBO, bonded as $Si\text{-}O^{-}M^{+}$, M = the modifying cations). One mole of network modifiers such as Na_2O and CaO normally contributes two moles of NBOs (Varshneya 1994), although deviation from this ratio may occur when there are large cations, *e.g.* Ba^{2+}, in glass network (Harding 1972, Zhao *et al.* 2000). The NBO fractions play a crucial role in the determination of dynamic properties of glass (Stebbins and Xu 1997) and hence in turn glass compositions can be tuned to achieve required NBO fractions that give rise to desirable glass properties.

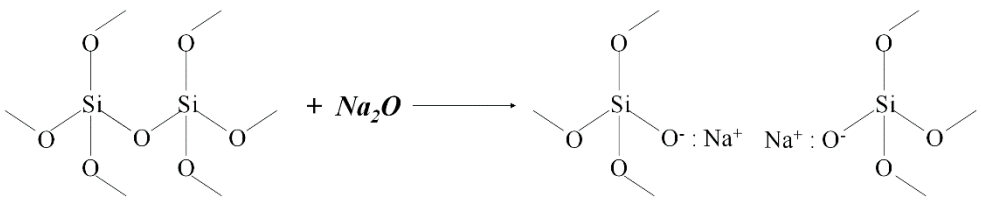

Figure 2-2 Depolymerisation of silicate glass network by a network modifier (*e.g.* Na_2O) addition.

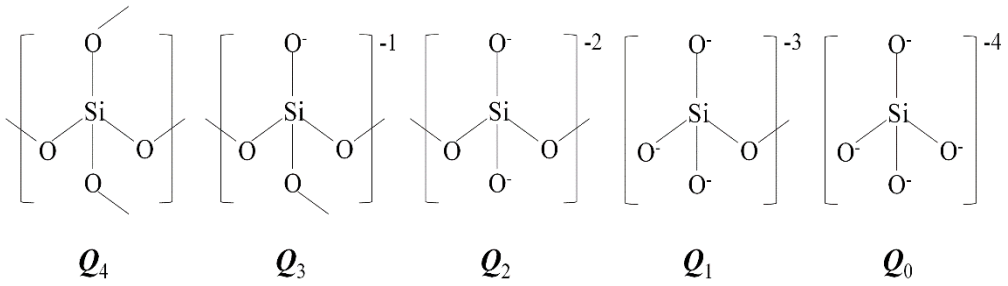

Figure 2-3 Different SiO_4 tetrahedral units Q_n in a silicate glass network.

The connectivity of silicate network can be expressed as Q_n in which the subscript *n* refers to the number of BOs in a SiO_4 tetrahedron. As illustrated in Figure 2-3, there are five *Q* species possible in silicate glass, from fully depolymerised unit Q_0 to fully polymerised unit Q_4. Therefore, a glass network with higher average *n* values has higher connectivity than that with lower average *n* values.

2.2.2. Borosilicate glass

Borosilicate glasses are a family of glasses in which the major network formers are SiO_2 and B_2O_3. They are famous for their extremely low thermal expansion coefficient (Lima and Monteiro 2001) and have been extensively used in lab equipment, optical device, cookware and astronomy (Varshneya 1994). In the nuclear industry, borosilicate glass is currently the major matrix in the vitrification of HLW (Ojovan and Lee 2005) due to its low melting temperature, good thermal and chemical stability, large compositional flexibility and high capacity to immobilise a diverse range of nuclear waste constituents (Plodinec 1982, Jantzen 1986, Donald 2010). A simplified pseudoternary phase diagram from Jantzen (2011) demonstrating the varied applications of borosilicate glass compositions is shown in Figure 2-4.

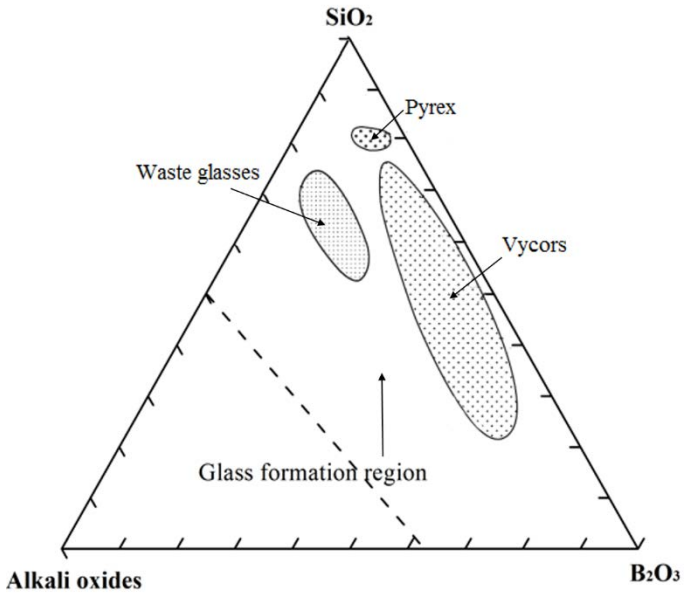

Figure 2-4 Pseudoternary phase diagram of the alkali-oxide-boron oxide system. Compositional ranges of commercial borosilicate glasses (Pyrex and Vycors) and nuclear borosilicate glasses are superimposed. Image from Jantzen (2011).

2.2.2.1. Structure of borosilicate glass

There are two mutually convertible boron structural units in borosilicate glass: BO_3 triangles and BO_4 tetrahedra, the portion of which are determined by the amount of network modifiers. The added network modifying cations can be either associated with a SiO_4 tetrahedron to create an NBO or consumed in the conversion of BO_3 to BO_4 units to create no NBO (Varshneya 1994). In the latter case, modifiers function as charge compensators to stabilise the negatively charged $[BO_4]^-$ units (usually one mole B_2O_3 consumes one mole Na_2O to compensate, but other species might be involved (Manara *et al.* 2009)). It has also been concluded (Yun and Bray 1978, Dell *et al.* 1983, Manara *et al.* 2009) that network modifiers preferably convert BO_3 to BO_4 at low modifier contents (R<~0.5, R is the molar ratio of network modifiers to B_2O_3) and only after a critical point they begin to proportionally associate with SiO_4 and BO_4 units to create NBOs.

As the amount of network modifiers increases, some glass properties such as thermal expansion coefficient and glass transition temperature show a minimum or maximum rather than a linear trend, the so-called “boron anomaly” (Ojovan and Lee 2005). It is

widely recognised that boron anomaly is attributed to the BO_3 to BO_4 conversion, but the point at which a minimum or maximum appears is not always consistent with the point at which NBO formation starts to occur (Varshneya 1994). Tetrahedral BO_4 units are more polymerised than trigonal BO_3 units, so the addition of network modifiers to borosilicate glass initially polymerises the glass network, rather than depolymerises it by the creation of NBOs. NBOs are not created until the conversion reaches saturation. In addition, the existence of this conversion makes borosilicate network more flexible, allowing more compositional variation to be carried out and more components to be accommodated.

The ratio of network formers to network modifiers and the ratio of different network formers are also influential on glass properties. Higher network former contents endow the glass with a higher connectivity while higher network modifiers depolymerise the glass network reducing the melting temperature. The ratio of network formers to network modifiers is normally around 2 to guarantee the glass forming ability (Ojovan and Lee 2005). Meanwhile, the ratio of SiO_2 to other network formers (B_2O_3 and Al_2O_3) in borosilicate nuclear glass should be higher than 1.5 to maintain the low radionuclide leachability even though the melting temperature may also be higher (Ojovan and Lee 2005).

2.2.2.2. Borosilicate glass in nuclear waste vitrification

Borosilicate glass was firstly investigated as a vitrification matrix in the US in the 1950s (Jantzen 1986) and later developed in European countries in the 1960s (Donald *et al.* 1997). Since the composition of nuclear waste varies among reactors and countries, the borosilicate glass formulations used for vitrification are also diverse (partly listed in Table 2-3.

The simplest borosilicate glass formulation put into practical vitrification is a mixed alkali borosilicate glass in which Na_2O and Li_2O are the major network modifiers. The high amount of alkalis reduces the glass melting temperature and meanwhile retards glass crystallisation tendency (Polyakova 2000). Moreover, as mentioned above, the thermal behaviour of glass can be optimised by the interaction between alkalis and boron structural units (the boron anomaly). Glass properties are further modified by adding a small amount of other oxides such as CaO and Al_2O_3. The addition of CaO

allows the glass matrices to incorporate more waste constituents while the addition of Al_2O_3 improves glass durability (however, because many nuclear wastes themselves contain considerable amount of Al, there is no need to add Al_2O_3 in the base glass).

Table 2-3 Compositions (wt%) of some basic borosilicate glasses for vitrification. (Data from Jantzen (2011) and Ojovan and Lee (2005), "others" include MgO, TiO_2, ZnO, *etc.*)

Oxide component	Country	Waste loading	SiO_2	B_2O_3	Na_2O	Li_2O	CaO	Al_2O_3	Others
Magnox	UK	25-31	61.63	21.93	11.09	5.35	-	-	-
UOX1	France	16.5	54.04	16.67	12.05	2.35	4.80	5.89	-
SM58	Belgium	11.1	63.93	13.82	5.17	4.16	4.27	1.35	7.31
Purex/HM HAW	USA	28-38	68.00	10.00	13.00	7.00	-	-	2.00
Hanford 76-88	USA	25	59.7	14.18	11.19	-	2.99	-	11.94
K-26	Russia	?	48.2	7.5	17.8	-	15.5	2.5	8.5
Tokai	Japan	18.29	56.97	17.38	8.54	3.66	3.66	6.13	3.66

There are a large quantity of studies on investigation of borosilicate nuclear waste glass. Chemical durability tests on the SON68 (R7-T7) glass pioneered in France (Gin *et al.* 2001) show that a layer of silicate gel forms on the surface of glass when placed in contact with water. This layer hinders the leaching out of radionuclides from the glass matrix. The effects of radioactive decays of the short-lived fission products such as ^{90}Sr and ^{137}Cs in the waste on the structure of surface gel of borosilicate glass are proven to be limited in time under geological conditions (Advocat *et al.* 2001). Frugier *et al.* (2008) proposed a model of dissolution kinetics of SON68 glass based on a series of durability tests, also indicating that the dissolution rate of glass is mainly controlled by the diffusion of water and the hydrolysed and solvated glass constituents in the surface gel. In addition, Fábián *et al.* (2007) and Jollivet *et al.* (2002) reported that glass has high hydrolytic stability and low mobility of large-sized radionuclides during the storage of the same waste-loaded glass.

A calcium-sodium borosilicate glass (K-26) was developed in Russia (Sobolev *et al.* 1990) to vitrify ILW in which the main radionuclides are radioactive caesium and strontium. Several tonnes of this glass were produced in blocks in 1980s and many of these blocks have been placed in a near surface environment for disposal evaluation since 1987 (Ojovan *et al.* 2005). Leaching experiments were performed by exposing the glass blocks to flowing non-saturated water at 1.7 m beneath the ground and covered by loamy soil (Ojovan *et al.* 2001, Ojovan *et al.* 2004, Ojovan *et al.* 2005, Ojovan *et al.* 2006). The leaching rate of caesium over 16 years is 2.2×10^{-7} g cm^{-2} d^{-1} in average whereas the hydrolysis rate of glass framework is 0.1 μm year^{-1}, suggesting that ion exchange diffusion will be dominant for hundreds of years in the geological repositories. It has also been observed (Ojovan *et al.* 2005) that the simulant inactive glass under laboratory conditions and the radioactive K-26 glass in underground conditions have similar leaching behaviours. Meanwhile, the specific radioactivity of active K-26 glass reduces by half after 12-year storage with ^{137}Cs as the only γ-emitter remaining in glass (Ojovan *et al.* 2001). Some borosilicate nuclear waste glasses developed in France and the UK also contain higher calcium levels (Calas *et al.* 2003, Short *et al.* 2008, Chouard *et al.* 2011) to avert the crystallisation of water-soluble alkali molybdates in glass. MoO_4^{2-} anions are preferentially associated with Ca^{2+} cations rather than Na^+ cations (Caurant *et al.* 2007) so that the crystallisation of Na_2MoO_4 is disfavoured; however, the resultant glasses are often not completely glassy but actually are glass composites. The details of molybdate containing glasses are discussed in Section 2.3.3.

A series of barium-sodium borosilicate glass compositions have been investigated in India to vitrify sulphate-bearing HLW in recent years (Kaushik *et al.* 2006, Mishra *et al.* 2006, Mishra *et al.* 2007, Mishra *et al.* 2008). Barium has some advantages compared to calcium in nuclear waste glass even though they both belong to alkali earth elements. Ba^{2+} is greatly larger than Ca^{2+}, showing a better miscibility and the highest depolymerisation in borosilicate glass network among all alkaline earth elements (Ramkumar *et al.* 2009). This means that more waste constituents such as sulphate can be incorporated. On the other hand, even if sulphate is not fully dissolved in the glass melt, it tends to form crystalline $BaSO_4$ which is one of the most stable minerals in nature, being a reliable barrier to prevent the dispersion of radionuclides

(Mishra *et al.* 2008). Meanwhile, Mishra *et al.* (2007) asserted that thorium solubility is also dramatically increased by 16 wt% to 20 wt% BaO addition. Thorium is a promising nuclear fuel which may be widely exploited in future and therefore a glass matrix with high thorium solubility is of practical importance in designing proper disposal for potential thorium cycle nuclear wastes. Moreover, the high BaO content significantly reduces the melting temperature of borosilicate glass. In a pilot vitrification plant in India, an SB-44 waste glass has been melted at 950 ºC (Kaushik *et al.* 2006). Lower melting temperature is favourable in reducing the evaporation of some volatile elements in nuclear waste, such as Tc and Na and thus improving the efficiency of vitrification. It is also reported (Singh *et al.* 2008, Tuscharoen *et al.* 2012) that the addition of barium enhances the ability of borosilicate glass to withstand X-ray and γ-ray irradiation, which is ascribed to the strong absorption of these rays by Ba^{2+}.

Borosilicate glass compositions are also used for nuclear waste vitrification in other nuclear countries such as China (Sheng *et al.* 1999), Japan (Inagaki *et al.* 1994) and Sweden (Werme *et al.* 1990). Nonetheless, they are not discussed here either because their information is limited or because they are close to the compositions mentioned above.

2.2.3. Aluminosilicate glass

Aluminosilicate glasses are a family of glasses in which SiO_2 and Al_2O_3 are the structural units. Aluminosilicates are of particular interest in geoscience because of their wide presence in magma. In the glass industry, based on their excellent mechanical, thermal and chemical properties, aluminosilicates have various applications including crystal display substrates (Potuzak *et al.* 2010), strengthened cover glasses (Tandia *et al.* 2012), laser host materials (Tiegel *et al.* 2013) and nuclear waste immobilisation hosts (Jantzen *et al.* 2010). Therefore, the structure and properties of aluminosilicate glasses and melts have been thoroughly investigated by geologists and glass scientists.

2.2.3.1. Structure of aluminosilicate glass

As an intermediate oxide, Al_2O_3 is able to function as both a network former and a

network modifier in aluminosilicate glasses. The roles of Al^{3+} ions in glass network are dependent on the ratio of Al_2O_3 content [Al_2O_3] to alkali and alkaline earth contents [M_2O + MO]. When [Al_2O_3] ≤ [MO + M_2O], Al^{3+} ions are predominantly four-fold coordinated to form AlO_4^- tetrahedra (Xiang *et al.* 2013). AlO_4^- tetrahedra are combined with SiO_4 tetrahedra in the network to form the backbone through Si-O-Si, Al-O-Si and Al-O-Al connections. However, like BO_4^- tetrahedra, AlO_4^- tetrahedra are negatively charged and hence require alkali or alkaline earth ions in the neighbourhood to compensate the charge so as to stabilise the network. Each mole of AlO_4^- tetrahedra consumes one mole M^+ or 0.5 mole M^{2+} and there are no NBOs created in this stage. After all the AlO_4^- tetrahedra have been charge compensated, the residual M^+ and/or M^{2+} begin to break network connections, functioning as network modifiers to create NBOs in a mole ratio of 1:2 (M_2O/MO: NBO). The difference between Al_2O_3 and B_2O_3 in glass network lies in the fact that Al^{3+} does not form 2-dimensional AlO_3 units unlike B^{3+} and hence in aluminosilicate glass there are no maxima or minima analogous to the "boron anomaly".

On the other hand, when [Al_2O_3] > [M_2O + MO], all of the M^+ and M^{2+} ions are consumed as charge compensators. As the charge compensator is insufficient, the excess Al^{3+} ions cannot form AlO_4^- structural units and instead they function as network modifiers in octahedral coordination. These Al^{3+} ions are located in the network interstices and each Al^{3+} ion is surrounded by three BOs and three NBOs in equivalence (Varshneya 1994). In summary, some Al^{3+} ions form AlO_4^- structural units to join the network backbone while other Al^{3+} ions function as network modifiers to create NBOs in a ratio of 1:3 (Al^{3+}: NBO).

In the aluminosilicate glasses of interest in this study, [Al_2O_3] is always lower than [M_2O + MO] and hence all the Al^{3+} ions are believed to be present as AlO_4^- tetrahedra entering the backbone of network. The addition of M_2O and MO is considered to charge compensate AlO_4^- tetrahedra first and then function as network modifiers.

2.2.3.2. Aluminosilicate glass in nuclear waste vitrification

Compared with borosilicate glasses, aluminosilicate glasses demonstrate higher chemical durability and thermal stability which favour nuclear waste vitrification (Jantzen *et al.* 2013). Moreover, the large abundance of aluminosilicate raw materials

in the world can reduce the cost of vitrification. Nevertheless, such advantages are overridden by the relatively high processing temperature and low waste loading capacity and as a result the application of aluminosilicates as immobilisation matrices is limited.

Investigations on using aluminosilicate glass formulations as vitrification matrices have been carried out in Canada since the late 1950s (Jantzen 1986). Natural nepheline syenite rock ($NaAlSi_3O_8$) was crushed and fused with nuclear waste at temperatures above 1350 ºC. The first active glass wasteform made from nepheline syenite with fission products was produced in 1958 (Bancroft 1960). Durability tests performed on 25 blocks containing 7.4 TBq in total suggests that these aluminosilicate glasses, which were buried below water table in a sandy-soil aquifer, are extremely chemically durable (Melnyk *et al.* 1984). The authors also found good agreement in the leaching behaviour between laboratory and field measurements over a 17 year period. However, in order to lower the processing temperature and reduce the loss of radionuclides by volatilisation, research on vitrification matrices was redirected to develop borosilicate glass compositions (Ewing *et al.* 1995).

Although the interest in using aluminosilicate glasses as vitrification candidates has faded, there are still a large number of studies with regard to the corrosion behaviour of naturally occurring basaltic glasses (45-61 wt%SiO_2 and 12-17 wt%Al_2O_3) (Leturcq *et al.* 1999, Techer *et al.* 2000, Crovisier *et al.* 2003, Donald 2010). These glasses have been present in nature over geological times and are considered as analogues to nuclear waste glasses for simulating the long-term corrosion in underground conditions. Comparative studies suggest that the long-term alteration mechanisms and kinetics between them are similar: the leaching rate diminishes rapidly after an initial period and an alteration film is then formed as a diffusion barrier which controls the reaction with water. Both the investigated basaltic glasses and simulated nuclear waste glasses show good chemical durability in experiments.

In recent years, calcium aluminosilicate glass compositions have been investigated for the incorporation of chloride (Siwadamrongpong *et al.* 2004, Schofield 2011). Although the issues and target in Siwadamrongpong *et al.* (2004) were the treatment of fly ash, and the investigated glasses were prepared under reducing atmosphere, this

work indicates the possibility of using calcium aluminosilicate glass compositions to incorporate chloride-rich nuclear waste. The maximal incorporated chloride amount is 10.6 at%Cl, which is far beyond the chloride solubility limit in ordinary glasses. Then, in Schofield's PhD thesis (2011), he investigated the loading limit and incorporation behaviour of chloride containing actinide waste surrogate in a calcium aluminosilicate glass composition. The cast glass was able to retain 7.92 at%Cl without causing phase separation and retained excellent chemical durability. The structural characteristics of these glasses are discussed in Section 2.3.2, where chloride incorporation in glass network is reviewed.

2.2.4. Raman spectroscopy

The chemical bonds in glasses can be detected by Raman and FTIR spectroscopies. For a specific bond, the vibrational energy of Raman scattering and infrared absorption is unique and thus the sequence of Raman and/or FTIR peaks can be used to identify bond information by comparison with known data. However, for glass samples, the Raman and FTIR peaks are broadened due to the disordered arrangement of atoms. From a statistical perspective, this broadening should be symmetric and hence the central frequencies of those bands are used in the assignment. Table 2-4 presents the general frequencies to which the Raman bands for borosilicate and aluminosilicate glasses are assigned.

The substitution of Al and B for Si in glass network results in distortion in neighbouring Si-O bonds and therefore the frequencies assigned to vibrations of Si-O bonds can be slightly shifted for aluminosilicate and borosilicate glasses. Since boron atoms are able to form both BO_3 triangles and BO_4^- tetrahedra, the bond information in borosilicate glasses is more complex than in aluminosilicate glasses where aluminium atoms only forms AlO_4^- tetrahedra. Hence there are more Raman bands for borosilicate glasses than for aluminosilicate glasses.

Although the alkali and alkaline earth cations are not sensitive to Raman spectroscopy, their addition indeed results in notable changes in Raman spectra of glasses. This is because of the effects of modifier incorporations on surrounding Si-O, Al-O and B-O bonds, which gives rise to distortions in these bonds. Usually, the addition of network modifiers results in a slight frequency shift of some Raman bands, coupled with

changes in relative intensities of bands assigned to different structural groups. Deconvolving the broad bands which are assigned to combinations of Si-O bonds in SiO_4 units with different connectivity provides a way of analysing the polymerisation of the glass network.

Table 2-4 Corresponding Raman frequencies (cm^{-1}) of vibrations in borosilicate and aluminosilicate glasses.

Frequency (cm^{-1})	Vibrations	References
450-580	Si-O-Si bending and rocking	(Furukawa and White 1981, Neuville and Mysen 1996)
530-550	Si-O-Si symmetric stretching and Si-O-Al deformation	(Neuville and Mysen 1996, Koroleva *et al.* 2011)
610-635	Metaborate rings ($B_3O_6^-$) and mixed borosilicate rings	(Koroleva *et al.* 2011) (Osipov *et al.* 2013)
765-775	Six-membered borate rings with one or two [BO_4] units	(Furukawa and White 1981)
750-790	Si-O-Al	(Mckeown *et al.* 1984)
805-810	Boroxy ring, symmetric	(Furukawa and White 1981)
~850	Si-O-Si asymmetric stretching Q_0	(McMillan 1984) (Lenoir *et al.* 2009)
~900	Si-O-Si asymmetric stretching Q_1	(Lenoir *et al.* 2009)
950-1000	Si-O-Si asymmetric stretching Q_2	(Lenoir *et al.* 2009)
1050-1100	Si-O-Si asymmetric stretching Q_3	(Lenoir *et al.* 2009)
1120-1190	Fully polymerised Q_4	(Lenoir *et al.* 2009)
1470-1480	BO_3 triangles	(Furukawa and White 1981, Osipov *et al.* 2013)

2.3. Chemistry of anionic species in glass

The aforementioned three difficult elements, sulphur, chlorine and molybdenum, have limited solubilities in the conventional used nuclear waste glasses, and hence can control the waste loading capacity of nuclear waste vitrification. It is therefore of great interest to understand the incorporation of sulphur, chlorine and molybdenum in glasses and to explore their solubility dependence on glass compositions, for the sake of improving their solubilities on the basis of reliable knowledge. Considerable studies have been carried out with regard to chemistries of sulphur, chlorine and molybdenum in glasses and in the following sections most of the relevant findings are summarised.

2.3.1. Sulphur

Sulphur is an important element in glasses and glass melts. In the commercial glass industry, sulphates have been long used as a fining agent (Beerkens 2003, Matyas and Hrma 2005). The understanding of sulphur chemistry in glass melts facilitates the optimisation of glass fining and the avoidance of forming corrosive sulphate layer. Meanwhile, sulphides are sometimes deliberately added to achieve amber colour glass (Behrens and Webster 2011). In the nuclear glass industry, particular attention has been paid to sulphur because of its poor solubility in borosilicate melts and the consequent issues caused by excess sulphate. Numerous researches (Jantzen *et al.* 2004, Tronche *et al.* 2009, Billings and Fox 2010) have been carried out to understand and maximise sulphate dissolution in glass in order to increase the waste loading in vitrification. Sulphur in silicate melt is also of geological interest because of the saturated sulphur content in magmas (Li and Ripley 2005, Liu *et al.* 2007, Jugo 2009). The study of sulphur in magma-like melts is relevant to the prediction of SO_2 emissions by volcanic eruptions and to the detection of sulphur-bearing ores in geological deposits. Generally speaking, while glass researchers focus more on sulphate species (S^{6+}) in silicate melts, the majority of sulphide (S^{2-}) studies are performed by geologists.

In the glasses prepared under neutral and oxidising atmospheres, *e.g.* commercial and nuclear glasses, sulphur occurs dominantly as sulphate (Bingham *et al.* 2010). This thesis is aimed to investigate the incorporation and solubility of some anions in glasses for nuclear waste use and therefore only sulphate (SO_4^{2-} or SO_3 equivalent) behaviours

in glass are involved here.

2.3.1.1. Sulphate solubility in glass

The dissolution of sulphur in silicate glass melt is a chemical process (Pye *et al.* 2005). Sulphur in glass of interest in this study is present as hexavalent S^{6+} and bonded with four oxygens to form a SO_4^{2-} tetrahedron. There are three equilibrium reactions (Equations 2-1 ~ 2-3) determining the dissolution of SO_4^{2-} in a silicate melt (Fincham and Richardson 1954, Holmquist 1966, Papadoloulos 1973), as detailed below.

Equation 2-1 expresses the mutual inverse relationship between bridging oxygens (O^0), free oxygen ions (O^{2-}) and non-bridging oxygens (O^-) in a melt. Since the concentration of O^{2-} ($[O^{2-}]$) in glass is usually very low (Papadoloulos 1973), the total concentration of oxygens [O] can be assumed to approximate the sum of $[O^0]$ and $[O^-]$. For a given composition, the fractions of O^0 and O^- are certain though calculation from glass composition may be cumbersome.

$$O^0 + O^{2-} \underset{}{\overset{K_1}{\rightleftharpoons}} 2O^- \qquad \text{Equation 2-1}$$

Equation 2-2 describes the decomposition of SO_4^{2-} into free oxygen ions and SO_3 gas in the melt. This is the primary reaction of sulphate dissolution and evaporation in melt, indicating that the concentration of SO_4^{2-} ions $[SO_4^{2-}]$ in melt is related to $[O^{2-}]$ and K_2, the equilibrium constant of Equation 2-2. $[O^{2-}]$ is determined by glass composition, especially the amount and species of network modifiers; K_2 varies with sulphate species in melt. Equation 2-3 is the further decomposition of SO_3 to SO_2 and O_2. At temperatures higher than 1000 ºC, SO_3 decomposition almost goes to completion.

$$SO_4^{2-} \underset{}{\overset{K_2}{\rightleftharpoons}} O^{2-} + SO_3 \uparrow \qquad \text{Equation 2-2}$$

$$SO_3 \underset{}{\overset{K_3}{\rightleftharpoons}} SO_2 + \frac{1}{2}O_2 \qquad \text{Equation 2-3}$$

Combining above three equilibrium equations together, the equilibrium concentration of sulphate $[SO_4^{2-}]$ in the melt can be expressed as Equation 2.4:

$$[SO_4^{2-}] = \frac{P_{SO_2} P_{O_2}^{1/2} [O^-]^2}{K_1 K_2 K_3 [O^0]}$$ Equation 2-4

where P_{SO2} and P_{O2} are the partial pressures of SO_2 and O_2, respectively. This indicates that, if melting atmosphere and temperature are kept constant, $[SO_4^{2-}]$ is proportional to $[O^-]^2/[O^0]$ (namely $[O^{2-}]$) and inversely proportional to K_2. $[O^-]^2/[O^0]$ can be tuned by adjusting the content and species of network modifiers whereas K_2 is controlled by the sulphate species in the melt.

Nevertheless, according to the thermodynamic data for sulphate decomposition from Stern and Weise (1966), K_2 of Na_2SO_4 is several orders of magnitude higher than K_2 of alkaline earth sulphates: K_2 (Na_2SO_4) >> K_2 ($BaSO_4$) >> K_2 ($CaSO_4$). Although these calculations are extrapolated from the data for sulphate crystals, it can be assumed that such significant difference among sulphate K_2 values remains applicable in a glass melt. Therefore, Na_2SO_4 will dominate sulphate dissociation until the Na_2O content is very low, and in the Na_2O abundant glasses the variation in alkaline earth species does not significantly alter K_2. Meanwhile, Papadoloulos (1973) found that the influence of K_2 on sulphate solubility is larger in silicate melts that do not contain alkalis; Ilyukhina *et al.* (2010) mentioned that a tiny amount of Na_2O could result in a significant reduction of sulphate solubility in an alkali-free borosilicate glass: both of them suggest that sulphate solubility is controlled by the possible sulphate species in the melt which has the highest dissociation equilibrium constant K_2.

On the other hand, the $[O^-]^2/[O^0]$ ratio can be readily adjusted by compositional variation, of which decreasing the SiO_2 content while increasing network modifier content in glass is the most direct. Holmquist (1966) investigated the binary SiO_2-Na_2O glass system with varying SiO_2/Na_2O ratios, showing that sulphate solubility drops from ~4 to less than 0.1 wt%SO_3 as the ratio increases from 1.5 to 2.5 in ambient atmosphere. This tendency has also been observed by Ooura and Hanada (1998) when investigating a ternary glass system (85-*x*)SiO_2-*x*MO-15Na_2O (M = divalent cations, x = 10 ~ 25). The authors reported a generally linear increase in sulphate solubility due to equimolar replacement of SiO_2 by MO.

The calculation and prediction of non-bridging oxygen fraction is convenient in simple

glasses; however, most nuclear waste glass compositions are complicated, making the calculation of the non-bridging oxygen fraction more difficult. A simplified approach is to categorise the components by their presumed contribution to the creation of non-bridging oxygens. Li *et al.* (2001) proposed a sequence of Al, P, Fe, B and Si for the interaction with alkalis so that network modifiers added to glass are preferentially consumed to compensate the negative charge of AlO_4^- and BO_4^- in aluminosilicate and borosilicate glasses. Only when this compensation is completed can the alkalis start to interact with SiO_4 to create non-bridging oxygens in a 1:1 ratio. By assuming this the fractions of non-bridging and bridging oxygens ($[O^-]$ and $[O^0]$) can be calculated. The authors plotted sulphate solubility as a function of calculated $[O^-]^2/[O^0]$, observing a non-linear increasing correlation in (alumino)-borosilicate glasses (phosphate glasses are not discussed here). Following this, Jantzen *et al.* (2004) investigated the relationship between sulphate solubility and the melt viscosity, which is a function of non-bridging oxygen fraction. A downward sulphate solubility tendency was fitted with increasing viscosity. Given the authors' definition that melt viscosity is inversely proportional to non-bridging oxygen fraction, the results are also considered to show an increase in sulphate solubility with increasing $[O^-]^2/[O^0]$.

Nevertheless, in both Li *et al.* (2001) and Jantzen *et al.* (2004), one mole of alkali or alkaline earth oxide was assumed to produce two moles of non-bridging oxygens no matter the species. Ignoring the specific modifier species does not affect the calculation results because their investigated glasses contain a limited level of large cations such as Ba^{2+} which may create more non-bridging oxygens. However it does mean that their proposed prediction models, despite fitting well to their own data, do not apply to more varied glass compositions, see for example, Ooura and Hanada (1998) where a complete substitution between a variety of divalent cations has been achieved. Ooura and Hanada (1998) observed an increasing sulphate solubility with the abundance of BaO > SrO > PbO > CaO > MgO > ZnO while other components stayed constant. This may arise from the different depolymerisation effect on the glass network due to the cations. Larger cations are believed to make glass network more depolymerised than smaller cations and hence the number of non-bridging oxygens created by one mole of larger cations is more than that created by one mole of smaller cations. Combined with the previous SiO_2/MO substitution results in Holmquist (1966)

and Ooura and Hanada (1998), it indicates that both the amount and the species of network modifiers are playing important roles in determining sulphate solubility in glass.

Bingham and Hand (2008) applied cation field strength to characterise glass composition for the prediction of sulphate solubility in glass. Cation field strength *F*, which is defined as Equation 2.5, is a parameter relating to the charge and radius of a cation:

$$F = Z / a^2 \qquad \text{Equation 2-5}$$

where *Z* is the valence of a cation and *a* is the cation-oxygen bond length in Å. Cation field strength can be used to judge whether a cation is network forming (high *F*) or network modifying (low *F*) in glass (Ojovan and Lee 2005). The *F* values of relevant cations in glass are listed in Table 2-5.

Table 2-5 Field strength *F* values of cations involved in this study. Values referred to Ojovan and Lee (2005) calculated from Shannon and Prewitt (1969) and Shannon (1976).

Cation	Valence	Coordination Number	*F*	Cation	Valence	Coordination Number	*F*
Si	+4	4	1.57	Mg	+2	6	0.45
B	+3	4	1.34	Ca	+2	8	0.33
Al	+3	4	0.96	Sr	+2	8	0.28
Na	+1	6	0.19	Ba	+2	8	0.25

Bingham and Hand (2008) observed a linear increase in logarithmic sulphate solubility [log (mol%SO_3)] with decreasing normalised cation field strength [Σ (Z/a^2), the sum of cation field strength of each component normalised to one mole cations]. The favouring of lower normalised cation field strength is probably because cations with lower field strengths contribute higher oxygen ion activities in the melt (Harding 1972) which improves sulphate dissolution. Although the fitting was derived from combined phosphate and borosilicate glasses, the overall results are more consistent with

phosphate compositions. However, for the individual series of borosilicate glasses, *e.g.* McKeown *et al.* (2001) and Lorier *et al.* (2005), similar trends could be obtained separately. While the model of Bingham and Hand (2008) provides a general approach to predict sulphate solubility in nuclear glasses, it seems better to separate silicate glasses from phosphate glasses when fitting sulphate solubility data.

Meantime following Ooura and Hanada (1998), some Indian researchers (Jahagirdar and Wattal 1998, Kaushik *et al.* 2006, Mishra *et al.* 2008) developed borosilicate glass compositions with high levels of lead or barium for vitrification of sulphate bearing HLW. Jahagirdar and Wattal (1998) recommended a WTR-62 glass, which contains 33 wt% PbO in its base composition, to vitrify HLW due to its excellent sulphate capacity and chemical durability. However, the waste-loaded glasses were reported to suffer severe phase separation during long-term storage (IAEA 2007) and hence this composition was later abandoned. Then, another borosilicate glass composition, which has a high BaO content (25 wt% in base), was proposed and investigated by Kaushik *et al.* (2006). This glass is able to contain more than 3 wt% SO_3 without causing phase separation while showing reliable leaching behaviour. It has been applied to large scale vitrification in India and no phase separation issue has been reported so far. Both lead and barium borosilicate glasses showing higher sulphate solubility are in accordance with the tendency reported in silicate glasses by Ooura and Hanada (1998), suggesting that the enhancement of sulphate solubility by such large cations is likely to be universal.

Another way to improve sulphate solubility in nuclear glass is to add some multivalent metals. A small amount of vanadium (V_2O_5) is reported (Manara *et al.* 2007) to have a beneficial effect on sulphate dissolution in melt. The authors attributed this benefit to the acceleration of the kinetics of sulphate dissolution and decomposition by vanadium addition. Titanium is another element that improves sulphate solubility in nuclear waste glasses (Ilyukhina *et al.* 2010); the mechanism of this improvement is not clear however. Such multivalent metals will make the general characterisation of glass compositions more difficult and they may also function differently with the traditional network modifiers, hence the contribution of such multivalent metals is not investigated in this thesis.

2.3.1.2. Sulphate incorporation in glass

The understanding of sulphate incorporation and its influence on glass structure and properties provides an insight into the controlling factors for sulphate capacity in glass. As mentioned previously, sulphur in glasses prepared under oxidising and neutral atmospheres is predominantly present as S^{6+} (SO_4^{2-}) (Bingham *et al.* 2010) and does not replace silicon to function as a network-forming element unless in the pure silica glass (Papadoloulos 1973) which however has a very limited capacity of incorporating sulphate. The studies regarding the environment of S^{6+} in glass network, *e.g.* X-ray absorption fine structure (XAFS) spectroscopy results (Brendebach *et al.* 2009) suggest that SO_4^{2-} tetrahedra are preferably associated with modifiers to form sulphate clusters, located in the voids of glass network. These authors also argued that SO_4^{2-} ions are most likely associated with Na^+ ions in clusters. However, Mishra *et al.* (2008) concluded that SO_4^{2-} ions are more likely associated with Ba^{2+} ions in a borosilicate glass system where sodium and barium coexist. This discrepancy may arise from the different modifiers present in their glasses. There is no strong chemical preference for SO_4^{2-} ions to associate with alkalis or alkaline earths, thus SO_4^{2-} ions may tend to associate with larger cations such as Ba^{2+} ions which is able to provide more space to attract SO_4^{2-} ions.

The presence of sulphate in glass can be detected by Raman spectroscopy (McKeown *et al.* 2001, McKeown *et al.* 2004, Manara *et al.* 2007, Lenoir *et al.* 2009, Klimm and Botcharnikov 2010, Lenoir *et al.* 2010). Four Raman bands are created due to the vibrations of SO_4^{2-} units, which are υ_1 centred at ~990 cm^{-1} assigned to the symmetric S-O stretching mode, υ_2 at ~460 cm^{-1} assigned to the symmetric O-S-O bending mode, υ_3 at ~1100 cm^{-1} assigned to the asymmetric S-O stretching mode and υ_4 at ~620 cm^{-1} assigned to the asymmetric O-S-O bending mode, respectively. For silicate glasses, υ_1 band is the only prominent one among them and the other bands are usually weak and hidden behind the bands assigned to vibrations of the silicate network. Moreover, Raman spectra of different alkali and/or alkaline earth sulphate crystals are similar, with the corresponding frequencies slightly shifted (Table 2-6). As seen in the table, the frequencies move to lower values with cations of larger radius within individual alkali or alkaline earth series. In addition, there is a slight difference between the frequencies of sulphate crystals and sulphate in glass due to the alteration of

environment of SO_4^{2-} ions when incorporated into the amorphous network, which complicates the identification of specific sulphate species in glasses. Normally, sulphate in an amorphous state gives rise to a lower frequency band than in a crystalline state.

Table 2-6 Frequencies of υ_1 band of some crystalline sulphates (McKeown *et al.* 2001).

Sulphate crystals	Frequency (cm^{-1})	Sulphate crystals	Frequency (cm^{-1})
Li_2SO_4	1017	$MgSO_4$	1020
Na_2SO_4	994	$CaSO_4$	1018
$NaK(SO_4)$	996	$CaSO_4 \cdot 2H_2O$	1007
K_2SO_4	984	$SrSO_4$	990
Cs_2SO_4	972	$BaSO_4$	988

The intensity of sulphate bands in Raman spectra reflects the concentration of sulphate in glass, providing the possibility of quantitatively analysing the relative amount of sulphate dissolved in glass. This is realised by the separation of sulphate bands from silicate bands and the deconvolution of silicate bands using mathematical methods (Ahmed *et al.* 1997, McKeown *et al.* 2001, Manara *et al.* 2007, Lenoir *et al.* 2009). Among these studies most are focused on the 800-1200 cm^{-1} region where υ_1 SO_4^{2-} band overlaps with the broad asymmetric stretching silicate band. By deconvolving this region into five or six Gaussian bands, the contribution of the signals from sulphate and from silicate is attained. As described in Lenoir *et al.* (2009), the intensity of deconvolved SO_4^{2-} band is dependent on the relative amount of sulphate to the other components in glass. Moreover, the reliable quantification for sulphate content in glass is based on the standard ratio between them for a glass with known sulphate content and glass composition. Then the sulphate content in other glasses can be obtained through comparison with the intensities or areas of sulphate bands.

2.3.2. Chlorine

There are not many studies regarding chlorine dissolution in silicate glass systems. In the commercial glass industry, sodium chloride is commonly used as an alternative

fining agent to sodium sulphate for production of high quality borosilicate glasses (Müller-Simon 2011, Stevenson 2012). Meanwhile, the addition of chloride to soda-lime-silica glasses is reported to be detrimental to the glass formation because it accelerates the phase separation between silica-rich precipitates and silica-poor matrices (Hoell *et al.* 1996, Kranold *et al.* 2001, Stevenson 2012). However, Cl^- solubility in these glasses is usually very low and these studies give little information about the incorporation of Cl^- ions in the glass network.

Investigations on chlorine in glass are also of significance in magma research where chlorides, mainly in the form of HCl and volatile metal chlorides, are an important component formed in the volatiles of some magmas which drive the degassing process (Webster *et al.* 1999, Stebbins and Du 2002). Considerable studies have been carried out to investigate the solubility and incorporation behaviour of chloride in magmatic (aluminosilicate) glasses. Generally speaking, the chlorine content (Cl^-) that is finally retained in magmatic glasses is very low (~ ppm), though its influence on glass properties can be significant.

As a troublesome element in nuclear waste vitrification, chlorine in nuclear glasses has been paid particular attention due to its low solubility and the issues it may cause (Metcalfe and Donald 2004, Ojovan and Lee 2005, Donald *et al.* 2007, Donald 2010). Many endeavours to avoid phase separation and deterioration of nuclear glasses due to excess chloride have been made, including the amelioration of basic glass compositions to have a higher Cl^- solubility (Ilyukhina *et al.* 2010, Schofield 2011), the use of vigorous stirring and fast cooling (Ojovan and Batyukhnova 2007) and the forming of glass ceramic materials (Metcalfe and Donald 2004). These studies, particularly those for new glasses with improved Cl^- solubility, provide some insight into the dissolution of Cl^- in glass network at greater levels. Nevertheless, the mechanisms of Cl^- incorporation in glass network and its solubility dependence on glass composition are still not fully understood.

2.3.2.1. Chloride solubility in glass

As mentioned previously, literature regarding chlorine solubility in silicate glasses and melts is limited. Chlorine (Cl^-) solubility has been observed to be dependent on melt composition, melting temperature and atmosphere as well as the coexistence of other

halogens (Dingwell and Hess 1998, Webster and De Vivo 2002, Siwadamrongpong *et al.* 2004, Zimova and Webb 2006). Here in this thesis it is mainly focused on the compositional dependence of chlorine solubility in glass and therefore only factors that are related to glass composition are discussed.

To the best of our knowledge, chlorine in either nuclear waste glasses or magmatic glasses is exclusively present as Cl^- ions when incorporated into glass network; in other words, chlorine (Cl) solubility is in fact equivalent to chloride (Cl^-) solubility in glass in the study. Like SO_4^{2-} ions, Cl^- ions are also dissolved into glass by incorporation into glass network, and in turn the bonding environment of Cl^- ions within glass network is determinant with regard to Cl^- solubility. Previous studies have suggested that Cl^- ions are associated with network modifying cations in all ordinary glasses, with exception of those pure or almost pure silica glasses where Si-Cl bonds occur (see next section). Therefore, the ability of a glass composition to incorporate chloride essentially relies on the network modifying cations.

The common variations in network modifiers in glass include the content and species, both of which can result in significant changes in chloride solubility in silicate glasses. Webster and De Vivo (2002) summarised the saturated Cl^- content in various magmatic aluminosilicate rock glasses. Their work suggests that the abundance of different elements has different effects on chloride solubility in glass, some advantageous while some others are disadvantageous. After excluding those glasses with the coexistence of F^- and Cl^-, the authors defined and determined the association coefficient of each cation on increasing chloride solubility. The order of association coefficient of some abundant elements is as following:

$$Mg \approx Ca > Fe > Na > K > Al > Li \approx Rb \approx Cs$$

It can be predicted that the abundance of alkaline earths are more influential than that of alkalis with regard to chloride solubility in (alumino-)silicate glasses. However, due to the restricted compositional range inherent in magmatic glass compositions, the influence of larger alkaline earth elements has not been investigated. More recently, Siwadamrongpong *et al.* (2004) investigated chloride solubility in a range of calcium aluminosilicate glasses with varying ratios of CaO to SiO_2 and Al_2O_3, in which

compositional variation is realised by altering the network modifier content. Increasing CaO content means a higher NBO fraction in glass, and the results (plotted in Figure 2-5) showed that a larger NBO fraction favours higher chloride solubility in glass.

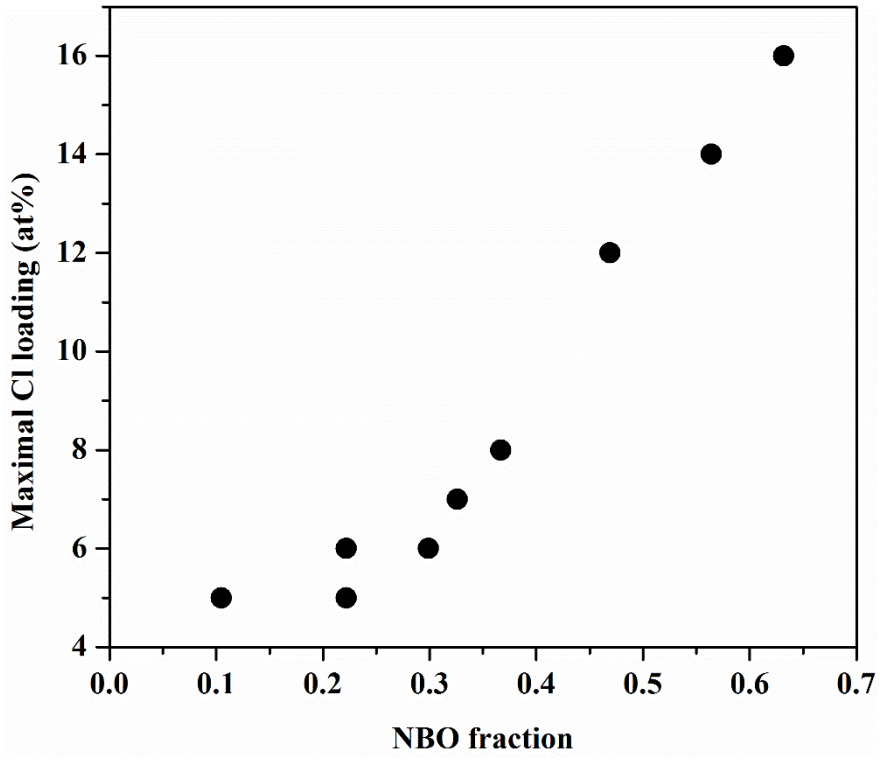

Figure 2-5 Cl loading limit versus NBO fraction of basic glass compositions (Siwadamrongpong *et al.* 2004), NBO fraction calculated as 2([CaO]-[Al_2O_3])/[O].

One must note that the glasses in Webster and De Vivo (2002) and Siwadamrongpong *et al.* (2004) have been prepared under distinct conditions either from each other or from glasses for nuclear waste use. Especially, the glasses in the former paper were prepared under ~2000 bars pressure rather than air pressure used in the latter. It is probably for this reason that the Cl^- solubilities between them vary significantly, resulting in comparability between the two studies being reduced. However, given the fact that the experimental conditions within each study are almost kept constant, the features of Cl^- solubility found in them are still relevant for future studies.

Schofield in his thesis (Schofield 2011) investigated the applicability of using calcium aluminosilicate glasses to immobilise simulated chloride-containing nuclear waste. It

is interesting that, despite the ambient and reducing atmospheres which are used during glass making in Schofield (2011) and Siwadamrongpong *et al.* (2004), respectively, the Cl^- solubilities in comparable compositions between them are generally close. This means that the melting atmosphere plays an insignificant role in the determination of chloride solubility and hence the difference in atmosphere is ignored in the future comparisons.

There are also a number of studies regarding chloride incorporation in phosphate glass compositions, such as another chapter in Schofield (2011) and Metcalfe and Donald (2004); however, due to the substantial difference between silicate and phosphate glass networks, these studies are not considered further here.

2.3.2.2. Chlorine incorporation in glass

It is known that chlorine occurs as Cl^- in glass network; however, the bonding environment of Cl^- ions is often controversial and contradictory in literature (Kiprianov *et al.* 2004). Earlier studies on halogens (F and Cl) in silicate glasses (see the review by Kiprianov and Karpukhina (2006)) concluded that they are preferably bonded with Si, functioning as bridging atoms in the silicate glass network by replacing bridging oxygens to form structural groups ≡Si–Hal Hal–Si≡ or ≡Si<$(Hal)_2$>Si≡ (Hal = F and Cl), as implied by electron paramagnetic resonance (EPR) results. Meanwhile, in glasses with a second network former (*e.g.* Al), the preferential bonds change to $[AlO_{3/2}Hal]^-$ (Kiprianov *et al.* 2004). Moreover, the Si-Cl connection is reported in a pure silica glass in Chmel and Svetlov (1996) with up to 6 mol% Cl dissolved.

On the other hand, many researchers argue that Cl^- ions do not bond with Si or other network formers but, instead, are associated with network modifying cations in the glass network. Based on the results from various compositions at ordinary pressure, Zimova and Webb (2006) indicates that Cl^- ions prefer to bond with divalent network modifying cations or with the charge compensating cations if there are no modifying cations. Evans *et al.* (2008) suggests that there is an absence of Si-Cl and Al-Cl bonds in a wide range of aluminosilicate glasses based on X-ray absorption near edge structure (XANES) results. Nuclear magnetic resonance (NMR) results obtained by Sandland *et al.* (2004) and Stebbins and Du (2002) also suggest that Cl^- ions are more

likely associated with alkali and alkaline earth cations, albeit with no strong preference between them. There are limited difference between the Raman and FTIR spectra of glasses with and without chloride additions (Marr *et al.* 1999, Schofield 2011), with no band attributed to Cl^- incorporation. Since the Si-Cl bond is not transparent in Raman spectroscopy (stretching mode at ~540 cm^{-1}) (Griffiths 1967, Chmel and Svetlov 1996) but the metallic chlorides are, it may imply that Cl^- ions, which are at least sufficient to influence glass network, are primarily associated with metallic cations, although the presence of a small proportion of Si-Cl cannot be excluded given the Cl content is much lower than the SiO_2 content.

The disagreement in the literature about the different incorporation mechanisms of chlorine in glasses among studies may arise from their varying glass compositions and preparation conditions. It is likely that the environment of Cl^- in glass network is very sensitive to these changes and the resultant findings become diverse and not always directly comparable. The compositional influence on Cl^- environment is mentioned in Veksler *et al.* (2012) when investigating chloride-silicate melts, where smaller alkaline earth cations (*e.g.* Mg^{2+} and Be^{2+}) are able to act as tetrahedral anionic complexes with Cl^- ions. However, as composition varies the environment of Cl^- is not constant and depends on the possible cations that surround them.

Not only the Cl^- incorporation mechanism but also the effects of Cl^- incorporation on glass properties diverge among researches. The most obvious divergence lies in the change in melt viscosity, namely polymerisation of glass, with the addition of chloride. Kiprianov *et al.* (2004) and Evans *et al.* (2008) argue that a small amount of Cl results in a slight but insignificant decrease in melt viscosity, while Siwadamrongpong *et al.* (2004) reports T_g reductions (indicative of a viscosity decrease) varying widely from insignificant to significant, depending on glass composition and varying with the CaO to (SiO_2+Al_2O_3) ratio. In contrast, Baker (1993) and Marr *et al.* (1999) assert that increasing chloride additions increase melt viscosity in the high temperature range. By measuring the viscosity of glass melts in a wider range, Dingwell and Hess (1998) and Zimova and Webb (2006) suggest that the viscosity change is varying with the viscosity range of melts themselves: increased in the low viscosity range (10^1 Pa·s) and decreased in the high viscosity range (10^{10} Pa·s). The correlation between the melt viscosity and melt temperature varies with temperature range and melt composition,

resulting in the divergent observations among studies. In this study, T_g is estimated from DTA curves of glass samples upon heating. Thus, the measurements are in a relatively high viscosity range and T_g and viscosity of glasses are expected to decrease with increasing chloride addition.

Regardless of whichever Cl^- incorporation mechanism applies, chloride addition results in decreased glass densities (Siwadamrongpong *et al.* 2004, Kiprianov and Karpukhina 2006, Schofield 2011). Such a decrease in glass density can be explained by the larger size of Cl compared to the size of O. However, this is against the hypothesis that Cl^- ions are located in the interstices of glass network, in which case the glass network should become more compact and dense.

2.3.3. Molybdenum

Molybdenum is not a common element that can be found in commercial silicate glass compositions and thus studies about the behaviour of Mo in silicate glasses are even fewer than those about S and Cl. The use of Mo electrodes during electric glass melting processes may introduce a small amount of Mo in glass through corrosion (Balazs and Rüssel 1988, Hwang *et al.* 2005, Vanmoortel *et al.* 2007); however, studies regarding this aspect are mainly concentrated on the understanding and protection of Mo electrodes from corrosion by a glass melt, rather than exploration of Mo dissolution in glass. The majority of research on Mo incorporation in silicate glasses comes from nuclear waste vitrification (Short 2004, Caurant *et al.* 2007, Dunnett *et al.* 2012), where MoO_3 is regarded as a challenging oxide due to its ready crystallisation.

2.3.3.1. Molybdenum solubility in glass

The studies about Mo dissolution in silicate-based glasses are quite limited, and most are concentrated on the speciation and localisation of Mo in the glass network (Galoisy *et al.* 2000, Caurant *et al.* 2007). Mo^{6+} is the predominant species in nuclear waste glass as well as other glasses prepared under oxidising and neutral atmospheres (Galoisy *et al.* 2000, Farges *et al.* 2006). Each hexavalent Mo is coordinated with four oxygens to form a molybdate unit $[MoO_4]^{2-}$, which is then associated with network modifiers and located within alkali and alkaline earth rich domain (Short *et al.* 2005, Hyatt *et al.* 2012). Consequently, Mo solubility in glass is effectively equivalent to

molybdate (MoO_4^{2-}, expressed as MoO_3) solubility in glass, for which the amount and species of network modifying cations are of great concern. Tailoring glass composition so as to improve molybdate solubility in borosilicate glasses has been undertaken by a number of workers (Do Quang *et al.* 2003, Caurant *et al.* 2007, Schuller *et al.* 2008, Chouard *et al.* 2011, Magnin *et al.* 2011), with the highest amount achieved at 2.5 mol%MoO_3 by quenching as a thin disc (Caurant *et al.* 2007).

The fraction of NBOs in glass can be always used as a simple tool to characterise glass compositions when they are not that complicated. Farges *et al.* (2006) studied the molybdate solubility dependence on the ratio of NBOs to silicon tetrahedra (*NBO*/T), asserting that higher *NBO*/T ratio is in favour of higher molybdate solubility in silicate glass. The network modifiers which are attached to non-bridging oxygens will stabilise $[MoO_4]^{2-}$ ions in network by mutual attraction.

The location of MoO_4^{2-} ions in the glass network suggests that the dissolution is related to the neighbourhood cations. Compared to sulphates, molybdates show a stronger separation tendency from the glass network and in many cases this controls the solubility limit of Mo in glass. In Caurant *et al.* (2007), the authors investigated the effects of boron addition on the crystallisation of molybdates in Mo-containing nuclear glasses. Although the addition of B_2O_3 polymerises the glass network, which is believed to reduce the incorporation capacity, the crystallisation of molybdates is retarded with increasing B_2O_3 content. This can be explained by the preferential consumption of Na^+ to compensate the negative charge of BO_4^- units, rather than Ca^{2+}. This then leaves more MoO_4^{2-} units to be connected with Ca^{2+}. The crystallisation tendency of $CaMoO_4$ is lower than that of Na_2MoO_4 and thus more molybdates can be retained in glass without phase separation. The glasses with precipitated powellite ($CaMoO_4$), a kind of glass ceramics, are considered acceptable in nuclear waste vitrification because the solubility of $CaMoO_4$ in water is low; many studies (Schuller *et al.* 2008, Magnin *et al.* 2011) are directed to tailor glass composition to ensure powellite and powellite-like phases being the only separated phase.

In addition, Uruga *et al.* (2008) performed a study to address MoO_3 excess in nuclear waste glasses by extracting either excess or dissolved MoO_3 from borosilicate melts loaded with nuclear waste using liquid copper during melting. The majority of MoO_3

content (>87%) was removed to the extractors (liquid copper) and thereby negating the issues of "yellow phase" (aggregates of molybdates with sulphates and chromates if MoO_3 is present in excess in nuclear glasses), but this method itself does not increase the Mo capacity of glass. And this method also needs the addition of Si powder to first reduce MoO_3 to Mo metal.

2.3.3.2. Molybdenum incorporation in glass

The ready crystallisation of molybdate from glass arises from the local environment of Mo^{6+} in glass network. The average Mo-O distance range is observed to be between 1.76 and 1.78 Å (Calas *et al.* 2003, Short *et al.* 2005, Farges *et al.* 2006, Caurant *et al.* 2010, Hyatt *et al.* 2012), which enables Mo^{6+} to have a high field strength range (1.89-1.94 $Å^{-2}$). As a result, Mo^{6+} cations in glass have a strong ordering effect on surrounding oxygens and hence MoO_4^{2-} units are easily separated from the silicate network (Caurant *et al.* 2007). Calas *et al.* (2003) and Hyatt *et al.* (2012) confirm that MoO_4^{2-} ions are preferentially associated with network modifying cations and are located in the alkali and alkaline earth enriched domain, providing the nuclei of the molybdate crystals which accounts for the readily molybdate crystallisation. In addition, there is no strong evidence for specific modifiers that MoO_4^{2-} units prefer to associate with in a glass network.

Either in molybdate crystals or in amorphous glasses MoO_4^{2-} ions are associated with metallic ions, thus the local environments of MoO_4^{2-} ions in crystals and in glasses are mutually referable. However, due to the amorphous nature of glass, Raman bands for MoO_4^{2-} in glass are broader than and slightly shifted compared with those in crystals. The incorporation of molybdate into glass network is conducive to a number of peaks in Raman spectra, which are generally assigned to four vibrational modes of MoO_4^{2-} ions: υ_1 mode (symmetric stretching) at 880-950 cm^{-1}, υ_2 mode (symmetric bending) at 280-340 cm^{-1}, υ_3 mode (asymmetric bending) at 790-850 cm^{-1} and υ_4 mode (asymmetric stretching) at 350-400 cm^{-1} (Ozeki *et al.* 1987, Pope and West 1995, Mahadevan Pillai *et al.* 1997, Saraiva *et al.* 2008). Among them the υ_1 mode is the most prominent for crystalline alkali or alkaline earth molybdates (the corresponding frequencies for each relevant molybdate crystal is listed in Table 2-7). The shift in frequencies indicates the interaction of different cations with MoO_4^{2-} and for glass

samples this shift is able to provide helpful information about the nature of MoO_4^{2-} association in the glass network. In general, the changes in Raman spectra caused by MoO_3 addition can be used as evidence of MoO_4^{2-} incorporation and for analysis of MoO_4^{2-} association in glass.

Table 2-7 Raman frequency of symmetric stretching vibration (υ_1) of MoO_4^{2-} in some molybdate crystals.

Molybdate species	υ_1 frequency (cm^{-1})	Reference
Na_2MoO_4	894-899	(Saraiva *et al.* 2008) (Chae *et al.* 2003)
K_2MoO_4	889-892	(Paraguassu *et al.* 2012)
$MgMoO_4$	930	(Ozeki *et al.* 1987)
$CaMoO_4$	879	RRUFF database (R050355)
$SrMoO_4$	888	(Petr *et al.* 2003)
$BaMoO_4$	890-892	(Ozeki *et al.* 1987, Vinod *et al.* 2006)

Due to the heavier mass of MoO_3, the addition of MoO_3 to glasses usually leads to increased glass densities, *e.g.* Henry *et al.* (2004). The addition of MoO_3 is observed to decrease T_g as well (Caurant *et al.* 2007, Caurant 2009); however, the authors cannot explain this phenomenon. According to the aforementioned localisation and association of MoO_4^{2-} ions, MoO_4^{2-} incorporation is expected to polymerise the glass network, which means increased T_g with increasing MoO_3 content in glass. Caurant (2009) attributes it to the increased size of depolymerised domains where MoO_4^{2-} ions are located, which overrides the increased connectivity of glass network, leading to the decrease in T_g. However, the evidence of this competition is not provided, and further investigation on the T_g reduction is necessary.

2.4. Summary

Vitrification is currently the primary choice for the immobilisation of high level waste and some intermediate level wastes. Among the candidate vitrification matrices borosilicate glasses are the most commonly used and have been thoroughly investigated. The addition of B_2O_3 to silicate glass lowers the vitrification processing temperature and enables more tuning of glass network to increase the loading capacity while retaining excellent basic properties. Aluminosilicate glasses have also been investigated for nuclear waste use, but their application is limited by the high processing temperatures required. However, some recent studies suggest they are capable of incorporating Cl^-.

Nevertheless, there are some troublesome elements that are abundant in nuclear waste but not readily dissolved in the glass matrices, among which S, Cl and Mo are three examples which are considered in this study. In nuclear glasses, S, Cl and Mo are all present as negative ions (SO_4^{2-}, Cl^- and MoO_4^{2-}) with low solubilities. Their solubilities are all found to be related to NBO fractions, namely the amount and species of network modifiers in glass. Increased NBO fractions lead to the higher capacity of the glass network to incorporate all of these anions, but Mo solubility may also be controlled by the separation tendency of molybdate from the silicate network at the same time.

Concerning the incorporation of these anionic species in glass, SO_4^{2-} and MoO_4^{2-} are both associated with network modifiers and located in the interstices of the glass network, while Cl^- is reportedly able to either act similarly to SO_4^{2-} and MoO_4^{2-} or to function as bridging atoms between network formers, depending on glass composition and preparation methods. The incorporation of SO_4^{2-} and MoO_4^{2-} results in increased glass densities and decreased T_gs, while the incorporation of Cl^- results in decreased glass densities and decreased T_gs (coupled however, increased viscosity at low viscosity range). In particular, there are some divergences regarding Cl^- incorporation behaviour in glass and further investigations are still necessary.

Raman spectra of glasses containing S, Cl and Mo provide helpful information about their incorporation in glass. The intense Raman bands assigned to vibrations of SO_4^{2-}

and MoO_4^{2-} can be used to confirm their presence and to analyse their comparative amount. Cl^- incorporation does not create any notable Raman band. In addition, glass polymerisation extent can be estimated from deconvolution of the silicate bands.

3. Experimental Procedures

3.1. Glass compositions

This thesis aims to investigate the incorporation behaviour and solubility dependence of sulphate, chloride and molybdate in glasses, all of these elements are potentially present in nuclear wastes. In this work two series of glasses have been considered as the incorporation hosts: borosilicate glasses (BS) and aluminosilicate glasses (AS).

3.1.1. Borosilicate glass series

The borosilicate glasses have the composition 50SiO_2, 15B_2O_3, 15Na_2O and 20MO in mole percent, where M is an alkaline earth (Mg, Ca, Sr or Ba or two of these in combination). This glass composition was initially designed as a hybrid of the K-26 glass (44.3SiO_2, 8.38B_2O_3, 20.3Na_2O, 21.6CaO, 0.83Fe_2O_3, 1.92Al_2O_3, mol%) developed in Russia and the SB44 glass (47.4SiO_2, 26.7B_2O_3, 14.3Na_2O, 11.6BaO, mol%) developed in India. While the former composition has been shown to have good chemical durability (Ojovan *et al.* 2001, Ojovan *et al.* 2005), the latter has been reported to be capable of immobilising sulphate-bearing wastes (Kaushik *et al.* 2006, Mishra *et al.* 2008). The selection of this hybrid is based on considerations regarding high capacity of anionic incorporation and satisfactory glass properties.

3.1.2. Aluminosilicate glass series

The aluminosilicate glasses have the composition 45SiO_2, 10Al_2O_3 and 45MO in mole percent, where M is again an alkaline earth (Mg, Ca, Sr or Ba or two of these in combination). This composition was developed from two calcium aluminosilicate glasses, one from Siwadamrongpong *et al.* (2004) which contains 38-56 mol% SiO_2, 6-20 mol% Al_2O_3 and 27-54 mol% CaO and the other from Schofield (2011) which simply contains 41.43 mol% SiO_2, 7.17 mol% Al_2O_3 and 51.4 mol% CaO. Both have shown extraordinary capacity to incorporate chlorine while maintaining good glass properties. It is worth noting that these glasses do not contain alkalis.

In both the borosilicate and aluminosilicate series, the species and abundance of alkaline earths were varied to investigate the influence of compositional variation on

sulphate, chloride and molybdate solubility in glass. Table 3-1 lists the nominal compositions of the base glasses.

Table 3-1 Nominal molar composition of the base glasses.

Samples	SiO_2	B_2O_3	Al_2O_3	Na_2O	BaO	SrO	CaO	MgO	Total
BBS	50	15	0	15	20	0	0	0	100
*SBBS*y*	50	15	0	15	24-4*y*	4*y*-4	0	0	100
SBS	50	15	0	15	0	20	0	0	100
CBS	50	15	0	15	0	0	20	0	100
MBS	50	15	0	15	0	0	0	20	100
BAS	45	0	10	0	45	0	0	0	100
SBAS	45	0	10	0	22.5	22.5	0	0	100
SAS	45	0	10	0	0	45	0	0	100
CAS	45	0	10	0	0	0	45	0	100
MCAS	45	0	10	0	0	0	22.5	22.5	100
MAS	45	0	10	0	0	0	0	45	100

**y* is equal to 2, 3, 4 and 5, respectively.

The samples in this thesis are labelled as "(base glass)-*x*(target element)", where *x* is the molar amount of the target anion added to 100% glass. For example, CBS-4Cl means 4 mol% Cl^- added to CBS base glass, SBS-3S means 3 mol% SO_3 added to SBS base glass and MAS-6M means 6 mol% MoO_3 added to MAS base glass.

3.2. Glass batching

Raw materials for glass batching are detailed in Table 3-2. It is assumed that all carbonates and hydroxides in batches will decompose to oxides in melt during heating and melting. Sulphate is regarded as a metal oxide combined with SO_3 to facilitate batching, even though sulphur is believed to occur as SO_4^{2-} in melts under oxidising atmosphere.

Table 3-2 Raw materials used for glass batching

Components	Raw Chemicals	Purity	Supplier
SiO_2	high purity silica, SiO_2	99.8%	Loch Aline, Tilcon, UK
B_2O_3	boric acid, H_3BO_3	99%	Acros Organics, UK
Al_2O_3	aluminium hydroxide, $Al(OH)_3$	99.5%	Fisher Chemical, UK
Na_2O	sodium carbonate, Na_2CO_3	99%	Brunner Mond, UK
	sodium sulphate, Na_2SO_4	99%	Fisher Chemical, UK
	sodium chloride, NaCl	99%	Fisher Chemical, UK
MgO	magnesium hydroxide, $Mg(OH)_2$	99%	Fisher Chemical, UK
	hexahydrate magnesium chloride, $MgCl_2 \cdot 6H_2O$	99%	Fisher Chemical, UK
	magnesium sulphate, $MgSO_4$	99%	Fisher Chemical, UK
CaO	calcium carbonate, $CaCO_3$	99%	Minfil l1220, UK
	calcium chloride, $CaCl_2$	99%	Fisher Chemical, UK
	calcium sulphate, $CaSO_4$	99%	Fisher Chemical, UK
SrO	strontium carbonate, $SrCO_3$	99%	Fisher Chemical, UK
BaO	barium carbonate, $BaCO_3$	99%	Fisher Chemical, UK
	bihydrate barium chloride, $BaCl_2 \cdot 2H_2O$	99%	Fisher Chemical, UK
	barium sulphate, $BaSO_4$	99%	Fisher Chemical, UK
MoO_3	molybdenum trioxide, MoO_3	99.5%	Fisher Chemical, UK

Sulphate and chloride in BS glasses were added as Na_2SO_4 and NaCl, respectively, and thus the amount of Na_2O batched as Na_2CO_3 was accordingly reduced. Sulphate and chloride in AS glasses were added as corresponding alkaline earth salts, and reductions were also made to the corresponding carbonates. Molybdate was added as molybdenum trioxide (MoO_3) and thus no change in batching of other oxides was caused.

Batches to make about 50 g of glass were weighed using an electronic scale with an accuracy of 0.01 g. The batches were then fully mixed and transferred to a sealed sample bag which were kept under dry circumstance prior to melting. The loss of batches during mixing due to adherence to the sample bag was controlled to be less than 0.5 wt% of the whole batch.

3.3. Glass making

The prepared batch was transferred into a mullite crucible which was placed in an electric furnace with a maximal temperature of 1500 °C. The batches were heated from room temperature to 1100 ºC (borosilicate glasses) or to 1450 ºC (aluminosilicate glasses), held for 3 hours, and afterwards the melt was poured into a stainless steel mould to form a tetragonal glass block. The glass block was immediately transferred into another electric furnace for annealing, during which it was held at 550 ºC (borosilicate glasses) or at 700 ºC (aluminosilicate glasses) for 1 hour, and cooled down to room temperature at 1 ºC/min (see Figure 3-1). All of the above procedures were carried out in an air atmosphere.

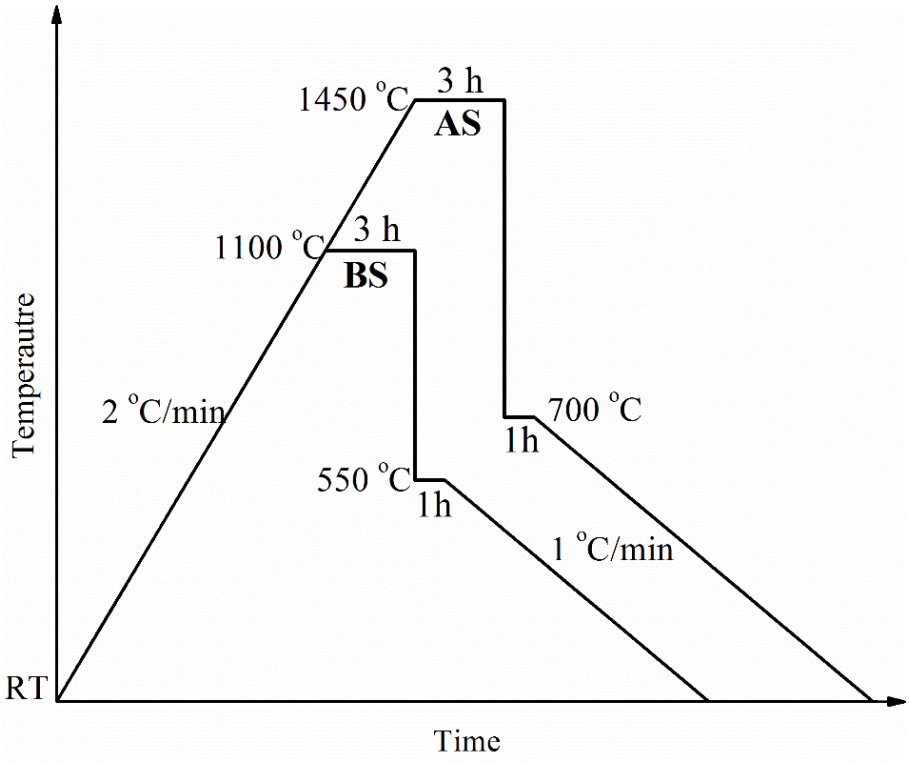

Figure 3-1 Schematic melting program of aluminosilicate glasses (AS) and borosilicate glasses (BS).

3.4. Characterisation

3.4.1. Density

Glass density was determined with a Mettler Toledo densimeter based on Archimedes' principle using deionised water as the immersion medium. The principle can be explained as follows:

The mass of a glass sample in air and in deionised water was weighed as m_1 and m_2, respectively. Hence, the volume of glass V_A, which equals the volume change of deionised water ΔV_W if glass is completely immersed, can be obtained by

$$V_A = \Delta V_W = \Delta m_W/\rho_W = (m_1 - m_2)/\rho_W \qquad \text{Equation 3-1}$$

where ρ_w, the density of deionised water, is known at a given temperature. Therefore, the density of glass ρ can be calculated using

$$\rho = m_1/V_A = \rho_W m_1/(m_1 - m_2) \qquad \text{Equation 3-2}$$

The precision of the equipment is 0.001 g cm^{-3}. Each glass sample was measured for five times; error bars are made according to the reproductive errors.

3.4.2. X-Ray Diffraction (XRD)

XRD was used to evaluate the amorphous nature of prepared glasses and to identify the crystalline phase in glasses which were partly crystallised or had a segregated layer when the sulphate, chloride or molybdate content exceeded their limit in the melt.

The principle of X-ray diffraction in crystals is illustrated in Figure 3-2. Diffraction occurs when a beam of incident X-rays of known wavelength (λ) strikes a sample at some specific angle (θ) which satisfies Bragg's Law:

$$2dsin\theta = n\lambda \qquad \text{Equation 3-3}$$

where n is an integer representing the order of diffraction and d is the spacing between two parallel atomic planes. Hence, given a fixed λ of X-rays, the interplanar spacings d in crystalline lattice give rise to characteristic diffraction angles θ. The diffraction

angle series, which are reflected as XRD patterns, are specific and unique for each species of crystals. As a result, XRD patterns provide information to identify crystalline structures.

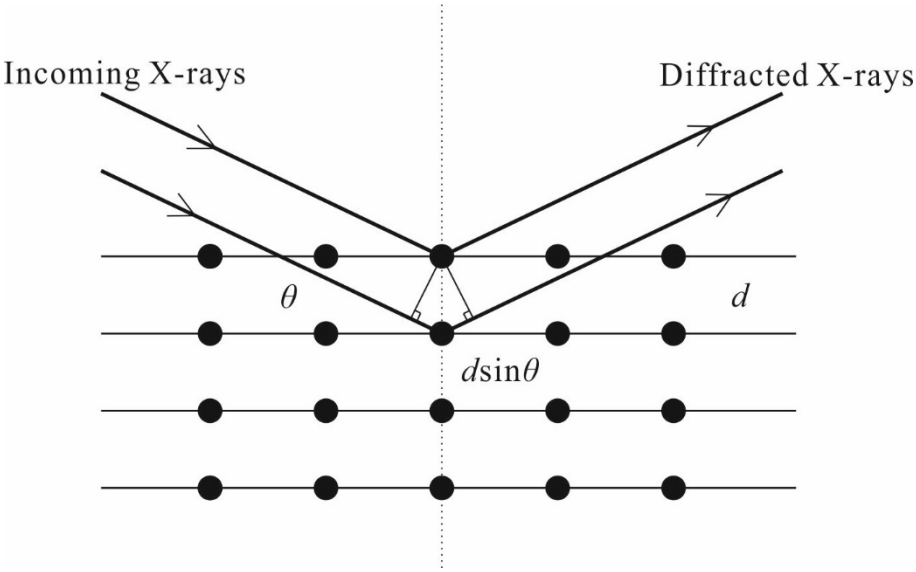

Figure 3-2 Schematic diagram of X-ray diffraction in crystals.

XRD patterns for crystals typically consist of a number of sharp peaks at certain diffraction angles whereas XRD patterns for amorphous materials are made up of a broad peak, the so called “glass hump”. The glass hump is due to the disordered nature of atomic arrangement in amorphous materials which results in widely scattered diffraction angles. In addition, XRD patterns for glass composites are normally composed of some crystalline peaks superimposed on the glass humps.

Crushed glass pieces were ground to fine powders in an agate mortar and sieved to <75 μm and collected for XRD analysis. Room temperature powder XRD was carried out in a Siemens D5000 X-Ray Diffractometer, using Cu-*K*α (λ=1.54056 Å) as the radiation source operating at 40 kV and 40 mA. The samples were scanned over the range of 10-60 °2θ with a step size of 0.05° and 7 s dwell time (14 s for partially crystallised glass).

Some molybdenum containing aluminosilicate glasses were also analysed with high temperature powder XRD (HT-XRD) in a Siemens D5000 HT-XRD diffractometer. The settings are same as for room temperature XRD except that the dwell time was 10

s. HT-XRD patterns were recorded at 30 ºC, target high temperatures and 30 ºC again after cooling, respectively. The heating rate conforms to that used in the DTA measurements namely 10 ºC min^{-1} while the cooling rate was 400 ºC min^{-1}.

The obtained XRD data were analysed with Sleve+ software (licenced to the Department of MSE, The University of Sheffield) for phase identification using the International Centre for Diffraction Data (ICDD) database PDF4 (2012) .

3.4.3. Differential thermal analysis (DTA) and thermogravimetric analysis (TGA)

DTA and TGA were used to investigate the thermal behaviours of the prepared glasses over a temperature range. A DTA curve records thermal reactions of samples on heating or cooling by comparison with an inert reference undergoing identical thermal treatment. A TGA curve is simultaneously recorded while DTA analysis is running, revealing the mass change of samples during heating. A DTA curve is able to show temperatures of glass transition, crystallisation and melting, as well as dehydration, oxidation and evaporation if applicable.

The glass transition temperature (T_g) was estimated from the onset of first endothermic peak in a DTA curve, an example shown in Figure 3-3. For borosilicate glasses this peak appears at 500~600 ºC whereas for aluminosilicate glass it normally is between 700 and 800 ºC. The crystallisation peak, which is exothermic and expected to appear at higher temperature than the glass transition peak, is not apparent in many samples studied here, thus an estimation of the glass crystallisation temperature (T_c) was not performed for all samples.

Powders for DTA and TGA analysis were prepared through an identical approach for XRD analysis. DTA and TGA curves were recorded simultaneously in a Perkin Elmer STA8000 using platinum crucible in static air flow. Approximately 40 mg (balance sensitivity 0.2 μg) powders with equivalent weight of alumina as the inert reference were measured from room temperature to 1000 °C (temperature precision ±0.5 ºC) at 10 °C min^{-1}. No cooling curves were acquired for the samples.

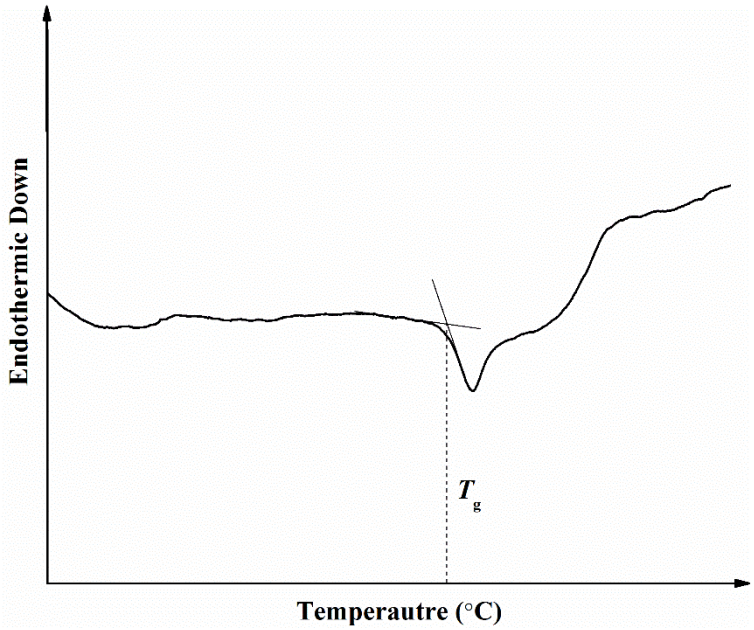

Figure 3-3 A typical DTA curve of glass and the estimation of T_g.

3.4.4. Raman Spectroscopy

Raman spectroscopy was used to identify the chemical bonds in glasses and to assess the structural change of glasses caused by sulphate, chloride and molybdate incorporation. It is based on the inelastic scattering of light incident on samples and provides the information of vibrational, rotational and other low-frequency modes in a system.

As illustrated in Figure 3.4, the scattered radiation arising when monochromatic radiation (ω_i) is incident on samples can be divided into two categories: Rayleigh scattering in which the frequency of the scattered radiation remains at ω_i and Raman scattering in which the frequency of scattered radiation shifts to ω_f. The Raman shift $\Delta\omega = |\omega_i - \omega_f|$ is only specific to the vibrational and rotational states of the samples regardless of the frequency of incident radiation. Therefore, the observed Raman shifts can be used to identify the chemical and structural information of samples.

Glass bars were sliced to ~5 mm thick using a Buehler low speed saw with a diamond blade at speed of 4 rev/s, using oil as a lubricant. The top surfaces of these slices were then polished to 1200 SiC grit, rinsed with isopropanol and later thoroughly dried. Raman spectroscopy measurement was performed upon the polished plane of the glass

slices in a Renishaw Invia Raman spectrometer equipped with a CCD detector, using the green line laser (514.5 nm) at a 20 mW power. The energy range 0-2000 cm^{-1} was scanned with a resolution of 1 cm^{-1} and exposure time of 10 s. 10 spectra were accumulated for each sample. Calibration with silicon was undertaken each time the spectrometer was used. The interference due to cosmic rays was removed by running two scans prior to recording a spectrum to ensure that interruption peaks do not appear in the final spectrum.

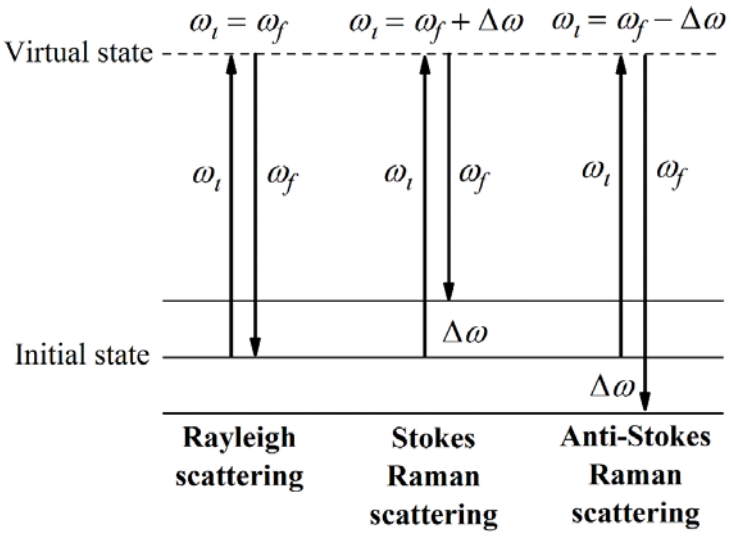

Figure 3-4 Frequency difference between incident and scattered radiation in Rayleigh and Raman scattering. Stokes and anti-Stokes Raman scattering refers to a lower and a higher scattered frequency, respectively.

Like diffraction angles in XRD, Raman shifts are dispersed in Raman scattering of amorphous materials and as a result a Raman spectrum for glass typically consists of some broad bands against Raman shift. For the detectable vibrational modes in crystalline materials, the Raman shift is concentrated and the resulting Raman spectrum consists of some sharp peaks.

3.4.5. Fourier Transform Infrared Spectroscopy (FTIR)

FTIR is similar but complementary to Raman spectroscopy which measures the vibrational characteristics of molecules in a system. While Raman spectroscopy is

more sensitive to symmetric bonds, FTIR spectroscopy requires a change in dipole during vibration.

Infrared spectroscopy is a technique based on the absorption of infrared radiations by chemical bonds in molecules at certain frequencies. Such frequencies, at which radiations are absorbed, correspond to the energy difference among different states of bonds and hence a series of these frequencies are unique to every molecule. Consequently, an infrared spectrum showing the frequencies of absorption can be used to identify structural information about materials.

The difficulty in infrared spectroscopy lies in the wide frequency range to be scanned. FTIR spectroscopy utilises an interferometer originally designed by Michelson and a subsequent mathematical procedure called Fourier transformation to convert a time-dependent function to a frequency-dependent function. It enables a wide range of infrared frequencies to be measured simultaneously rather than individually.

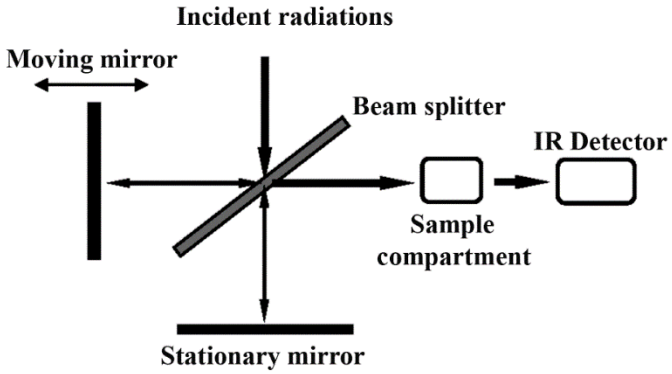

Figure 3-5 Schematic diagram of Michelson interferometer used in FTIR spectroscope.

The basic form of FTIR spectroscope using a Michelson interferometer is shown in Figure 3-5. A beam of polychromatic infrared radiation is split by a beam splitter to two halves, one half reflected to a movable mirror and the other travelling to a stationary mirror. Ideally these two mirrors are perpendicular to each other. The motion of the movable mirror results in path difference δ between the two beams when they are recombined at the beam splitter. If the velocity of the movable mirror is

constant at v, then $\delta = 2vt$ (t is time). Interference occurs constructively or destructively depending on the relation of δ and λ (radiation wavelength). The intensity of radiation for λ at the detector I(δ) is hence a cosine wave proportional to initial intensity I(λ) with a frequency f:

$$I(\delta) \propto I(\lambda)\cos(\frac{4nvt}{\lambda}) \qquad \text{Equation 3-4}$$

$$f = \frac{2v}{\lambda} \qquad \text{Equation 3-5}$$

Hence, the inteferogram of polychromatic radiations is a sum of cosine waves for each radiation wavelength λ. After Fourier transformation, the inteferogram is transformed from time domain to frequency domain and a spectrum versus wavenumbers is attained.

Powdered samples as prepared for XRD analysis were used for FTIR measurement in a Pelkin-Elmer Frontier FTIR spectroscope. About 4 mg of sample powder was fully ground with 200 mg KBr powder and pressed into a thin disk prior to analysis. The FTIR scanning ranged between 400 and 4000 cm^{-1}, with a resolution of 4 cm^{-1} and 8 accumulations. Background scanning was carried out in the beginning of every use of machine. Both transmittance and absorbance data were obtained during measurements.

3.4.6. Scanning electron microscopy (SEM) and attached energy dispersive X-ray spectroscopy (EDX)

SEM was used to observe the microstructural features and to identify the homogeneity of the prepared samples. As shown in Figure 3-6, a beam of accelerated electrons are focused by electromagnetic lenses to create an electron probe on the specimen. The specimen surface is then scanned by the probe with the help of scanning coils. The interaction of electrons with the specimen surface results in emissions which are collected by a detector and displayed on screen. The useful emitted radiations are usually secondary electrons and/or backscattered electrons for surface observations and X-rays for elemental analysis. The interaction volume of SEM is also drawn in Figure 3-6.

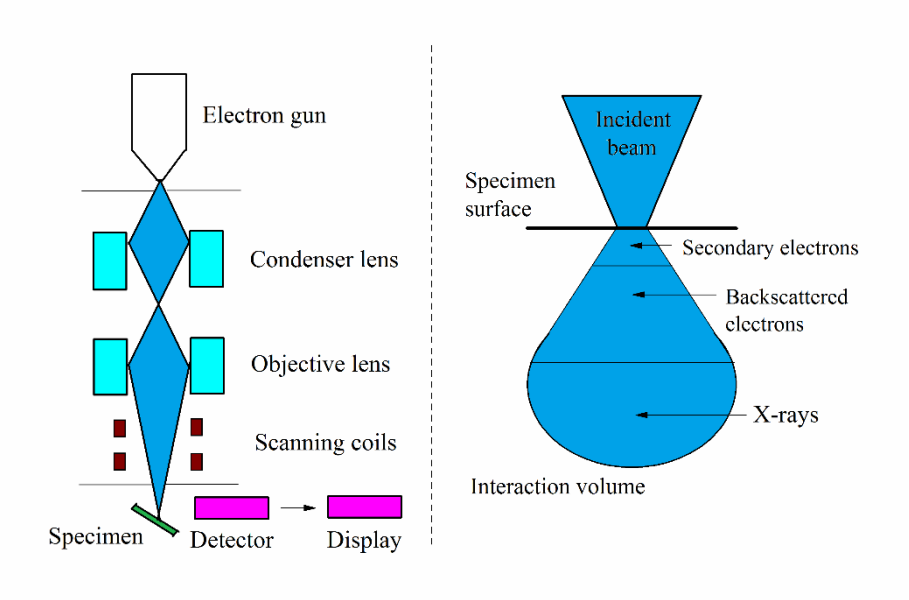

Figure 3-6 The main components of a typical SEM machine and the interaction volume of incident electrons.

Both secondary and backscattered electrons can be used to observe the microstructural features of samples. Secondary electrons originate from the inelastic collision of incident electrons with the *k*-orbital electrons of atoms of specimen and the resultant secondary electron images (SEI) directly reflect the topological features of specimen surface. Backscattered electrons are generated by the elastic collisions with the specimen's atoms, the intensity of which is dependent on the atomic number of atoms in question. Higher numbered atoms contribute more backscattered electrons, resulting in contrast between the signals of backscattered electrons from points of different compositions. Hence, backscattered electron images (BEI) can be used to observe different phases in microstructures and to assess the micro-homogeneity of samples. Characteristic X-rays are emitted from the excited atoms struck by incident electrons. The frequencies of emitted X-rays are unique to each element and thus by analysing the proportions of frequencies of X-rays collected by EDX detector the compositional analysis of individual points can be achieved. However, the resolution of quantitative EDX is limited by the size of interaction volume, so features smaller than 1 μm^2 cannot be quantitatively analysed. In addition, elements lighter than carbon are not readily detected and differentiated by EDX, giving difficulties in analysing borosilicate glass compositions.

Glasses were sectioned into thin slices using a Buehler slow saw with a diamond blade lubricated by oil. The glass slices were then mounted into epoxy resin, successively ground from 400 to 1200 grade silicon carbide papers with running water and polished using 6 to 1 μm diamond pastes. The polished samples were thoroughly rinsed with isopropanol and dried. Afterwards, the samples were coated with carbon and painted with silver paste to increase conductivity. SEM observations were performed with a JEOL JSM6400 SEM machine at magnifications of 100x to 4000x and were performed with an FEI Inspect F SEM machine if higher magnifications (1500x to 80,000x) were required. Quantitative EDX analysis was carried out with an energy dispersive X-ray spectrometer (INCA, Oxford Instruments) attached to the JEOL JSM6400 SEM. Calibration was undertaken with cobalt for each sample (by recording a spectrum of cobalt oxide under same conditions at first). The sulphate and molybdate containing glass compositions were normalised to oxides whereas the chloride containing glass compositions were normalised to atoms because Cl^- cannot be expressed as an oxide. In addition, elemental distribution was performed on some samples by X-ray mapping within an area of 1600 μm^2 in glass during EDX analysis.

3.4.7. Transmission electron microscopy (TEM)

In order to observe the separated particles within partly crystallised glasses at a higher magnification (13,500x to 105,000x) and to identify the crystal phase of these particles, some relevant samples were selected for TEM observations.

A TEM machine uses accelerated electrons which are then focused by the condenser lens. When striking a thin specimen, part of the incident electrons transit through whereas part of the electrons are scattered by atoms in specimen acting as a diffraction grating. As illustrated in Figure 3-7, the diffracted electrons form diffraction spots on the back focal plane after being focused by the objective lens while the transmitted electrons are recombined with diffracted electrons to form an image of specimen on the image plane (Bendersky and Gayle 2001). Thus TEM is able to give information about both the topology and the microstructure of specimen.

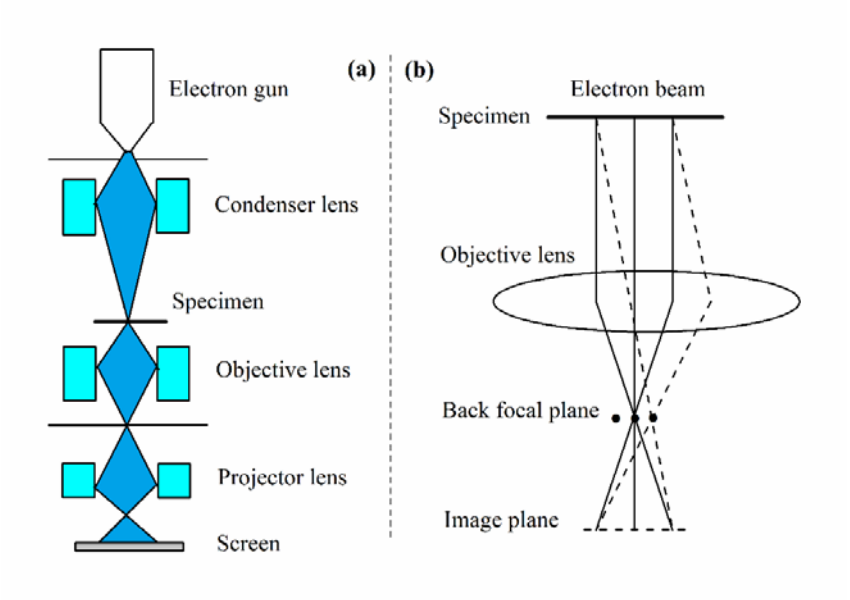

Figure 3-7 (*a*) typical layout of a TEM machine and (*b*) the diagram showing the principle of TEM imaging process (Bendersky and Gayle 2001).

For TEM observation, glass samples were crushed into small pieces. Some pieces were then selected to be ground with acetone for 20 min in an agate pestle and mortar. One drop of the resultant suspension was loaded onto a holey carbon-filmed copper grid. TEM observation was performed with a Philips 420 microscope, operating at 120 kV at an emission of 4. The images of samples and diffraction patterns were recorded by exposure to photographic films which were thereafter developed and scanned to digital pictures.

3.4.8. Inductively coupled plasma optical emission spectroscopy (ICP-OES)

Because of the difficulty in measuring boron by EDX, some borosilicate glasses were analysed with ICP-OES to obtain their boron content. Atoms and ions of samples are excited by inductively coupled plasma, emanating electromagnetic radiations which are characteristic of each element. Hence the concentration of an element can be obtained from the intensity of its specific radiations.

Glass samples were crushed and ground to fine powders and then sieved to <75 μm. Afterwards, the sample powders were dissolved in hydrofluoric acid (HF) for analysis. The dissolution of glass powders and the ICP-OES measurement were performed by the Sheffield Assay Office (Sheffield, UK).

4. Sulphur in glass

4.1. Introduction

This chapter describes the incorporation and the solubility dependence of sulphate in the borosilicate and aluminosilicate glasses studied ($50SiO_2$-$15B_2O_3$-$15Na_2O$-20MO and $45SiO_2$-$10Al_2O_3$-45MO, mol%, M = Mg, Ca, Sr and Ba). Compositional variation is achieved by equimolar substitution between the alkaline earth oxides to investigate sulphate solubility dependence on the modifier species and their amounts in the glass. The changes in glass properties and structure caused by sulphate incorporation have also been assessed, by density measurement, XRD, DTA, Raman and FTIR spectroscopies. SEM and TEM are used to characterise the phase separation in the partly crystallised glasses which contain excess sulphate.

4.2. Results

4.2.1. Sulphate retention and solubility

Glass compositions were measured by EDX and ICP-OES (for some boron containing glasses). The normalised molar compositions are listed in Table 4-1 with comparison of nominal values.

Firstly, borosilicate glasses exhibit excellent sulphate retention (more than 90% SO_3 retained until saturation) whereas aluminosilicate glasses do not retain sulphate at all, with 2.91 mol% batched but less than 0.10 mol% retained. Thus the results and discussion of sulphate incorporation here are focused on the borosilicate glasses.

Secondly, borosilicate glasses are compositionally consistent and generally close to the batched compositions. The slightly higher content of SiO_2 and the introduction of Al_2O_3 are due to the slight dissolution of mullite crucibles into melt during melting. EDX analysis for a used crucible (Figure 4-1) suggests that there is negligible diffusion of components from melt to crucible. The reactions between the melt and crucible are believed not to have had significant influence on the results of sulphate dissolution in glass.

Table 4-1 Measured and nominal compositions (mol%, normalised to 100%) of prepared glasses with increasing SO_3 additions.

Sample	***x***	**SiO_2**	**B_2O_3**	**Al_2O_3**	**Na_2O**	**BaO**	**SrO**	**CaO**	**MgO**	**SO_3**	**Total**
BBS-*x*S	0	50.86 (50.00)	(15.00)	4.26 (0)	12.43 (15.00)	17.45 (20.00)	-	-	-	0.00 (0.00)	100.00 (100.00)
	3	49.48 (48.54)	(14.56)	1.35 (0)	12.75 (14.56)	19.02 (19.42)	-	-	-	2.84 (2.91)	100.00 (100.00)
	4	49.77 (48.08)	(14.42)	1.14 (0)	13.45 (14.42)	17.69 (19.23)	-	-	-	3.53 (3.85)	100.00 (100.00)
hc	5	-	-	-	-	-	-	-	-	-	
SBBS2-*x*S	0	51.04 (50.00)	(15.00)	2.95 (0)	12.36 (15.00)	13.92 (16.00)	3.73 (4.00)	-	-	0.00 (0.00)	100.00 (100.00)
	3	49.89 (48.54)	(14.56)	1.02 (0)	13.67 (14.56)	14.32 (15.53)	3.72 (3.88)	-	-	2.82 (2.91)	100.00 (100.00)
sc	4	-	-	-	-	-	-	-	-	-	
SBBS3-*x*S	0	51.64 (50.00)	(15.00)	3.00 (0)	12.76 (15.00)	10.62 (12.00)	6.98 (8.00)	-	-	0.00 (0.00)	100.00 (100.00)
	3	50.21 (48.54)	(14.56)	1.24 (0)	13.45 (14.56)	10.77 (11.65)	6.96 (7.77)	-	-	2.81 (2.91)	100.00 (100.00)
SBBS4-*x*S	0	52.09 (50.00)	(15.00)	3.16 (0)	12.42 (15.00)	7.01 (8.00)	10.32 (12.00)	-	-	0.00 (0.00)	100.00 (100.00)
	1	50.24 (49.50)	(14.85)	1.56 (0)	14.24 (14.85)	7.55 (7.92)	10.60 (11.88)	-	-	0.96 (0.99)	100.00 (100.00)
	2	50.67 (49.02)	(14.71)	1.23 (0)	13.38 (14.71)	7.43 (7.84)	10.70 (11.76)	-	-	1.88 (1.96)	100.00 (100.00)
	3	49.84 (48.54)	(14.56)	1.22 (0)	12.99 (14.56)	7.64 (7.77)	11.02 (11.65)	-	-	2.73 (2.91)	100.00 (100.00)
sc	4	48.66 (48.08)	(14.42)	1.20 (0)	14.03 (14.42)	7.88 (7.69)	10.26 (11.54)	-	-	3.55 (3.85)	100.00 (100.00)
SBBS5-*x*S	0	51.54 (50.00)	(15.00)	2.87 (0)	12.85 (15.00)	3.69 (4.00)	14.05 (16.00)	-	-	0.00 (0.00)	100.00 (100.00)
	3	49.56 (48.54)	(14.56)	1.68 (0)	13.33 (14.56)	3.46 (3.88)	14.66 (15.53)	-	-	2.75 (2.91)	100.00 (100.00)
SBS-*x*S	0	52.12 (50.00)	(15.00)	3.41 (0)	12.50 (15.00)	-	16.97 (20.00)	-	-	0.00 (0.00)	100.00 (100.00)
	3	50.05 (48.54)	(14.56)	1.03 (0)	13.67 (14.56)	-	18.01 (19.42)	-	-	2.68 (2.91)	100.00 (100.00)
hc	4	-	-	-	-	-	-	-	-	-	
CBS-*x*S	0	51.45 (50.00)	(15.00)	1.12 (0)	12.99 (15.00)	-	-	19.44 (20.00)	-	0.00 (0.00)	100.00 (100.00)
	2	50.56 (49.02)	(14.71)	0.33 (0)	13.45 (14.71)	-	-	19.13 (19.61)	-	1.82 (1.96)	100.00 (100.00)
hc	3	-	-	-	-	-	-	-	-	-	
MBS-*x*S	0	50.56 (50.00)	(15.00)	1.77 (0)	13.56 (15.00)	-	-	-	19.10	0.00 (0.00)	100.00 (100.00)
sc	1	-	-	-	-	-	-	-	-	-	

"*sc*" and "*hc*" means the glass is slightly crystallised and heavily crystallised, respectively.

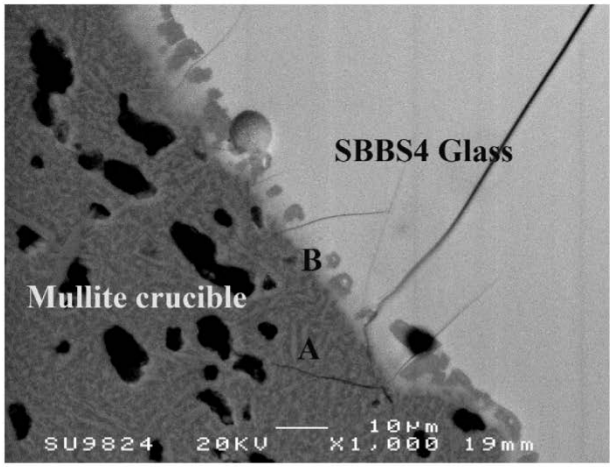

Oxides	Crucible	Interface
SiO_2	58.73	63.41
Al_2O_3	40.19	29.35
Na_2O	1.08	5.28
SrO	-	0.69
BaO	-	1.27

Figure 4-1 backscattered electron image of the cross section of a used crucible; Right: EDX results of (A) inner crucible and (B) interface between crucible and glass.

4.2.1.1. Sulphate retention versus sulphate loading

While aluminosilicate glasses show limited sulphate retention, borosilicate glasses are able to retain the majority of loaded sulphate. Figure 4-2 shows the correlation between sulphate retention rate and sulphate loading in SBBS4 glass. At low levels almost 100% of sulphate can be retained in the glass but this rate gradually decreases to around 90% at the saturation point where phase separation occurs. However, further sulphate addition does not increase the amount of sulphate in the glass and the excess sulphate remains outside the glass.

4.2.1.2. Sulphate retention versus melting temperature

The influence of melting temperature on sulphate retention in glass has been evaluated by melting SBBS4-3S glass (2.91 mol%SO_3) at temperatures ranging between 1050 and 1300 ºC. As shown in Figure 4-3, sulphate content gradually declines from 2.96 mol% at 1050 ºC to 2.30 mol% at 1200 ºC, and then plummets to as low as 0.96 mol% SO_3 at 1250 ºC. Bulk glass was not obtained from the melt processed at 1300 ºC because of the severe corrosion; the residual glass pieces were found to contain 0.13 mol%SO_3. Meanwhile, the SiO_2 content steadily increases with increasing melting temperature, which indicates an increase in the dissolution of crucible walls to melt and/or the evaporation of volatiles (B and Na) during melting.

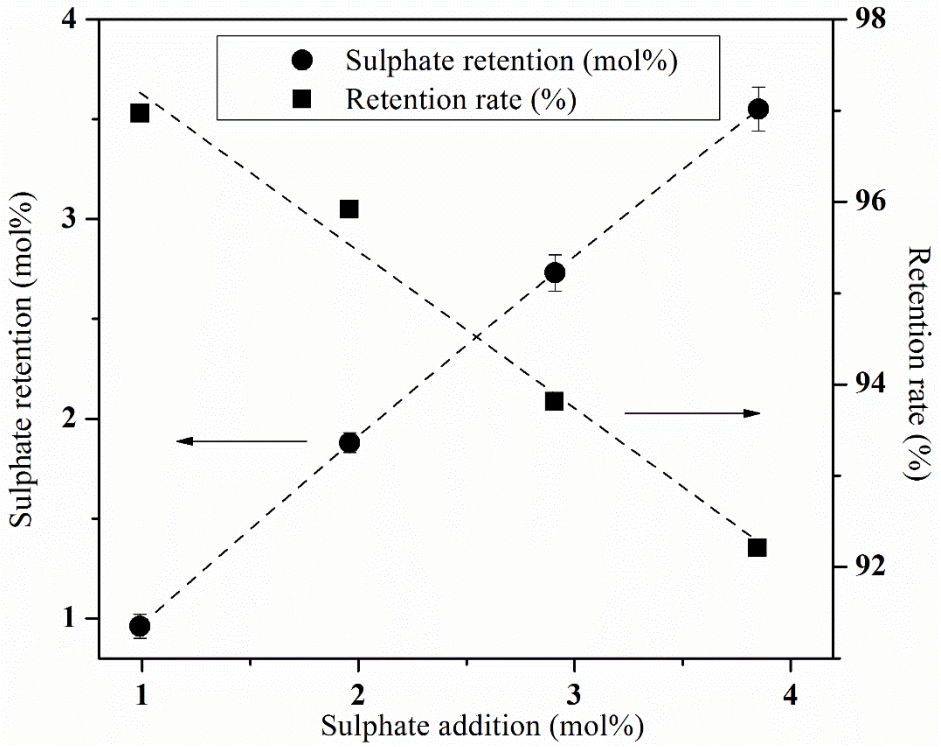

Figure 4-2 Absolute sulphate retention and relative retention rate of sulphate in SBBS4 glass (for detailed composition see Table 4-1). Sulphate content is expressed as mol% SO_3. Dashed lines are added as guides to the eyes.

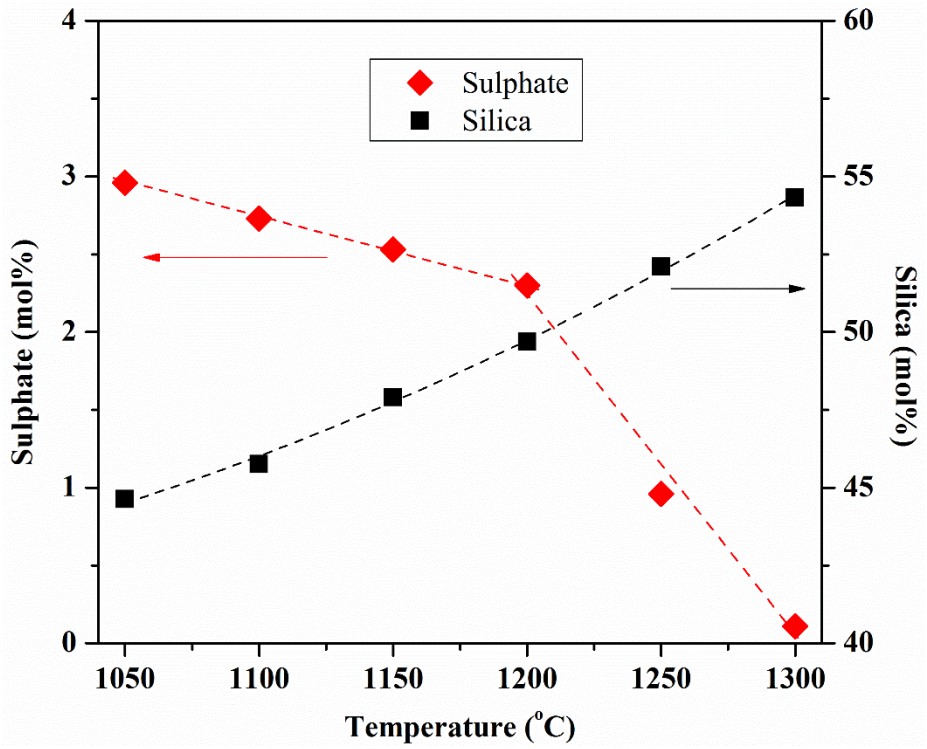

Figure 4-3 Sulphate content (mol% SO_3) and silica content (SiO_2 mol%) in SBBS4 glass melted at different temperatures. Dashed lines are added as guides to the eyes.

4.2.1.3. Sulphate solubility dependence on glass composition

In this study, sulphate solubility is defined as the measured sulphate content (mol% SO_3) in the glass to which maximal sulphate has been added while remaining homogeneous after annealing. The tendency of sulphate solubility with changing alkaline earths in glass is displayed in Figure 4-4. Sulphate solubility increases with the abundance of larger alkaline earths in glass: magnesium borosilicate glass (MBS) has the lowest (0.99 mol%) while barium borosilicate glass (BBS) has the highest sulphate solubility (3.53 mol%). A series of mixed strontium-barium borosilicate glasses (SBBS2-5S) have been prepared; all of them remain homogenous up to 2.91 mol% SO_3 addition and become phase separated at 3.85 mol% SO_3 addition, but the crystallisation extent is reduced as the barium ratio increases.

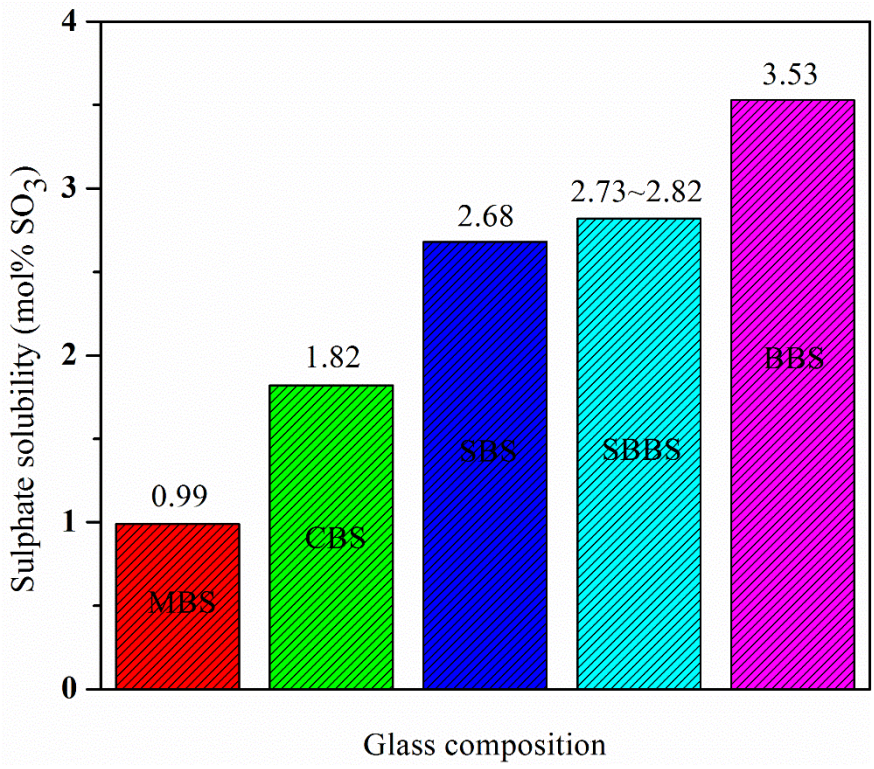

Figure 4-4 Sulphate solubility (as defined above) trend in sodium-alkaline earth-borosilicate glasses ($50SiO_2$-$15B_2O_3$-$15Na_2O$-20MO, mol%, M = Mg, Ca, Sr and Ba). MBS-1S glass was apparently inhomogeneous so its solubility limit is noted as the batched value. SBBS glass is a family of glasses containing varying proportion of Sr and Ba; they are plotted as a solubility range.

4.2.2. Sulphate incorporation in glass

Sulphate incorporation results in significant changes in glass structure and properties. Assessments in this study mainly concentrate on strontium and/or barium borosilicate glasses which can contain high levels of sulphate. The compositions with low sulphate solubility (< 2 mol%SO_3) are only analysed with density measurement, XRD and Raman microscopy.

4.2.2.1. Density

The densities of three glass compositions with increasing sulphate additions are shown in Figure 4-5. For all prepared glass compositions sulphate incorporation results in an increase (fitted best by a quadratic) in density until saturation is reached. Excess sulphate added to glass does not increase or sometimes even slightly decreases glass density. In addition, the density gap between base glass and sulphate-saturated glass varies between glass compositions.

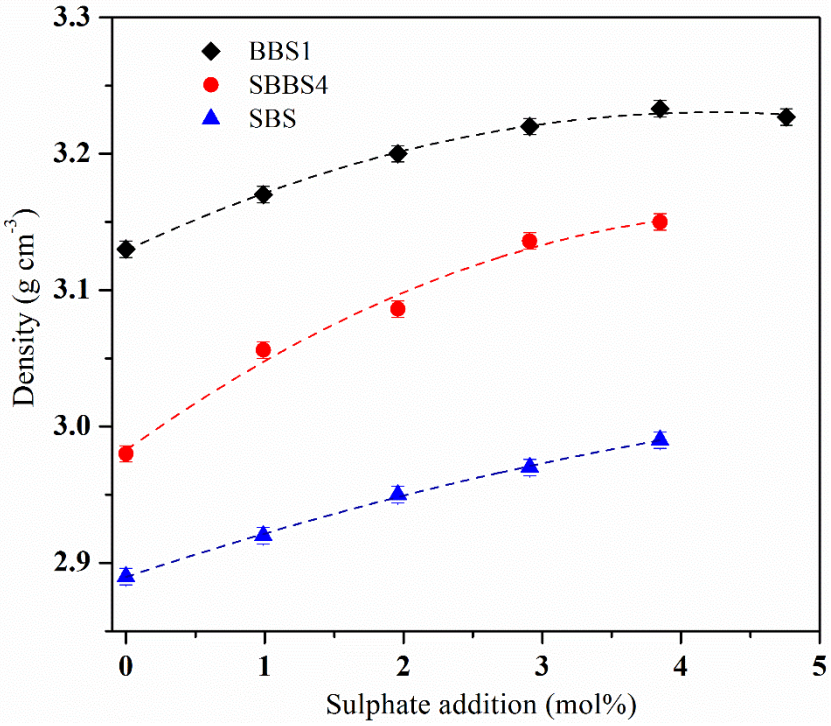

Figure 4-5 Density change with increasing sulphate additions in some prepared glass compositions: SBS (20MO = 20SrO, blue triangle symbol), SBBS4 (20MO = 12SrO + 8BaO, red circular symbol) and BBS (20MO = 20BaO, black diamond symbol); other components are constant at 50 mol% SiO_2, 15 mol% B_2O_3 and 15 mol% Na_2O.

4.2.2.2. X-Ray Diffraction

Figure 4-6 presents the XRD patterns of prepared glasses with no sulphate, dissolved sulphate and overloaded sulphate. The visibly homogeneous glasses (without or with fully dissolved sulphate) appear to be completely amorphous whereas the glasses with overloaded sulphate are identified as partially crystalline due to the tiny crystalline peaks in XRD patterns.

The position of the broad glass hump shifts to lower diffraction angles as CaO is substituted by SrO and then by BaO, which is expected because Ba^{2+} is larger than Sr^{2+} than Ca^{2+} and hence there is a resultant network expansion in BBS glass. The glasses with MgO do not agree with this trend probably because of the different MBS network (Mg^{2+} is able to function as a network former in silicate glass).

As for the crystalline peaks, Figure 4-6 marks the phase to which the peaks are most likely assigned. It must be pointed out that these peaks are not sufficient to allow phase analysis to be performed as many of them are inconspicuous and ambiguous. The phase identification is based on the comparison with the XRD patterns of potential sulphate phases. It can be seen that the crystals in opaque SBS-4S, SBBS4-4S and BBS-5S glasses (M = Sr and/or Ba) may be alkaline earth sulphates while the crystals in inhomogeneous CBS-3S and MBS-2S glasses (M = Ca or Mg) are most likely to be Na_2SO_4 or Na_2SO_4 crystals with Na^+ partly substituted by Ca^{2+} or Mg^{2+}. The segregated layer, which is formed on glass surface when sulphate addition in glass far exceeds its capacity, is identified to be composed of Na_2SO_4 with a small amount of alkaline earth sulphates.

The influence of glass cooling rate on sulphate solubility has also been investigated by making a same glass composition with annealing and splat quenching, respectively. While the annealed SBBS-4S glass bulk appears opaque (partly crystallised), the splat quenched SBBS-4S glass pieces are visibly transparent. XRD comparison (Figure 4-7) suggests that there is no/limited crystal formation in the splat quenched sample.

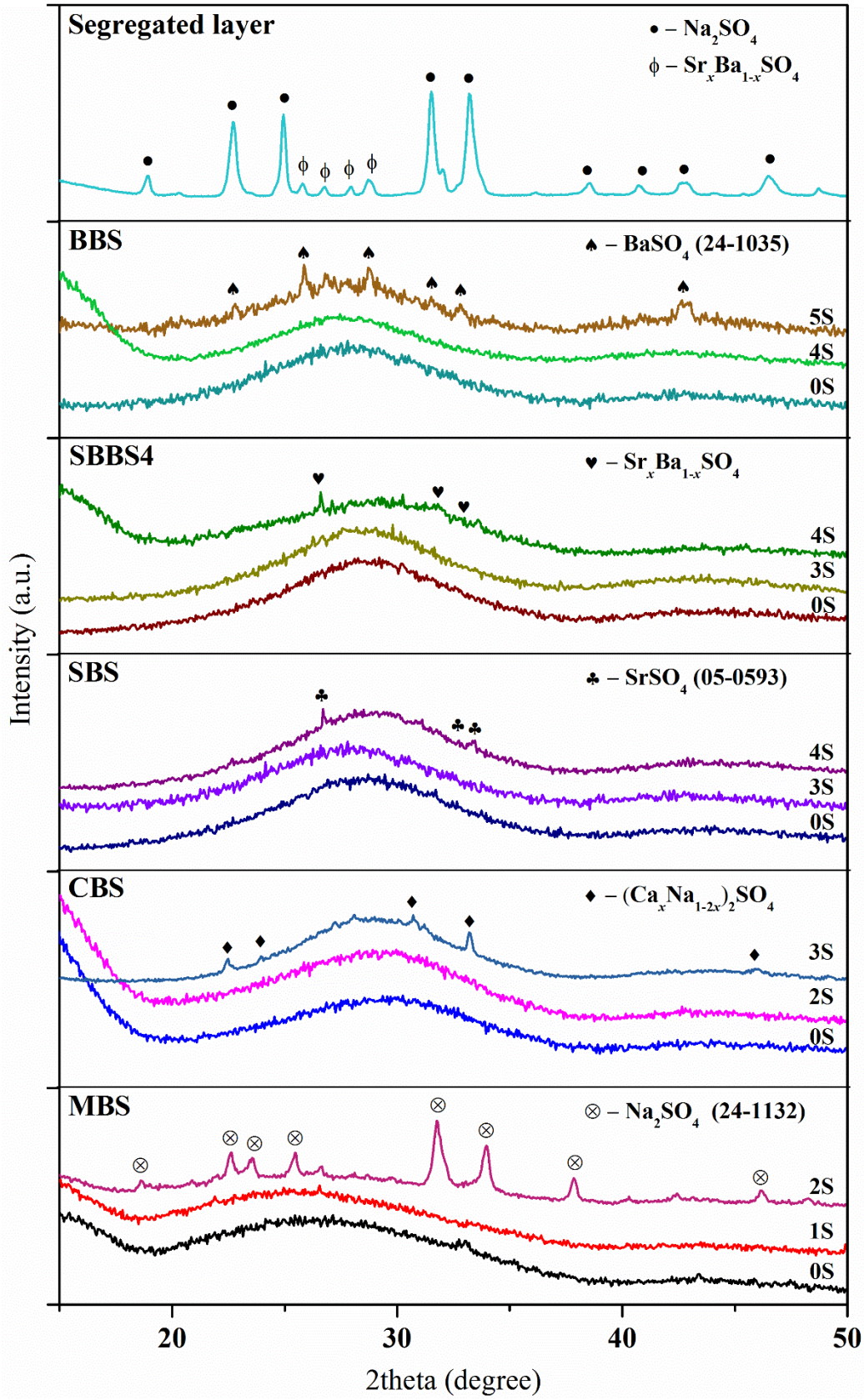

Figure 4-6 XRD patterns of prepared glasses with and without sulphate addition. For detailed composition please see Table 4-1.

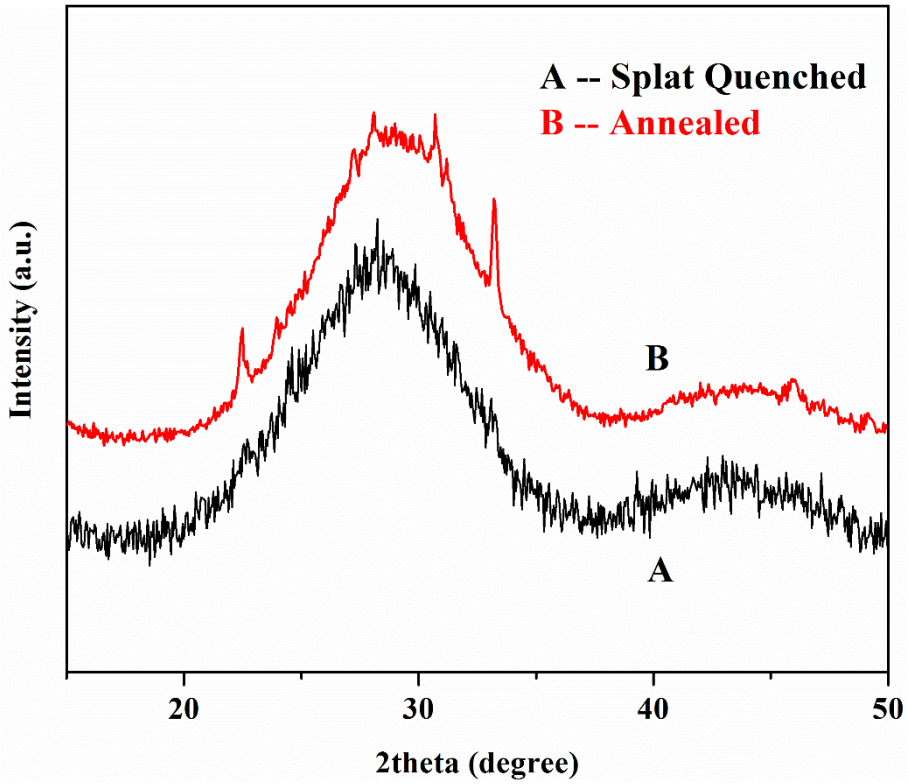

Figure 4-7 XRD patterns of SBBS-4S glass ($50SiO_2$-$15B_2O_3$-$15Na_2O$-12SrO-8BaO + $4SO_3$, mol%): (A) splat quenched and (B) annealed at 550 ºC for 1 h.

4.2.2.3. Differential thermal analysis

The influence of sulphate incorporation on thermal behaviours of glasses has been investigated with DTA. Figure 4-8 shows the typical change of DTA curves along with increasing sulphate addition in SBBS4 glass. The glasses demonstrate good thermal stability within the measured temperature range; the glass transition temperature T_g is estimated from the onset of first endothermic peak. Sulphate addition has resulted in an up to 45 ºC reduction of T_g, from 569 ºC in base glass to 524 ºC at 4 mol% SO_3 addition. The decrease in T_g suggests that sulphate incorporation reduces the energy required for structural relaxation of glass network.

TGA measurement was done simultaneously with DTA analysis. There is no larger than 1% fluctuation (0.04 of 40 mg) throughout heating, so it is deemed that samples do not suffer mass changes during heating from room temperature to 1000 ºC.

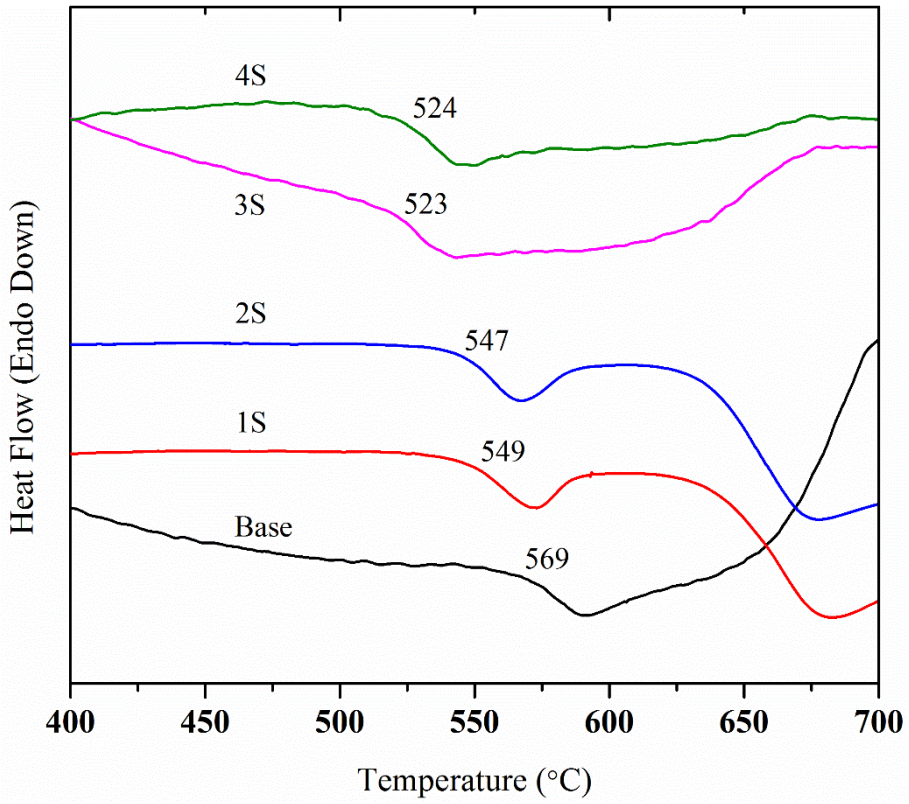

Figure 4-8 DTA curves of SBBS4 glass with different sulphate additions. SBBS4-*x*S glass composition: $50SiO_2$-$15B_2O_3$-$15Na_2O$-12SrO-8BaO + xSO_3, mol%.

4.2.2.4. Raman Spectroscopy

Figure 4-9 (*a*)-(*e*) are Raman spectra of SBBS4 glass with increasing sulphate loadings. There are three broad band regions in the spectrum of the base glass: 450~750 cm^{-1} region assigned to Si-O bending motions or Si-O-B rings, 850~1200 cm^{-1} region assigned to Si-O stretching motions in SiO_4 unit and 1350~1600 cm^{-1} region assigned to B-O stretching motions in borate triangles (BO_3). The incorporation of sulphate in glass is conducive to the creation of three new bands, which are υ_2 band centred at ~460 cm^{-1} assigned to the O-S-O symmetric bending mode, υ_4 band centred at ~630 cm^{-1} assigned to the asymmetric O-S-O bending mode, and υ_1 band centred at ~990 cm^{-1} assigned to the S-O symmetric stretching mode, respectively. The weak band υ_3 which is assigned to the S-O asymmetric stretching mode and located at ~1200 cm^{-1}, is not observed probably because it is hidden by the broad Si-O band between 850 and 1200 cm^{-1}. Figure 4-9(*f*) indicates that the segregated phase in SBBS4-4S glass is made up of crystalline sulphates; however, the cations to which SO_4^{2-} ions are bonded

cannot be identified by Raman spectroscopy.

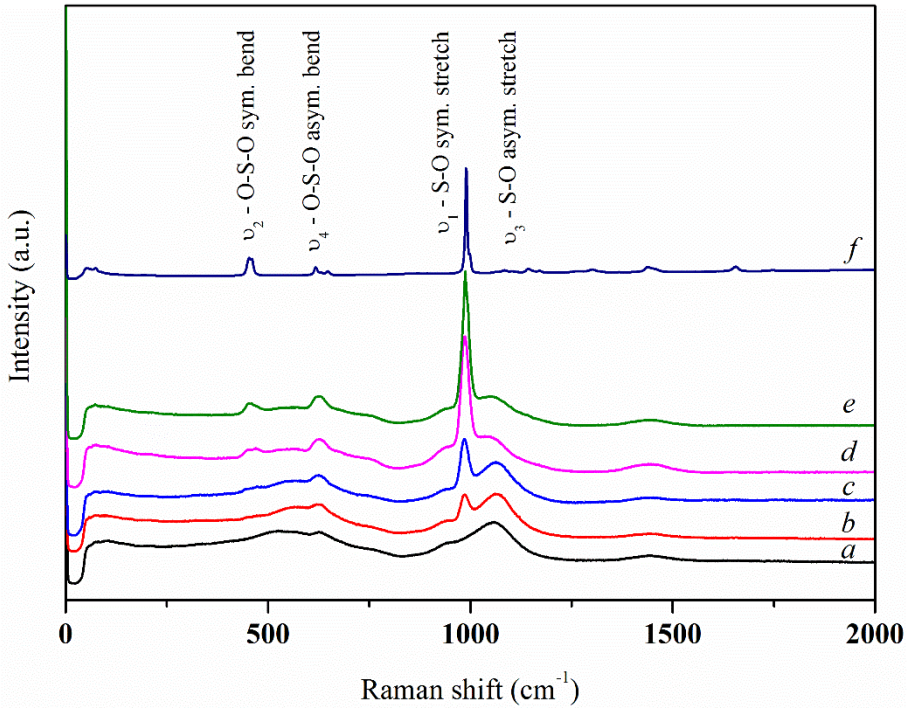

Figure 4-9 Raman spectra of SBBS4 glass with increasing sulphate additions. (*a*) Base; (*b*) 1 mol%SO_3; (*c*) 2 mol%SO_3; (*d*) 3 mol%SO_3; (*e*) 4 mol%SO_3; (*f*) Segregated phase on (*e*). SBBS4 composition (mol%): 50SiO_2-15B_2O_3-15Na_2O-12SrO-8BaO + *x*SO_3.

Deconvolution of the Raman spectra was performed with software Peakfit 4.1.2 for the region 850 - 1200 cm^{-1} which covers the Si-O stretching and S-O stretching modes. The deconvolution procedures followed McKeown *et al.* (2001) and Lenoir *et al.* (2009) where quantitative analysis for Raman spectra of sulphur containing glasses has been achieved. After linear baseline subtraction, this region was deconvolved to five Gaussian bands, four of which are assigned to Si-O bonds in different silicate tetrahedra Q_n (*n* denotes the number of bridging oxygen per tetrahedron, two Q_3 bands are considered due to the different modifier species that a SiO_4 unit can associate in glass network) and one assigned to υ_1 band of the SO_4^{2-} tetrahedron. An example deconvolution is shown in Figure 4-10.

The normalised Q_2 and Q_3 areas are plotted in Figure 4-11*a* (Q_4 area not plotted since it is less than 5% and did not change much). It can be seen that the Q_2 to Q_3 ratio initially slightly decreases until 1.96 mol%SO_3 addition and then largely increases

after that.

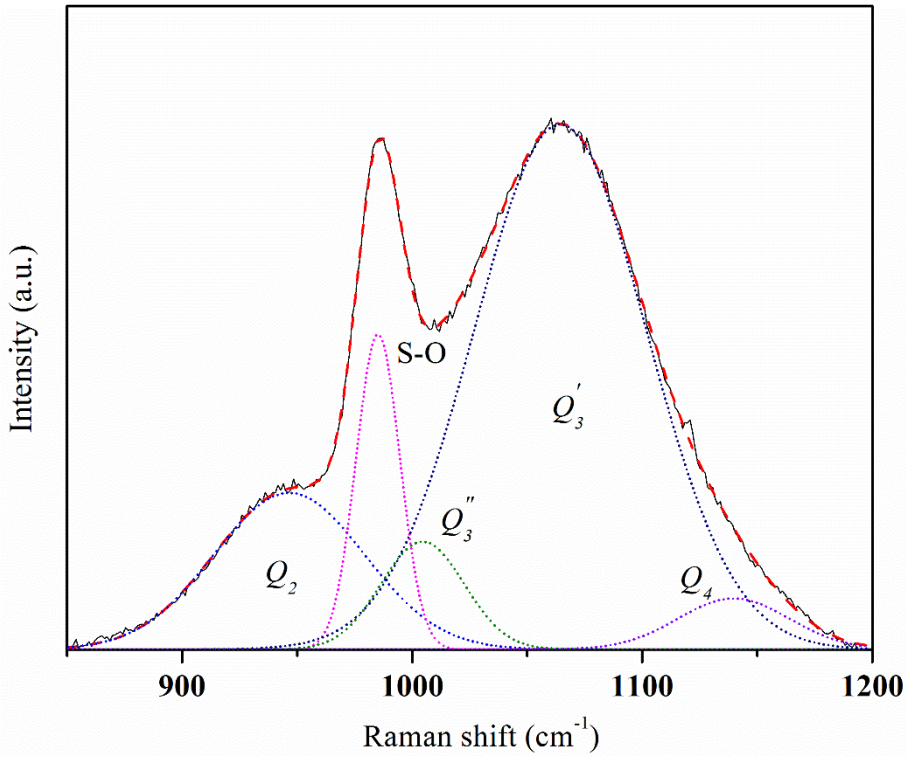

Figure 4-10 Deconvolution of the 850-1200 cm^{-1} region of the Raman spectrum of SBBS4-1S glass.

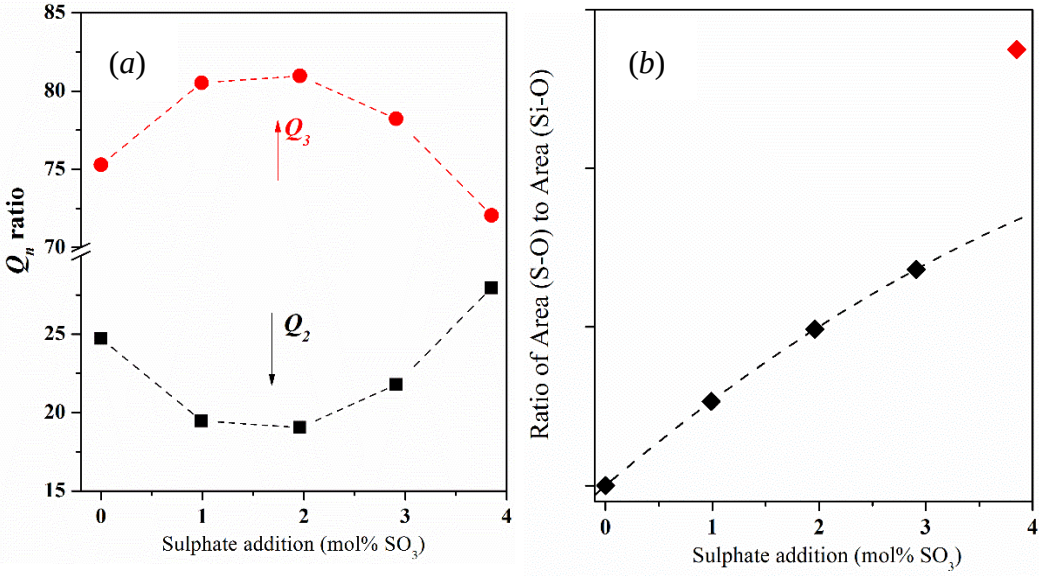

Figure 4-11 Deconvolution results of 850-1200 cm^{-1} band region of Raman spectra of SBBS4 glass with different sulphate addition: (*a*) Q_2 and Q_3 proportion, respectively; (*b*) the ratio of S-O stretching band area to whole Si-O stretching band area.

Meanwhile, Figure 4-11*b* suggests that SO_4^{2-} incorporation in glass network is in line within 2.91 mol% SO_3 addition whereas the S-O/Si-O ratio apparently deviates from the trend at 3.85 mol% SO_3 addition.

Raman scattering does not respond to the metal-oxide ionic bond and thus the obtained Raman spectrum only reflects the presence of SO_4^{2-} ions but not the specific cations with which SO_4^{2-} ions are associated. However, varying field strengths enable cations to have different distortion effect on the nearby SO_4^{2-} ions thereby leading to slight shift in Raman frequencies. Figure 4-12 plots the centre frequencies of S-O symmetric stretching band in the Raman spectra of all the strontium-barium borosilicate glasses with same amount of sulphate addition. The equivalent substitution of SrO by BaO leads to a linear decrease in Raman frequencies from 988.5 cm^{-1} at 20 mol% SrO (SBS-3S) to 983.0 cm^{-1} at 20 mol% BaO (BBS-3S). This result proves the preferable association of SO_4^{2-} ions with alkaline earth cations in glass network.

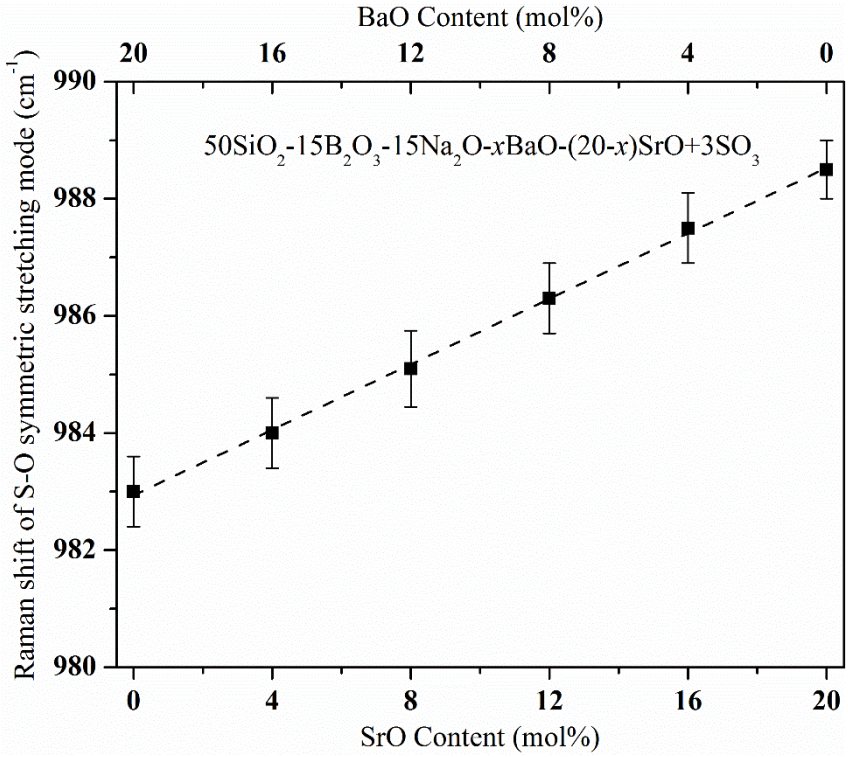

Figure 4-12 Raman shift of S-O stretching vibration against the abundance of SrO and BaO in glasses with 3 mol% SO_3 addition.

SBBS4-3S glass processed at different melting temperatures has also been examined

with Raman spectroscopy. As shown in Figure 4-13, increasing melting temperature leads to decreasing SO_4^{2-} ions being incorporated into glass network as the relative intensity of S-O symmetric stretching band (dash circle) declines. The large reduction in intensity at 1250 ºC agrees with the compositional analysis by EDX which indicates intense sulphate evaporation by this point.

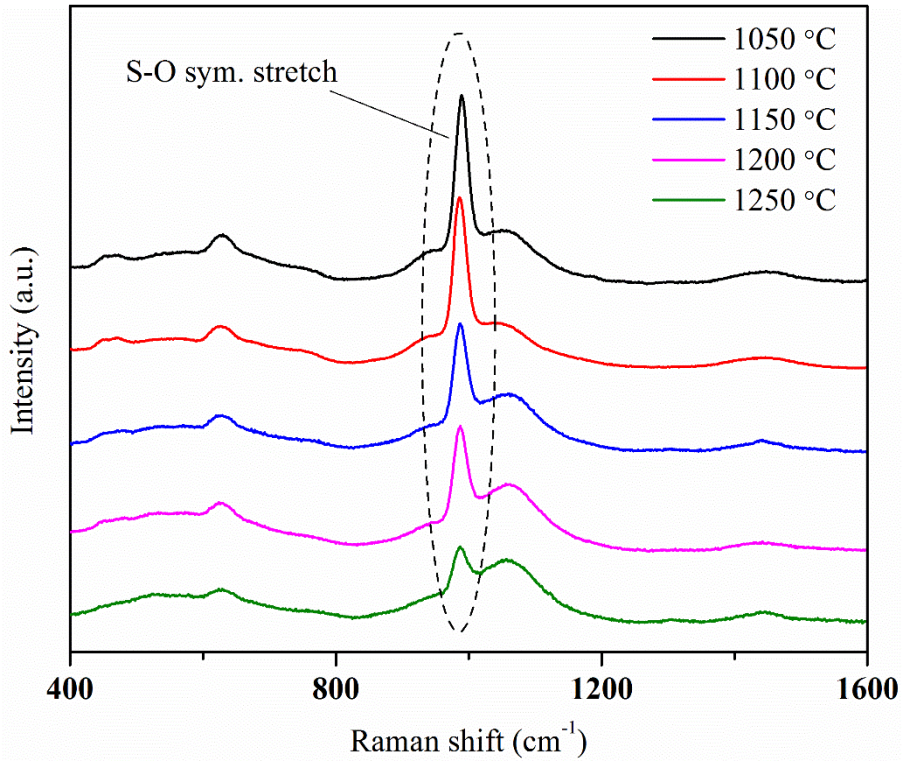

Figure 4-13 Raman spectra of SBBS4-3S glass against different melting temperatures. The dashed circled band is assigned to S-O symmetric stretching mode.

4.2.2.5. FTIR Spectroscopy

An FTIR spectrum gives supplementary information to a Raman spectrum of a sample. Figure 4-14 presents FTIR spectra (absorbance) of SBBS4 glasses with 0-4 mol% SO_3 additions. The incorporation of SO_4^{2-} ions into glass network creates a band at ~620 cm^{-1} assigned to S-O asymmetric bending mode (υ_4), the intensity of which increases with increasing SO_3 additions. The changes in 800-1300 cm^{-1} region are not prominent probably because the bands assigned to Si-O bond dominate in this region and overlay the bands assigned to S-O bond and hence the contribution of S-O bond vibrations cannot be reflected. However, a small shoulder begins to appear at ~1150 cm^{-1} with

increasing sulphate content, probably assigned to the asymmetric stretching vibration mode of the S-O bond (υ_3).

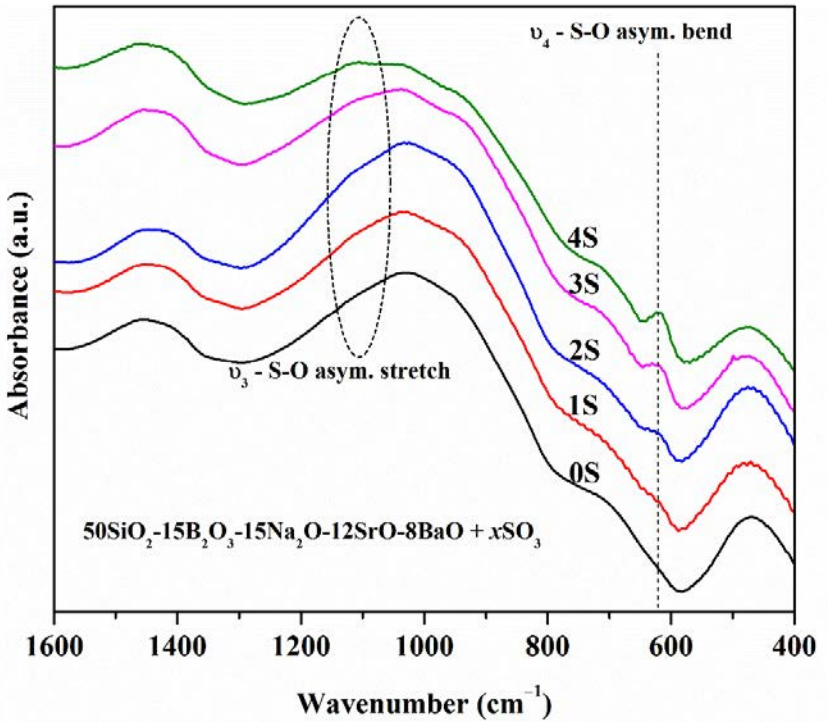

Figure 4-14 FTIR spectra of SBBS4 glass with 0-4 mol% SO_3 loadings.

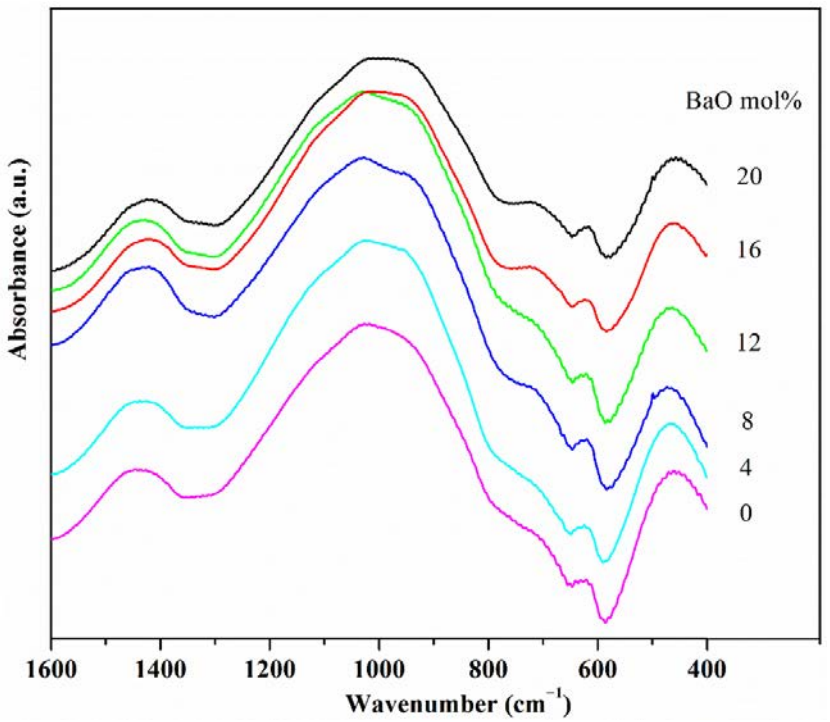

Figure 4-15 FTIR spectra of glass ($50SiO_2$-$15B_2O_3$-$15Na_2O$-xBaO-(20-x)SrO, mol%, x = 0, 4, 8, 12, 16 and 20, respectively) with 3 mol% SO_3 addition.

The effect of compositional variation on FTIR spectra of glasses containing same level of sulphate is displayed in Figure 4-15. The substitution of Sr with Ba does not cause a notable change in the spectra; only a small shoulder can be observed at ~950 cm^{-1} in the spectra of mixed Sr-Ba glasses (BaO = 4, 8 and 12 mol%, respectively). The shift of sulphate bands against compositional change cannot be discerned clearly due to their low intensity and broad nature.

4.2.3. Microstructural analysis for phase separation

4.2.3.1. SEM and EDX

The micro-homogeneity of prepared glasses was assessed with backscattered electron (BSE) images in SEM. It is observed that the visibly transparent glasses (*e.g.* BBS-3S) are featureless in BSE image (Figure 4-16*a*) while the sulphate-overloaded glasses (*e.g.* BBS-5S) contain a number of tiny separated particles (Figure 4-16*b*). It appears that the glass can remain homogeneous in microstructure as long as the sulphate capacity is not exceeded. Meanwhile, in the optically opaque glass, the separated phases are widely and randomly distributed within the glass matrix.

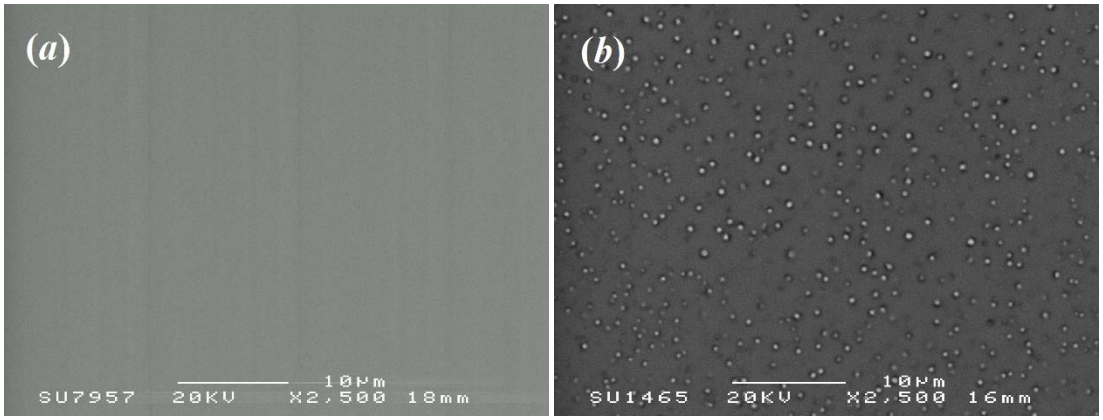

Figure 4-16 Backscattered electron images of (*a*) BBS-3S glass (homogeneous) and (*b*) BBS-5S glass (optically opaque), respectively.

Figure 4-17 shows secondary electron images of phase separation in BBS-5S glass and SBBS4-4S glass fracture surface (unpolished) at higher magnifications, respectively. The precipitated particles in BBS-5S glass are droplet-like, about 500 nm in diameter and randomly dispersed within the glass matrix. Similar features are

observed on the particles in SBBS4-4S glass fracture surface; however, the particles are readily removed from fracture surface during sample processing, leaving glass matrix with empty pores. A BSE image of a polished SBBS4-4S glass slice is shown in Figure 4-18. There are many remaining phases trapped in the pores, which are crystal-like according to their morphologies and distinct from surrounding base glass. The brighter colour of these particles than glass matrix under BSE observation indicates these particles are of higher density.

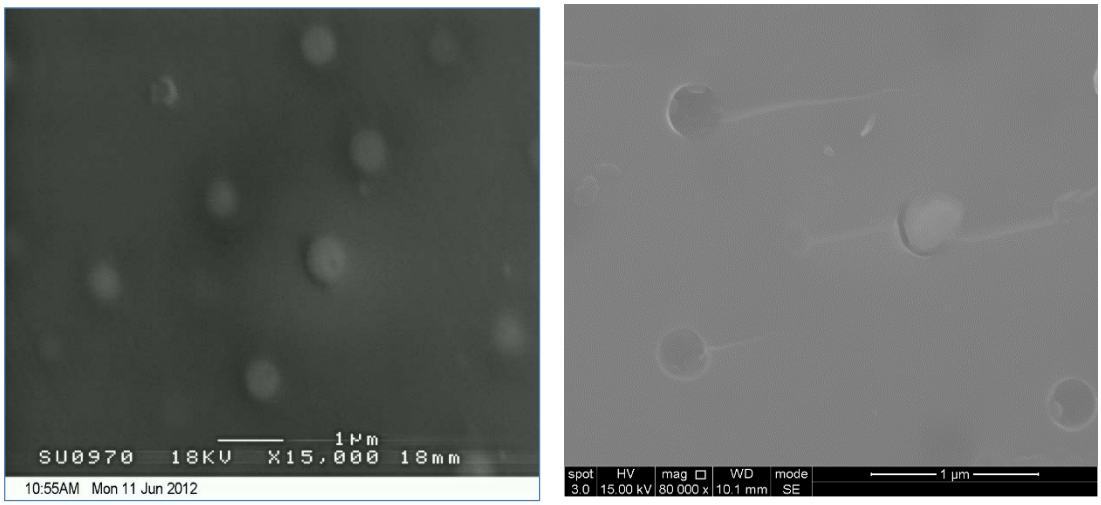

Figure 4-17 Secondary electron images of BBS-5S glass (left) and SBBS4-4S glass (right). The right image is from an unpolished fracture surface of SBBS4-4S glass.

EDX analysis has been done upon areas A and B marked in Figure 4-18; the spectra obtained are presented in Figure 4-19. As the particle size is smaller than the resolution limit of EDX (1 μm^2), it is not sensible to perform quantitative measurement upon the separated phase. However, by the comparison of EDX spectra between A and B it can be seen that the separated phase is more enriched in Ba and S and less enriched in Na compared with surrounding glass areas. The changes in Sr and Si contents are not obtained as the Sr band and Si band in EDX spectra overlap. Therefore, the EDX result implies that the separated phase is most likely to be $BaSO_4$ or $Ba/SrSO_4$ crystals.

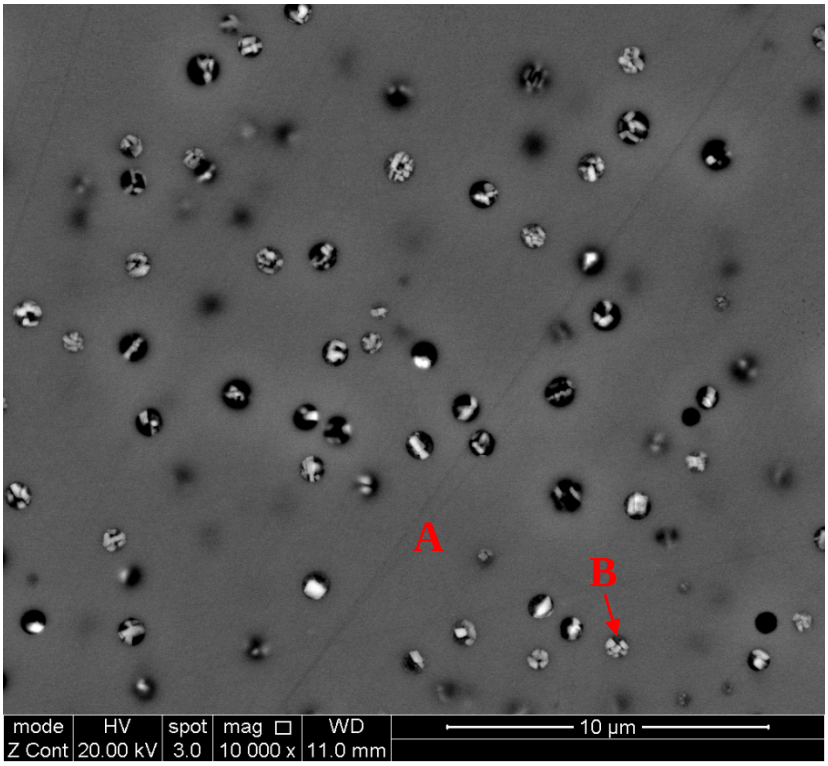

Figure 4-18 Backscattered electron image of SBBS4-4S glass: (A) glass matrix and (B) remaining trapped separated phase.

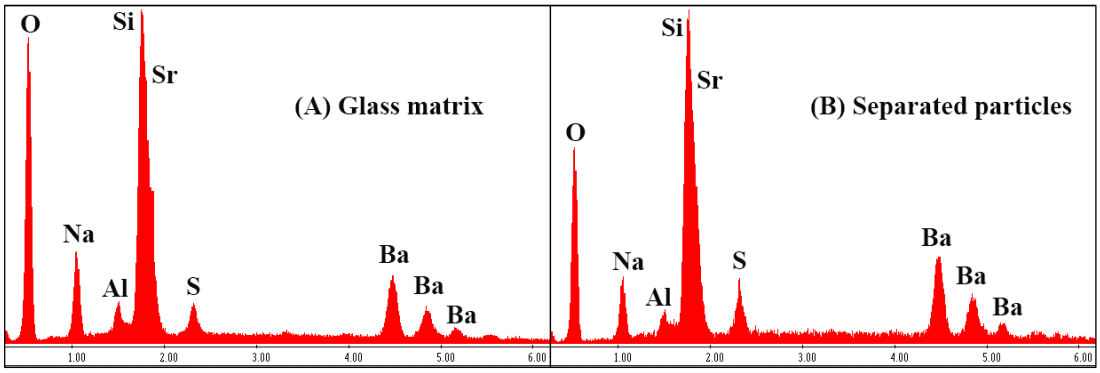

Figure 4-19 EDX spectra of SBBS4-4S (A) glass matrix and (B) separated particles. Spectra are obtained from areas marked in Figure 4-18.

4.2.3.2. TEM

Figure 4-20(*a*) and (*c*) are two TEM images of BBS-5S samples and Figure 4-20(*b*) and (*d*) are the electron diffraction patterns of those selected areas where crystals are found. The diffraction patterns in Figure 4-20(*b*) are made up of series of diffraction

spots, among which the series likely due to the [010] plane diffraction of orthorhombic $BaSO_4$ crystal is apparently dominant; the diffraction patterns in Figure 4-20 (*d*) are made up of a number of diffraction rings, indicating that it is a multi-crystal area which contains crystals ($BaSO_4$) in a variety of orientations. From Figure 4-20 (*c*) it can be seen that the morphology of crystals are distinct from that of surrounding glass pieces (which hold the crystals in the picture).

Figure 4-21 presents a single particle in SBBS4-4S glass and its electron diffraction patterns. This isolated crystal probably separated out from the glass base during the grinding in acetone when preparing specimens. The diffraction spots are indexed to be assigned to the $BaSO_4/SrSO_4$ [011] plane diffraction.

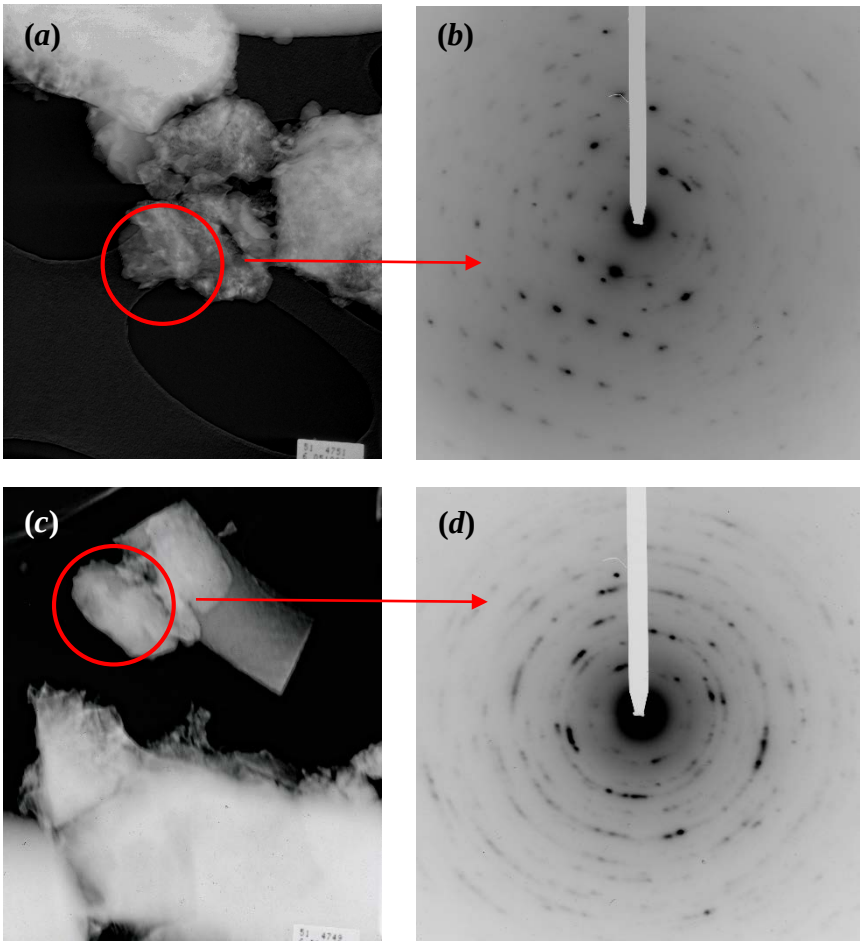

Figure 4-20 TEM observations of BBS-5S sample: (*a*) and (*c*) are two different pieces of sample while (*b*) and (*d*) are their corresponding electron diffraction patterns.

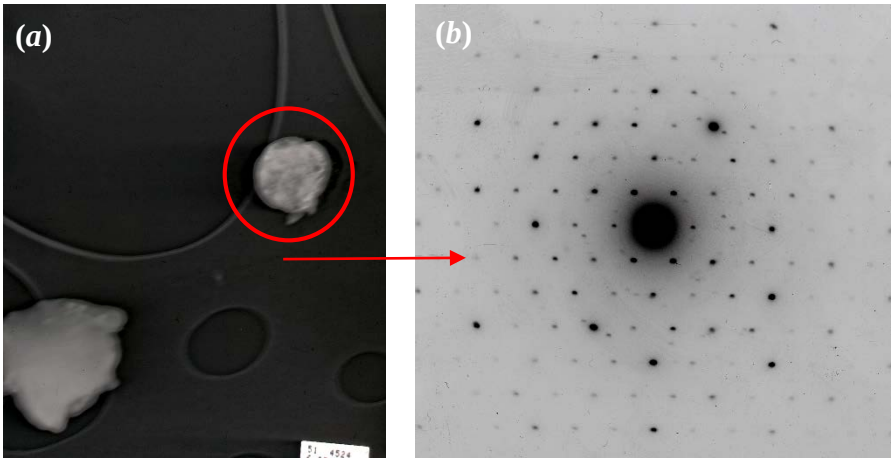

Figure 4-21 TEM image and diffraction patterns of one particle of SBBS4-4S glass.

4.3. Discussion

4.3.1. Sulphate retention and solubility in glass

4.3.1.1. Sulphate retention

Higher sulphate retention in glass is essential to the vitrification of sulphate bearing waste because it reduces the corrosion by the exhaust gases during melting and thereby ensuring the efficiency and safety of vitrification process. The compositional analysis indicates that sulphate retention rate is more dependent on melting temperature than on melt composition in this study. Residual sulphate content in glass is dramatically reduced as melting temperature increases to 1250 ºC, which agrees with Nagashima and Katsura (1973) and Beerkens (2003) who reported decreasing sulphate retention with increasing melting temperature.

The decreasing sulphate retention caused by increasing melting temperature can be attributed to the decomposition of sulphate (SO_4^{2-}) during melting. Since there is no evidence of sulphate diffusion into the crucible during melting, it is deemed that all sulphate loss is due to sulphate evaporation. According to Halle and Stern (1980), decomposition dominates over vaporisation in sulphate evaporation in the melting temperature range of this study. The decomposition reaction of SO_4^{2-} to SO_2 and O_2 gases in the melt, which is expressed in Equation 2-2, is endothermic because its enthalpy change (ΔH) is positive whichever modifiers SO_4^{2-} ions are associated with (ΔH data are referred to Mohazzabi and Searcy (1976) and Halle and Stern (1980); SO_4^{2-} ions are assumed to connect with alkali and alkaline earth cations only). This means increasing melting temperature will facilitate sulphate decomposition at high temperature and hence lower sulphate retention in glass. As can be seen in Figure 4-3, the melting temperature of SBBS4-3S glass should be controlled to be between 1050 and 1150 ºC to ensure a high sulphate retention and as a result most borosilicate glasses in this chapter were prepared at 1100 ºC. The sulphate decomposition mechanism is also able to explain the limited retention of sulphate in aluminosilicate glasses as most sulphate could have been decomposed and evaporated out from the melt at the processing temperature (1450 ºC).

Sulphate retention is also related to sulphate loading in glass. The more sulphate added,

the lower the retention rate achieved. This can be explained by the increasing difficulty for SO_4^{2-} ions to enter the voids of glass network when approaching saturation. And in the glass melts with oversaturated sulphate, excess sulphate will remain outside of glass matrices after cooling, resulting in a much lower sulphate retention than the theoretical value.

4.3.1.2. Sulphate solubility

There have been a number of works investigating the sulphate solubility dependence on glass compositions (Jantzen *et al.* 2004, Beerkens 2007, Liu *et al.* 2007, Bingham and Hand 2008), which have proposed many empirical models to describe the correlation between sulphate solubility and some compositional parameters. However, these models do not agree well with each other, and no one can be used for universal prediction so far. A more universally applicable model is still needed.

Here in this chapter the contribution of alkaline earth oxides to sulphate solubility in glass has been assessed. Results indicate that the improvement of sulphate solubility with the same abundance of alkaline earths follows the order Ba > Sr > Ca > Mg while other components remain constant. As discussed in the literature review (Section 2.3.1), Na_2SO_4 decomposition dominates sulphate dissociation when Na and alkaline earths are both present in melt. The substitution between alkaline earth sulphates should not significantly impact sulphate solubility. Therefore, sulphate solubility improvement is most likely a result of increasing oxygen ion activity $[O^{2-}]$ (Equations 2-1 and 2-4).

Oxygen ion activity is related to network modifiers species and content; cations with lower field strength (Z/a^2) are believed to contribute higher oxygen ion activity in the melt (Harding 1972) and thus the abundance of cations with low field strength is beneficial to enhance sulphate solubility in melt. If their charge is identical, larger cations (*e.g.* Ba^{2+}) have the lower field strength than smaller cations (*e.g.* Mg^{2+}). Therefore, as observed in this study, higher sulphate solubility is achieved by equimolar substitution from MgO to BaO in alkaline earth oxides.

In Chapter 8, the solubility results here will be combined with comparable literature data to establish some empirical models of sulphate solubility dependence on a variety

of compositional parameters, trying to find the best applicable one which can be used for the prediction of sulphate solubility in glass.

4.3.2. The effects of sulphate incorporation on glass structure and properties

The glass density increased by sulphate incorporation indicates that $[SO_4]^{2-}$ ions have entered the interstitial space of glass network to make it more compact, like observed in Manara *et al.* (2007). It is possible that sulphate incorporation also causes slight network expansion because the increasing density appears to vary quadratically. In addition, the varying density increment with different compositions suggests that the capacity of sulphate incorporation in different glass is not the same.

The decrease in T_g caused by sulphate addition agrees with Mishra *et al.* (2008) but disagrees with the results of Manara *et al.* (2007). The disagreement with Manara *et al.* (2007) may result from its poor sulphate retention level (less than 20% with 5 wt%SO_3 loading) which makes it less comparable. Mishra *et al.* (2008) attributes the change in T_g to the interactions of SO_4^{2-} ions with the glass network at low loading and with network modifiers at high loading, respectively. However, according to the Raman spectra deconvolution result (Figure 4-11), sulphate incorporation slightly polymerises glass until 1.96 mol% SO_3 addition, which would result in a small increase in T_g. This implies that the two interactions may coexist along with sulphate incorporation and the strong interaction between SO_4^{2-} ions and network modifiers, which is supposed to reduce the energy required for the structural relaxation of borosilicate glass network, is overwhelming in determining T_g.

As plotted in Figure 4-11, sulphate incorporation initially polymerises the glass network and depolymerises it thereafter. The polymerisation may occur through the following reaction:

$$2Si-O:Na^{+}+SO_4^{2-}=Si-O-Si+Na_2SO_4 \qquad \text{(Equation 4-1)}$$

In this case, SO_4^{2-} will be present as Na_2SO_4 or MSO_4 clusters in the voids of glass network. The association of modifying cations with sulphate leaves more structural units connected, leading to the polymerisation of network. Such sulphate clusters have been reported by Brendebach *et al.* (2009) with X-ray absorption fine structure (XAFS)

data from sulphate containing glasses.

While network polymerisation is observed in glasses containing low level of sulphate (Tsujimura *et al.* 2004, Manara *et al.* 2007, Morizet *et al.* 2013), network depolymerisation occurs here, Sokolov *et al.* (2003) and Mishra *et al.* (2008) in which sulphate content is much more abundant. The depolymerisation mechanism is difficult to explain; one possibility is that SO_4^{2-} ions interact with SO_4 structural units, forming Si-O-S units to disconnect the silicate network:

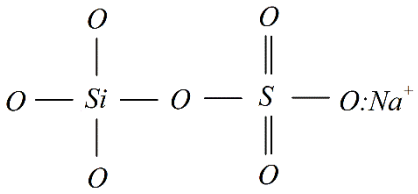

In this case, SO_4^{2-} unit terminates SiO_4 linkage and the glass network is likely to be depolymerised. Nevertheless, no evidence so far has been found yet for the existence of Si-O-S unit in the prepared glasses.

The increasing ratio of the S-O band area to whole Q_n area in Figure 4-11 confirms the incorporation of SO_4^{2-} ions in the glass network. This ratio steadily increases with sulphate addition as long as sulphate is fully dissolved; however, it jumps to extraordinarily high value in SBBS4-4S glass within which sulphate crystals are formed. The Raman signal of sulphate crystals is much higher than SO_4^{2-} dissolved in glass, so the intensity of the S-O band deviates to a higher ratio.

Figure 4-12 provides the information about the associated cations of SO_4^{2-} ions in glass network. The decrease in Raman frequency of SO_4^{2-} υ_1 mode with the substitution of BaO for SrO indicates that SO_4^{2-} ions are largely associated with Sr^{2+} and Ba^{2+}. There is no strong preference for SO_4^{2-} ions to connect alkalis or alkaline earths in glass, but the larger cations are able to provide more space for the association of sulphate. Therefore, more SO_4^{2-} ions are supposed to surround Ba^{2+} or Sr^{2+} ions rather than Na^+ ions in glass network. $BaSO_4$ and $SrSO_4$ are predominantly present as sulphate clusters in glass. Moreover, Ba^{2+} ions have a stronger distortion effect than Sr^{2+} ions on SO_4^{2-} ions, resulting in SO_4^{2-} ions associated with Ba^{2+} ions having lower

Raman frequencies. Consequently, the equimolar substitution of BaO for SrO leads to a linear decrease in υ_1 frequency.

4.3.3. Phase separation in glass containing excess sulphate

According to XRD and EDX results, the phase separation in glass caused by excess sulphate occurs through two different ways. One way is the liquid-liquid separation from critically saturated melt upon cooling, resulting in droplet-like particles forming within the glass matrix. The other is the floating surface layer which is composed of excess sulphate, resulting in a segregated layer on the glass surface.

Liquid-liquid separation occurs in the glasses containing critical amount of sulphate, such as SBS-4S, SBBS4-4S and BBS-5S. In the molten state, sulphate is completely dissolved in the borosilicate melt; however, during cooling, the incorporative capacity of sulphate in borosilicate network is reduced concomitantly. This leads to some excess sulphate being expelled from network, forming a number of droplets within the cooling melt. These droplets crystallise during cooling and demonstrate distinct morphologies from the surrounding glass matrix under electron microscope observation. XRD and EDX results suggest that the crystallised phase in the droplets is most likely to be alkaline earth sulphate, which agrees with the finding in the Raman spectra that SO_4^{2-} ions are preferably associated with larger alkaline earth cations (Ba^{2+}/Sr^{2+}) in glass.

It is worth noting that the occurrence of such liquid-liquid separation is dependent on the cooling rate. While the annealed SBBS4-4S glass appears opaque, the splat quenched SBBS4-4S glass pieces are transparent, showing no feature of crystals in XRD patterns and SEM images. It is likely because of the rapid quenching that the time allowing critically saturated sulphate to separate from melt is dramatically reduced, leading to less or even no crystallisation in the final glass. Thus the quenched glass will have a slightly higher sulphate solubility than annealed glass. Such difference is important because sulphate solubility in many papers, *e.g.* Mishra *et al.* (2008) and Lenoir *et al.* (2010), are reported in air quenched glasses. This discrepancy will be taken into account in Chapter 7 when combining the solubility results here with the previous literature data.

On the other hand, if sulphate has been already excessive in the melt, the residual sulphate which is unable to enter borosilicate network will remain outside of the melt, floating on the melt surface to form a segregated layer. This is in accordance with the description of "gall" (segregated sulphate layer in nuclear waste vitrification) by (Jantzen *et al.* (2004), Kaushik *et al.* (2006)) and other researchers. XRD result indicates that the segregated layer of SBBS4-5S glass comprises a majority of Na_2SO_4 with a minority of $SrSO_4$ and $BaSO_4$. The Raman spectrum of this layer closely resembles the spectrum of Na_2SO_4 crystals. Na_2SO_4 is the most thermally stable among possible sulphate species in melt (Papadoloulos 1973) and thus the excess SO_4^{2-} ions tend to connect with Na^+ to form a more stable Na_2SO_4 layer. The presence of a small amount of alkaline earth sulphates can be either expelled from the melt during cooling or separated from the melt during melting.

In addition, in calcium and magnesium borosilicate glasses, the separated phases are primarily Na_2SO_4 or Na_2SO_4 solid solutions as well when sulphate is slightly excessive in the melt. They do not form a segregated layer and instead they separate from the melt to form bulk crystals within the glass. As discussed above, SO_4^{2-} association is related to the cationic size of the modifiers. Ca^{2+} has a similar cationic radius to Na^+ so that the formed sulphate crystals are solid solution $(Ca_xNa_{1-2x})_2SO_4$. Mg^{2+} is smaller than Na^+ so that SO_4^{2-} is preferably associated with Na^+ and the separated phase is Na_2SO_4.

4.4. Conclusions

Series of borosilicate glasses ($50SiO_2$-$15B_2O_3$-$15Na_2O$-15MO) and aluminosilicate glasses ($45SiO_2$-$10Al_2O_3$-45MO) have been prepared to incorporate sulphate in this study. Based on the above results and discussion, the following conclusions can be drawn:

- Borosilicate glasses exhibit excellent sulphate retention while aluminosilicate glasses cannot retain sulphate at all. Both increasing melting temperature and increasing sulphate loading result in decreasing sulphate retention.
- The highest sulphate solubility found in this study was 3.53 mol%SO_3 in BBS-4S glass. Sulphate solubility is improved by the equimolar substitution of BaO for SrO for CaO for MgO, indicating that cations with lower field strength are beneficial in enhancing sulphate solubility.
- Sulphate incorporation increases glass density, decreases T_g and increases the intensity of Raman and FTIR bands assigned to SO_4^{2-} tetrahedra. Sulphate incorporation initially polymerises the glass network but depolymerises it after 1.96 mol%SO_3.
- SO_4^{2-} ions are preferably associated with larger cations such as Ba^{2+} and Sr^{2+} ions rather than Na^+ ions in glass network. The substitution of BaO for SrO leads to lower Raman frequencies of SO_4^{2-} vibration.
- The slow cooling of critically sulphate-saturated melt results in the formation of droplet-like particles within SBS, SBBS and BBS melts. These separated particles are submicron in size, randomly dispersed within glass and identified to be alkaline earth sulphate crystals. Apparently excess sulphate in melt results in the occurrence of segregated layer, which is primarily composed of Na_2SO_4.
- The separated phase in CBS-3S and MBS-2S glasses is $(Ca_xNa_{1-2x})_2SO_4$ ($x \leq 0.5$) solid solution and Na_2SO_4 crystals, respectively. This agrees with the assumption of SO_4^{2+} preferable association with larger cations in glass network.

5. Chlorine in glass

5.1. Introduction

This chapter describes the incorporation and the solubility dependence of chloride in borosilicate and aluminosilicate glass compositions ($15Na_2O$-$20MO$-$15B_2O_3$-$50SiO_2$) and $45MO$ -$10Al_2O_3$-$45SiO_2$, respectively, mol%, where M = Mg, Ca, Sr, Ba or a combination). Compositional variation is achieved by equimolar substitution between alkaline earth oxides with the aim of investigating chloride solubility dependence on the species and amount of modifiers in glass. The changes in glass properties and structure caused by chloride incorporation have also been assessed, by techniques including density, XRD, DTA, Raman and FTIR spectroscopies. SEM and TEM are used to characterise the phase separation in the partly crystallised glasses which contain excess chloride.

5.2. Results

5.2.1. Chloride loading limit, retention and solubility in glass

5.2.1.1. Glass compositions

The EDX measured compositions of borosilicate and aluminosilicate glasses are listed together with their nominal values in Table 5-1 and Table 5-2, respectively. Chlorine is expected to occur as Cl^- in glass and hence glass components cannot be simply expressed as oxides (network modifying cations are partly associated with chlorine). Consequently, in this chapter, glass composition is expressed as atomic percentage (at%).

The measured compositions are generally consistent with the target values. The slight increase of SiO_2 and Al_2O_3 will arise from the partial dissolution of the mullite crucibles and it can be seen that the glasses containing Cl suffer much less crucible corrosion than the base glasses. In borosilicate glasses, there is up to 2 at% sodium loss in borosilicate glass while the alkaline earth contents are apparently not reduced. In aluminosilicate glasses, there is up to 4 at% loss of alkaline earth content (the evaporation is less significant in BAS glasses, possibly because of their slight lower melting temperature 1400 ºC compared to 1450 ºC used for the CAS and MAS glasses). There is significant loss of chlorine from the glass and, interestingly, the chlorine retention rate seems to be independent of temperature, but sensitive to the glass composition, as presented in next section.

Table 5-1 Borosilicate glass compositions (at%): measured by EDX (in bold) and nominal (in brackets), oxygen content is not included.

Sample		Si		B*	Al		Na		Alkaline earth		Cl		Total
BBS-	0Cl	**16.09**	(16.13)	(9.68)	**2.70**	(0)	**7.86**	(9.68)	**Ba 5.52**	(6.45)	**0**	(0)	41.85 (41.94)
	4Cl	**16.60**	(16.03)	(9.62)	**0.86**	(0)	**7.98**	(9.62)	**6.52**	(6.41)	**0.78**	(1.28)	42.36 (42.96)
	8Cl	**16.46**	(15.92)	(9.55)	**0.69**	(0)	**8.02**	(9.55)	**6.51**	(6.37)	**1.46**	(2.55)	42.69 (43.94)
	10Cl	**16.65**	(15.87)	(9.52)	**0.68**	(0)	**7.90**	(9.52)	**6.37**	(6.35)	**2.06**	(3.17)	43.18 (44.43)
	14Cl	**16.83**	(15.77)	(9.46)	**0.61**	(0)	**7.48**	(9.46)	**6.46**	(6.31)	**2.54**	(4.42)	43.38 (45.42)
	15Cl (*hc*)	**17.07**	(15.75)	(9.45)	**0.60**	(0)	**7.49**	(9.45)	**6.40**	(6.30)	**2.77**	(4.72)	43.78 (45.67)
SBBS4-	0Cl	**16.33**	(16.13)	(9.68)	**3.29**	(0)	**7.05**	(9.68)	**Ba 2.15** (2.58)	**Sr 3.23** (3.87)	**0**	(0)	41.73 (41.94)
	3Cl	**16.36**	(16.05)	(9.63)	**0.59**	(0)	**8.66**	(9.63)	**2.47** (2.57)	**3.63** (3.85)	**0.63**	(0.96)	41.97 (42.69)
	6Cl	**16.71**	(15.97)	(9.58)	**0.38**	(0)	**8.46**	(9.58)	**2.54** (2.56)	**3.77** (3.83)	**1.25**	(1.92)	42.69 (43.44)
	10Cl	**16.99**	(15.87)	(9.52)	**0.24**	(0)	**7.78**	(9.52)	**2.55** (2.54)	**3.84** (3.81)	**1.85**	(3.17)	42.77 (44.43)
	12Cl (*sc*)	**16.75**	(15.82)	(9.49)	**0.13**	(0)	**8.12**	(9.49)	**2.67** (2.53)	**3.91** (3.80)	**2.56**	(3.80)	43.63 (44.93)
	15Cl (*sl*)	**17.08**	(15.75)	(9.45)	**0**	(0)	**7.27**	(9.45)	**2.59** (2.52)	**4.05** (3.78)	**2.46**	(4.72)	42.80 (45.67)
SBS-	0Cl	**16.70**	(16.13)	(9.68)	**2.18**	(0)	**8.01**	(9.68)	**Sr 5.44**	(6.45)	**0**	(0)	42.01 (41.94)
	10Cl	**16.93**	(15.87)	(9.52)	**0.15**	(0)	**7.62**	(9.52)	**6.48**	(6.35)	**1.63**	(3.17)	42.33 (44.43)
	12Cl (*hc*)	**-**	-	-	**-**	-	**-**	-	**-**	-	**-**	-	
CBS-	0Cl	**17.10**	(16.13)	(9.68)	**0.30**	(0)	**9.24**	(9.68)	**Ca 6.34**	(6.45)	**0**	(0)	42.66 (41.94)
	4Cl	**16.85**	(16.03)	(9.62)	**0.19**	(0)	**8.34**	(9.62)	**6.30**	(6.41)	**0.77**	(1.28)	42.07 (42.96)
	8Cl	**17.49**	(15.92)	(9.55)	**0**	(0)	**7.84**	(9.55)	**6.11**	(6.37)	**1.19**	(2.55)	42.18 (43.94)
	10Cl (*sc*)	**17.15**	(15.87)	(9.52)	**0.08**	(0)	**7.38**	(9.52)	**6.61**	(6.35)	**1.14**	(3.17)	41.88 (44.43)
	16Cl (*sl*)	**17.73**	(15.72)	(9.43)	**0**	(0)	**6.25**	(9.43)	**6.56**	(6.29)	**1.42**	(5.03)	44.57 (45.90)
MBS-	0Cl	**15.33**	(16.13)	(9.68)	**1.16**	(0)	**8.85**	(9.67)	**Mg 6.83**	(6.45)	**0**	(0)	41.85 (41.94)
	4Cl	**16.24**	(16.03)	(9.62)	**0.21**	(0)	**8.61**	(9.62)	**7.33**	(6.41)	**0.57**	(1.28)	42.58 (42.96)
	6Cl (*sc*)	**16.35**	(15.97)	(9.58)	**0.08**	(0)	**8.52**	(9.58)	**7.49**	(6.39)	**0.58**	(1.92)	42.60 (43.44)
	8Cl (*hc*)	**-**	-	-	**-**	-	**-**	-	**-**	-	**-**	-	

"*" Target boron content. ICP-OES analysis for some typical glasses has shown that boron evaporation is very limited at the melting temperature. "*sc*", "*hc*" and "*sl*" means the glass is slightly crystallised, heavily crystallised or with a segregated layer, respectively.

Table 5-2 Aluminosilicate glass compositions (at%): measured by EDX (in bold) and nominal (in brackets), oxygen content is not included.

Sample	Si		Al		Alkaline Earth		Cl		Total
BAS*-					Ba				
0Cl	**15.77**	(16.36)	**8.15**	(7.27)	**16.17**	(16.36)	**0**	(0)	40.09 (39.99)
5Cl	**16.56**	(16.22)	**7.55**	(7.21)	**15.38**	(16.22)	**1.36**	(1.80)	40.85 (41.45)
10Cl	**16.52**	(16.07)	**7.32**	(7.14)	**15.32**	(16.07)	**2.96**	(3.57)	42.12 (42.85)
15Cl (*sc, cr*)	**17.71**	(15.93)	**6.89**	(7.08)	**13.78**	(15.93)	**4.24**	(5.31)	42.62 (44.25)
20Cl (*hc, cr*)	**17.59**	(15.79)	**6.77**	(7.02)	**13.75**	(15.79)	**5.61**	(7.02)	43.72 (45.65)
SBAS-					Ba	Sr			
15Cl (*cr*)	**17.22**	(15.93)	**7.93**	(7.08)	**7.26** (7.96)	**7.33** (7.96)	**3.69**	(5.31)	47.07 (44.25)
CAS-					Ca				
0Cl	**16.83**	(16.36)	**10.08**	(7.27)	**12.15**	(16.36)	**0**	(0)	39.06 (39.99)
5Cl	**16.83**	(16.14)	**8.60**	(7.18)	**13.85**	(15.93)	**0.58**	(1.36)	39.86 (40.61)
10Cl	**16.85**	(15.93)	**9.14**	(7.08)	**13.07**	(15.51)	**0.89**	(2.70)	39.95 (41.22)
20Cl	**17.10**	(15.52)	**9.09**	(6.90)	**12.73**	(14.72)	**1.06**	(5.30)	39.98 (42.44)
25Cl	**16.95**	(15.32)	**9.32**	(6.81)	**12.66**	(14.35)	**1.08**	(6.57)	40.01 (43.05)
30Cl	**17.18**	(15.12)	**9.10**	(6.72)	**12.58**	(13.99)	**1.11**	(7.81)	39.97 (43.64)
35Cl (*sc*)	**17.39**	(14.93)	**8.77**	(6.64)	**12.64**	(13.64)	**1.25**	(9.04)	40.05 (44.25)
MAS-					Mg				
0Cl	**18.40**	(16.36)	**10.76**	(7.27)	**12.98**	(16.36)	**0**	(0)	42.14 (39.99)
5Cl (*sc, cr*)	**16.14**	(16.22)	**8.70**	(7.21)	**14.91**	(16.22)	**<0.1**	(1.80)	39.75 (41.45)
10Cl (*hc, cr*)	**17.94**	(16.07)	**7.82**	(7.14)	**13.32**	(16.07)	**<0.1**	(3.57)	39.08 (42.85)

"*" BAS and SBAS glasses were melted at 1400 ºC while the others were melted at 1450 ºC. The reduction in melting temperature for the BAS glasses is to enable the casting process as they are very fluid at 1450 ºC.

"*sc*" and "*hc*" means the glass is slightly crystallised and heavily crystallised, respectively.

"*cr*" means glass was cracked during casting or annealing

5.2.1.2. Loading limit

Excess chlorine added to glass results in the occurrence of phase separation during melting and/or cooling. The chlorine loading limit is therefore defined as the maximal chlorine addition that gives rise to a homogeneous glass for the compositions tested.

Among all borosilicate glasses the barium borosilicate glass (BBS) exhibits the highest chlorine loading limit. BBS glasses with 1.28, 2.55, 3.17, 4.42 and 4.72 at%Cl addition respectively (BBS-*x*Cl, *x* = 4, 8, 10, 14 and 15, respectively) have been produced and phase separation occurs in the cooling of BBS-15Cl glass. The loading limit of BBS glass is therefore regarded as being 4.42 at%Cl (BBS-14Cl).

Combined barium-strontium borosilicate glasses (SBBS4) with 0.96, 1.92, 3.17, 3.80 and 4.72 at%Cl addition (SBBS4-*x*Cl, *x* = 3, 6, 10, 12, 15, respectively) have been produced. Slight phase separation occurs in SBBS4-12Cl glass and a segregated layer is observed to form on the phase separated SBBS4-15Cl glass. The loading limit of SBBS4 glass is hence regarded as being 3.17 at%Cl (SBBS4-10Cl).

Strontium borosilicate glasses (SBS) with 3.17 and 3.80 at%Cl addition (SBS-*x*Cl, *x* = 10 and 12, respectively) have been produced. SBS-10Cl glass is homogeneous while SBS-12Cl glass is phase separated. Hence the chlorine loading limit of SBS glass is also taken as 3.17 at%Cl (SBS-10Cl).

Calcium borosilicate glasses (CBS) with 1.28, 2.55, 3.17 and 5.03 at%Cl addition (CBS-*x*Cl, *x* = 4, 8, 10 and 16, respectively) have been produced. Phase separation starts to occur in CBS-10Cl glass and a segregated layer is observed to form on the surface of phase separated CBS-16Cl glass bulk. The loading limit of CBS glass is regarded as being 2.55 at%Cl (CBS-8Cl). Magnesium borosilicate glasses (MBS) with 1.28, 1.92 and 2.55 at%Cl additions (MBS-*x*Cl, *x* = 4, 6 and 8, respectively) have been produced. MBS-6Cl and MBS-8Cl are both phase separated but no segregated layer is formed. The loading limit of MBS glass is regarded as being 1.28 at%Cl (MBS-4Cl).

In comparison, the chlorine loading limit in aluminosilicate glasses is as described below. Barium aluminosilicate glasses (BAS) with 1.80, 3.57, 5.31 and 7.02 at%Cl additions (BAS-*x*Cl, *x* = 5, 10, 15 and 20, respectively) have been produced. Phase

separation occurs in BAS-15Cl and -20Cl glasses during cooling, together with severe cracking throughout glass bodies. The loading limit of BAS glass is regarded as being 3.57 at%Cl (BAS-10Cl). A combined strontium-barium aluminosilicate glass with 5.31 at%Cl (SBAS-15Cl) has also been produced, showing a severe cracking upon casting. Calcium aluminosilicate glasses (CAS) with 1.36, 2.70, 5.30, 6.57, 7.84 and 9.04 at%Cl (CAS-*x*Cl, x = 5, 10, 15, 20, 25, 30 and 35, respectively) have been produced. Slight phase separation is only observed on the surface of CAS-35Cl glass and hence the loading limit of CAS glass is regarded as being 7.81 at%Cl (CAS-30Cl). Magnesium aluminosilicate glasses (MAS) with 1.80 and 3.57 at%Cl addition (MAS-*x*Cl, x = 5 and 10, respectively) have been produced. Both glasses are visibly phase separated and cracked after cooling. Therefore no chlorine could be incorporated into a homogeneous MAS glass in this study.

5.2.1.3. Chlorine retention in glass

Figure 5-1 indicates the correlation between chlorine retention and chlorine addition in borosilicate glasses. A chlorine retention rate range of 60-67% is achieved at initial additions (<1.28 at%Cl) in CBS, SBBS4 and BBS glasses, with little difference among compositions. MBS glass is less capable of incorporating chlorine compared with other borosilicate glasses studied even at 1.28 at%Cl addition.

As the chlorine addition to the glass increases, differences in the chlorine retention among the compositions studied becomes apparent. MBS glass firstly reaches chlorine saturation at 1.92 at%Cl addition in MBS-6Cl glass where the retained chlorine is not higher than that in MBS-4Cl glass. The chlorine retention rate in CBS glass is decreased from 60% to 47% in CBS-8Cl glass and falls further to 36% in the partly crystallised CBS-10Cl glass (glassy part). Meanwhile, SBBS4 glass has a 67% retention rate at 3.80 at%Cl addition in SBBS4-12Cl glass which slightly crystallises during cooling. Further Cl addition (4.72 at%Cl) in SBBS4-15Cl glass results in a segregated layer forming on glass surface; the glass bulk has a slightly lower chlorine content. BBS glass exhibits similar chlorine retention behaviour to SBBS4 glass, retaining 65% chlorine at 3.17 at%Cl addition and 57% chlorine at 4.42 at%Cl, respectively. In the heavily crystallised BBS-15Cl glass (4.72 at%Cl addition), however, the retained chlorine is 2.77 at%Cl, even higher than the homogeneous glass.

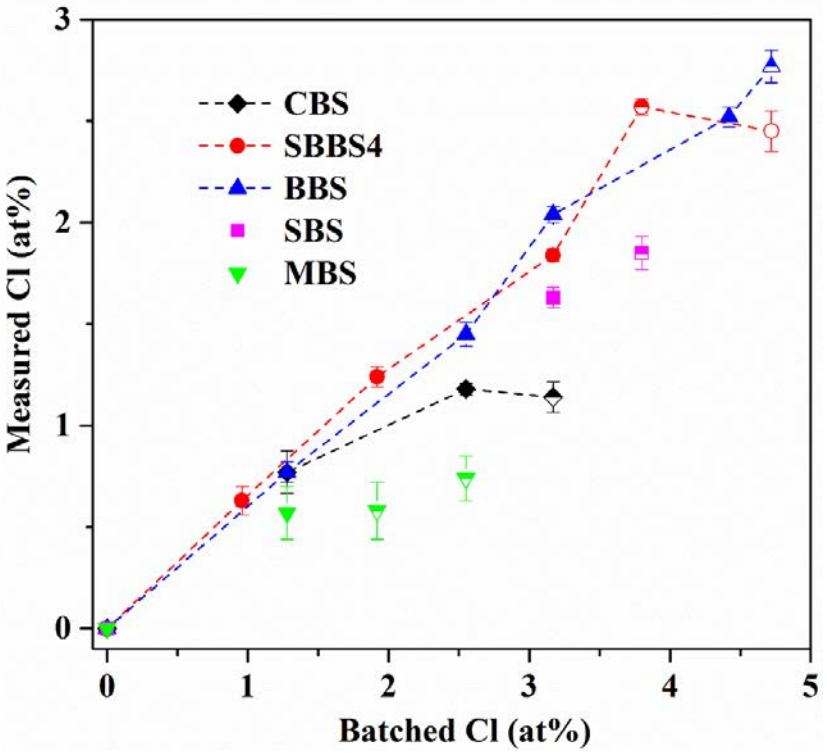

Figure 5-1 Measured Cl content versus the batched Cl content for the borosilicate glasses. Half-filled symbols are for the partly crystallised glasses whereas hollow symbols are for those with a segregated layer, hereinafter the same.

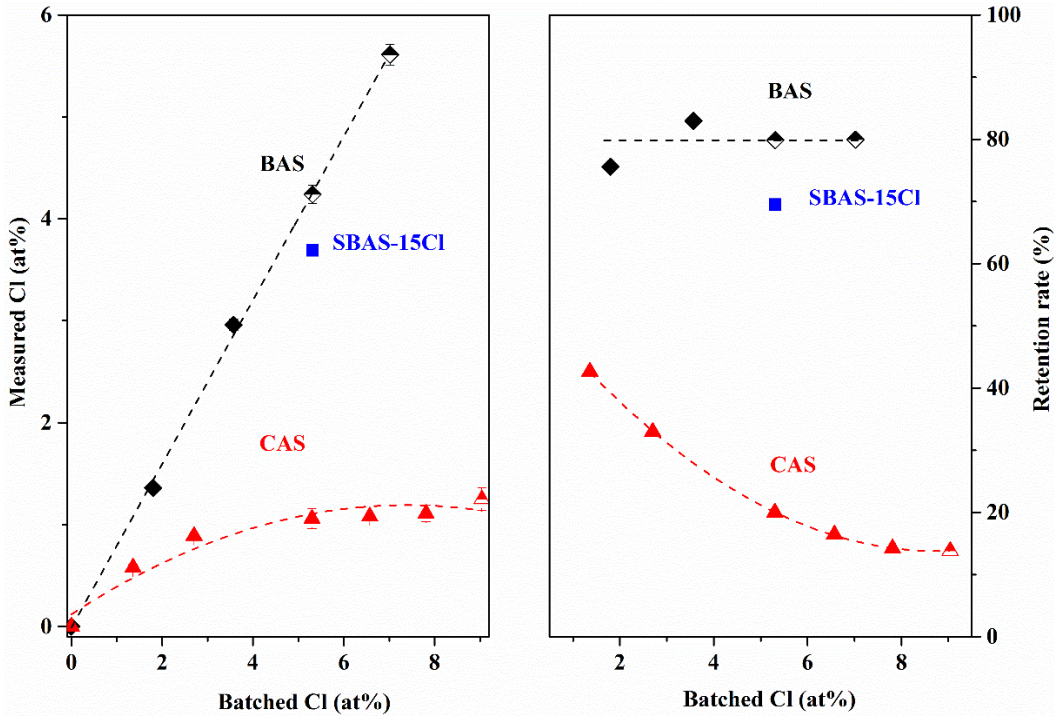

Figure 5-2 Measured Cl content (left) and the chlorine retention rate (right) of BAS and CAS glasses with increasing Cl addition. Dashed lines added to guide the eyes.

Chlorine retention in aluminosilicate glasses is largely dependent on the alkaline earth species in glass. As shown in Figure 5-2, BAS glass has a greater than 80% chlorine retention rate even when it becomes phase separated (BAS-15Cl and BAS-20Cl glasses) whereas CAS has a less than 40% chlorine retention rate at 1.36 at%Cl addition followed by a rapid reduction with increasing Cl additions. SBAS glass with 5.31 at%Cl addition batched as $BaCl_2$ was prepared, showing 3.69 at%Cl content in the final product. The retention rate in SBAS glass is 10% less than in BAS glass. Moreover, MAS glass does not retain chlorine at all although chlorine addition in glass leads to the occurrence of phase separation upon casting.

It is worth noting that BAS glass has a higher chlorine retention than borosilicate glasses which are melted at much lower temperature (1100 ºC). CAS and MAS glasses melted at 1450 ºC however have poor retention ability. It seems that glass composition plays a more important role than melting temperature in determining chlorine retention in glass.

5.2.1.4. Chlorine solubility in glass

Similar to the sulphur solubility, chlorine solubility in a glass composition is defined as the chlorine content retained in the glass at the chlorine loading limit when phase separation occurs. Hence in the borosilicate glass series, the measured chlorine contents in BBS-14Cl, SBBS4-10Cl, SBS-10Cl, CBS-8Cl and MBS-4Cl glasses are regarded as the chlorine solubility in BBS, SBBS4, SBS, CBS and MBS glasses, respectively. In the aluminosilicate glass series, however, MAS glass has no chlorine solubility as it does not retain chlorine at all, whereas the chlorine solubilities for CAS and BAS glasses are obtained from the CAS-30Cl and BAS-10Cl glasses, respectively. As the chlorine retention rate in CAS glass is very low compared to that in BAS glass, BAS glass exhibits a much higher chlorine solubility than CAS glass even though its apparent loading limit before phase separation is much lower.

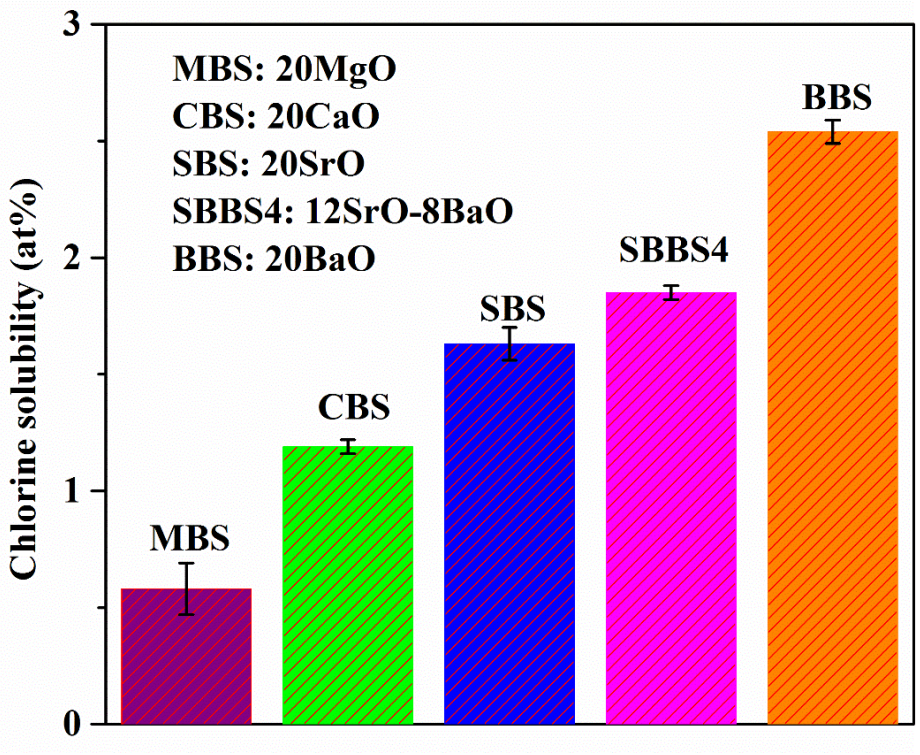

Figure 5-3 Chlorine solubility in borosilicate glass compositions ($15Na_2O$-20MO-$15B_2O_3$-$50SiO_2$, mol%).

As shown in Figure 5-3, when other components are kept constant, chlorine solubility in borosilicate glasses increases in the order Ba > 0.4Ba + 0.6Sr > Sr > Ca > Mg: while BBS glass shows a chlorine solubility of 2.54 at%Cl, MBS glass only shows a chlorine solubility of 0.57 at%Cl. Moreover, SBBS4 glass exhibits a higher chlorine solubility than SBS glass though both limit glasses studied were loaded with 3.17 at%Cl. Equimolar replacement of larger alkaline earths for smaller ones seems to be most beneficial for chlorine solubility in borosilicate glass.

Meanwhile, as mentioned above, chlorine solubility in aluminosilicate glasses shows a very different behaviour: BAS glass has a chlorine solubility of 2.96 at%Cl following a 3.57 at%Cl addition. This value is much higher than that in CAS glass (1.11 at%Cl) which, however, is able to remain homogeneous with a 7.81 at%Cl addition. SBAS-15Cl glass contains 3.69 at%Cl at 5.31 at%Cl addition, but the glass was heavily cracked during casting. MAS and SAS (expected) glasses do not have chlorine solubility because their melting temperature is higher than the boiling point of $MgCl_2$

(1412 ºC) and $SrCl_2$ (1250 ºC). At the temperature of melting, all chloride ions (may) have been evaporated from melt with alkaline earth cations.

5.2.1.5. Chlorine solubility and chlorine capacity

It must be pointed out that the chlorine solubility as defined here does not give the maximal amount of chlorine that can be incorporated into glass network. Conversely, chlorine content in the glassy region of many partly crystallised glasses can be higher than the defined solubility. Especially in BAS glass, chlorine content linearly increases in the phase separated BAS-15Cl and BAS-20Cl glasses, which indicates that maximal chlorine capacity in the glass network has not been reached when phase separation occurs. However, these glasses are not fully homogeneous and their chlorine content is not recognised as the chlorine solubility in this study.

In addition, in the borosilicate glasses with a segregated chloride layer (SBBS4-15Cl and CBS-16Cl), the chlorine content in glass bulk is lower than the value in glasses with less chloride addition (*e.g.* SBBS4-12Cl and CBS-10Cl). It suggests that there may be a maximum of chlorine content along with chlorine additions.

5.2.2. Chloride incorporation in glass

5.2.2.1. Density

The density changes with chlorine incorporation in CBS, SBBS4 and BBS glass series are plotted in Figure 5-4. Within the compositions investigated, glass density conforms to a similar fashion of an initial increase followed by a gradual decline with increasing chlorine content in glass. The slow downward tendency of glass density continues to the glasses which are partly crystallised or which contain a segregated layer (densities were measured after removal of the segregated layer). For CBS glass the glass density is lower than the base glass as chlorine incorporation approaches saturation while for SBBS4 and BBS glasses the glass density is still higher than the base glass even though it is decreasing as chlorine incorporation increases.

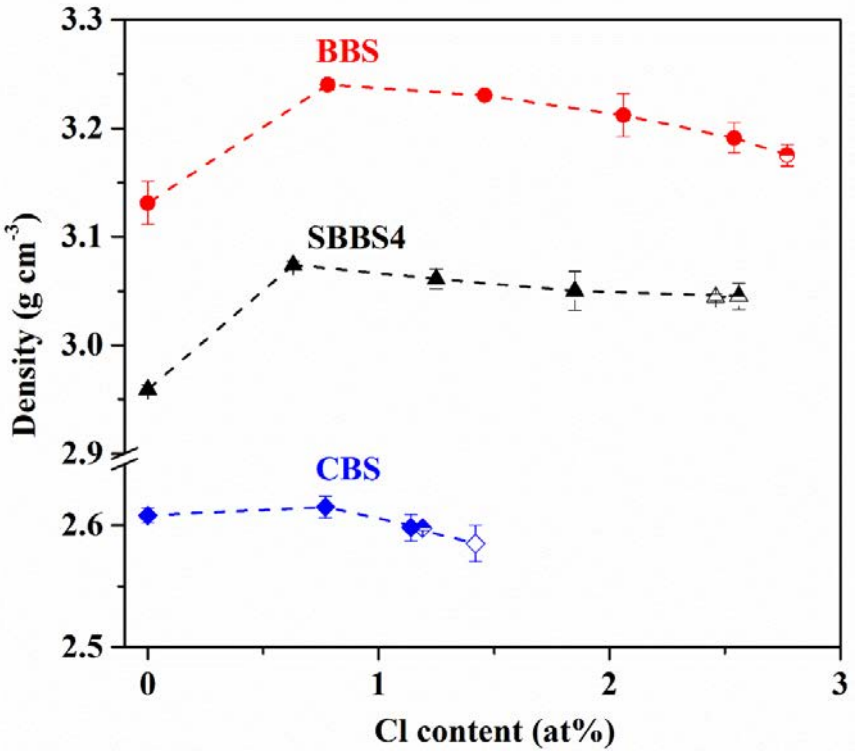

Figure 5-4 Density changes with chlorine incorporation in borosilicate glasses (● BBS series, ▲ SBBS4 series and ♦ CBS series).

The density changes of CAS and BAS glasses with increasing chlorine contents are plotted in Figure 5-5. Similar to borosilicate glasses, these two aluminosilicate glass series also reveal a density maximum at initial chlorine incorporation followed by a smooth reduction at higher chlorine contents. In particular the glass density continues decreasing in BAS-15Cl and BAS-20Cl glasses in spite of severe phase separation. Given that chlorine content in BAS-15Cl and BAS-20Cl glasses is still increasing, the density reduction in them can be deemed as an outcome of continued chlorine incorporation into the glass network combined with phase separation. Meanwhile, although the loading limit of chlorine in CAS glass is high, the retained chlorine content is in fact relatively low. Consequently, the density change in CAS glass is not that significant compared with BAS glass.

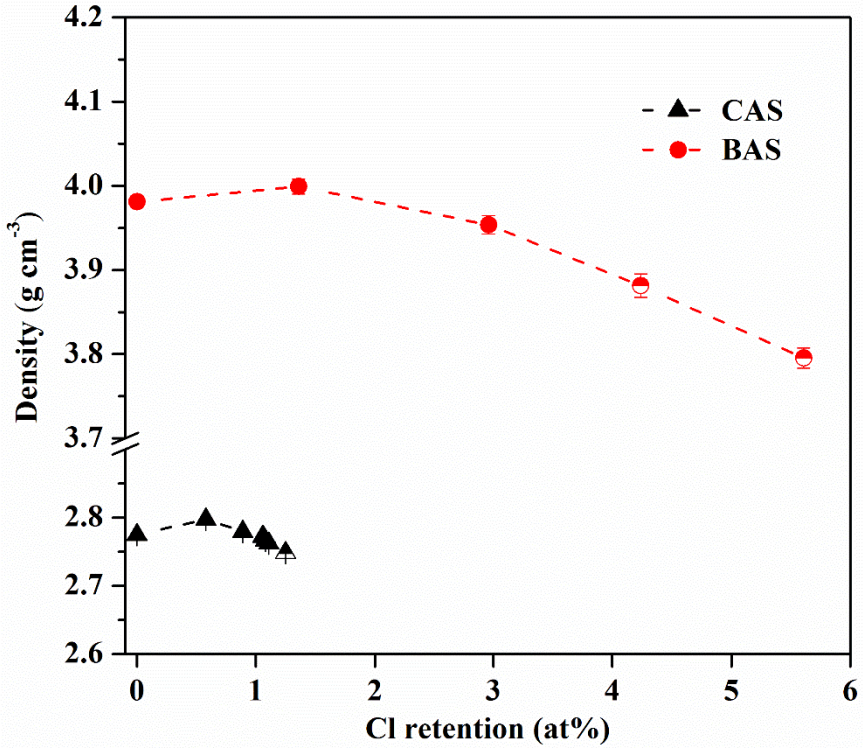

Figure 5-5 Density changes with chlorine incorporation in aluminosilicate glasses (● BAS series and ▲ CAS series).

In summary, density maxima can be observed in both borosilicate and aluminosilicate glasses with a small amount of chlorine incorporation. Further chlorine incorporation leads to steadily decreased glass densities which continues even when the glass becomes phase separated.

5.2.2.2. XRD

The XRD patterns of borosilicate glasses with different chloride additions are shown in Figure 5-6 (MBS and CBS) and Figure 5-7 (SBBS4 and BBS), respectively. The glasses with subcritical chloride additions have completely amorphous XRD patterns, showing two broad humps between 20 and 60 º2θ. Crystalline peaks are visible in the patterns for the partially crystallised glasses and the glasses with a segregated layer. The separated phase in partially crystallised glasses such as BBS-15Cl, CBS-16Cl bulk, MBS-6Cl and MBS-8Cl is identified to be quartz (PDF4#00-046-1045) whereas there are no conspicuous peaks in the patterns of SBBS4-12Cl, SBS-12Cl and CBS-10Cl glasses which are also inhomogeneous. In BBS-15Cl and MBS-8Cl glasses, there is also evidence for the existence of cristobalite (PDF4#00-039-1425, strongest peak

at $2\theta = 21.8^{o}$). Moreover the segregated layer forming on the surface of CBS-16Cl and SBBS4-15Cl glasses, which was removed from glass bulk surface and collected for analysis, is identified to be NaCl (PDF#00-005-0628) in both cases.

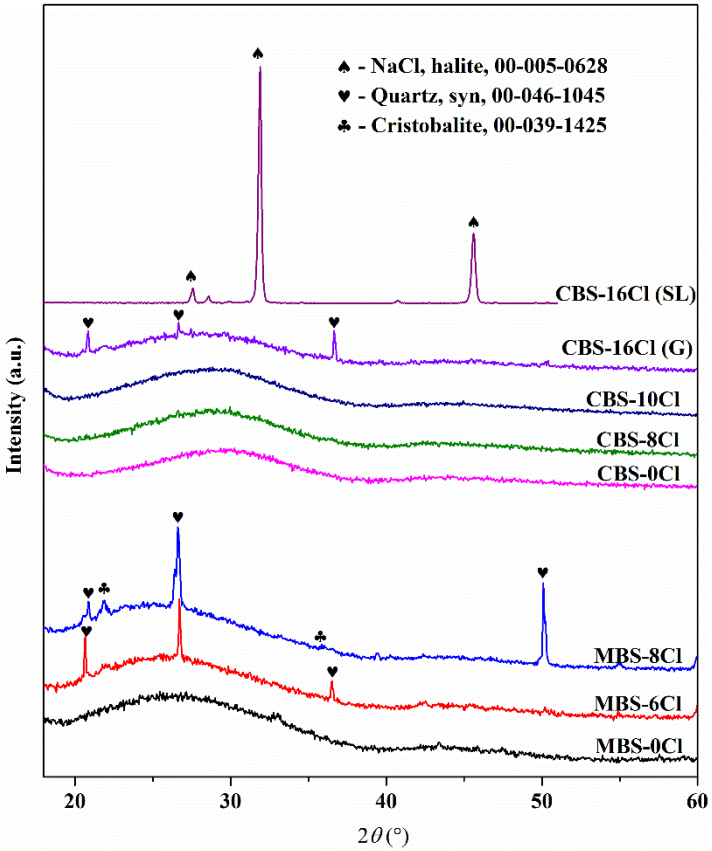

Figure 5-6 XRD patterns of MBS and CBS glasses with chlorine. CBS-16Cl (G) and (SL) means the glass bulk and segregated layer of CBS-16Cl sample, respectively.

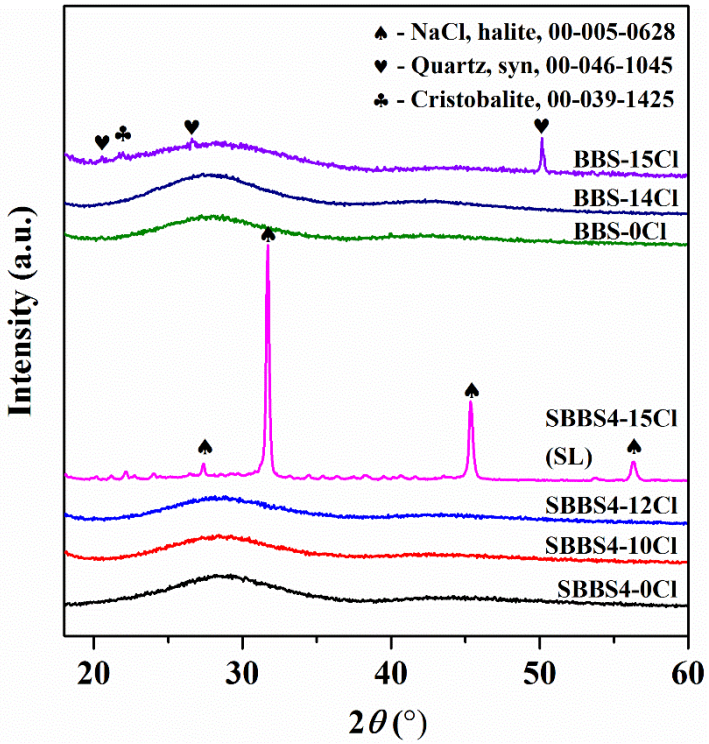

Figure 5-7 XRD patterns of SBBS4 and BBS glasses with chlorine. SBBS4-15Cl (SL) is the segregated layer removed from the surface of SBBS4-15Cl sample.

The XRD patterns for the aluminosilicate glasses are displayed in Figure 5-8. BAS-5Cl and BAS-10Cl glasses are completely amorphous whereas BAS-15Cl and BAS-20Cl glasses, which phase separated during cooling, show a number of crystalline peaks in XRD patterns. These peaks are in accordance with the patterns for barium aluminosilicate ($BaAl_2Si_2O_8$) phases with the best agreement being with the hexagonal form (hexacelsian, PDF4#00-028-0125). However, due to the limited number of peaks and the effects of glass matrix, accurate phase identification cannot be made from the current XRD results. The prepared CAS glasses all have amorphous XRD patterns even though some phase separated material can be observed in CAS-35Cl glass. It is interesting that, even though no chlorine is retained, MAS-5Cl and MAS-10Cl glasses are phase separated. The crystalline peaks are compatible with the patterns of a number of magnesium silicate or aluminosilicate crystals and agree best with that for quenched pyrope ($Mg_3Al_2Si_3O_{12}$, PDF4#00-035-0310).

According to the XRD results, chlorine is not present in the separated phase of either borosilicate glasses or aluminosilicate glasses unless there is a segregated layer formed

on the glass surface. The factor that limits chlorine solubility in these glasses is not the capacity for chlorine incorporation, but the tendency of crystallisation of glass network components: quartz and/or cristobalite in borosilicate glasses and aluminosilicate salts in aluminosilicate glasses. In contrast, the segregated layer is composed of NaCl regardless of glass composition.

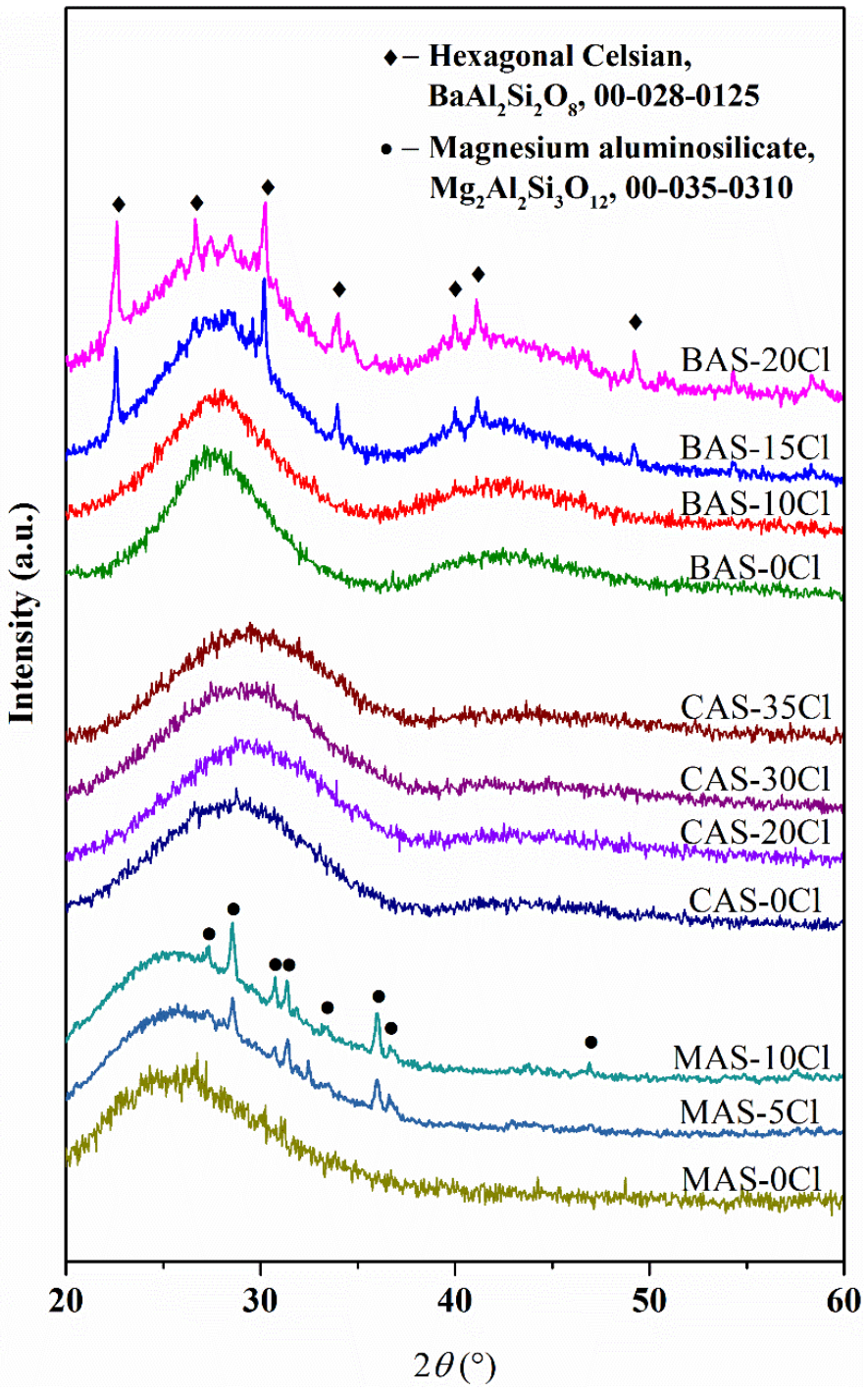

Figure 5-8 XRD patterns of aluminosilicate glasses with different chlorine additions.

5.2.2.3. DTA

Figure 5-9 presents the DTA curves of SBBS4 glass with different chlorine additions and Figure 5-10 shows the correlation between T_g and the real Cl^- content. The glasses show good thermal stability until T_g no matter whether they are homogeneous or not. T_g slightly decreases with initial incorporation of chlorine until SBBS4-6Cl glass (1.25 at%Cl), maintains unchanged in SBBS4-10Cl glass (1.85 at%Cl), followed by a further decline in SBBS4-12Cl glass (2.56 at%Cl) which is phase separated. Moreover, in the inhomogeneous SBBS4-12Cl and SBBS4-15Cl glasses, some prominent endothermic peaks appear between 700 and 800 ºC, which are probably due to the melting of chlorides (melting point of NaCl is 801 ºC, but can be lowered with the coexistence of other cations) in glass.

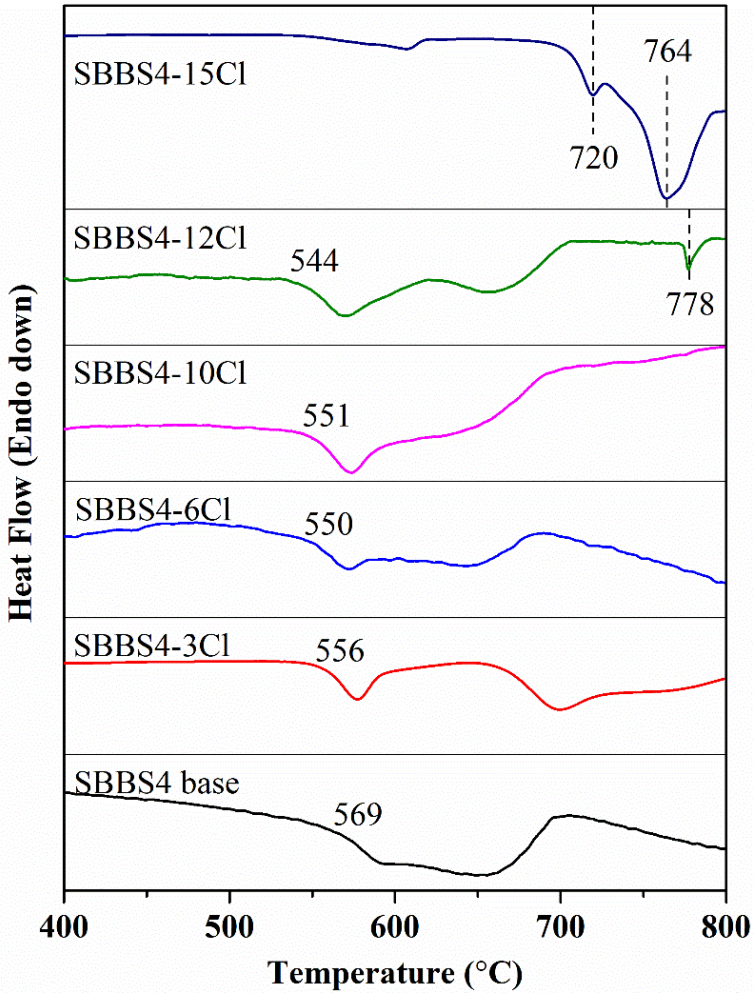

Figure 5-9 DTA curves of chlorine-containing SBBS4 glasses [mol%, $50SiO_2$-$15B_2O_3$-$(15-x/2)Na_2O$-12SrO-8BaO-xNaCl, x = 0, 3, 6, 10, 12 and 15, respectively]

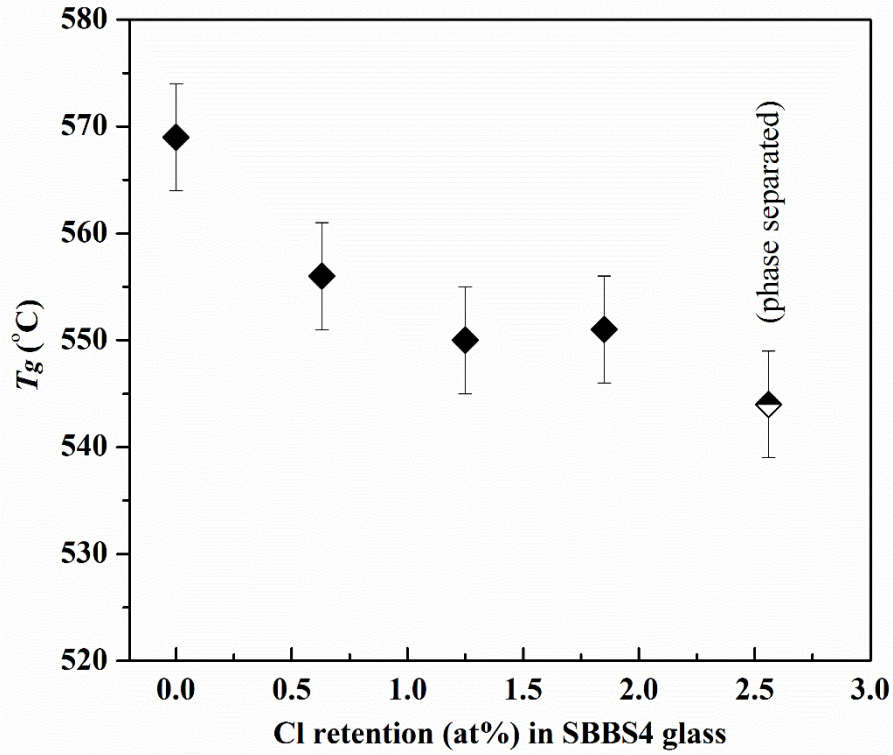

Figure 5-10 T_g change with increasing Cl content retained in SBBS4 glass.

Figure 5-11 presents the DTA curves of BAS glass with increasing chlorine additions and Figure 5-12 shows the T_g change with the retained chlorine contents. Likewise in SBBS4 glass, chlorine incorporation in BAS glass also decreases T_g from 662 ºC to 631 ºC in BAS-5Cl glass (1.36 at%Cl) initially, then maintains unchanged until BAS-15Cl glass (4.24 at%Cl) which is slightly phase separated, and followed by a plunge to 605 ºC in BAS-20Cl glass (5.61 at%Cl) which is heavily crystallised. There is also an obvious downward tendency for the first exothermic peak, as plotted in Figure 5-12, showing that the first crystallisation temperature of glass T_{c1} decreases with increasing chloride content from 828 ºC in base glass to 741 ºC in BAS-20Cl glass. Meanwhile, there is an intense exothermic peak starting from 900 ºC in all these glasses, the onset of which initially decreases between 0 and 2.96 at%Cl incorporation and then increases in BAS-15Cl and BAS-20Cl glasses. The mechanism of this exothermic reaction is likely related to the phase transition between aluminosilicate phases as highlighted in the high temperature XRD results in Chapter 6. In addition, there is a small exothermic peak occurring at 690 ºC in BAS-15Cl glass, probably because of the phase transition of hexacelsian at this temperature (Xu *et al.* 2002).

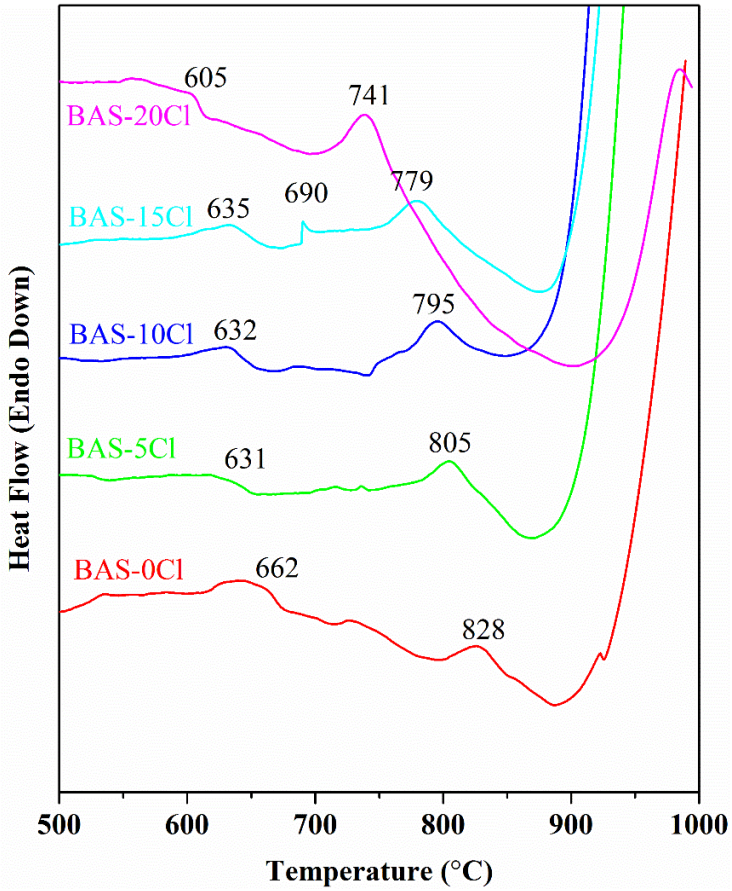

Figure 5-11 DTA curves of BAS glass with increasing chlorine additions.

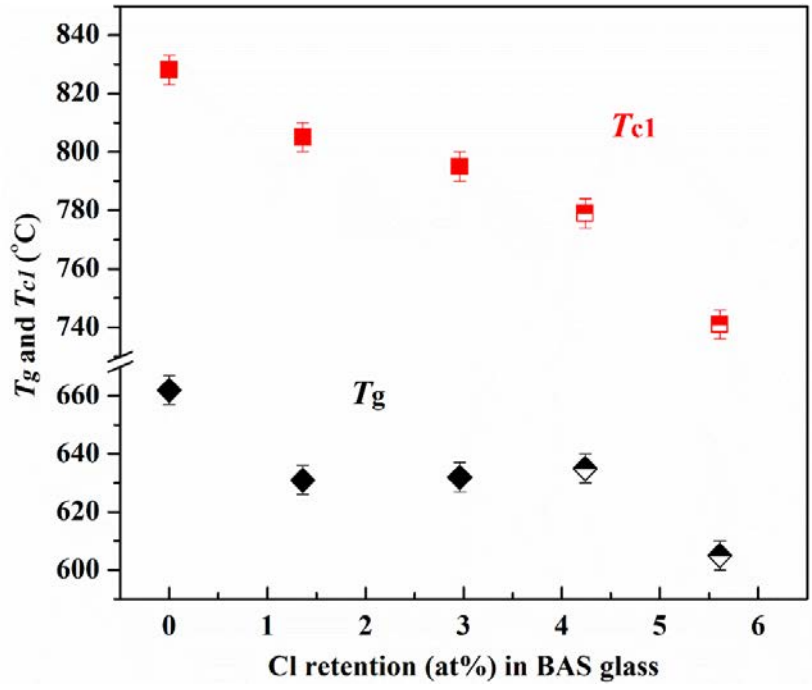

Figure 5-12 T_g change with increasing Cl content retained in BAS glass. The half-filled symbols are for the partly crystallised glasses.

5.2.2.4. Raman spectroscopy

The incorporation of chlorine in borosilicate glass network does not result in any new bands in the Raman spectra, as shown in Figure 5-13 (*a*) and (*b*). Only one notable change is observed that the band at 530 cm^{-1} in base glass shifts to ~570 cm^{-1} when chloride is incorporated and this does not further change with increasing chloride content.

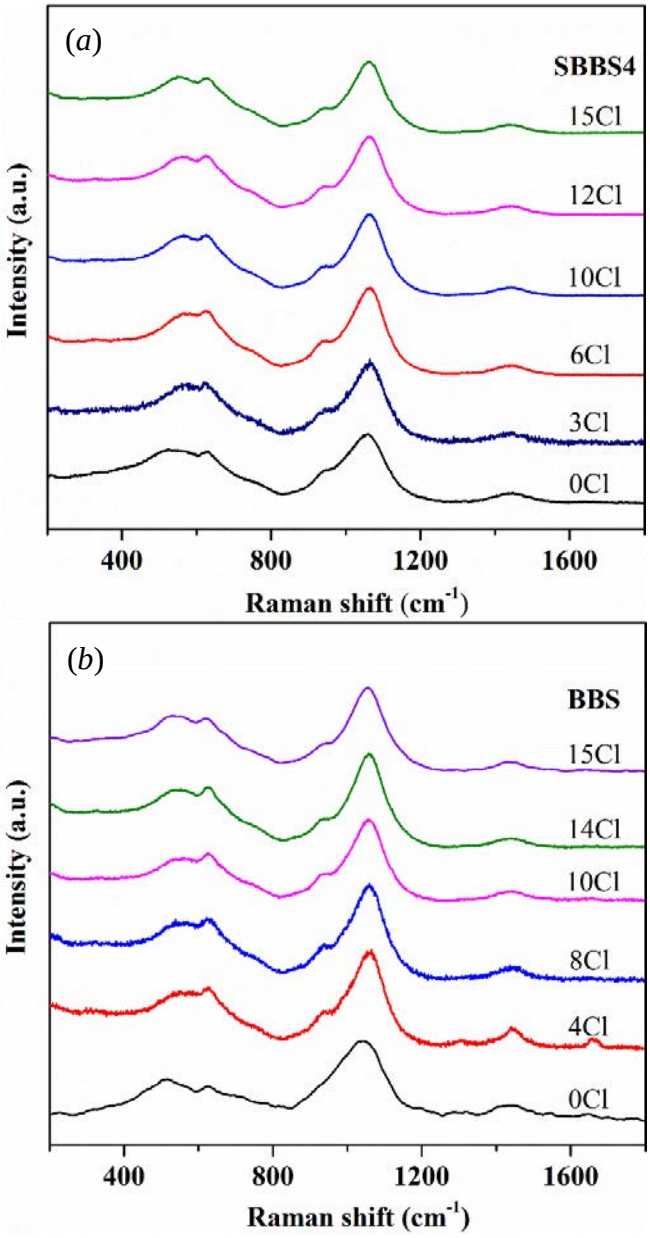

Figure 5-13 Raman spectra of (*a*) SBBS4 and (*b*) BBS glasses with chlorine additions.

The chloride bonds are not Raman active, given the above hypothesis that Cl^- are only associated with metallic cations in glass (Zhu 2006, Sun 2012), thus the incorporation of Cl^- in glass network cannot be directly assessed. The effects of Cl^- incorporation on glass network are studied with the Q_n proportions estimated from the deconvolution of 800-1200 cm^{-1} band assigned to Si-O stretching modes. The deconvolution procedures have been described in Section 4.2.2.4 so are not presented here.

Q_n proportions indicate the depolymerisation extent of the glass. Figure 5-14 (*a*) and (*b*) shows the results of deconvolution in SBBS4 and BBS glasses, respectively. Chlorine incorporation in SBBS4 glass initially slightly decreases Q_3 and increases Q_2 proportions, which signifies a small amount of depolymerisation of the glass network provided that Q_4 proportion is less than 2% throughout the samples. Whereas, further chlorine incorporation leads to higher Q_3 and lower Q_2 proportions, indicative of a more polymerised glass network. As for BBS glass, chlorine incorporation also initially decreases Q_3 and increases Q_2 ratios; however, increasing chlorine incorporation does not cause any change in Q_2 and Q_3 proportions until BBS-15Cl glass, in which phase separation occurs heavily, shows a more polymerised network.

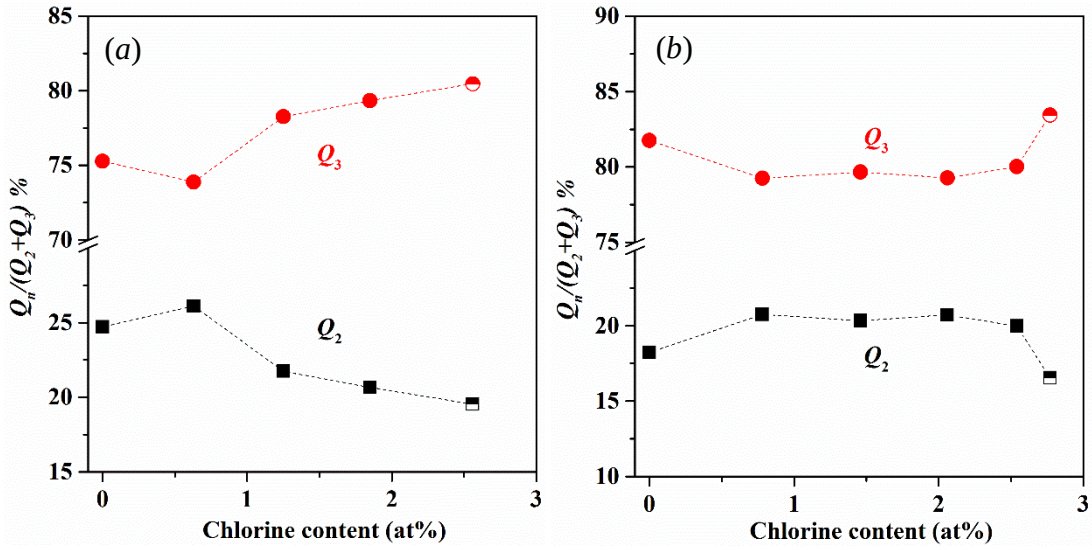

Figure 5-14 Q_2 and Q_3 proportions deconvolved from Raman spectra of (*a*) SBBS4 and (*b*) BBS glasses, respectively, with increasing chlorine content.

Similar to borosilicate glasses, aluminosilicate glasses (CAS and BAS glasses) do not show any notable new Raman bands with chlorine incorporation (Figure 5-15).

However, as phase separation occurs, a number of sharp peaks emerge in BAS-15Cl and BAS-20Cl (Figure 5-15*a*). These peaks agree very well with the Raman peaks of crystalline hexacelsian (Kremenovic *et al.* 2003), indicating that the separated phase in BAS-15Cl and BAS-20Cl glasses is hexacelsian.

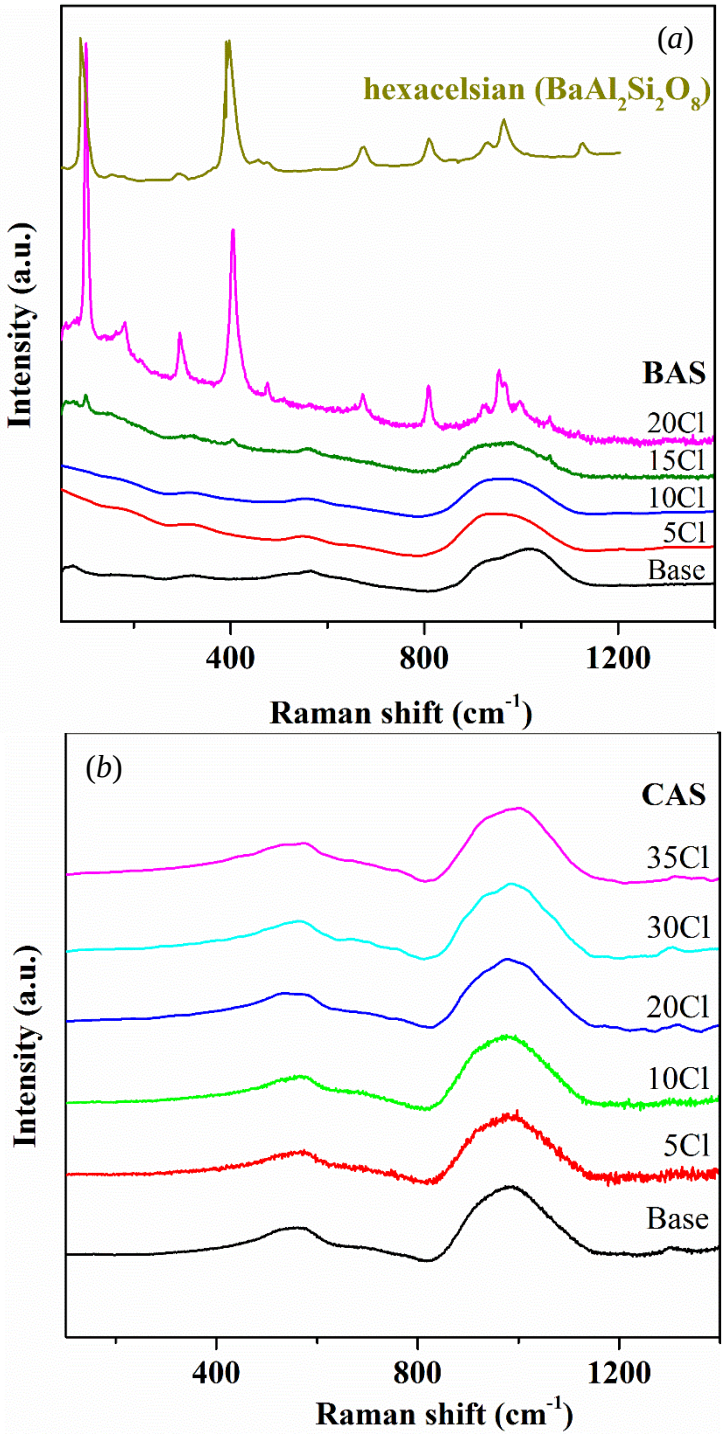

Figure 5-15 Raman spectra of (*a*) BAS and (*b*) CAS glasses with chlorine additions. Raman spectrum of hexacelsian is extracted from Kremenovic *et al.* (2003).

Raman spectra of CAS glasses (Figure 5-15*b*) show insignificant change with chlorine additions, which is in accordance with visible observation and XRD results that phase separation does not occur until CAS-35Cl glass. Only a slight shift to higher frequency of 800-1200 cm^{-1} broad band can be observed with increasing chlorine additions. It must be mentioned that the chlorine really incorporated into glass network is very low though the batched amount is high, this may be the reason for the limited change in the Raman spectra.

The polymerisation tendencies of BAS and CAS glasses with chlorine incorporation are analysed with the deconvolution of 800-1200 cm^{-1} Raman band which is assigned to Si-O symmetric stretching modes; results of Q_n proportions and average Q_n numbers are shown in Figure 5-16 and Figure 5-17, respectively. In both series, initial chlorine incorporation results in increased average Q_n numbers, with increasing Q_4 proportions at the expense of Q_2 and Q_3, which indicates a polymerisation of network. In BAS glass, this polymerisation process continues in BAS-10Cl glass where 2.96 at%Cl is incorporated while in the slightly crystallised BAS-15Cl glass Q_n proportions significantly changes and average Q_n number begins to decrease. In CAS glass, after the initial polymerisation, further chlorine incorporation results in increasing Q_1 and Q_2 proportions and decreasing Q_3 and Q_4 proportions, contributing to a decreased average *n* and a depolymerised glass network.

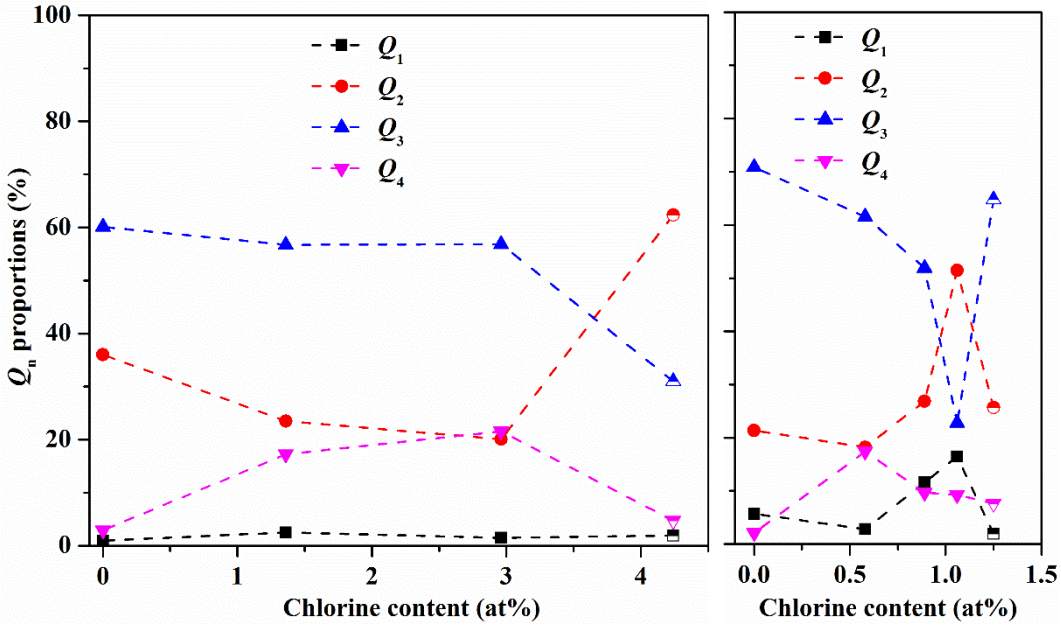

Figure 5-16 Q_n proportions deconvolved from Raman spectra of (*a*) BAS and (*b*) CAS glasses with increasing chlorine incorporation.

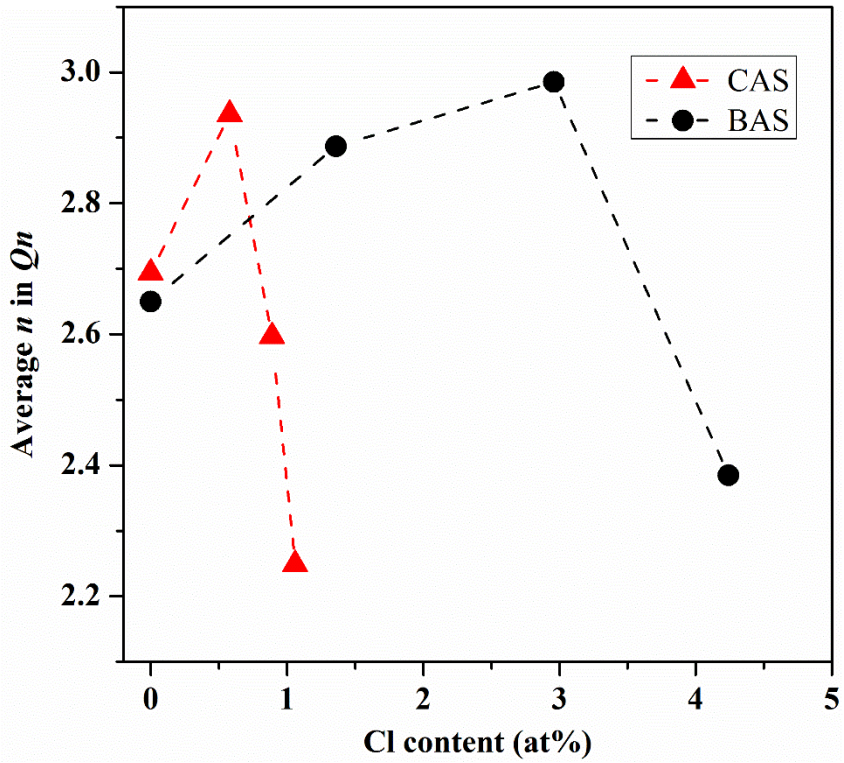

Figure 5-17 Average *n* in Q_n of CAS and BAS glasses, calculated from deconvolution of the 800-1200 cm^{-1} Raman region.

5.2.2.5. FTIR

The absorbance FTIR spectra of CBS and SBBS4 glasses with increasing chlorine additions are shown in Figure 5-18. As with the Raman spectra, chlorine incorporation does not create any new band in FTIR spectra except some sharp peaks are observed in the SBBS4-15Cl sample which is a mixture of glassy bulk and segregated layer.

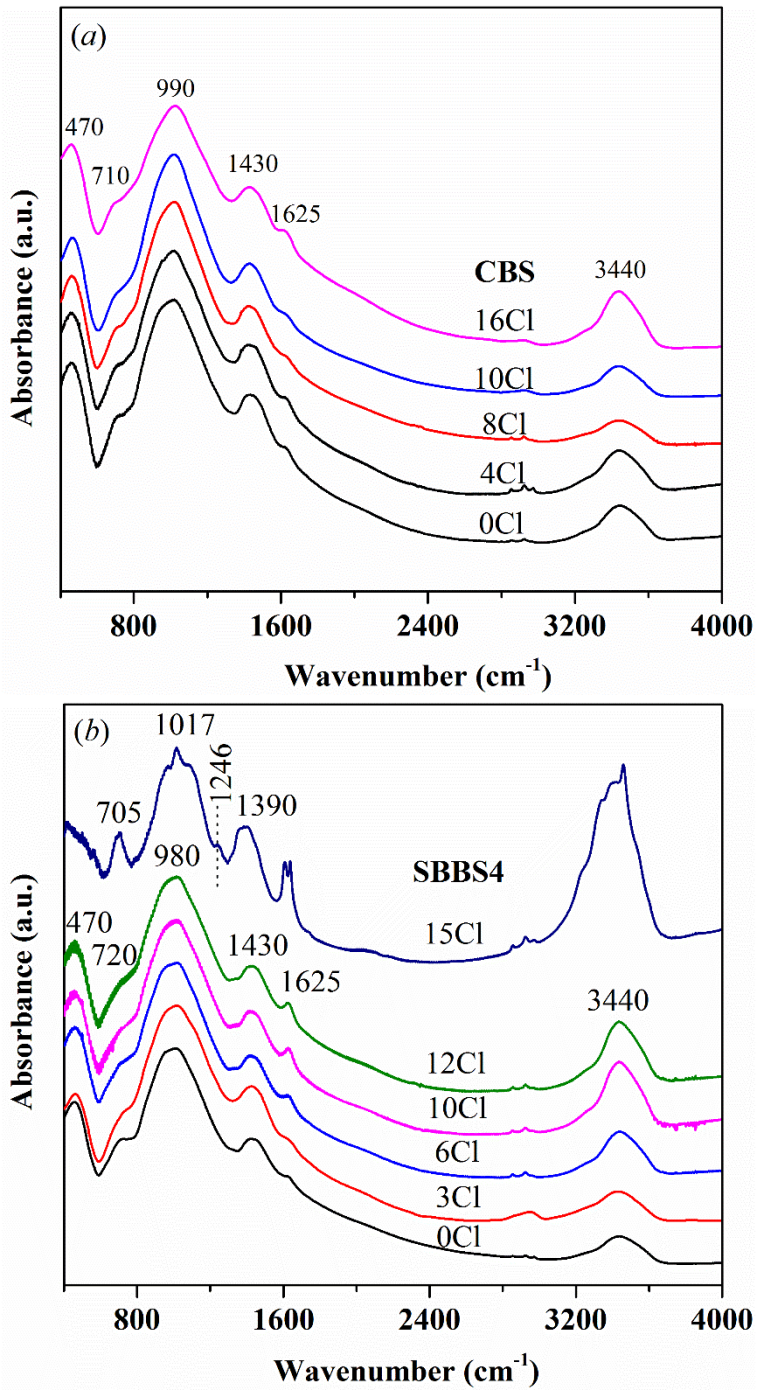

Figure 5-18 FTIR spectra of (*a*) CBS and (*b*) SBBS4 glasses with chlorine.

Nevertheless, an effect of chlorine incorporation on the FTIR spectrum can be seen in the shift of existing bands that are assigned to glass network. Figure 5-19 plots the change of IR frequencies of ~470 cm^{-1} band (assigned to Si-O-Si bending vibrations) and ~980 cm^{-1} band (assigned to Si-O-Si stretching vibrations) along with increasing chlorine incorporation in CBS and SBBS4 glasses, respectively. In both glass series, the ~980 cm^{-1} band shifts to a higher frequency with initial chlorine incorporation and then shifts to a lower frequency with further chlorine incorporation. Conversely, the ~470 cm^{-1} band shifts to lower frequency with initial chlorine incorporation and a higher frequency with further incorporation.

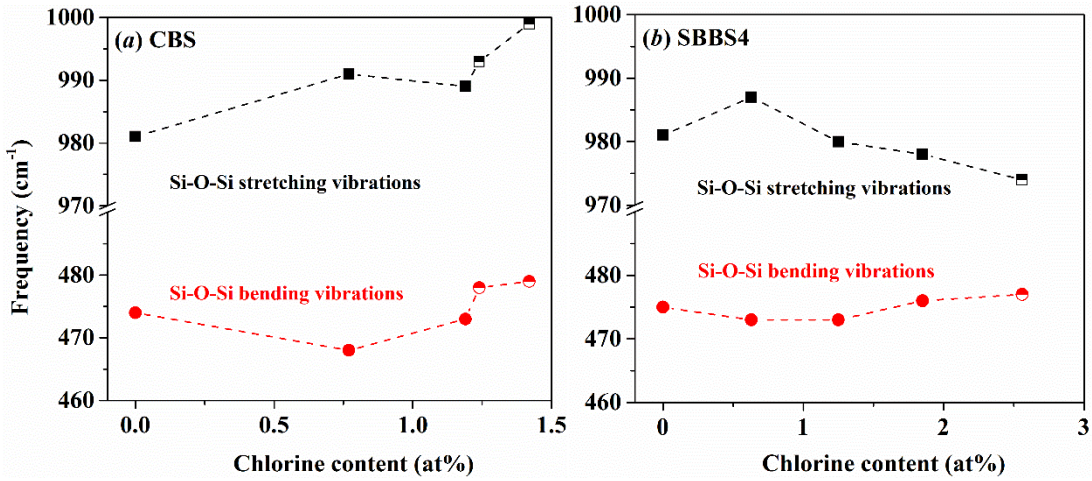

Figure 5-19 Frequency shifts of peaks of FTIR spectra of (*a*) CBS and (*b*) SBBS4 glasses with increasing chlorine content, respectively.

In addition, the split and sharp peaks of SBBS4-15Cl sample at 1625 and 3440 cm^{-1}, which are assigned to O-H-O scissor motion and O-H stretching vibration of molecular water, indicate that the sample has absorbed some water after preparation. Moreover, the intense peaks at 705, 1017 and 1246 cm^{-1} in the same sample are in good agreement with the IR frequencies of some borate glasses described by Gautam *et al.* (2012): the 705 cm^{-1} band can be assigned to B-O-B bending vibrations, the 1017 cm^{-1} band can be assigned to B-O stretching vibrations in BO_4 unit sand 1246 cm^{-1} can be assigned to B-O stretching vibrations in BO_3 units. The 470 cm^{-1} band assigned to Si-O-Si bending vibrations also disappears in the SBBS4-15Cl sample.

FTIR spectra of BAS glass with different chlorine additions are shown in Figure 5-20. No band is created due to chlorine incorporation whereas in the phase separated BAS-15Cl and BAS-20Cl glasses' spectra a shoulder at 670 cm^{-1} appears. Together with the Raman observation, this band is probably assigned to Si-O-Al stretching vibrations (662 cm^{-1}) of hexacelsian (Aronne *et al.* 2002); however, other characteristic bands (481, 934 and 1223 cm^{-1}) that are assigned to hexacelsian are not observed here, probably because of the severe overlapping with the bands assigned to the glass network.

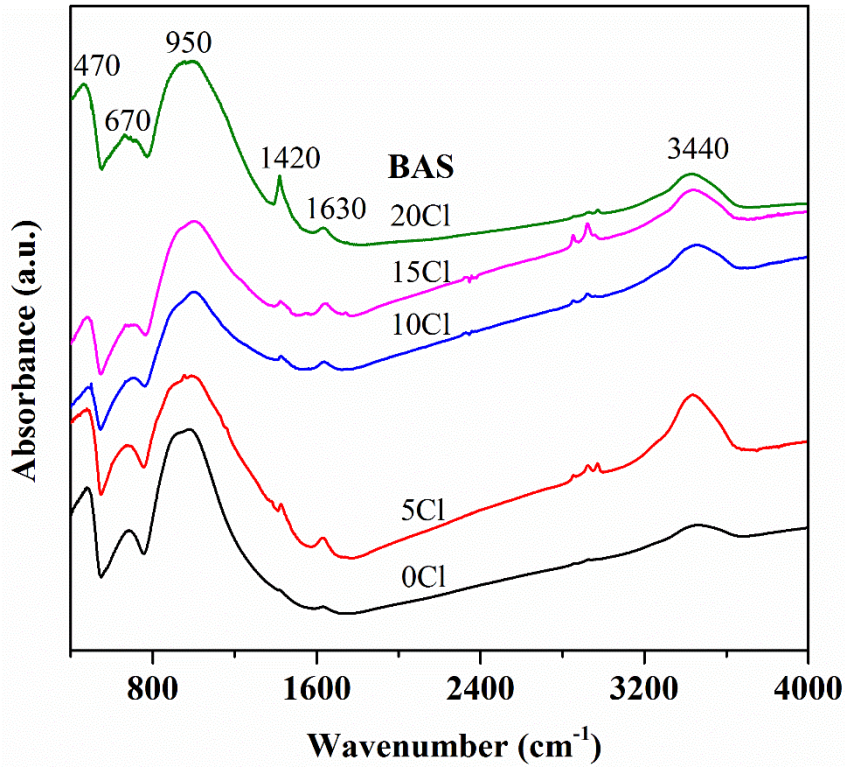

Figure 5-20 FTIR spectra of BAS glass with increasing chlorine additions.

Generally speaking, chlorine incorporation does not result in new bands either in the Raman or FTIR spectra. This is due to the occurrence of metal chloride ionic bonds in the investigated glasses, *e.g.* Na-Cl or Ba-Cl, being transparent in green light or infrared illumination. The absence of bands assigned to Si-Cl bond (main band at ~610 cm^{-1}, referred to infrared spectrum of $SiCl_4$, CAS No.10026-04-7, from the National Institute of Standards and Technology, NIST, USA) suggests that chlorine does not

directly connect with silicon in these glasses to form a structural unit, but associates with network modifying cations like an NBO does in glass network.

5.2.3. Microstructure

5.2.3.1. SEM

The separated phases occurring in those partly crystallised glasses have been observed by SEM. Figure 5-21 (*a*) and (*b*) are the backscattered electron images of MBS-6Cl and MBS-8Cl glasses, respectively, both showing the features of separated particles within glass matrix. The particles are 100-200 μm in diameter, randomly dispersed and irregularly shaped. Almost all the particles are cracked internally and some cracks even extend to the surrounding glass matrix. EDX analysis for the particles and glass base suggests that the particles are only composed of Si and O with a stoichiometric ratio close to 1:2 (SiO_2), whereas Cl, Na and Mg are only present in the glass region of the MBS-8Cl sample.

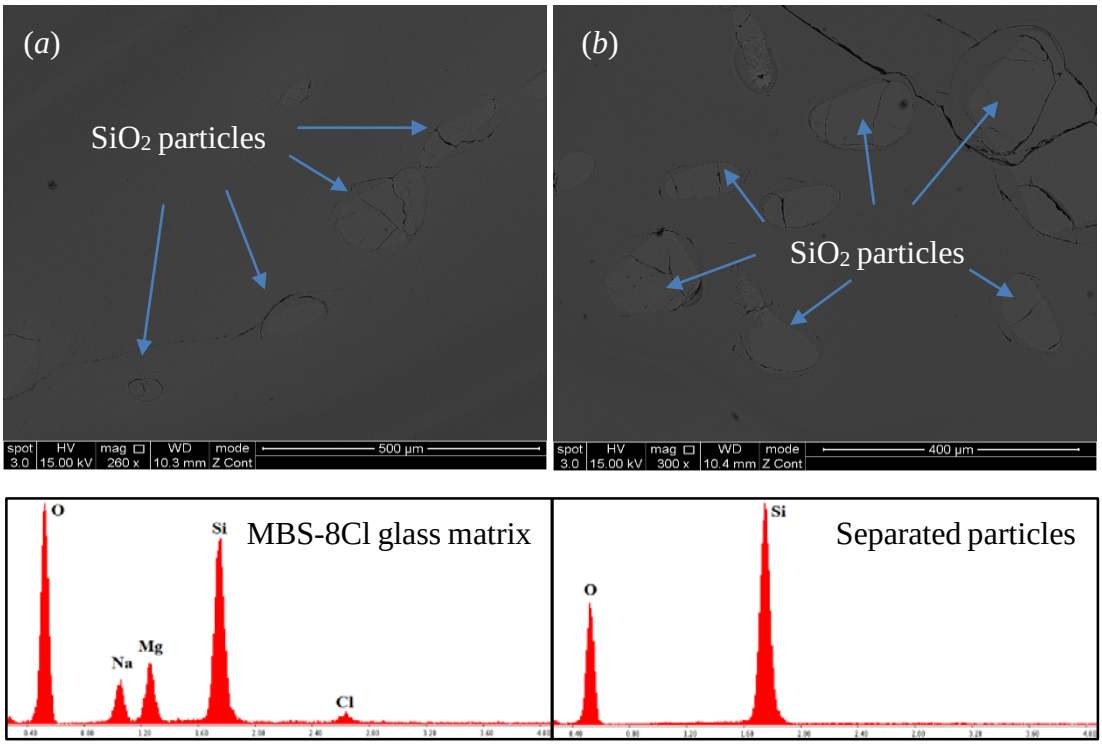

Figure 5-21 BSE images of separated particles in (*a*) MBS-6Cl and (*b*) MBS-8Cl glasses. Below are the EDX spectra of MBS-8Cl glass matrix and separated particles, respectively.

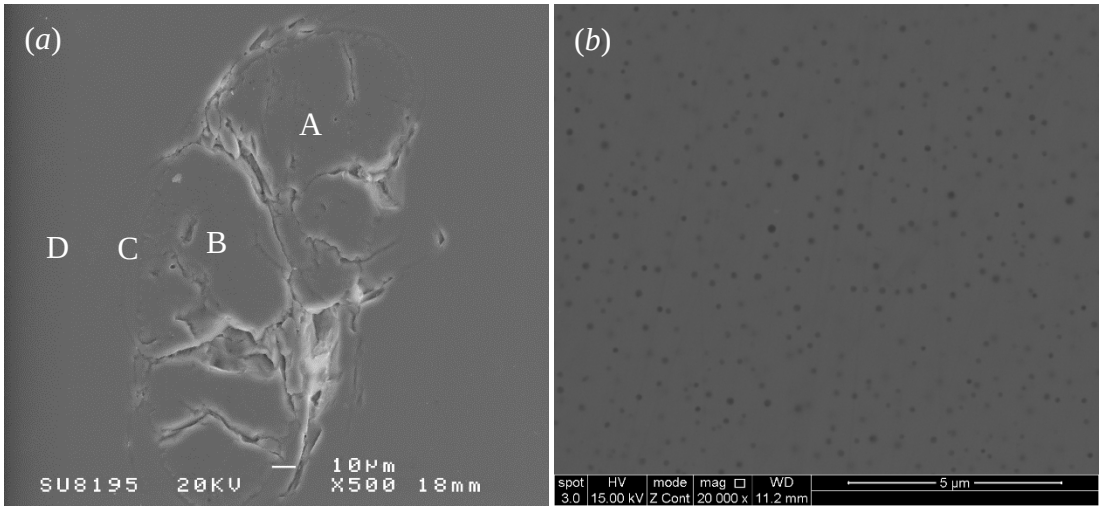

Figure 5-22 (*a*) SE image of glass bulk of CBS-16Cl sample and (*b*) BSE image of glassy region of BBS-15Cl glass.

Large particles (100-200 µm in diameter) can also be observed in the glass bulk of CBS-16Cl sample, one example shown in Figure 5-22(*a*). They are randomly shaped and distributed within glass. EDX analysis (Table 5-3) suggests that the particles are SiO_2 while Cl, Na and Ca are only present in glass matrix. Figure 5-22(*b*) exhibits the dispersion of separated particles in BBS-15Cl glass. Unlike the particles in MBS and CBS glasses, the particles in BBS-15Cl glass are much smaller (100-200 nm in diameter). They are formed as spheres and randomly distributed within the crystallised region. These particles are too small for quantitative EDX analysis.

Table 5-3 EDX results (at%) of different regions of CBS-16Cl glass bulk as shown in Figure 5-22(*a*).

Region	Si	Na	Ca	Cl	O
A	31.25	0	0	0	68.75
B	31.11	0	0	0	68.89
C	19.04	5.91	6.23	1.16	67.66
D	18.17	6.42	6.82	1.41	67.18

Based on the morphologies of separated particles, it is likely that those in MBS and CBS glasses are from undissolved SiO_2 from the glass batches while those in BBS

glass are formed within glass matrices during cooling; the mechanisms of phase separation differ among borosilicate glass compositions.

Figure 5-23 shows BSE images of phase separated MAS and BAS glasses with excess chlorine additions. According to Figure 5-23(*a*) and (*b*), the separated phase in MAS-5Cl and MAS-10Cl glasses is tabular and cracked and there is little difference between these two glasses. EDX results (Figure 5-24(*a*)-(*d*)) confirm that chlorine is neither in the glass matrix nor in the separated phase, although chlorine addition is believed to be the primary reason for phase separation. The separated phase contains more Si and Al and slightly less Mg than the glass matrix, with a stoichiometry close to that of magnesium aluminosilicate $2MgO•Al_2O_3•3SiO_2$ which is the most likely phase according to XRD patterns.

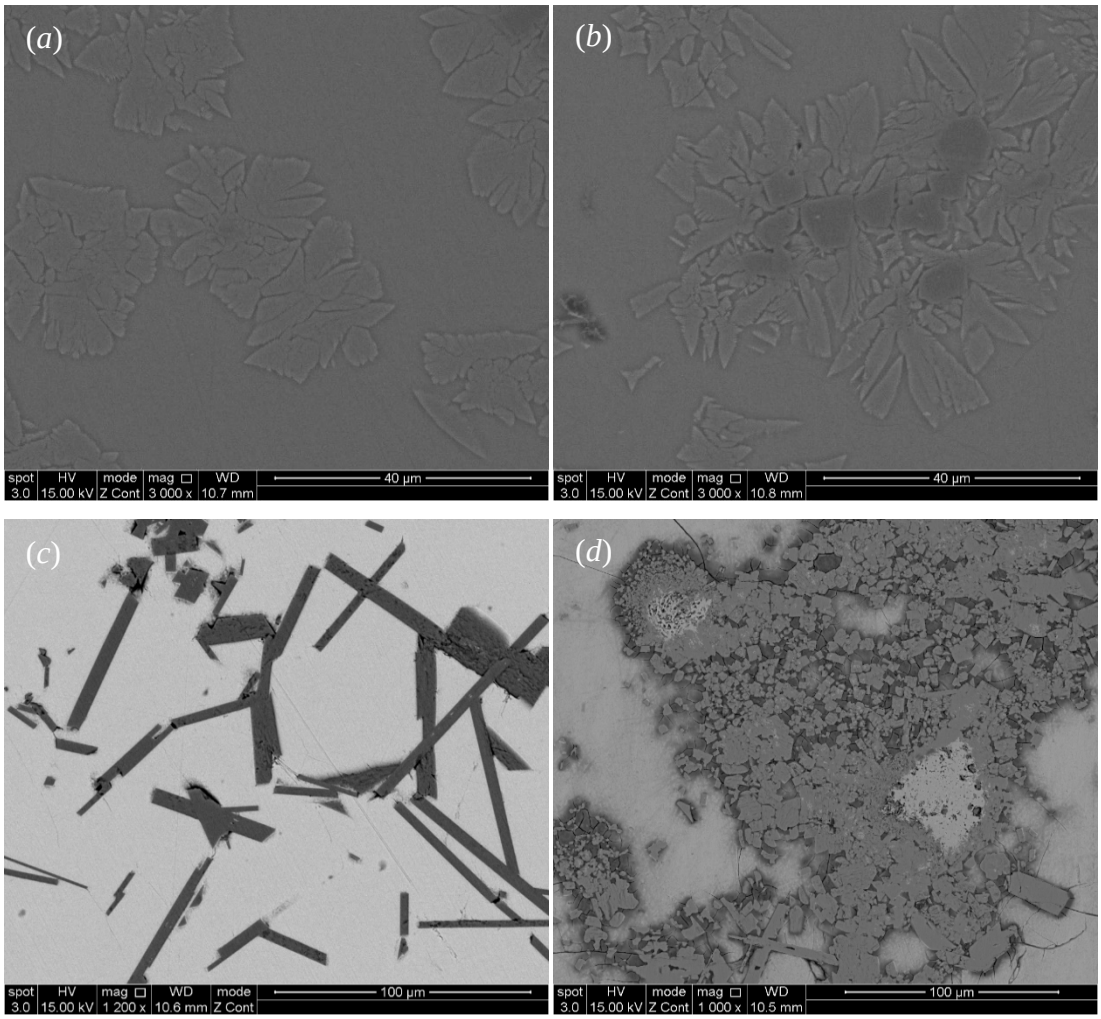

Figure 5-23 BSE images of separated precipitates in crystallised region of (*a*) MAS-5Cl, (*b*) MAS-10Cl, (*c*) BAS-15Cl and (*d*) BAS-20Cl glasses, respectively.

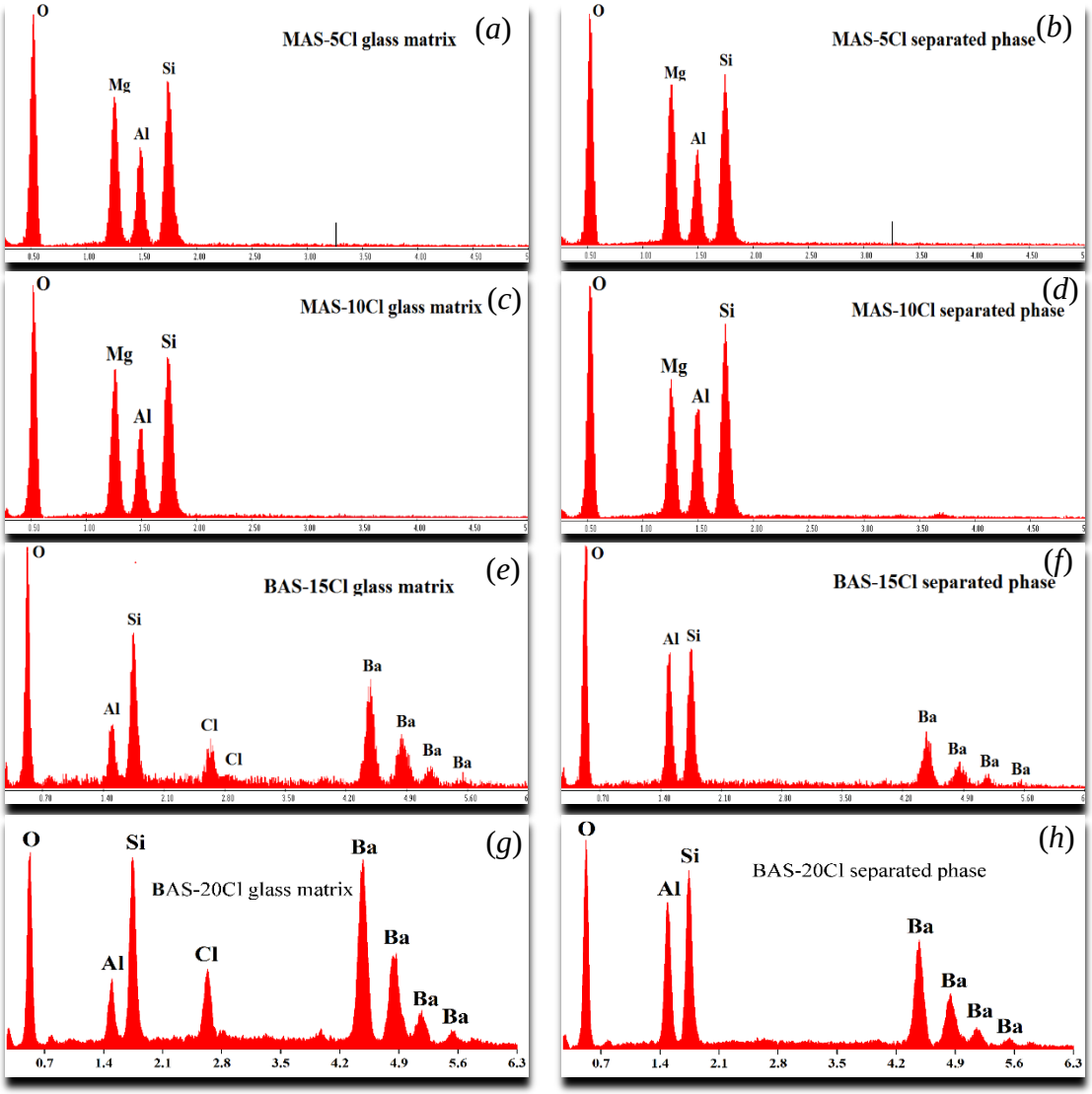

Figure 5-24 EDX spectra of BAS-20Cl glass matrix and needle-like precipitates in crystallised region of BAS-20Cl glass, respectively.

On the other hand, BAS-15Cl glass (Figure 5-23(*a*)) shows a number of needle-like and plate-like separated crystals which are distinct from the glass matrix. These needles and plates are widely distributed in the crystallised region, with a width range of 5 to 20 µm and a length up to 100 µm. However, in BAS-20Cl glass (Figure 5-23(*b*)), the separated phase particles are aggregated together, suggesting a higher rate of growth of separated phase. In this case, the particles are mostly in a rectangular or smooth shaped. EDX spectra of glass matrix and separated phase in each glass are displayed in Figure 5-24(*e*) and (*f*), which indicates that Cl is not present in separated phase at all but present in significant amounts in the glass matrix. The normalised

stoichiometry of the needles and plates is $23.9BaO•25.5Al_2O_3•50.6SiO_2$, very close to $25BaO•25Al_2O_3•50SiO_2$, the formula of hexacelsian which is suggested by Raman results to be the separated phase.

5.2.3.2. TEM

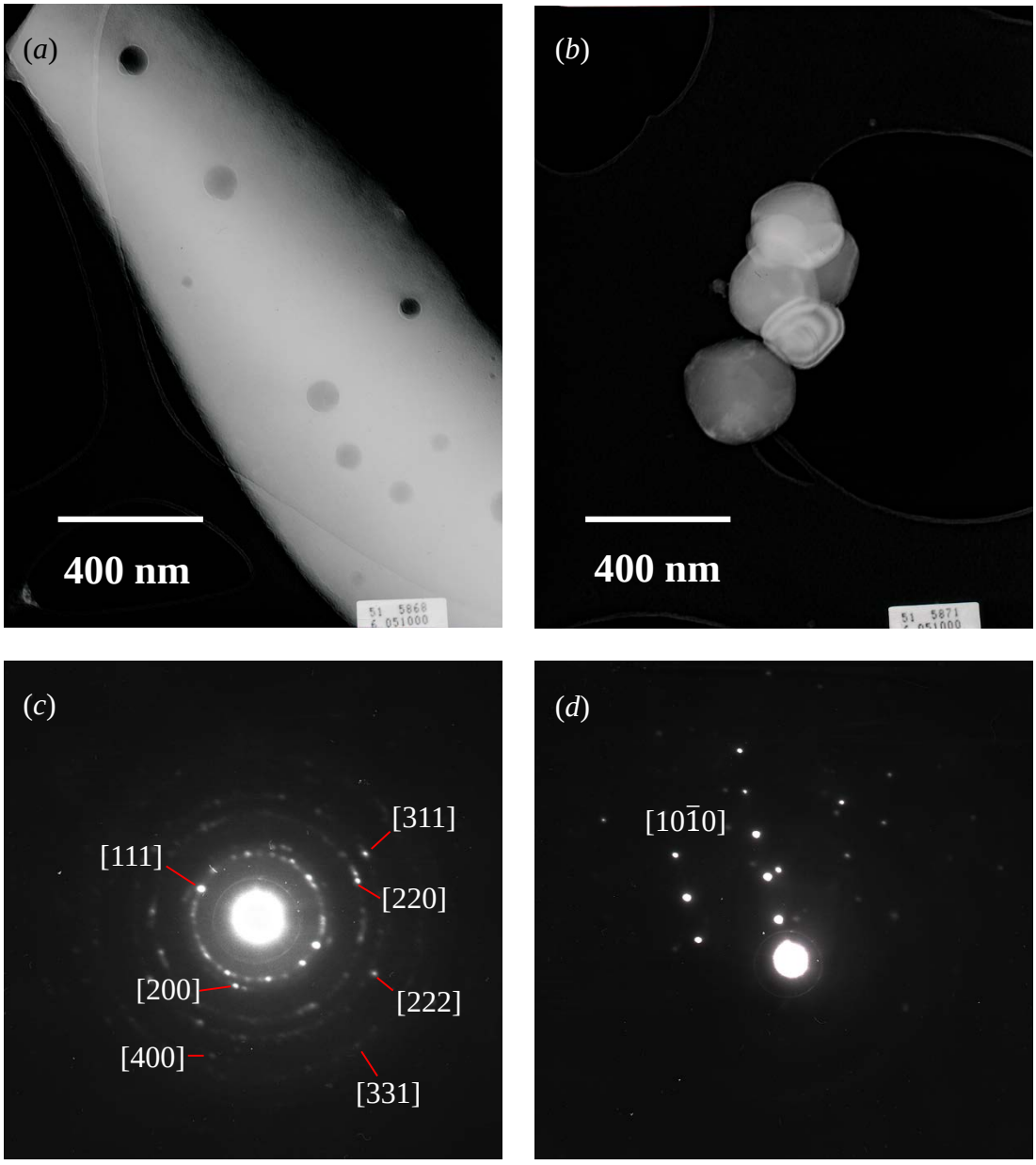

Figure 5-25 TEM images and some electron diffraction patterns of separated phase in BBS-15Cl glass.

As seen in Figure 5-25(*a*), a number of spherical particles or vacant holes can be found within glass matrix of BBS-15Cl glass. The holes may be formed when the separated particles escaped from the matrix during grinding; some isolated spherical particles are found on the grid in spite of a bit larger size, as shown in Figure 5-25(*b*). It agrees with the SEM results that the separated phase in BBS-15Cl glass is spherical and of 100-200 nm in diameter. Figure 5-25(*c*) gives the electron diffraction pattern of a whole piece which contains separated particles, showing a series of diffraction rings (discrete bright diffraction spots) that are in accordance with the feature of cubic face-centred structure (*fcc*). It is possible that these particles are the *fcc* cristobalite (a high temperature form) as the XRD-identified quartz is hexagonal. NaCl also shows an *fcc* structure but XRD patterns (Figure 5-7) do not see any evidence for the presence of NaCl. Figure 5-25(*d*) shows a number of diffraction spots belonging to multiple single crystals, among which the brightest series is likely due to the $[10\bar{1}0]$ diffraction axis of hexagonal low quartz.

Figure 5-26 displays TEM images and some electron diffraction patterns of the separated phase in BAS-20Cl glass. As can be seen in the images, the crystallised region shows a distinct morphology from the glass matrix: the glass matrix is homogeneous and exhibits no features under TEM observation while the crystallised regions contain some needle-like (Figure 5-26*b*) or irregular regions (Figure 5-26 *a* and *c*) which are darker than surrounding areas. The electron diffraction patterns of these regions proves that they are crystalline, and the indexing of the diffraction spots indicates that the patterns for area A, B, C and D in TEM images are assigned to the $[1\bar{1}01]$, $[10\bar{1}2]$, [0001] and [0001] diffraction axes of hexagonal celsian, respectively.

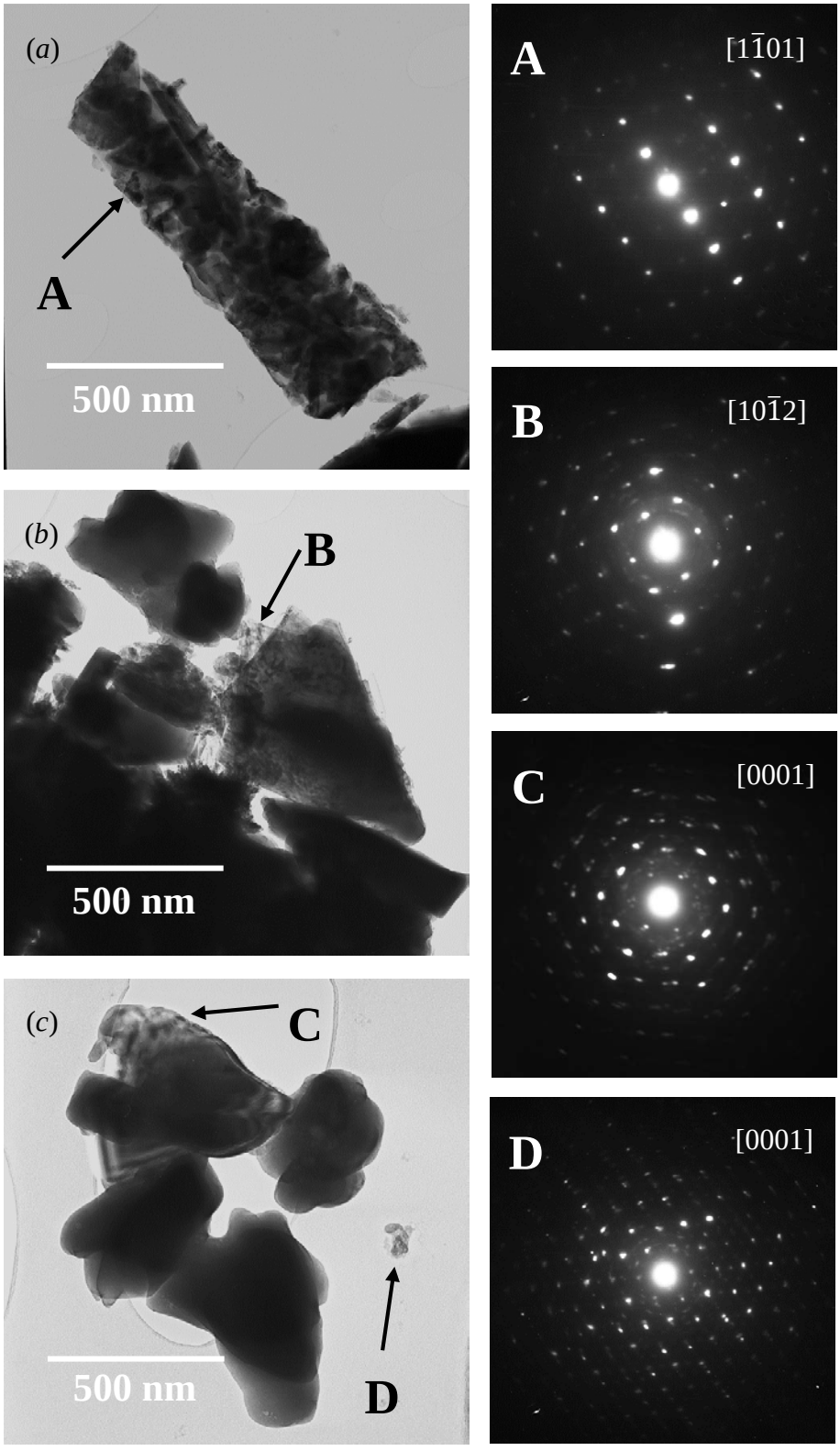

Figure 5-26 TEM images and corresponding electron diffraction patterns of separated phase in BAS-20Cl sample.

5.3. Discussion

5.3.1. Chloride retention and solubility in glass

5.3.1.1. Borosilicate glass

Generally speaking, the prepared borosilicate glasses have a chlorine retention of 50-65% when chlorine incorporation in glass is not approaching the saturation limit. This range is much higher than the average value 33% in borosilicate nuclear waste glasses prepared in laboratory crucibles (Hrma 2010). A higher chlorine retention rate of 80±5% has been achieved in pilot scale glasses (Goles and Nakaoka 1990, Feng *et al.* 1996, Hrma 2010), but they are melted in larger melters for 384 h to continuously make >100 kg products, in which case the surface to volume ratio is lower and so is the chloride evaporation. Moreover, the absolute chlorine content in these nuclear glasses, either at laboratory scale or pilot scale, is relatively low, *e.g.* 0.54 at% in P10-G-129A glass (McKeown *et al.* 2011) and 0.08 at% in PSCM-23 glass (Goles and Nakaoka 1990). In this study, the maximal chlorine retention in a homogeneous glass is 2.54 at%Cl in BBS-14Cl glass, a very much higher value than the literature figures. In comparison with the previously reported borosilicate glasses, the borosilicate glasses prepared in this study not only exhibit a better capacity of chlorine incorporation but also possess an excellent chlorine retention rate.

Meanwhile, despite the insignificant variation in chlorine retention rate among glass compositions at initial chlorine incorporation levels, chlorine retention rate becomes largely variable among the glass compositions with higher chlorine additions. According to Table 5-1 and Figure 5-1, the improvement of chlorine retention by equimolar replacement of alkaline earths conforms to the order of Ba> 0.6Sr+0.4Ba> Sr> Ca> Mg at higher chlorine loadings. This sequence may be related to the same sequence of chlorine solubility in these glasses. When the chlorine incorporation is approaching saturation, the added chlorine will have greater difficulty in entering the glass, resulting in more chloride being evaporated during melting. As a result, at 3.17 at%Cl addition, CBS glass only retains 1.14 at%Cl as the glass network has been almost saturated with chlorine whereas BBS glass retains as high as 2.06 at%Cl, as the network still has space to accommodate more chlorine.

Figure 5-27 plots the relationship between chlorine solubility and glass composition. The theoretical percentage of the total cation field strength of the base glass due to alkaline earths is used to characterise the compositional variation. It is clear that alkaline earths with lower cation field strengths are more beneficial to chlorine incorporation in borosilicate glass. Larger cations such as Ba^{2+} and Sr^{2+} are more able than smaller cations such as Ca^{2+} to expand and affect glass network (the lower T_g of Ba-containing glasses than Ca-containing glasses suggests that the rearrangement of glass network is easier when Ba^{2+} are present). Based on the assumption that Cl^- ions are only located in the interstitial space of glass network to associate with network modifying cations, larger cations, which are of lower field strength, have more space to attract and accommodate Cl^- ions. Thus the capacity of glass network to incorporate chlorine is increased.

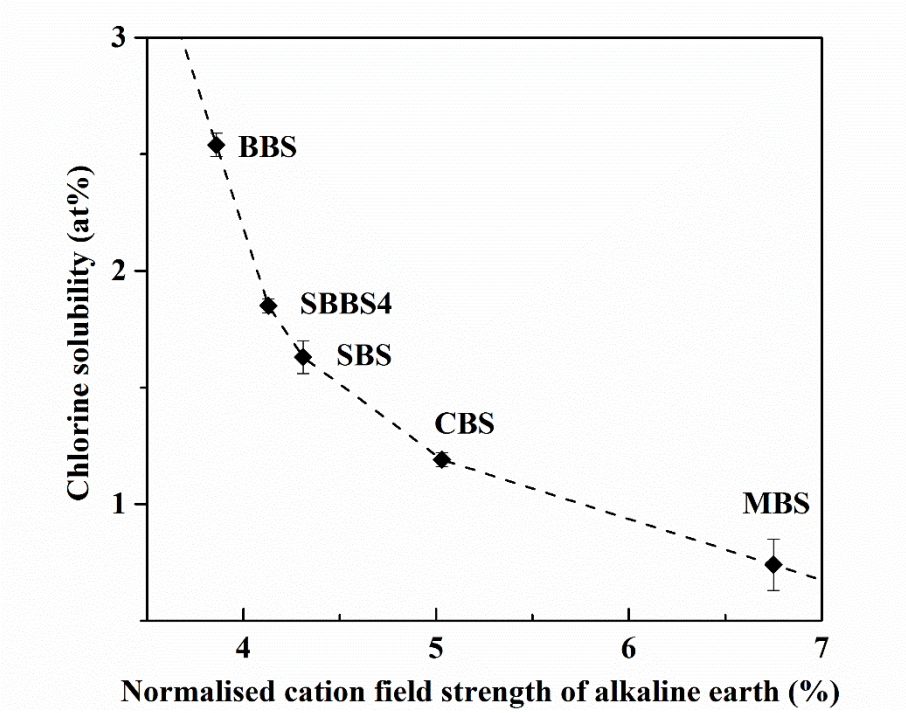

Figure 5-27 Chlorine solubility versus the proportion of cation field strength of alkaline earths in glass.

5.3.1.2. Aluminosilicate glass

The chlorine retention and solubility behaviours in aluminosilicate glasses are quite different from those in borosilicate glasses. BAS glass shows an excellent chlorine

retention rate (80±3%) coupled with a chlorine solubility of 2.96 at%Cl. Up to 5.61 at%Cl can be incorporated in the glassy region of phase separated BAS-20Cl sample. The high chlorine retention rate in BAS glass agrees with the retention rate in a barium silicate glass ($BaSi_2O_5$) reported by Stebbins and Du (2002) where 1.5 wt% chlorine is retained at 1.7 wt% addition; however, the authors produced the glasses in a closed system which minimises evaporative losses. Chlorine retention in SBAS-15Cl glass in which half BaO is replaced by SrO is 10% lower than BAS-15Cl glass, indicating that barium is better than strontium in terms of chlorine retention in glass. The melting and boiling points of alkaline earth chlorides are listed in Appendix I. The boiling point of different chloride may be the reason of various chloride retention rate among glass compositions.

CAS glass which remains homogeneous until 7.81 at%Cl addition however it has a less than 40% chlorine retention rate with a solubility of 1.11 at%Cl. The poor chlorine retention in CAS glass may arise from the use of hydrated calcium chloride as the chlorine precursor in this study. Schofield (2011) mentioned in his PhD thesis that hydrated $CaCl_2$ can be readily and significantly evaporated (probably via vaporisation) from the melt during melting. The chlorine loss can be reduced by preheating batches to 1000 ºC and cooling to room temperature prior to starting the melting program. In a future study, a preheating program should be investigated to compare its effect on chlorine retention in CAS glass. A ≥90% chlorine retention is achieved in a series of calcium aluminosilicate glasses in Siwadamrongpong *et al.* (2004). Nevertheless, the glasses were prepared under reducing atmosphere which inhibits chlorine evaporation, making the results less comparable. As to chlorine solubility, chlorine incorporation in CAS glass seems to have reached saturation quite early at ~1.1 at%Cl; however, this may be a result affected by the evaporation of hydrated calcium chloride.

In summary, both chlorine retention and chlorine solubility in aluminosilicate glasses decrease as BaO > SrO > CaO > MgO, but the exact dependence in each composition may be a combination of glass network and the nature of corresponding chlorides.

5.3.1.3. Effect of melting temperature on chlorine dissolution in glass

It seems that melting temperature is overwhelmed by melt composition in determining chlorine retention and solubility in glass: BAS glass processed at 1400 ºC is able to

incorporate more chlorine than BBS glass processed at 1100 ºC while CBS glass processed at 1100 ºC is able to incorporate and retain more chlorine than CAS glass processed at 1450 ºC. This suggests that processing temperature can be of a secondary consideration when designing glass compositions to immobilise chloride bearing nuclear waste.

5.3.2. Chloride incorporation in glass

Chlorine incorporation results in a variety of changes in glass structure and properties. According to Figure 5-4 and Figure 5-5, both borosilicate and aluminosilicate glasses show a density maximum with increasing chlorine incorporation. The chloride anions Cl^- are associated with network modifying cations such as Na^+ and Ca^{2+}; in this case two Cl^- ions replace one O^{2-} in the glass network. Cl^- is heavier but larger than O^{2-} (r_{Cl^-} = 181 Å, $r_{O^{2-}}$ = 138 Å) so the resulting density is balanced between the mass change and the network change such as expansion and depolymerisation. Therefore, the slightly increased density at initial chlorine incorporation can be explained on the grounds that, at this stage, Cl^- ions are located in the interstitial space among glass network to associate network modifying cations, which does not cause significant network expansion and hence the mass change dominates the density change of glass. However, increasing Cl^- content in glass results in more network modifying cations disassociating from non-bridging oxygens to associate with Cl^- (Evans *et al.* 2008) to form chloride clusters among glass network:

$$Si-O:Ca:O-Si + 2Cl^- = CaCl_2 + 2Si-O \qquad \text{Equation 5-1}$$

The above reaction polymerises glass network but the formation of chloride clusters leads to expansion in network and thus a reduced glass density. The more chlorine incorporated, the greater the expansion of the glass network.

The change in polymerisation of glass network can be reflected by the deconvolution results of Raman spectra. In borosilicate glasses (Figure 5-14), chlorine incorporation initially decreases the Q_3/Q_2 ratio, which is indicative of depolymerisation, and later increases the Q_3/Q_2 ratio until phase separation, suggesting a polymerisation process. As mentioned above, a small amount of chlorine directly enter the interstitial space of glass network, by which Cl^- ions are associated with network modifying cations as

O_3Si-O:CaCl. In BAS glasses (Figure 5-16*a*), chlorine incorporation results in a steady increase in Q_4 ratio at the consumption of Q_2 and Q_3 until phase separation, indicating that chlorine incorporation contributes to polymerisation of the BAS glass network. However, according to Figure 5-16*b*, after the initial polymerisation effect by chlorine incorporation (increased Q_4 proportion with decreased Q_2 and Q_3 proportions), CAS glass turns to be depolymerised with further chlorine addition by which Q_2 proportion increases while Q_3 and Q_4 proportions decreases until phase separation.

The shift in IR frequency at ~980 cm^{-1} also experiences an initial increase followed by a later decrease (Figure 5-19). The increased vibration frequency suggests that the Si-O bond length in SiO_4 tetrahedra is decreased, a signifier of a compacted network backbone. This can be a result of the attraction of Cl^- ions to network modifying cations, by which the association of network modifying cations with non-bridging oxygens is weakened and hence the associated Si-O bonds are shortened. Another possibility is that when filling the network voids Cl^- ions actually elbow out the surrounding atoms so as to make the network compact. These two effects, which may coexist, contribute to a slight increase in vibration frequency of SiO_4 unit with initial Cl^- incorporation. On the other hand, the slightly decreased frequency with further chlorine incorporation indicates that the average Si-O bond in SiO_4 tetrahedra is lengthened.

The glass transition temperature T_g is lowered by initial chlorine incorporation in both borosilicate and aluminosilicate glasses. Afterwards, T_g shows insignificant change with increasing chlorine incorporation until phase separation. The decreasing T_g from SBBS4 base to SBBS4-3Cl glass agrees with the structural change obtained by Raman spectroscopy that the glass is depolymerised. However, the increased polymerisation with further chloride incorporation does not agree with the unchanged T_g in this range. This may be because the large amount of chloride clusters destabilise glass network, which lowers the energy required for structural relaxation of the glass network and thus results in a decreased T_g. Therefore, as the two effects are counterbalanced, T_g does not change much along with further chlorine incorporation in SBBS4 glass. The T_g changes in BAS glass are similar.

Nevertheless, apart from the changes in T_g, chlorine incorporation also leads to shift of glass crystallisation temperature T_{c1} and the temperature for another intense exothermic reaction, T_{c2m} in BAS glass. The decreased T_{c1} suggests that glass is more prone to suffer devitrification upon heating when the chlorine content in glass is increased. The second crystallisation peak T_{c2} is common in alkaline earth aluminosilicate glasses prepared in this study (*e.g.* CAS and MAS glasses in next chapter) and is likely ascribed to a phase transition between the crystallised alkaline earth aluminosilicates. The starting point of this peak is decreased with increasing chlorine content in BAS glass; however, for the phase separated BAS-15Cl and BAS-20Cl glasses, this point is back to higher temperatures again. This indicates that chlorine in glass network is beneficial to reduce the temperature required for the phase transition, but this effect will be overridden by barium aluminosilicate crystals if they are already present in the glass.

5.3.3. Phase separation

Chlorine solubility in glass is not controlled by the capacity of glass to incorporate chlorine, but instead it is limited by the occurrence of crystallisation of non-chlorine components in glass. Figure 5-6 and Figure 5-7 suggest that borosilicate glasses with slightly excess chloride will become phase separated through the crystallisation of β-quartz (hexagonal) within glass matrix. Cubic SiO_2 β-cristobalite may also exist as a minor phase in the separated phase according to the XRD patterns though its peaks are not conspicuous. The crystallisation of SiO_2 is not affected by glass composition, indicating that it is a universal phenomenon in such borosilicate glasses that SiO_2 will separate out from glass network prior to chloride. A segregated chloride layer only occurs when chlorine addition is greatly in excess. The remaining chloride cannot be evaporated completely during melting because the melting temperature of borosilicate glasses is low (1100 ºC). It seems that the excess chloride will not stay inside the melt; however, all excess chloride aggregates together on the melt surface to form a chloride layer (identified to be NaCl in borosilicate glass series). The aggregation of chloride also explains the absence of chloride crystals in the separated glass bulk phase.

Separated phase in aluminosilicate glasses is achieved in BAS and MAS glasses; the surface layer on CAS-35Cl glass is so subtle that XRD cannot identify it. Like the

phase separation borosilicate glasses, the separated phase in BAS and MAS glasses is also non-chloride. XRD and Raman results (Figure 5-8 and Figure 5-15) suggest that the separated phase in BAS-15Cl and BAS-20Cl is most likely to be hexacelsian, a high temperature polymorph of celsian ($BaAl_2Si_2O_8$). This identification is supported by the EDX analysis on the separated phase in BAS-20Cl glass that has a very close stoichiometry. Because the chlorine content in BAS-15Cl and BAS-20Cl glass regions continues increasing, it is worth investigating the compositions of these glass regions to incorporate chloride while avoiding the occurrence of separation of hexacelsian. It is interesting that MAS-5Cl and MAS-10Cl glasses are phase separated but actually chlorine is neither retained in glass nor is present in the separated phase. Based on XRD and EDX analysis, the separated phase in MAS-5Cl and MAS-10Cl glasses is mainly magnesium aluminosilicate ($Mg_2Al_2Si_3O_{12}$). Compared with MAS base glass, MAS-5Cl glass contains less Al_2O_3 and SiO_2 and more MgO, which indicates that chlorine addition retards the melt-crucible interaction. Moreover, while all chlorine in MAS glass has been evaporated, the magnesium content in glass is not significantly reduced. Therefore, Cl^- ions are probably not lost via the vaporisation of $MgCl_2$. One possibility is that the reaction of $MgCl_2$ with oxygen during heating:

$$MgCl_2 + \frac{1}{2}O_2(g) = MgO + Cl_2(g) \qquad \text{Equation 5-2}$$

This reaction is able to appreciably take place in atmosphere pressure at temperatures higher than 300 ºC (Allen and Clark 1966, Ball 1977). As the melting in this study was carried out in an open system with a gas extractor, the released Cl_2 will be exhausted and the reaction continuously moves to the right side. Finally, Cl^- ions in batches or melt are all removed as Cl_2 and the product contains no chlorine.

The morphology of separated phases differs significantly among glass compositions according to the SEM observation in Figure 5-21 and Figure 5-22. While the separated particles in crystallised MBS and CBS glasses are large (100-200 μm in diameter) and irregularly shaped, the separated particles in crystallised SBBS4 and BBS glasses are very small (100-200 nm in diameter) and mostly droplet-like, although the separated phases are all the same. There is no evidence of crystalline orientation in the separated particles, so they are deemed to be formed through liquid-liquid separation on cooling

of melt. The strikingly large particle size in MBS-8Cl and CBS-16Cl glasses perhaps arises from the aggregation of SiO_2 droplets before the melt becomes rigid on cooling. The aggregated SiO_2 then start to crystallise as β-quartz or β-cristobalite. Meanwhile, the separation tendency of SiO_2 from SBBS4-12Cl and BBS-15Cl glasses is lower (*e.g.* phase separation in BBS-15Cl glass was not observed until annealing). There may not be enough time to allow the liquid droplets to aggregate and therefore the droplets remained isolated within glass matrix and crystallise as temperature reduces.

The morphology of separated phase in aluminosilicate glasses is distinct from that in borosilicate glasses. The precipitated hexacelsian particles in BAS-15Cl and BAS-20Cl glasses show an apparent orientation of crystalline growth (needles, plates and rectangles), which suggests that these particles are formed through nucleation and crystal growth within glass upon cooling. The crystallisation extent in BAS-20Cl glass is significantly larger than in BAS-15Cl glass, signifying that the nucleation is driven by increasing chlorine content in the glass. Meanwhile, the separated particles in MAS-5Cl and MAS-10Cl glasses are plate-like or flower-like, which is also indicative of nucleation and crystal growth. Both the barium and magnesium aluminosilicate crystals are prone to gather together and their large size (in microns) indicates that they crystallise rapidly during cooling.

In summary, both borosilicate and aluminosilicate glasses are phase separated when chlorine addition exceeds a critical point. However, chloride in glass network is only the driving force for phase separation; chlorine itself is not present in the separated phases. Phase separation in borosilicate glasses occurs as liquid-liquid separation and crystallisation whereas phase separation in aluminosilicate glasses occurs as nucleation and crystal growth.

5.4. Conclusions

In this chapter, both borosilicate glasses ($50SiO_2$-$15B_2O_3$-$15Na_2O$-20MO, mol%) and aluminosilicate glasses ($45SiO_2$-$10Al_2O_3$-45MO, mol%) with chlorine additions have been successfully prepared. Based on the above results and discussion, the following conclusions about chlorine in glass can be drawn:

- Chlorine solubility in borosilicate glasses reveals an increasing tendency with the equimolar substitution of larger to smaller alkaline earths: Ba>Sr>Ca>Mg; BBS glass has the highest solubility of 2.54 at%Cl.
- Chlorine solubility in aluminosilicate glasses is obtained in CAS and BAS glass, respectively; BAS glass has a much higher solubility of 2.96 at%Cl.
- Chlorine retention is more dependent on glass composition than melting temperature.
- Initial chlorine incorporation results in density maxima in both borosilicate and aluminosilicate glasses; the glass transition temperature is notably reduced by initial chlorine incorporation while maintains unchanged with further chlorine incorporation.
- Chlorine incorporation does not yield any Raman/FTIR band. In borosilicate glasses, chlorine incorporation initially leads to depolymerisation of network and later polymerised or unchanged network with increasing chlorine content. In aluminosilicate glasses chlorine incorporation monotonically depolymerises the glass network until the occurrence of phase separation.
- The first phase to separate from borosilicate glasses when the chlorine content exceeds loading limit is low quartz (SiO_2). Dependent on glass composition, a minority of cristobalite (SiO_2) can also be found. A segregated NaCl layer is formed on glass surface when chlorine addition is far beyond loading limit.
- The separated phases in aluminosilicate glasses (BAS and MAS) are alkaline earth aluminosilicates. Chlorine solubility is controlled by the stability of glass network. The separated phase is needle-like or plate-like in BAS glass while is flower-like in MAS glass.
- It is interesting that chlorine addition results in phase separation in MAS glass but chlorine itself is neither retained in glass nor in the separated phase.

6. Molybdenum in glass

6.1. Introduction

In this chapter, the solubility tendency and incorporation behaviour of molybdate in borosilicate and aluminosilicate glasses are presented. The base glass compositions are identical to those in the sulphur and chlorine chapters (4 and 5), namely 20MO-15Na_2O-15B_2O_3-50SiO_2 for borosilicate glass and 45MO -10Al_2O_3-45SiO_2 for aluminosilicate glass. Both formula are in mole percentage and M refers to alkaline earth elements. The effects of different alkaline earth on molybdate solubility in glass are assessed by equimolar substitution. The range of techniques outlined in Chapter 3 have been utilised to understand the effects of molybdate incorporation on the glass structure and properties.

6.2. Results

6.2.1. Loading limit

6.2.1.1. Borosilicate glasses

Barium borosilicate (BBS) glasses with 1.96 and 2.44 mol%MoO_3 additions (BBS-*x*M, x = 2 and 2.5, respectively) have been prepared. BBS-2M glass is homogeneous whereas BBS-2.5M is heavily crystallised. The MoO_3 loading limit of BBS glass is regarded as being 1.96 mol%.

Combined strontium and barium borosilicate (SBBS3) glasses with 0.99, 1.96, 2.44 and 2.91 mol%MoO_3 additions (SBBS3-*x*M, x = 1, 2, 2.5 and 3, respectively) have been prepared. SBBS3-1M and SBBS3-2M glasses are homogeneous while SBBS3-2.5M and SBBS3-3M have crystallised. The MoO_3 loading limit of SBBS3 glass is also regarded as being 1.96 mol%.

Strontium borosilicate (SBS) glasses with 1.96, 2.44 and 2.91 mol%MoO_3 additions (SBS-*x*M, x = 2, 2.5 and 3, respectively) have been prepared. Only SBS-2M glass is homogeneous while the other two samples have crystallised. The crystallisation extent of SBS-2.5M is lower than that of SBBS3-2.5M and BBS-2.5M glasses though they are all phase separated. The MoO_3 loading limit of SBS glass is regarded as being 1.96 mol%.

Calcium borosilicate (CBS) glasses with 0.99, 1.96, 2.44, 2.91, 3.38 and 3.85 mol% MoO_3 (CBS-*x*M, x = 1, 2, 2.5, 3, 3.5 and 4, respectively) have been prepared. Phase separation occurs in CBS-3.5M glass (as galls and within the glass matrix) and CBS-4M glass (segregated layer and within glass matrix). The MoO_3 loading limit of CBS glass is regarded as being 2.91 mol%.

Magnesium borosilicate (MBS) glasses 0.99, 1.96, 2.91 and 3.85 mol%MoO_3 (CBS-*x*M, x = 1, 2, 3, and 4, respectively) have been prepared. Phase separation occurs within all glasses and a segregated layer is formed on the surface of MBS-4M glass. The MoO_3 loading limit of MBS glass is less than 0.99 mol%.

Therefore, the loading limit of MoO_3 (mol%) in borosilicate glasses follows: CBS

(2.91) > SBS = SBBS3 = BBS (1.96) > MBS (<0.99).

6.2.1.2. Aluminosilicate glasses

Barium aluminosilicate (BAS) glasses with 1.96, 2.44 and 2.91 mol% MoO_3 additions (BAS-*x*M, *x* = 2, 2.5 and 3, respectively) have been prepared. BAS-2M glass is visibly transparent, BAS-2.5M glass is slightly crystallised whereas BAS-3M glass is heavily crystallised. MoO_3 loading limit is regarded as 1.96 mol%.

Combined strontium and barium aluminosilicate (SBAS) glasses with 1.96, 2.44 and 2.91 mol%MoO_3 additions (SBAS-*x*M, *x* = 2, 2.5 and 3, respectively) have been prepared. Like the BAS glass series, SBAS-2M glass is visibly transparent, SBAS-2.5M glass is partly crystallised whereas SBAS-3M glass is heavily crystallised. The MoO_3 loading limit is regarded as 1.96 mol%.

Strontium aluminosilicate (SAS) glasses with 2.44 and 2.91 mol%MoO_3 additions (SAS-*x*M, *x* = 2.5 and 3, respectively) have been prepared. SAS-2.5M glass is visibly transparent whereas SAS-3M glass is partly crystallised. The MoO_3 loading limit is hence regarded as the 2.44 mol%.

Calcium aluminosilicate (CAS) glasses with 0.99, 1.96, 2.91 and 3.85 mol% MoO_3 (CAS-*x*M, *x* = 1, 2, 3, and 4, respectively) have been prepared. Crystallisation occurs in CAS-4M only whereas other glasses are homogeneous. The MoO_3 loading limit in CAS glass is regarded as being 2.91 mol%.

Combined calcium and magnesium aluminosilicate (CMAS) glass with 3.85 mol% MoO_3 addition (CMAS-4M) is partly crystallised as CAS-4M glass. CMAS glass is believed to have a MoO_3 loading limit close to CAS glass (2.91 mol%).

Magnesium aluminosilicate (MAS) glasses with 0.99, 1.96, 2.91, 3.85, 4.76, 5.66, 6.54 and 7.41 mol%MoO_3 additions (MAS-*x*M, *x* = 1, 2, 3, 4, 5, 6, 7 and 8, respectively) have been prepared. Crystallisation starts to occur in MAS-8M glass and thus MoO_3 loading limit is regarded as 6.54 mol% in MAS-7M glass.

Therefore, the loading limit of MoO_3 (mol%) in aluminosilicate glasses is: MAS (6.54%) > CAS = CMAS (2.91%) > SAS (2.44%) > SBAS = BAS (1.96%).

6.2.2. Glass compositions

The EDX measured glass compositions are displayed in Table 6-1 (borosilicate glasses) and Table 6-2 (aluminosilicate glasses) in comparison with the nominal values. Target boron content is used as previous ICP-OES measurement suggests that there is limited loss of boron in borosilicate glasses processed at 1100 ºC (see Chapter 4).

As seen in Table 6-1, the addition of MoO_3 significantly reduces the amount of Al_2O_3 in borosilicate glasses, which indicates that adding MoO_3 to the melt is helpful in reducing the corrosion of the mullite crucibles by the melt. After the initial reduction the Al_2O_3 content does not notably decline with increasing MoO_3 addition until phase separation. The addition of MoO_3 does not significantly impact the Na_2O and alkaline earth oxide contents in most of the homogeneous glasses. Their slightly lower than nominal amounts are probably due to the slight evaporation of glass melts.

As seen in Table 6-2, MoO_3 addition also reduces the fraction of Al_2O_3 in the aluminosilicate glasses arising from corrosion of the mullite crucible by the melt. There is significant loss of alkaline earth content in CAS and MAS glasses when MoO_3 is initially added, whereas this loss appears to change insignificantly with increasing MoO_3 loadings.

Generally, glasses containing MoO_3 result in less crucible dissolution during melting than the base glasses. In most homogeneous glasses, the difference between measured and nominal contents of each component is within 2.5 mol%, except CAS and MAS glasses where CaO and MgO content is ~6 mol% less than the batches, respectively.

Table 6-1 Measured (by EDX) and nominal (in brackets) borosilicate glass compositions (mol%).

Sample	***x***	**SiO_2**	**B_2O_3**	**Al_2O_3**	**Na_2O**	**MO**		**MoO_3**	**Total**
BBS-*x*M						BaO			
	0	50.86 (50.00)	(15.00)	4.26	12.43 (15.00)	17.45 (20.00)		0.00 (0.00)	100.00 (100.00)
	2	48.06 (49.02)	(14.71)	1.91	14.32 (14.71)	19.09 (19.61)		1.92 (1.96)	100.00 (100.00)
sc	2.5	49.48 (48.78)	(14.63)	1.59	13.38 (14.63)	18.46 (19.51)		2.45 (2.44)	100.00 (100.00)
SBBS3-*x*M						BaO	SrO		
	0	51.64 (50.00)	(15.00)	3.00	12.76 (15.00)	10.62 (12.00)	6.98 (8.00)	0.00 (0.00)	100.00 (100.00)
	1	47.81 (49.50)	(14.85)	1.76	14.48 (14.85)	12.43 (11.88)	7.55 (7.92)	1.12 (0.99)	100.00 (100.00)
	2	50.53 (49.02)	(14.71)	1.62	12.63 (14.71)	11.06 (11.76)	7.49 (7.84)	1.97 (1.96)	100.00 (100.00)
sc	2.5	49.97 (48.78)	(14.63)	1.66	12.33 (14.63)	11.35 (11.71)	7.93 (7.80)	2.13 (2.43)	100.00 (100.00)
hc	3	47.70 (48.54)	(14.56)	1.19	12.26 (14.56)	12.65 (11.65)	8.35 (7.77)	3.30 (2.91)	100.00 (100.00)
SBS-*x*M						SrO			
	0	52.12 (50.00)	(15.00)	3.41	12.50 (15.00)	16.97 (20.00)		0.00 (0.00)	100.00 (100.00)
	2	48.05 (49.02)	(14.71)	1.10	14.44 (14.71)	19.80 (19.61)		1.92 (1.96)	100.00 (100.00)
sc	2.5	50.14 (48.78)	(14.63)	0.99	12.93 (14.63)	18.85 (19.51)		2.44 (2.44)	100.00 (100.00)
CBS-*x*M						CaO			
	0	51.45 (50.00)	(15.00)	1.12	12.99 (15.00)	19.44 (20.00)		0.00 (0.00)	100.00 (100.00)
	1	50.15 (49.50)	(14.85)	0.44	12.95 (14.85)	20.58 (19.80)		1.02 (0.99)	100.00 (100.00)
	2	48.79 (49.02)	(14.71)	0.10	12.72 (14.71)	21.39 (19.61)		2.29 (1.96)	100.00 (100.00)
	2.5	48.42 (48.78)	(14.63)	0.29	14.27 (14.63)	19.59 (19.51)		2.80 (2.44)	100.00 (100.00)
	3	49.43 (48.54)	(14.56)	1.09	13.97 (14.56)	18.11 (19.42)		2.84 (2.91)	100.00 (100.00)
sc	3.5	47.91 (48.31)	(14.49)	0.61	13.10 (14.49)	20.50 (19.32)		3.39 (3.38)	100.00 (100.00)
hc+sl	4	-	-	-	-	-		-	
MBS-*x*M						MgO			
	0	50.56 (50.00)	(15.00)	1.77	13.56 (15.00)	19.10 (20.00)		0.00 (0.00)	100.00 (100.00)
sc	1	48.41 (49.50)	(14.85)	0.01	15.15 (14.85)	20.55 (20.00)		1.02 (0.99)	100.00 (100.00)
hc	2-4	-	-	-	-	-		-	

"*sc*" and "*hc*" means the glass is slightly crystallised and heavily crystallised, respectively; "*sl*" means the glass has a segregated layer.

Table 6-2 Measured (by EDX) and nominal (in brackets) aluminosilicate glass compositions (mol%).

Sample	*x*	SiO_2	Al_2O_3	MO		MoO_3	Total
BAS-*x*M				BaO			
	0	43.79 (45.00)	11.31 (10.00)	44.90 (45.00)		0.00 (0.00)	100.00 (100.00)
	2	44.59 (44.12)	10.25 (9.80)	43.31 (44.12)		1.85 (1.96)	100.00 (100.00)
sc	2.5	44.51 (43.90)	10.27 (9.76)	42.73 (43.90)		2.49 (2.44)	100.00 (100.00)
hc	3	-	-	-		-	
SBAS-*x*M				BaO	SrO		
	0	44.64 (45.00)	11.16 (10.00)	22.50 (22.50)	21.70 (22.50)	0.00 (0.00)	100.00 (100.00)
	2	44.94 (44.12)	10.35 (9.80)	21.29 (22.06)	21.41 (22.06)	2.01 (1.96)	100.00 (100.00)
sc	2.5	45.32 (43.90)	10.43 (9.76)	20.70 (21.95)	21.00 (21.95)	2.55 (2.44)	100.00 (100.00)
hc	3	-	-	-		-	
SAS-*x*M				SrO			
	0	46.93 (45.00)	11.36 (10.00)	41.71 (45.00)		0.00 (0.00)	100.00 (100.00)
	2.5	44.98 (43.90)	10.92 (9.76)	41.78 (43.90)		2.32 (2.44)	100.00 (100.00)
sc	3	44.24 (43.69)	10.88 (9.71)	42.17 (43.69)		2.71 (2.91)	100.00 (100.00)
CAS-*x*M				CaO			
	0	49.47 (45.00)	14.82 (10.00)	35.71 (45.00)		0.00 (0.00)	100.00 (100.00)
	1	46.00 (44.55)	12.26 (9.90)	40.79 (44.55)		0.96 (0.99)	100.00 (100.00)
	2	47.54 (44.12)	12.21 (9.80)	38.34 (44.12)		1.92 (1.96)	100.00 (100.00)
	3	46.97 (43.69)	12.25 (9.71)	37.98 (43.69)		2.81 (2.91)	100.00 (100.00)
sc	4	47.18 (43.27)	11.92 (9.62)	37.20 (43.27)		3.70 (3.85)	100.00 (100.00)
CMAS-*x*M				CaO	MgO		
sc	4	47.06 (43.27)	13.09 (9.62)	18.46 (21.63)	17.96 (21.63)	3.43 (3.85)	100.00 (100.00)
MAS-*x*M				MgO			
	0	50.06 (45.00)	14.63 (10.00)	35.31 (45.00)		0.00 (0.00)	100.00 (100.00)
	1	46.99 (44.55)	11.49 (9.90)	40.58 (44.55)		0.94 (0.99)	100.00 (100.00)
	2	46.57 (44.12)	11.69 (9.80)	39.95 (44.12)		1.78 (1.96)	100.00 (100.00)
	3	46.24 (43.69)	11.82 (9.71)	39.18 (43.69)		2.76 (2.91)	100.00 (100.00)
	4	46.01 (43.27)	11.91 (9.62)	38.38 (43.27)		3.71 (3.85)	100.00 (100.00)
	5	46.07 (42.86)	12.13 (9.52)	37.34 (42.86)		4.46 (4.76)	100.00 (100.00)
	6	46.33 (42.45)	12.49 (9.43)	36.02 (42.45)		5.16 (5.66)	100.00 (100.00)
	7	46.10 (42.06)	12.36 (9.35)	36.21 (42.06)		5.34 (6.54)	100.00 (100.00)
sc	8	46.84 (41.67)	12.72 (9.26)	35.14 (41.67)		5.30 (7.41)	100.00 (100.00)

"*sc*" and "*hc*" means the glass is slightly crystallised and heavily crystallised, respectively.

6.2.3. Molybdenum retention and solubility

6.2.3.1. MoO_3 retention

The MoO_3 retention rate in borosilicate and aluminosilicate glasses are both extremely high. According to Figure 6-1, MoO_3 retention rate is close to 100% in borosilicate glasses regardless of base glass composition and MoO_3 addition. According to Figure 6-2 (*a*), MoO_3 retention rate in MAS glass remains higher than 90% until MAS-6M glass, after which MoO_3 retention seems to have reached the limit and hence remains unchanged in MAS-7M and MAS-8M glasses. Nevertheless, the MoO_3 in other aluminosilicate glass compositions is essentially all retained even when the MoO_3 added is excessive and phase separation occurs. In summary, excluding the MAS glasses with high MoO_3 loadings (MAS-6M to MAS-8M glasses), the near-to-100% MoO_3 retention rate in both borosilicate and aluminosilicate glasses does not vary with glass composition or with increasing MoO_3 content in glass in spite of substantial phase separation.

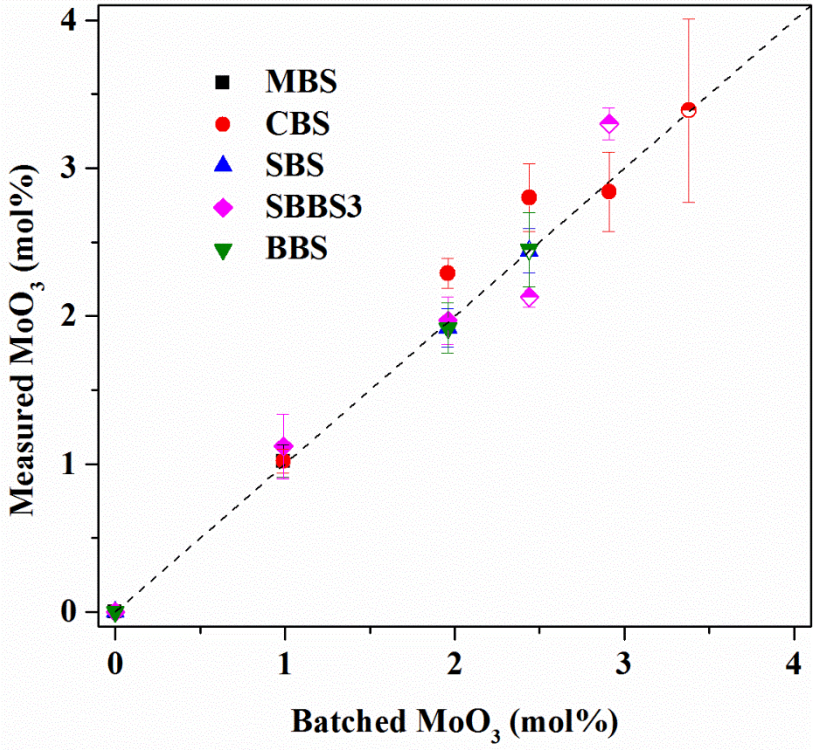

Figure 6-1 MoO_3 retention in borosilicate glasses. The half-filled symbols are for the crystallised glasses, hereinafter the same. The dashed line is the line for 100% retention.

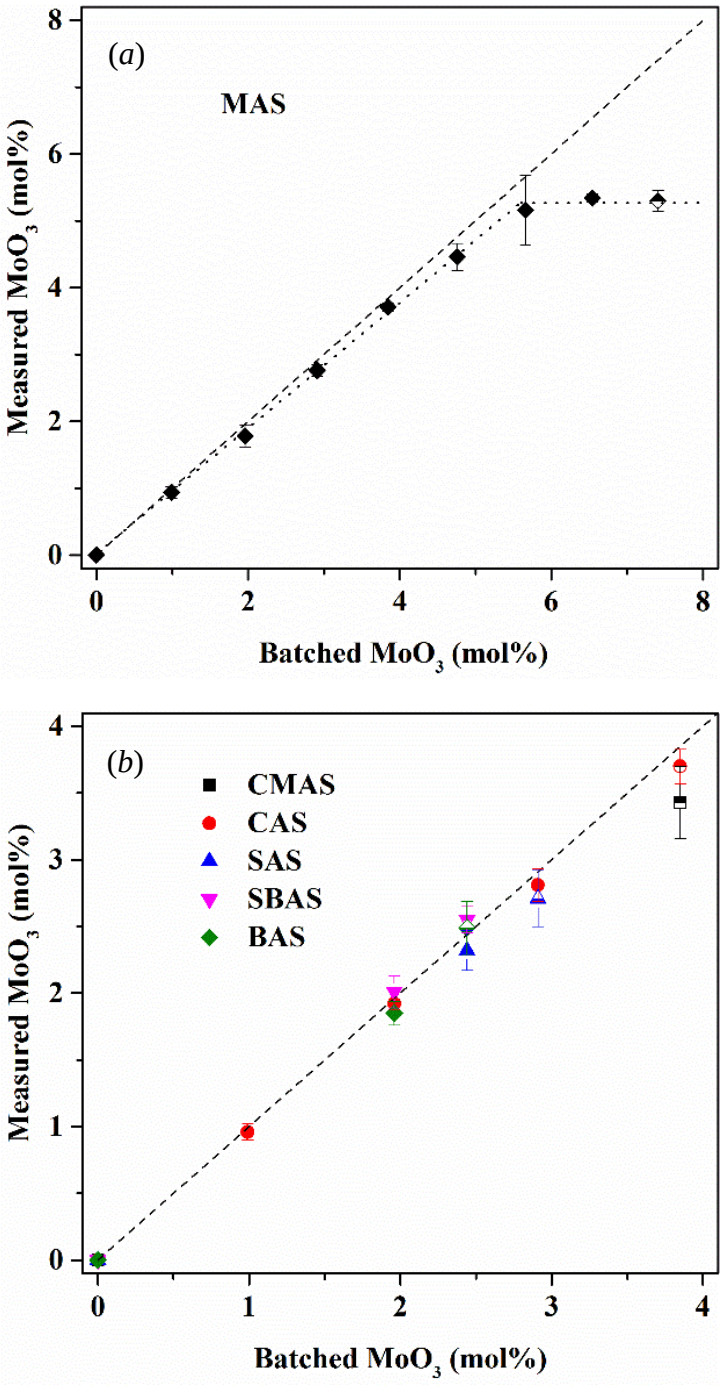

Figure 6-2 MoO_3 retention in aluminosilicate glasses: (*a*) MAS glasses and (*b*) other glasses. The dashed line is the 100% retention line.

The effect of melting temperature on MoO_3 retention was not investigated, but the near-to-100% retention rate in both borosilicate and aluminosilicate glasses (melted at 1100 and 1400/1450 ºC, respectively) suggests that the evaporation of MoO_3 should be very limited at temperatures lower than 1450 ºC. Therefore, glass melting

temperature has not been taken into account when comparing the molybdate incorporation data with the literature.

6.2.3.2. MoO_3 solubility

MoO_3 solubility is defined as the measured MoO_3 content in the glass with the measured MoO_3 loading limit. Figure 6-3 shows the MoO_3 solubility charts of borosilicate and aluminosilicate glasses, respectively. Similar to MoO_3 loading limit, MoO_3 solubility in borosilicate glasses (Figure 6-3*a*) also exhibits an increase with the equimolar substitution of Ca to Sr to Ba; however, the substitution of Mg results in very poor MoO_3 solubility. Meanwhile, MoO_3 solubility in aluminosilicate glasses (Figure 6-3*b*) monotonically decreases with the equimolar substitution of smaller by larger alkaline earths, increasing from 1.85 mol% in BAS glass to 5.34 mol% in MAS glass. It can also be seen that the glasses with combined SrO and BaO (SBBS3 and SBAS) have a MoO_3 solubility that is slightly higher than that obtained with BaO only and lower than that obtained with SrO only. The partial replacement of BaO by SrO does not increase the loading limit, but does slightly increase MoO_3 solubility in glass.

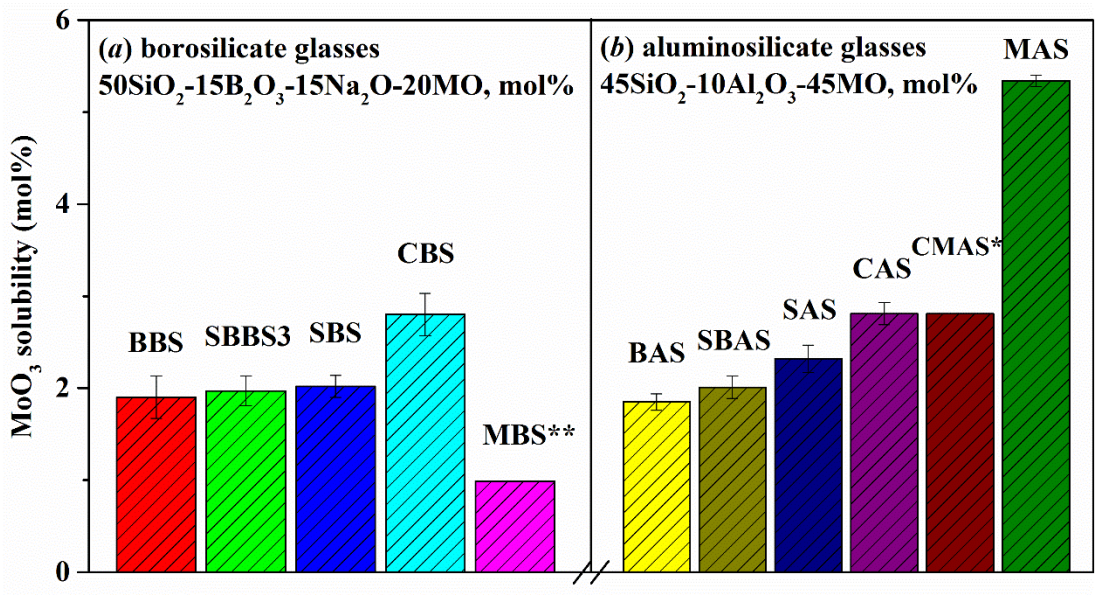

Figure 6-3 Measured MoO_3 solubilities in (*a*) borosilicate glasses and (*b*) aluminosilicate glasses, respectively. "*": exact MoO_3 solubility in CMAS glass is not achieved, but it should be similar to that in CAS glass. "**": MBS-1M is already crystallised so MoO_3 solubility in MBS glass is less than 0.99 mol%.

6.2.4. Density

6.2.4.1. Borosilicate glasses

As shown in Figure 6-4, MoO_3 incorporation in borosilicate glass compositions results in increased glass densities. Density of CBS glass increases from 2.608 g cm^{-3} for the base glass to 2.653 g cm^{-3} for CBS-1M glass (0.99 mol%MoO_3 addition) initially. The increasing trend continues with increasing MoO_3 content in glass albeit at a decreasing rate, the density reaching the highest of 2.680 g cm^{-3} for CBS-3M glass. Subsequently the MoO_3 content exceeds the solubility limit leading to phase separation, and CBS glass density does not further increase so that the CBS-3.5M sample has a density of 2.679 g cm^{-3}.

A similar increasing trend of density is also found in SBS, SBBS3 and BBS glasses with increasing MoO_3 incorporation. However, with the occurrence of phase separation, glass density slightly decreases in SBS-2.5M and BBS-2.5M glasses whereas it continues to increase in SBBS3-2.5M glass. This may be due to the relatively low MoO_3 content in SBBS3-2.5M glass compared with the other two (shown in Figure 6-1). The densities of MBS samples are not plotted because all of the Mo-containing MBS glasses are phase separated.

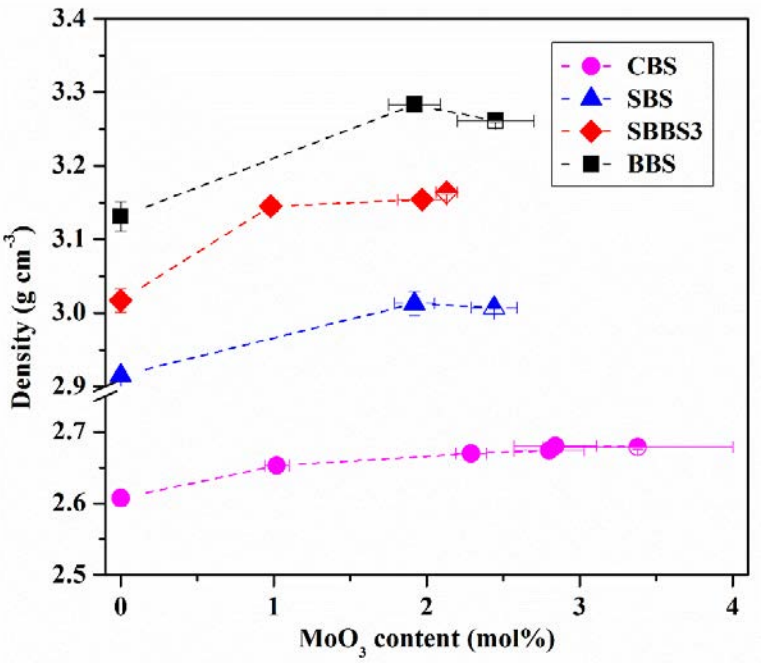

Figure 6-4 Density of borosilicate glasses with different MoO_3 contents. The dashed lines were added to guide the eyes.

6.2.4.2. Aluminosilicate glasses

As plotted in Figure 6-5, MoO_3 incorporation in aluminosilicate glasses also results in increased glass densities. The density of MAS glass steadily increases from 2.696 g cm^{-3} for the base glass to 2.775 g cm^{-3} for MAS-6M glass. Subsequently although the MoO_3 content in MAS-7M and MAS-8M glasses does not further increase, their densities continue to increase to 2.782 and 2.790 g cm^{-3}, respectively. Similarly, the density of CAS glass significantly increases from 2.770 g cm^{-3} for the base glass to 2.826 g cm^{-3} for CAS-1M glass and gradually reaches 2.847 g cm^{-3} for CAS-3M glass. Then, glass density continues increasing to 2.861 g cm^{-3} for the phase separated CAS-4M glass.

On the other hand, the densities of SAS, SBAS and BAS glass series behave in a different fashion with increasing MoO_3 content. After initial MoO_3 incorporation which results in increased glass densities, further MoO_3 addition slightly reduces the densities for phase separated glasses. In addition, CMAS-4M glass has a density of 2.795 g cm^{-3}, which is between the density of the CAS-4M and MAS-4M glasses.

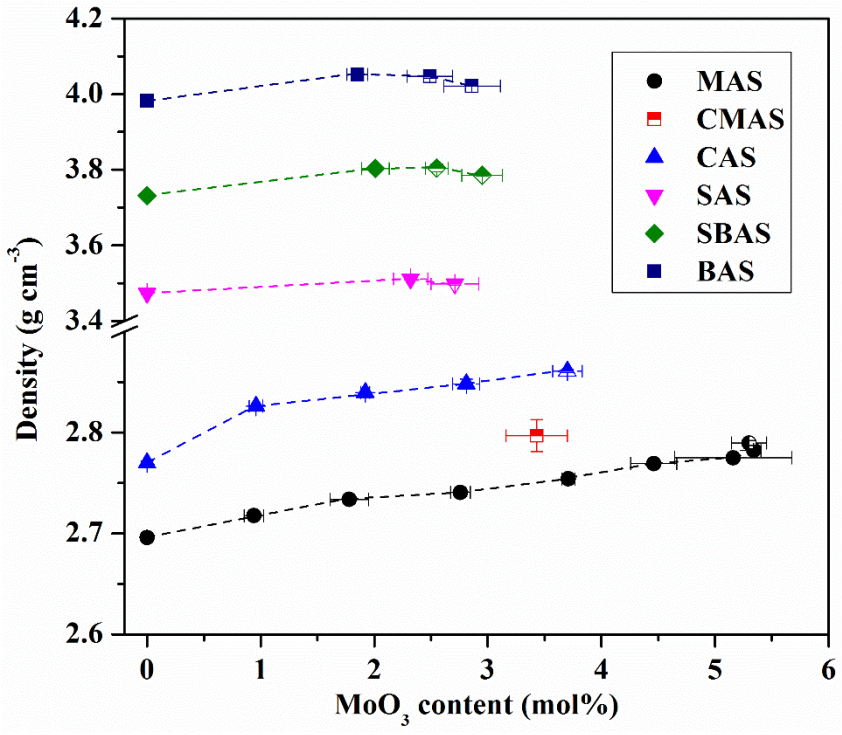

Figure 6-5 Density of aluminosilicate glasses with different MoO_3 contents. The dashed lines were added as guides to the eyes.

6.2.5. XRD

6.2.5.1. Borosilicate glasses

The XRD patterns of borosilicate glasses with different MoO_3 additions are shown in Figure 6-6 to Figure 6-8. Among all Mo-containing MBS glasses (Figure 6-6) only MBS-1M glass shows an amorphous XRD pattern even though optical inspection shows that it is still not completely homogeneous. The other MBS glasses however show evidence for the presence of crystalline phases: the XRD patterns of MBS-3M and MBS-4M glasses show a number of crystalline peaks, among which the peaks at 2θ = 15.1º, 18.9º, 20.1º, 20.7º, 22.7º, 23.5º, 26.0º, 28.5º, 29.7º, 30.6º and 31.3º are assigned to sodium-magnesium molybdate solid solution $Na_{2.4}Mg_{0.8}(MoO_4)_2$ (PDF4 (2012), 00-030-1211) while the peaks at 2θ = 17.1º, 27.8º, 32.7º, 43.0º, 49.1º and 53.2º are assigned to sodium molybdate Na_2MoO_4 (PDF4 (2012), 00-012-0773); MBS-2M glass has an intense peak at 2θ = 30.6º which is attributed to $Na_{2.4}Mg_{0.8}(MoO_4)_2$. The segregated layer of MBS-4M glass can also be identified to be a mixture of $Na_{2.4}Mg_{0.8}(MoO_4)_2$ and Na_2MoO_4, where the former phase still dominates.

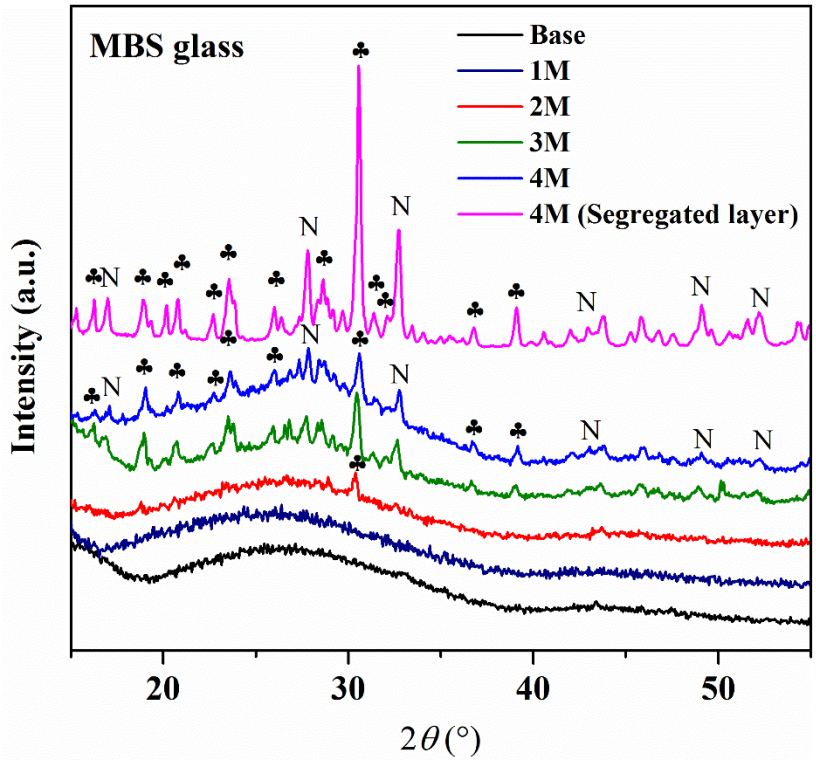

Figure 6-6 XRD patterns of MBS glasses with different MoO_3 additions. "♣" – peaks assigned to $Na_{2.4}Mg_{0.8}(MoO_4)_2$ crystals; "N" – peaks assigned to Na_2MoO_4 crystals.

Figure 6-7 shows XRD patterns of CBS glasses with different MoO_3 contents. CBS glass shows an amorphous pattern until CBS-3M glass after which the CBS samples have some crystalline peaks. CBS-3.5M glass shows distinct peaks at 2θ = 18.6º, 28.8º, 31.3º, 34.4º, 47.1º and 54.1º which are attributed to powellite $CaMoO_4$ (PDF4 (2012), 00-029-0351) while two minor peaks centred at 2θ = 27.7º and 32.6º, which can be assigned to Na_2MoO_4, are also observed. The much higher intensities of peaks attributed to $CaMoO_4$ indicates that at this stage $CaMoO_4$ is the dominant phase. However, XRD patterns for the heavily crystallised CBS-4M glass are different, with the emergence of a number of peaks belonging to hydrated sodium molybdate (Na_2MoO_4•$2H_2O$, PDF4 (2012), 00-034-0076), at 2θ = 21.2º, 24.7º, 27.0º, 28.3º, 30.0º, 33.6º and 41.5º, respectively. Meanwhile, the relative intensities of peaks assigned to Na_2MoO_4 and/or Na_2MoO_4•$2H_2O$ to the peaks assigned to $CaMoO_4$ are increased for the CBS-4M sample, indicating that the excess MoO_4^{2-} ions are mainly separated with Na^+ ions from glass network. Moreover, the segregated layer of CBS-4M glass, which is directly collected by removal from glass surface, is identified to be a mixture of $CaMoO_4$ and Na_2MoO_4.

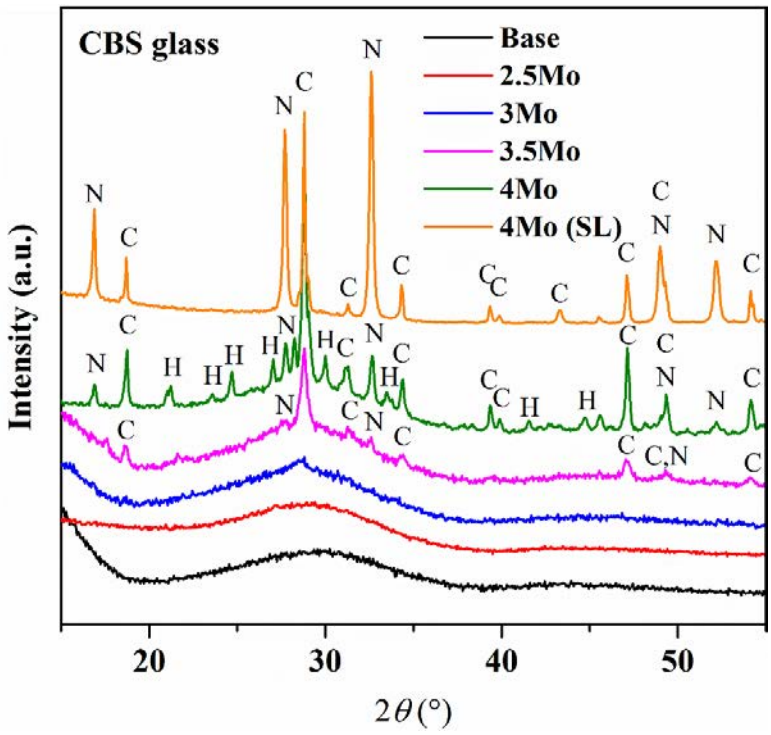

Figure 6-7 XRD patterns of CBS glasses with different MoO_3 additions. Peaks marked with "C", "N" and "H" are assigned to $CaMoO_4$, Na_2MoO_4 and Na_2MoO_4•$2H_2O$ crystals, respectively.

XRD patterns of SBS, SBBS3 and BBS glasses with MoO_3 additions are shown in Figure 6-8. SBS-2M glass displays a completely amorphous pattern while SBS-2.5M glass shows one tiny inconspicuous peak at 2θ = 27.8º. Although BBS-2M and SBBS3-2M glasses are visibly transparent, their XRD spectra exhibit a small crystalline peak at 2θ = 26.5º. As the MoO_3 content increases in BBS-2.5M and SBBS3-2.5M glass, a series of peaks at 2θ = 26.5º, 27.8º, 32.1º, 43.0º, 46.2º, 48.5º and 54.0º are found in their XRD patterns. Moreover, the XRD peaks for heavily crystallised SBBS3-3M glass exhibit a same feature but with a slight shift (~0.2º 2θ) to higher angles.

By comparison with the XRD patterns of crystalline barium and strontium molybdates (PDF4 (2012), $SrMoO_4$/00-008-0842 and $BaMoO_4$/00-029-0193, simulated patterns are plotted in Figure 6-8), the evident peaks for BBS and SBBS3 glasses are assigned to $BaMoO_4$ while the inconspicuous peak at 2θ = 27.8º for SBS-2.5M glass may be attributed to the (112) plane of $SrMoO_4$. The slightly higher shift of peaks for SBBS3-3M glass perhaps indicates a partial substitution of Sr^{2+} for Ba^{2+} in $BaMoO_4$ crystals, to form a $Ba_{1-x}Sr_xMoO_4$ solid solution, though the possibility of system error resulting in this shift cannot be excluded.

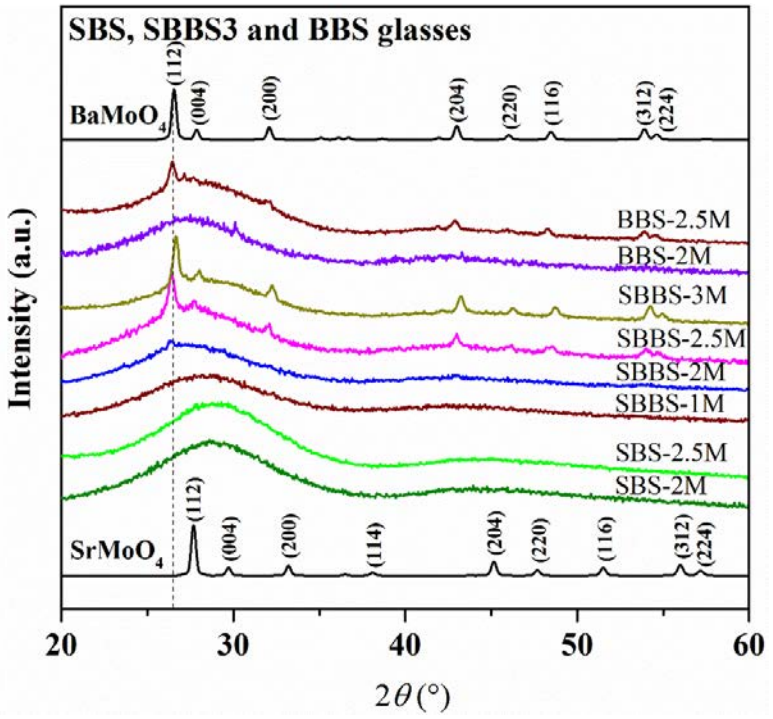

Figure 6-8 XRD patterns of BBS, SBBS3 and SBS glasses with different MoO_3 additions. Simulated patterns for $BaMoO_4$ and $SrMoO_4$ crystals are from ICDD.

6.2.5.2. Aluminosilicate glasses

Amorphous XRD patterns are observed from MAS base to MAS-7M glass while some crystalline peaks are found in the XRD trace of the MAS-8M sample, as shown in Figure 6-9. The peaks in the MAS-8M sample agree best with $MgMoO_4$ (PDF4 (2012), 00-021-0961) crystals and as a result the crystallised phase within MAS-8M glass matrix is thought most likely to be $MgMoO_4$.

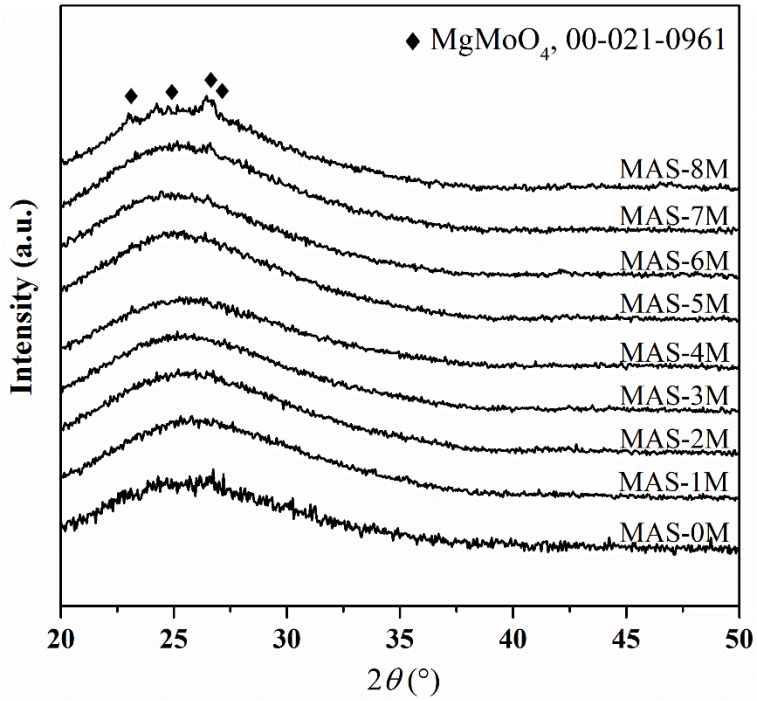

Figure 6-9 XRD patterns of MAS glass with increasing MoO_3 additions.

Figure 6-10 shows the XRD patterns of CAS glass with different MoO_3 additions. CAS glass remains completely amorphous until CAS-2M glass. Then CAS-3M glass shows a notable crystalline peak at 27.2º 2θ even though the glass is transparent. Apart from this peak, CAS-4M glass also shows some other peaks at 2θ = 28.6º, 34.4º and 47.0º, which can be assigned to the (112), (200) and (204) planes of $CaMoO_4$ crystals, respectively. This is thought to be the formation of $CaMoO_4$ crystals that results in opacity in CAS-4M glass. The single peak at 27.2º 2θ is difficult to assign; one possible phase is the orthorhombic molybdite (MoO_3, PDF4 (2012) 00-035-0609) which has an intense peak at 27.3º 2θ assigned to its (021) plane, but further techniques are required to corroborate this possibility.

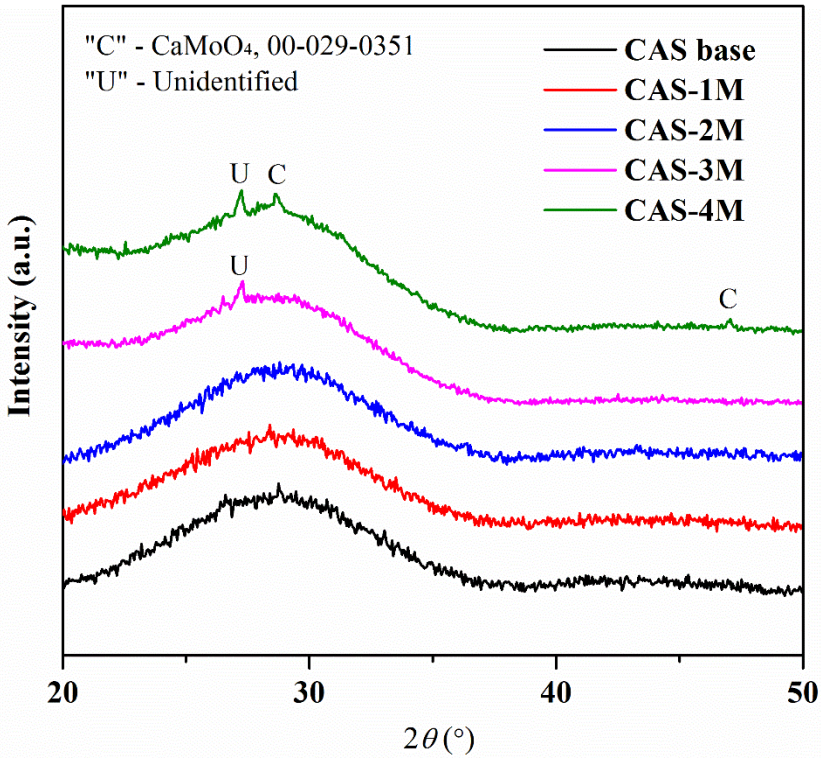

Figure 6-10 XRD patterns of CAS glass with increasing MoO_3 additions.

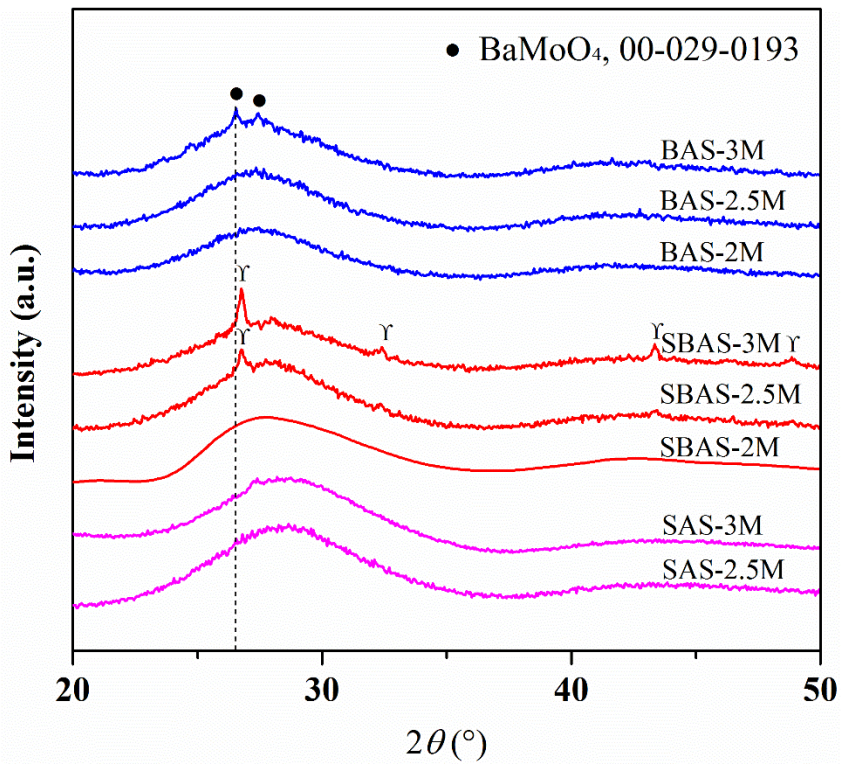

Figure 6-11 XRD patterns of SAS, SBAS and BAS glasses with different MoO_3 additions. Peaks marked with "γ" likely belong to $Ba_xSr_{1-x}MoO_4$ solid solution.

According to Figure 6-11, crystalline peaks are observed in the XRD patterns of BAS-3M, SBAS-2.5M and SBAS-3M samples. The positions of these peaks agree with the patterns of $BaMoO_4$ crystals, which suggests that the crystallised phases are either $BaMoO_4$ or $Ba_{1-x}Sr_xMoO_4$ solid solution (there is slight shift of diffraction angles at 2θ = ~26.8º). The crystallisation in SAS-3M glass is not prominent and it is impossible to identify the separated phase within its glass matrix. When two alkaline earths coexist in glass, excess MoO_4^{2-} ions are preferentially associated with the larger alkaline earth.

6.2.6. DTA

6.2.6.1. Borosilicate glasses

The prepared Mo-containing borosilicate glasses have a good thermal stability until glass transition temperature T_g which is estimated from the onset of the first endothermic peak. Figure 6-12 and Figure 6-13 shows DTA curves of CBS and SBBS3 glasses with MoO_3 incorporation, respectively.

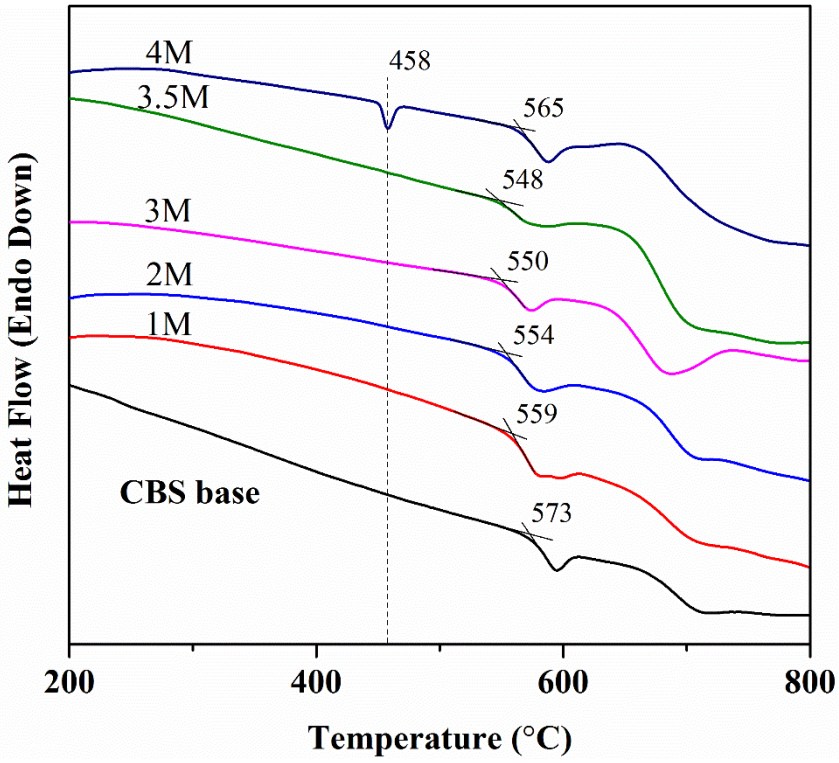

Figure 6-12 DTA curves of CBS glass with increasing MoO_3 additions.

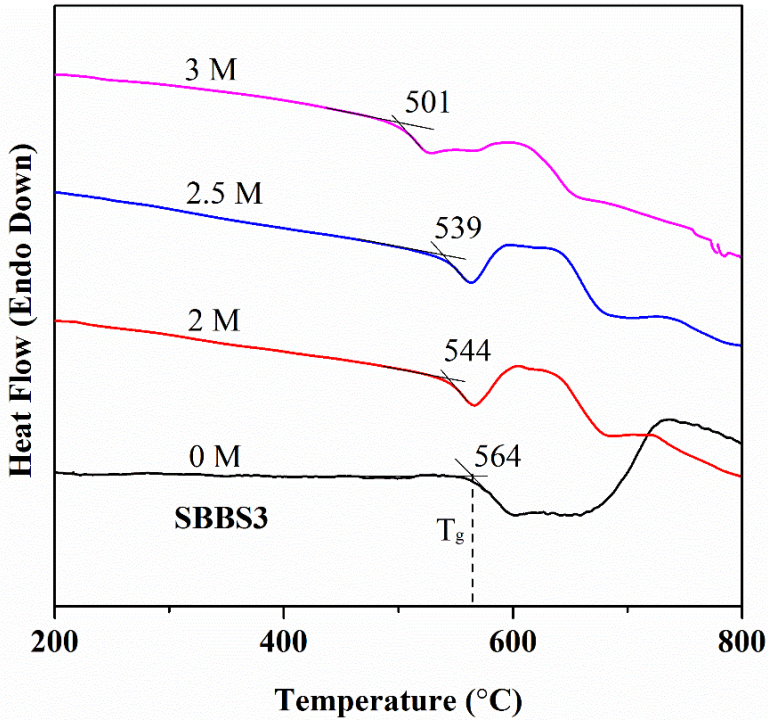

Figure 6-13 DTA curves of SBBS3 glass with increasing MoO_3 additions.

It is clear that MoO_3 incorporation in CBS glass results in notable reduction of T_g from 573 ºC of the CBS base glass to 559 ºC for CBS-1M glass. Afterwards, T_g slightly reduces to 548 ºC of CBS-3.5M glass which has been partly crystallised. However, the heavily crystallised CBS-4M glass shows an increased T_g of 565 ºC, even higher than that of CAS-1M glass. Moreover, there is an endothermic peak centred at 458 ºC before the glass transition. TGA result indicates that there is no mass change at this temperature range, so this peak is possibly due to phase transition of Na_2MoO_4 (a stable orthorhombic polymorph at 440-590 ºC, PDF4 (2012) 00-026-0967) or melting of other components in glass. In addition, the crystallisation hump after the glass transition peak is smooth for all samples, which may suggest that the devitrification process of these glasses is not dramatic.

The incorporation of MoO_3 into SBBS3 glass reduces T_g from 564 ºC for the base glass to 544 ºC for SBBS3-2M glass. Such a reduction continues down to 539 ºC in the slightly crystallised SBBS3-2.5M sample and to 501 ºC in the heavily crystallised SBBS3-3M sample. MoO_3 incorporation also reduces T_c of SBBS3 glasses: in the base glass the crystallisation exothermic plateau begins at ~700 ºC but in the loaded glasses it begins at ~570 ºC. The crystallisation plateau in SBBS3-3M glass is less apparent,

probably due to the presence of a large amount of molybdate crystals in it.

Generally speaking, MoO_3 incorporation in borosilicate glass does not impact the glass thermal stability. However, it reduces the glass transition and crystallisation temperatures and this decreasing tendency can be accelerated as molybdate induced phase separation occurs within the glass.

6.2.6.2. Aluminosilicate glasses

Figure 6-14 shows two typical DTA curves of MAS glasses. MAS-0M to MAS-6M glasses have a curve like the black solid one whereas MAS-7M and MAS-8M glasses have a curve like the red dashed one; the main difference is the disappearance of the second and sharp exothermic peak in the red dashed curve. All the curves exhibit no features until T_g is reached, which suggests the good thermal stability of MAS glasses. The two exothermic peaks recorded after T_g indicate two distinct crystallisation events upon heating. The relations between the temperatures at which the above thermal reactions occur and the molybdate addition in glass are plotted in Figure 6-15. Both T_g and T_{c1} (first crystallisation temperature) exhibit similar downwards linear trends with increasing molybdate content, reducing from 775 ºC for the base glass to 741 ºC for MAS-8M and from 831 ºC for the base glass to 794 ºC for MAS-8M, respectively. For those samples exhibiting a subsequent crystallisation T_{c2} (second crystallisation temperature) also exhibits a downwards linear trend reducing from 1010 ºC to 923 ºC for MAS-6M glasses.

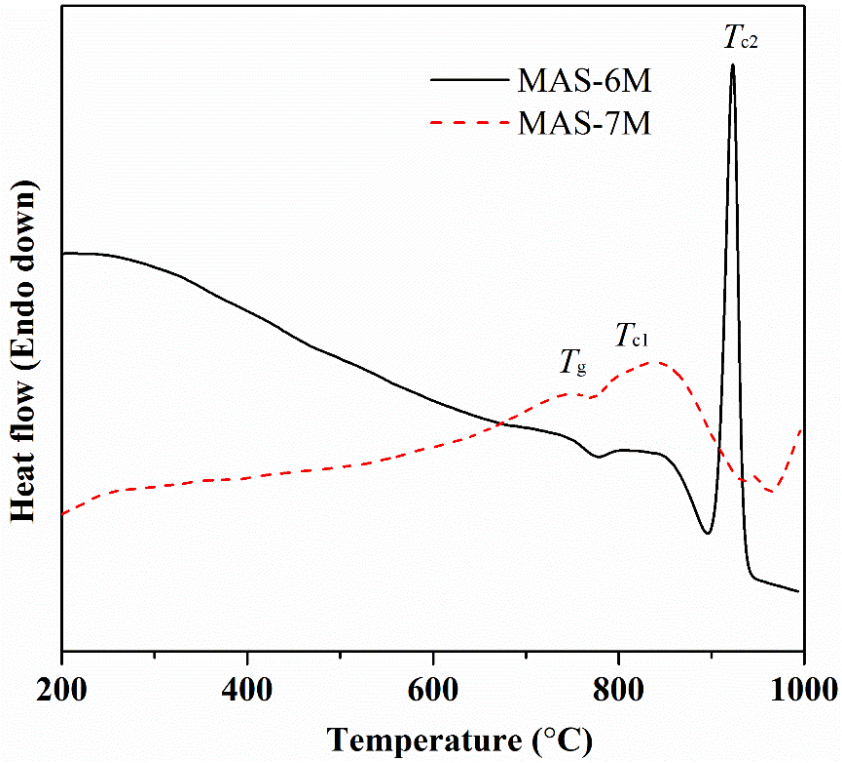

Figure 6-14 Two typical DTA curves of MAS glass with MoO_3 additions. MAS-6M curve (black and solid) represents MAS-0M to MAS-6M glasses and MAS-7M line (red and dash) represents MAS-7M and MAS-8M glasses.

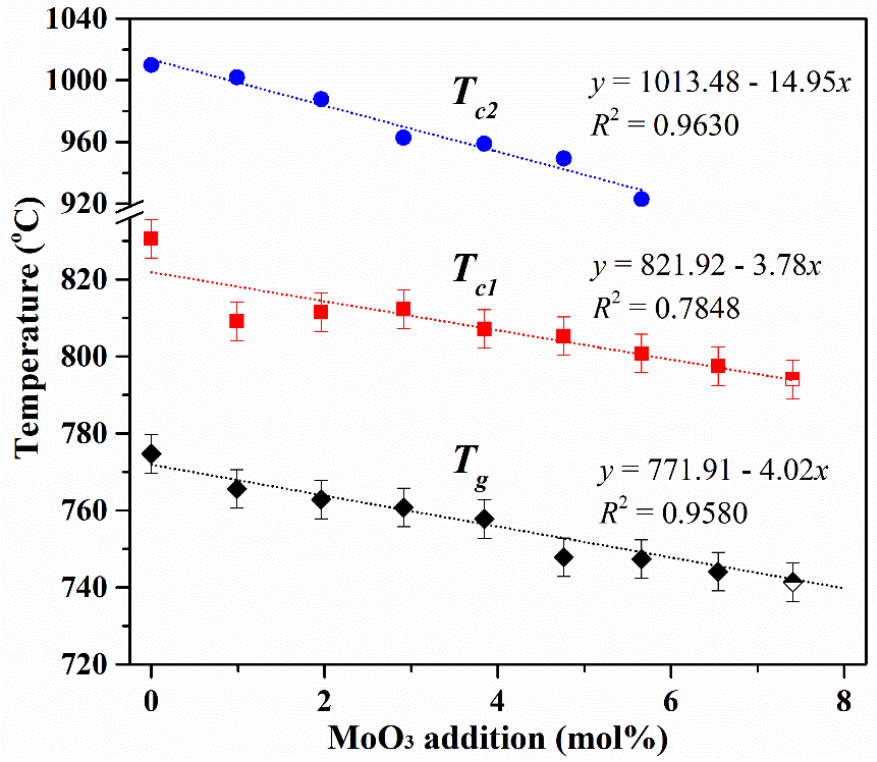

Figure 6-15 Changes in T_g, T_{c1} and T_{c2} of MAS glass with increasing MoO_3 addition.

The DTA curves of CAS glass with increasing MoO_3 additions are shown in Figure 6-16. Initial MoO_3 incorporation results in a notable reduction in T_g from 792 ºC for the CAS base glass to 779 ºC for CAS-1M glass while further MoO_3 incorporation only slightly reduces T_g until 775 ºC for CAS-3M glass. This downward trend also continues for the phase separated CAS-4M glass. Like the MAS glasses, CAS glasses also show two crystallisation peaks after the glass transition. The first crystallisation temperature T_{c1} is monotonically reduced from CAS-0M to CAS-3M glasses and then slightly increased for CAS-4M glass. The same behaviour is observed for the starting point of the second and intense exothermic peak which signifies another crystallisation, although the entire peak was not recorded for CAS-2M to CAS-4M glasses.

In addition, the DTA curves of SAS, SBAS and BAS glasses containing MoO_3 are not shown here, but T_g and T_c (if applicable) for these glasses are listed in Appendix I. A general similar trend of decreasing T_g with increasing MoO_3 content is found for these glasses regardless of the occurrence of phase separation. However, the crystallisation peaks, especially the second one, are not apparent as in MAS and CAS glasses.

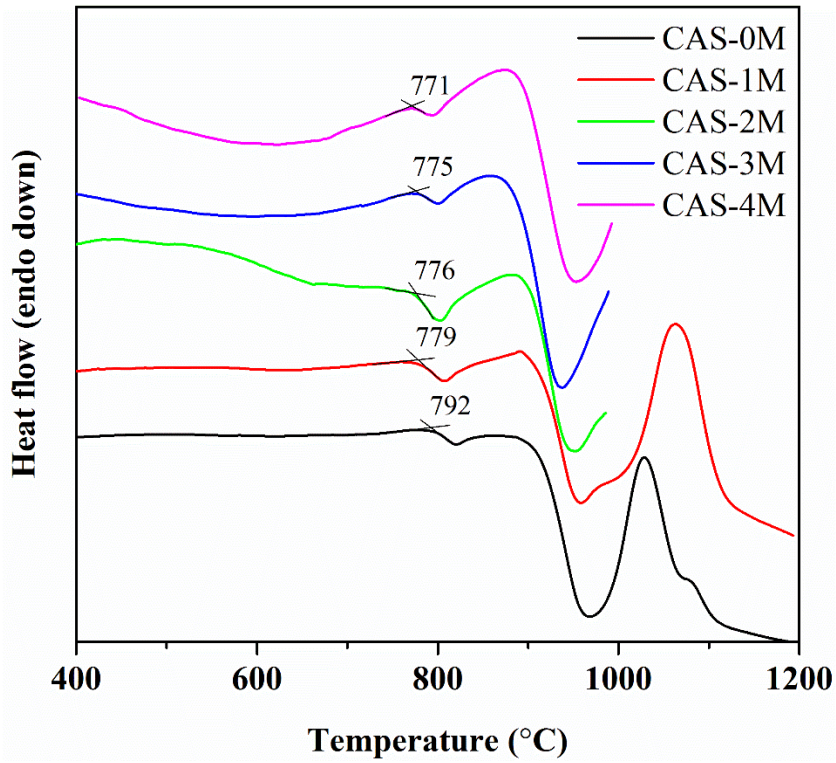

Figure 6-16 DTA curves of CAS glass with increasing MoO_3 additions.

6.2.7. High temperature XRD (HT-XRD)

In order to investigate the nature of the second and intense exothermic peak in DTA curves of MAS glasses, HT-XRD has been performed to analyse the crystalline phases present at different temperatures. Results of 900 to 1000 ºC heat treatments are shown in Figure 6-17.

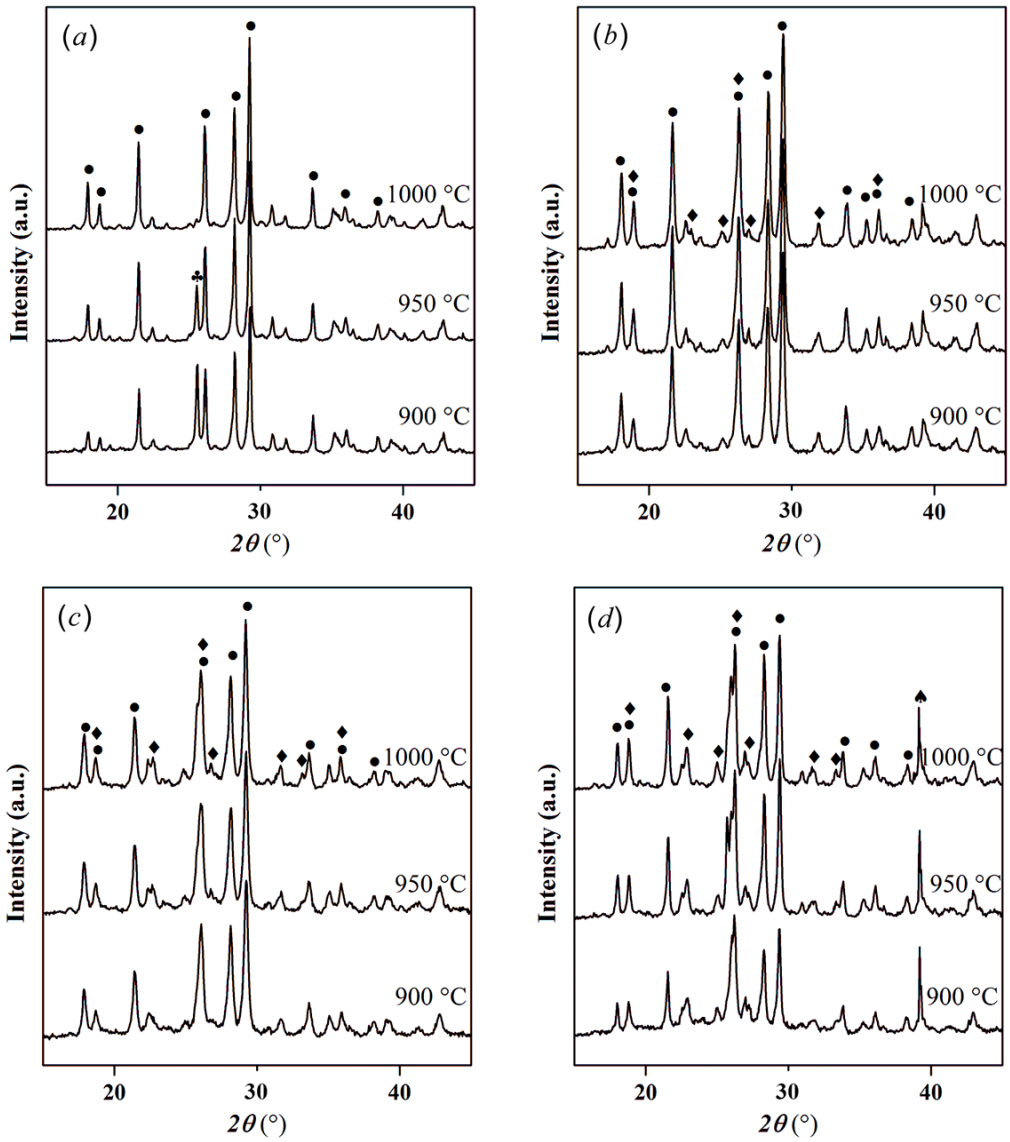

Figure 6-17 High temperature XRD patterns of (*a*) MAS-0M, (*b*) MAS-3M, (*c*) MAS-6M and (*d*) MAS-7M glasses at 900, 950 and 1000 ºC, respectively. ("●" - cordierite/indialite $Mg_2Al_4Si_5O_{18}$, PDF4 (2012), 00-012-0303/00-013-0293; "♣" - metastable $Mg_2Al_4Si_5O_{18}$ at 900 ºC, PDF4 (2012), 00-014-0249; "♦" - $MgMoO_4$, PDF4 (2012), 00-021-0961; "♠" - platinum sample holder)

After the first glass crystallisation at ~800 ºC, the main phase of each glass is cordierite ($Mg_2Al_4Si_5O_{18}$, PDF4 (2012), 00-012-0303) which crystallises from the base glass network. Meanwhile, a number of relatively low intensity peaks assigned to $MgMoO_4$ (PDF4 (2012), 00-021-0961) can be found in molybdate containing glasses at 2θ = 22.6º (021), 25.0º (201), 26.8º ($\bar{1}12$) and 33.2º ($\bar{3}12$) and overlapping with peaks of cordierite at 2θ = 18.7º ($\bar{2}01$), 31.6º ($\bar{1}31$) and 36.0º (400). In the temperature range 900 to 1000 ºC, the peaks of $MgMoO_4$ appear and are intensified in the MAS-3M and MAS-6M glasses whereas in the MAS-7M glass the relative intensity does not change with increasing temperature. However, a peak at 25.7 º2θ appears at 950 ºC and merges with the neighbouring peak at 26.0 º2θ at 1000 ºC in the MAS-7M sample. In addition, the XRD patterns of MAS-0M glass indicate little change except a peak at 25.6 º2θ which vanishes between 900 and 1000 ºC

6.2.8. Raman spectroscopy

6.2.8.1. Borosilicate glasses

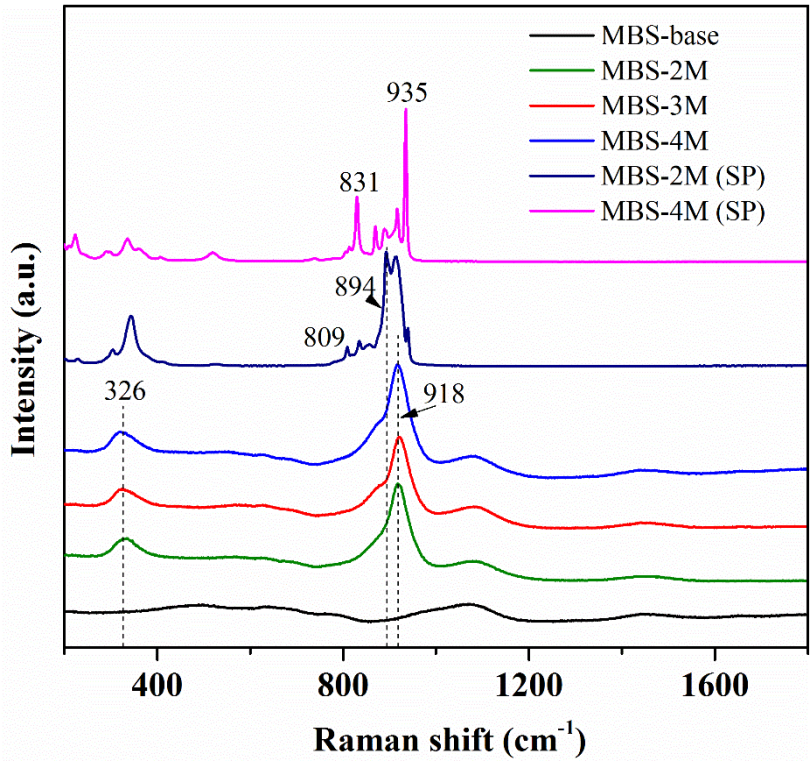

Figure 6-18 Raman spectra of MBS glasses with increasing MoO_3 additions.

Figure 6-18 shows Raman spectra of MBS glass series as well as the separated phases within MBS-2M and MBS-4M glasses. The broad band ranged between 850 and 1200 cm^{-1} is assigned to Si-O stretching vibrations of SiO_4 structural units. The addition of MoO_3 results in two bands positioned at 326 and 918 cm^{-1}. The 326 cm^{-1} band is a convolution of the symmetric and asymmetric bending vibration modes (v_2 and v_4) in MoO_4^{2-} tetrahedra while the 918 cm^{-1} band is a convolution of the symmetric and asymmetric stretching vibration modes (v_1 and v_3) in MoO_4^{2-} tetrahedra. The vibration frequencies of MoO_4^{2-} tetrahedra are given in Saraiva *et al.* (2008) and Ozeki *et al.* (1987) for alkali and alkaline earth molybdate crystals. In amorphous materials such as glass, the variable local environment means that only two broad bands are attained.

While the 326 and 918 cm^{-1} bands still remain for the glassy region of each sample, the separated phases inside them display different Raman spectra where the broad bands are split and a number of new peaks are created in the 809 and 935 cm^{-1} region. The assignment of these peaks is difficult because a variety of molybdates may have vibrational frequencies in this region, but the significant differences between the patterns of separated phases in MBS-2M and MBS-4M glasses suggests that the crystals in them are not the same. Based on the XRD results (Figure 6-6), the peaks at 831 and 935 cm^{-1} are likely to be due to Na_2MoO_4 whereas the peaks at 809 and 894 cm^{-1} are likely to be due to $Na_{2.4}Mg_{0.8}MoO_4$.

According to Figure 6-19, MoO_3 incorporation in CBS glass results in creation of two bands which are centred at 321 and 911 cm^{-1}, respectively. Similar to those for MBS glass, each of these two bands is a convolution of several neighbouring broad bands. The pattern remains similar until CBS-2.5M glass and after that a narrow peak centred at 874 cm^{-1} appears on the shoulder of the 911 cm^{-1} band for CBS-3M glass. This peak is intensified for CBS-3.5M and CBS-4M glasses, coupled with emergence of three other peaks at 390, 789 and 843 cm^{-1}. The peaks agree well with the Raman spectrum of $CaMoO_4$ crystals reported by Ozeki *et al.* (1987) and hence it can be concluded that the separated phase within CBS-3.5M and CBS-4M glasses is primarily $CaMoO_4$. Meanwhile, the segregated layer of CBS-4M glass shows a different Raman spectrum where there are two intense peaks centred at 832 and 898 cm^{-1}, respectively. As this layer has been identified by XRD to be a mixture of $CaMoO_4$ and Na_2MO_4, the 832 and 898 cm^{-1} peaks are most likely assignable to Na_2MoO_4 crystals.

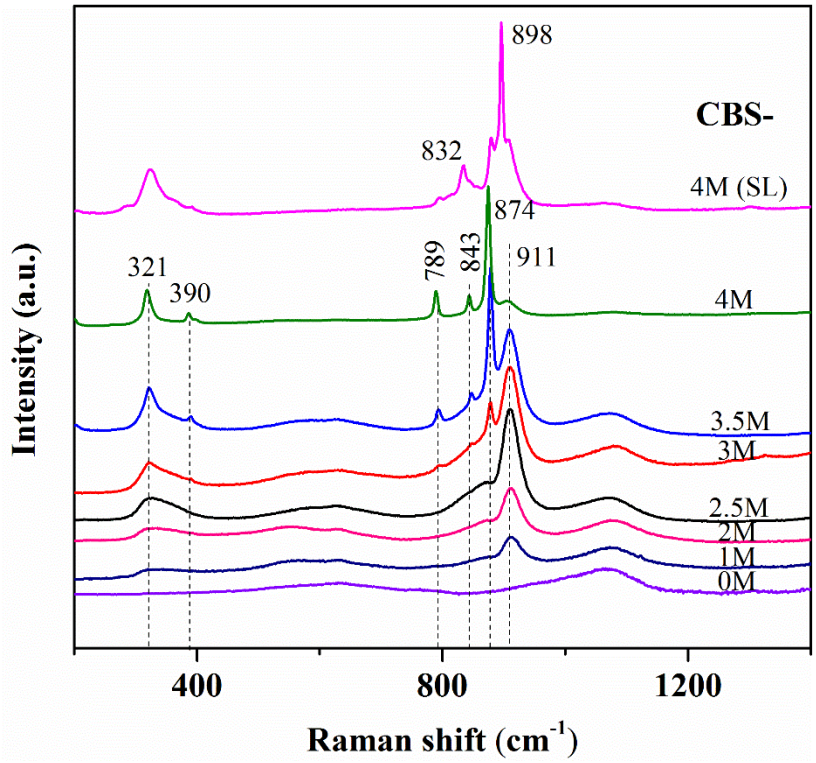

Figure 6-19 Raman spectra of CBS glasses with increasing MoO_3 additions.

Figure 6-20 shows Raman spectra of SBBS3 glass series together with BBS-2.5M and SBS-2.5M glasses. The incorporation of MoO_3 in SBBS3 glass creates two MoO_4^{2-} bands assigned to the υ_1 (902 cm^{-1}) and υ_3 (327 cm^{-1}) modes, respectively. The position of the 902 cm^{-1} band moves to 900 cm^{-1} in BBS glass and 904 cm^{-1} in SBS glass, indicating that the local environment of MoO_4^{2-} in SBBS3 glass is influenced by both Ba^{2+} and Sr^{2+} ions. Regarding the peaks assigned to crystalline molybdates in the spectra of phase separated glasses, the main difference arises from the position of the υ_1 mode. While the υ_1 peak is located at 893 cm^{-1} for both BBS-2.5M and SBBS-2.5M glasses, this peak shifts to 887 cm^{-1} for SBS-3M glass. This means that the separated phase in SBBS-2.5M glass is the same as or similar to the separated phase in BBS-2.5M glass, namely $BaMoO_4$. Therefore, MoO_4^{2-} ions are jointly associated with Sr^{2+} and Ba^{2+} in glass with the coexistence of Ba^{2+}, Sr^{2+} and Na^{+} ions, but prone to separate out from network with Ba^{2+} when exceeding its loading limit.

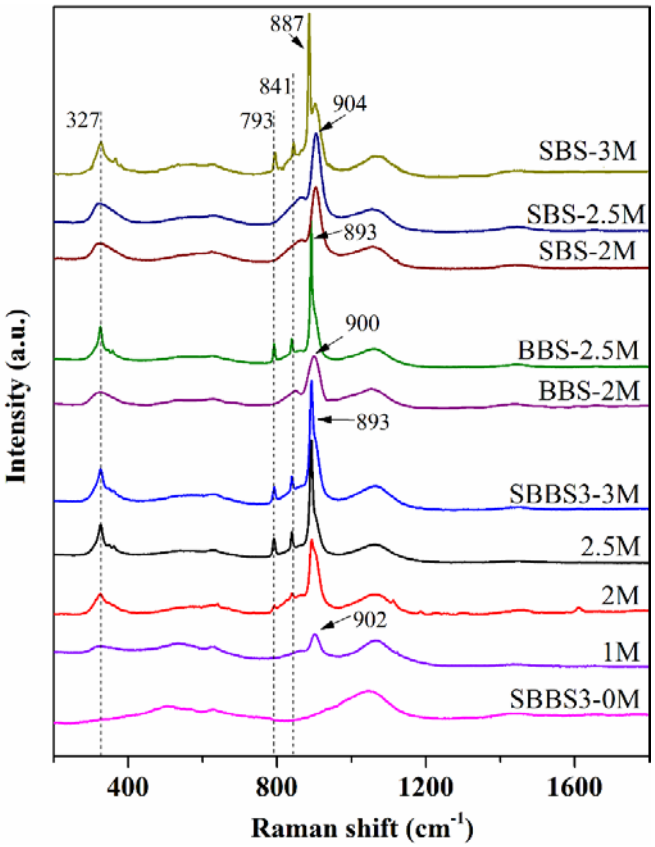

Figure 6-20 Raman spectra of SBBS3 glasses with increasing MoO_3 additions.

6.2.8.2. Aluminosilicate glasses

The Raman spectra of aluminosilicate glasses suffer significant fluorescence and as a result proper treatments have to be carried out before presenting the corrected spectra. Firstly the background was extrapolated from an exponential function fitting the interval between 1300 and 2000 cm^{-1} where no Raman signal should be detected. Secondly, the subtracted intensity was multiplied by the Long correction factor (Long 1977) which is dependent on frequency and temperature (temperature is constant in this study). Finally the corrected intensity is normalised by that of the silicate band at ~550 cm^{-1} which is believed to be unaffected by MoO_3 incorporation. The 550 cm^{-1} band is assigned to Si-O-Si bending vibrations while the silicate band between 850 and 1200 cm^{-1} is assigned to Si-O stretching vibrations; It is assumed that the relative area ratio of these two bands remain the same throughout glasses. Therefore, the area of molybdate stretching band, which overlaps with silicate stretching band at 800-1200 cm^{-1} interval, can be obtained by subtracting the area of silicate stretching band from the whole area in this region.

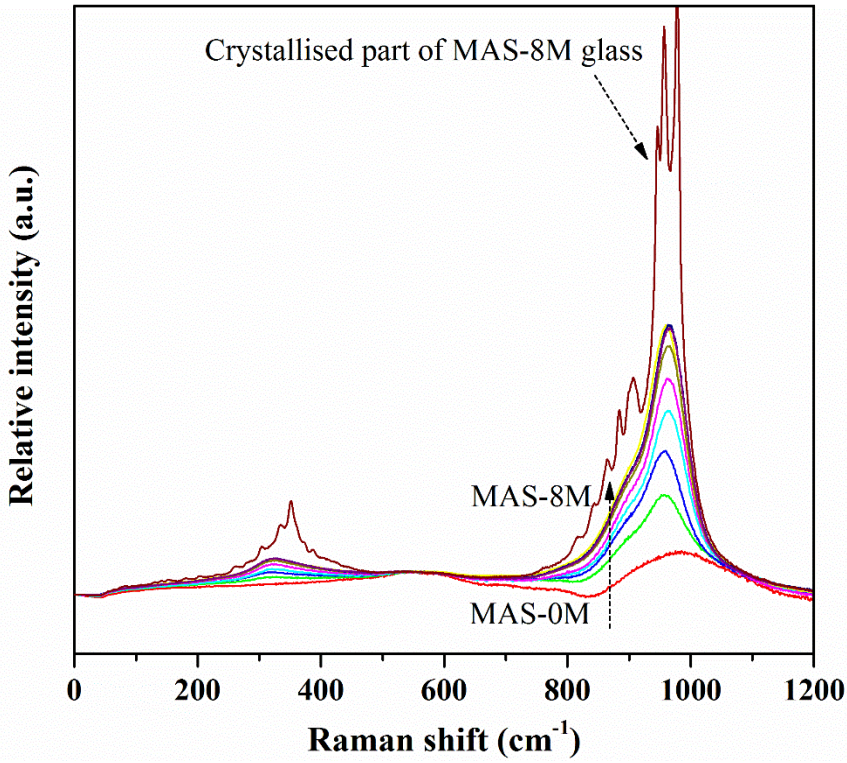

Figure 6-21 Corrected and normalised Raman spectra of MAS glasses with different MoO_3 additions.

Figure 6-21 shows the corrected Raman spectra of MAS glass series. MAS-0M (base) glass reveals two prominent broad bands centred at 980 cm^{-1} and 550 cm^{-1}, which are assigned to the vibrations of Si-O stretching modes and Si-O-Si bending modes in depolymerised structural units (McMillan 1989, Neuville and Mysen 1996), respectively. MoO_3 incorporation in MAS glass results in two broad bands positioned at 320 and 965 cm^{-1}, respectively, likewise in the Mo-containing borosilicate glasses. These two bands remain scattered from MAS-1M to the glassy part of MAS-8M sample and their relative intensities increase with increasing MoO_3 content in glass. In the crystallised part of the MAS-8M sample, these two bands are split into a number of sharp peaks which prove the existence of a crystalline molybdate phase. According to XRD results, these peaks are most likely assigned to $MgMoO_4$.

Raman spectra of CAS glasses (Figure 6-22) indicate that MoO_3 incorporation results in one broad band located at 300-400 cm^{-1} and another broad band centred at 919 cm^{-1}. In agreement with XRD results, only CAS-4M glass shows crystalline peaks in Raman spectra. The series of peaks at 322, 389, 792, 847 and 878 cm^{-1} match with the

patterns of $CaMoO_4$ crystals (Ozeki *et al.* 1987) and resembles the peaks seen in phase separated CBS-4M glass (within 4 cm^{-1} shift). It is worth noting that in Raman spectra of CAS-3M and CAS-4M glasses there are no peaks assigned to crystals other than $CaMoO_4$, but in their XRD patterns there is an unidentified crystalline peak at 2θ = 27.2°. It is possible that the XRD peak is attributed to a phase not from the glass, or the phase responsible for the XRD peak is not sensitive in Raman spectroscopy.

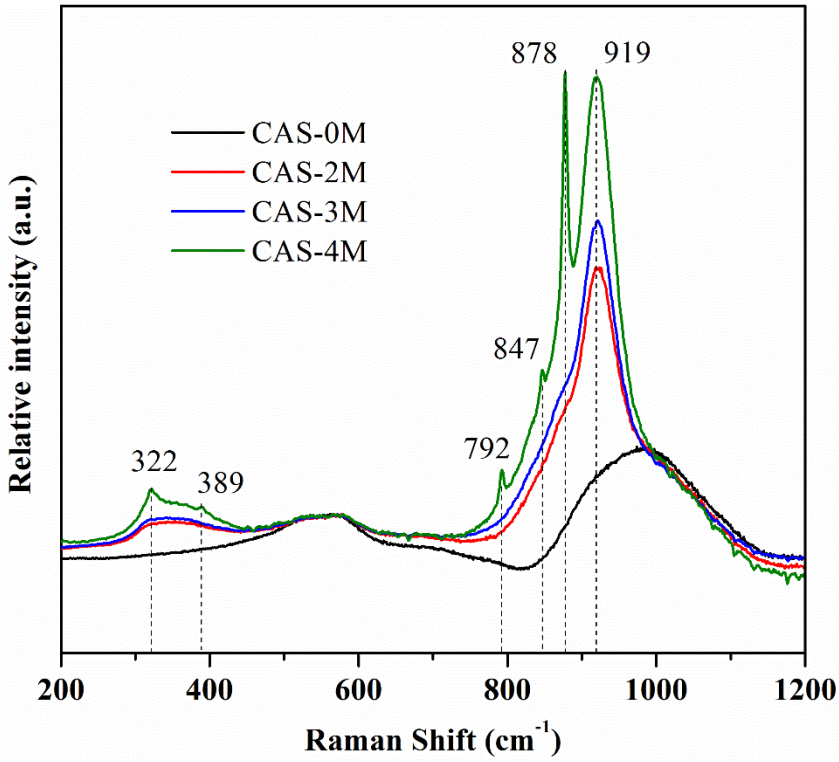

Figure 6-22 Corrected and normalised Raman spectra of CAS glass series.

Since the fluorescence influence on Raman spectra of SAS, SBAS and BAS glasses is not strong, the obtained Raman spectra are not modified with background subtraction. As shown in Figure 6-23, MoO_3 incorporation in SAS, SBAS and BAS glasses also results in two bands located at ~320 cm^{-1} and ~900 cm^{-1}, respectively. The centre of the latter band shifts from 906 cm^{-1} for SAS glass to 902 cm^{-1} for SBAS glass and to 898 cm^{-1} for BAS glass, which indicates that the MoO_4^{2-} environment in glass is strongly related to alkaline earth species and amount. However, all these three glass compositions show a nearly identical series of frequencies of crystalline peaks (at 326, 791, 841 and 893 cm^{-1}, respectively) when they are phase separated. Theoretically the Raman spectra of $BaMoO_4$ and $SrMoO_4$ crystals are very similar (Ozeki *et al.* 1987)

and thus it is difficult to differentiate the alkaline earth cations with which MoO_4^{2-} ions are associated in crystallised phases by Raman spectroscopy.

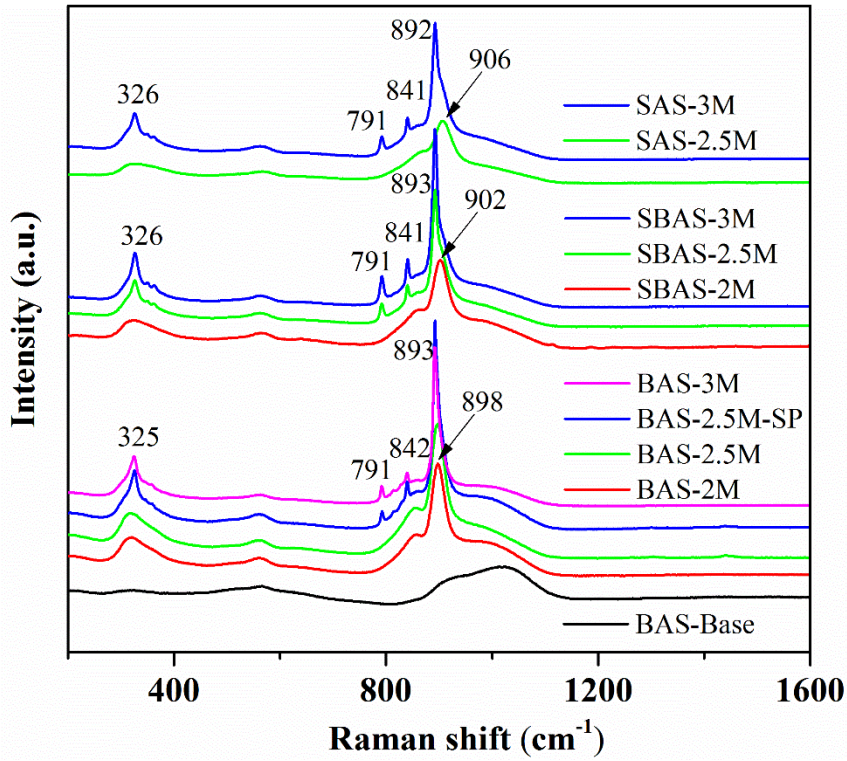

Figure 6-23 Raman spectra of SAS, SBAS and BAS glass series.

6.2.9. FTIR

6.2.9.1. Borosilicate glasses

FTIR spectra of CBS glass series are shown in Figure 6-24. CBS base glass shows broad bands located at 400-600 cm^{-1}, ~700 cm^{-1}, 800-1250 cm^{-1}, 1400-1550 cm^{-1} and 1650 cm^{-1}. According to Uchino *et al.* (1989) and Darwish and Gomaa (2006), the band located at 1650 cm^{-1} is assigned to vibrations of water (from the residual water as impurity in sample or moisture in the air; FTIR is sensitive to its presence), the band located at 1400-1550 cm^{-1} is assigned to B-O stretching vibrations in BO_3 units, the band between 800 and 1250 cm^{-1} is assigned to Si-O and/or B-O stretching vibrations in SiO_4/BO_4 units, the band at ~700 cm^{-1} is assigned to oxygen between two BO_3 units and the band at 400-600 cm^{-1} is assigned to Si-O bending or O-Si-O rocking vibrations.

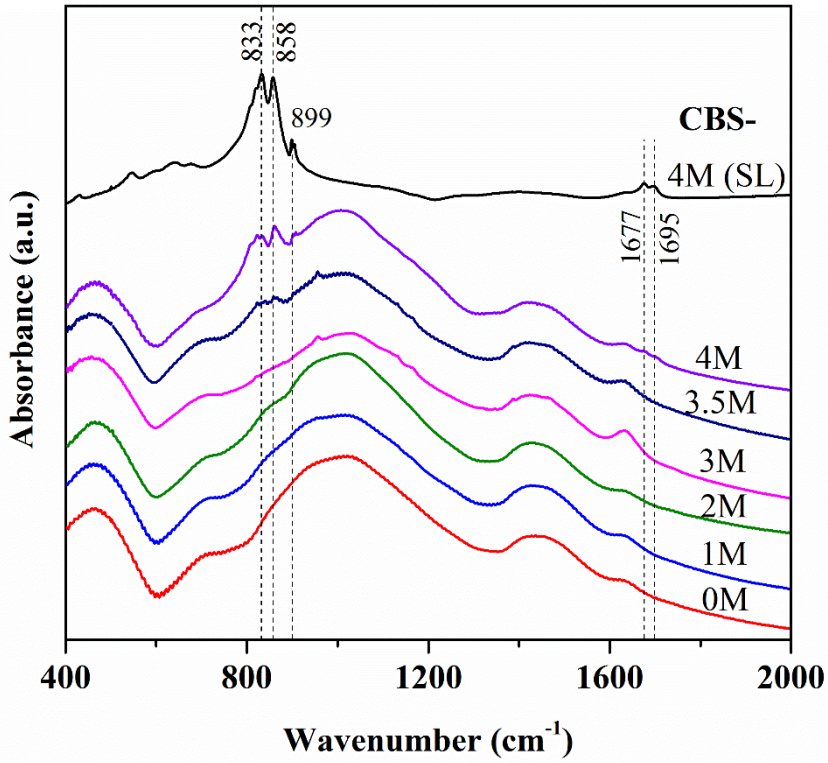

Figure 6-24 FTIR spectra of CBS glass series. CBS-4M (SL) means the segregated layer of CBS-4M glass.

MoO_3 incorporation in CBS glass does not result in significant change in FTIR spectra; only a small shoulder at ~850 cm^{-1} is observed and its relative intensity increases with increasing MoO_3 content. In the spectra of phase separated CBS-3.5M and CBS-4M glasses, this shoulder is split into two peaks at 833 and 858 cm^{-1}, respectively. Three other bands located at 899, 1677 and 1695 cm^{-1} are also observed in the spectra of CBS-4M glass and its segregated layer. The positions of 833, 858 and 899 bands are in good agreement with the FTIR spectrum of Na_2MoO_4 (Miller and Wilkins 1952). $CaMoO_4$ exhibits a strong absorption peak at 827 cm^{-1} in its FTIR spectrum (Ansari *et al.* 2014) thus the non-Gaussian band at 833 cm^{-1} is likely a convolution of two bands which are attributed to Na_2MoO_4 and $CaMoO_4$, respectively. The bands at 1677 and 1695 cm^{-1} can be attributed to both phases according to their reference spectra.

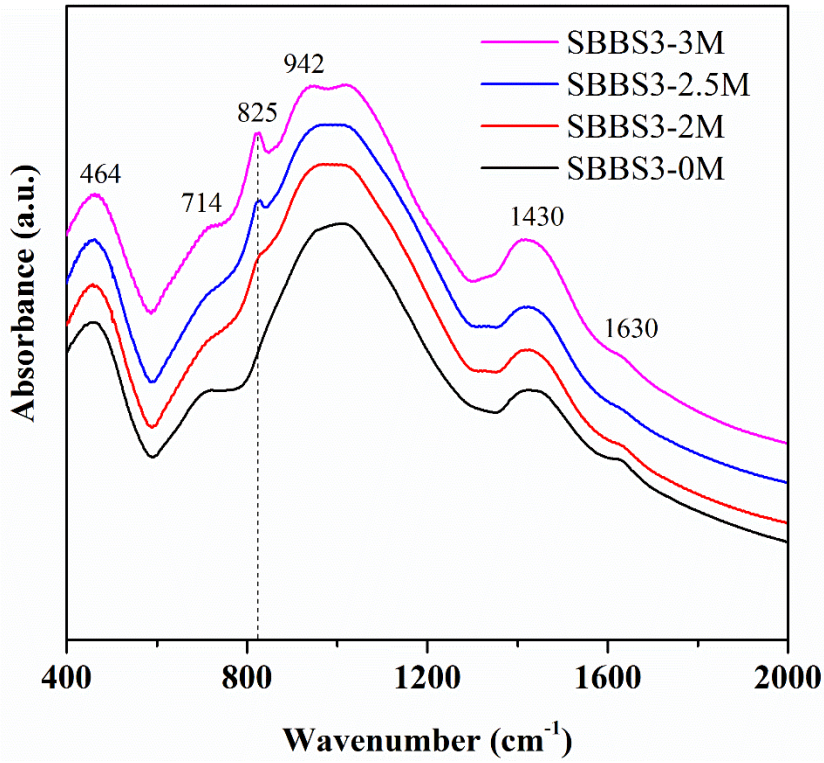

Figure 6-25 FTIR spectra of SBBS3 glasses with increasing MoO_3 additions.

The FTIR spectrum of SBBS3 base glass is analogous to the spectrum of CBS base glass and the assignments of the bands are as described above. The incorporation of MoO_3 into SBBS3 glass results in a shoulder appearing on the broad 800-1200 cm^{-1} band, as seen in Figure 6-25. The shoulder centred at 822 cm^{-1} becomes narrower and more intense in SBBS3-2.5M glass which is slightly crystallised, whereas in the heavily crystallised SBBS3-3M glass this shoulder is further intensified together with the emergence of another shoulder at 942 cm^{-1}. The 822 cm^{-1} band is likely due to crystalline $SrMoO_4$ which has a main absorption band at 825 cm^{-1} (B6000473, NIST database) or crystalline $BaMoO_4$ which has a main absorption band at 810 cm^{-1} (Phuruangrat *et al.* 2009) or their solid solutions in glass. The 942 cm^{-1} band cannot be assigned to stretching vibrations of MoO_4^{2-} units either in $BaMoO_4$/$SrMoO_4$ or in Na_2MoO_4; the band is possibly caused by structural change in the heavily crystallised glass.

Figure 6-26 compares FTIR spectra of different phase separated borosilicate glasses. BBS-2.5 glass has a MoO_4^{2-} band at 822 cm^{-1} whereas SBS-2.5M glass has a MoO_4^{2-} band at 826 cm^{-1}, indicating that the environment of MoO_4^{2-} ions in SBBS3-2.5M

glass is closer to that in BBS-2.5M glass rather than that in SBS-2.5M glass. The crystallised phase in SBBS3-2.5M glass is more likely to be $BaMoO_4$. MBS-2M glass shows a shoulder at 860 cm^{-1} which, like the 858 cm^{-1} band in CBS-3.5M glass, is assigned to vibrations of MoO_4^{2-} units associated with Na^+. Generally speaking, the band assigned to MoO_4^{2-} vibrations shifts to lower frequency as larger alkaline earths in phase separated glasses are substituted by smaller ones.

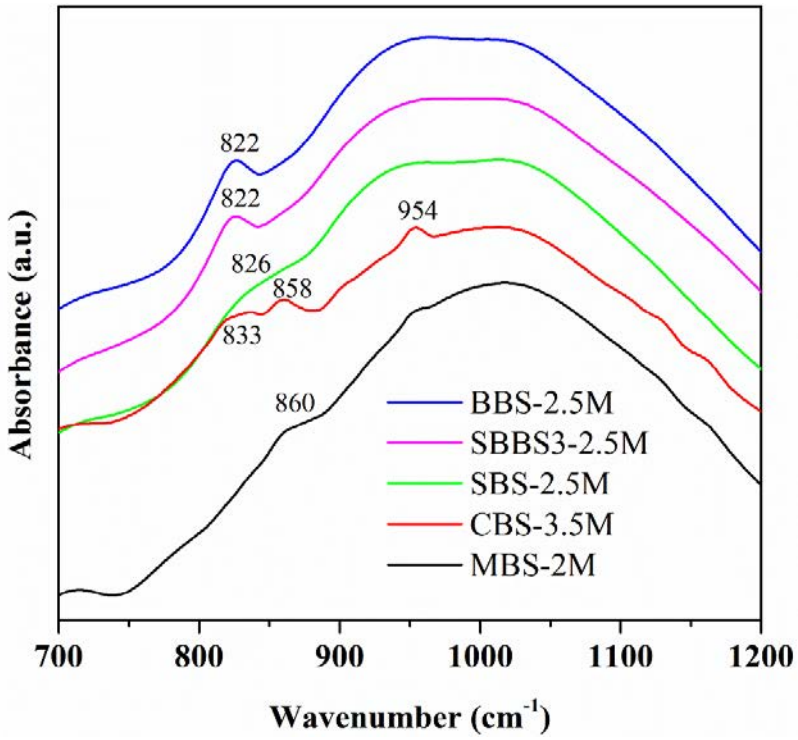

Figure 6-26 FTIR spectra of phase separated borosilicate glasses.

6.2.9.2. Aluminosilicate glasses

As seen in Figure 6-27, CAS base glass shows a series of scattered bands at ~480, ~698, 800-1200 and ~1627 cm^{-1}, which are assigned to Si-O bending vibration, Si-O-(Si, Al) symmetric stretching vibration, Si-O-(Si, Al) asymmetric stretching vibrations and vibration of water, respectively (Schofield 2011).

MoO_3 incorporation in CAS glass does not cause any prominent band in the FTIR spectrum; only the intensity of the main band ranged in 800-1200 cm^{-1} is increased with increasing MoO_3 content, which is likely due to the superimposition of MoO_4^{2-} band (800-900 cm^{-1}) in this region. Even in the spectrum of phase separated CAS-4M

glass there is no additional peak for the crystalline phase ($CaMoO_4$), thus the relative amount of $CaMoO_4$ in glass is still low.

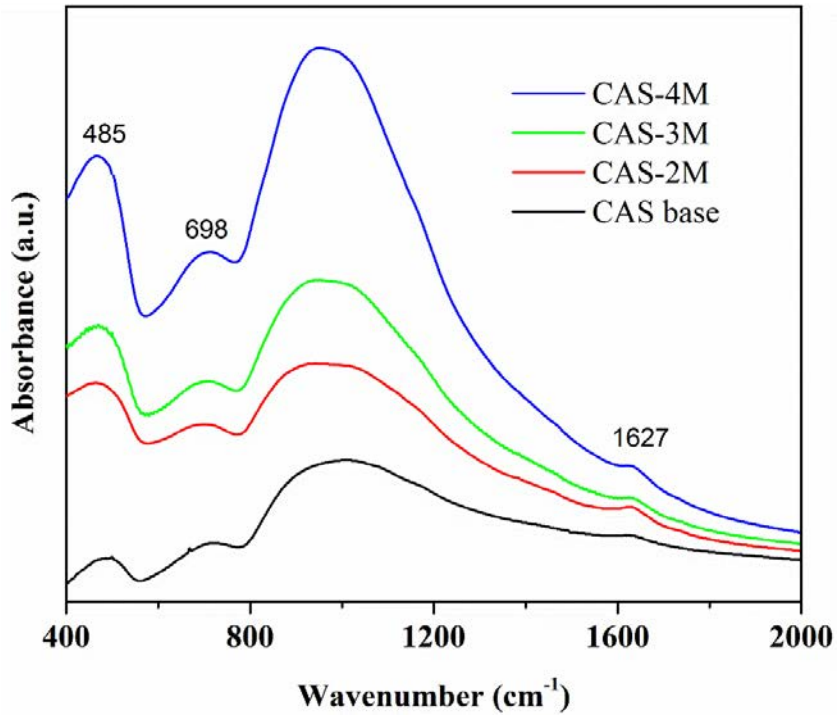

Figure 6-27 FTIR spectra of CAS glasses with increasing MoO_3 additions.

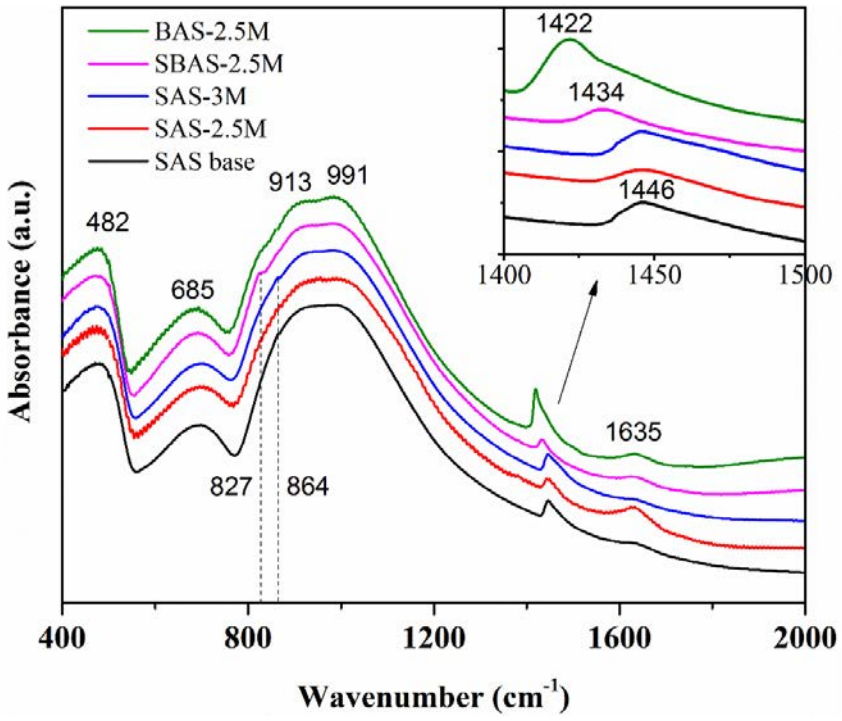

Figure 6-28 FTIR spectra of SAS glasses with increasing MoO_3 additions, in comparison with spectra of BAS-2.5M and SBAS-2.5M glasses.

Figure 6-28 shows that the incorporation of MoO_3 in SAS glass does not result in any new band until phase separated SAS-3M glass which has a small peak at 864 cm^{-1}. At the same time, SBAS-2.5M glass has a smaller peak at 827 cm^{-1} while BAS-2.5M glass also has a shoulder at this frequency. These frequencies are assigned to the stretching vibrations of MoO_4^{2-} ions and it appears that MoO_4^{2-} ions in strontium-barium combined SBAS-2.5M glass have a local environment closer to that in BAS-2.5M glass than that in SAS-2.5M glass. Moreover, the peak at 1446 cm^{-1} in SAS glasses shifts to lower frequencies of 1434 cm^{-1} in SBAS-2.5M glass and 1422 cm^{-1} in BAS-2.5M glass.

6.2.10. SEM

The microstructure of phase separated Mo-containing glasses has been observed with SEM in both backscattered electron (BSE) and secondary electron (SE) modes.

6.2.10.1. Borosilicate glasses

Figure 6-29 (*a*) and (*b*) shows the secondary electron images of CBS-3.5M and CBS-4M samples, respectively. Both samples are opaque and separated particles can be observed in both glass matrices under high magnification. It appears that such separated particles are both randomly dispersed and that they have a spherical or square shape while showing different sizes in each glass (average diameter of particles in CBS-3.5M and CBS-4M glasses is 500 nm and 1 μm, respectively).

EDX analysis has been performed to compare the compositional difference between separated particles and glass matrices in CBS-4M glass (areas marked in Figure 6-29 (*b*)). As shown in Figure 6-30, the separated particles are much more enriched in Mo and Ca compared with glass matrix, while Na and Si are apparently more abundant in glass matrix. This indicates that the separated particles are probably $CaMoO_4$. In addition, the scarce Na in separated particles suggests that the XRD peaks assigned to Na_2MoO_4 phases may arise from the residual segregated layer in glass.

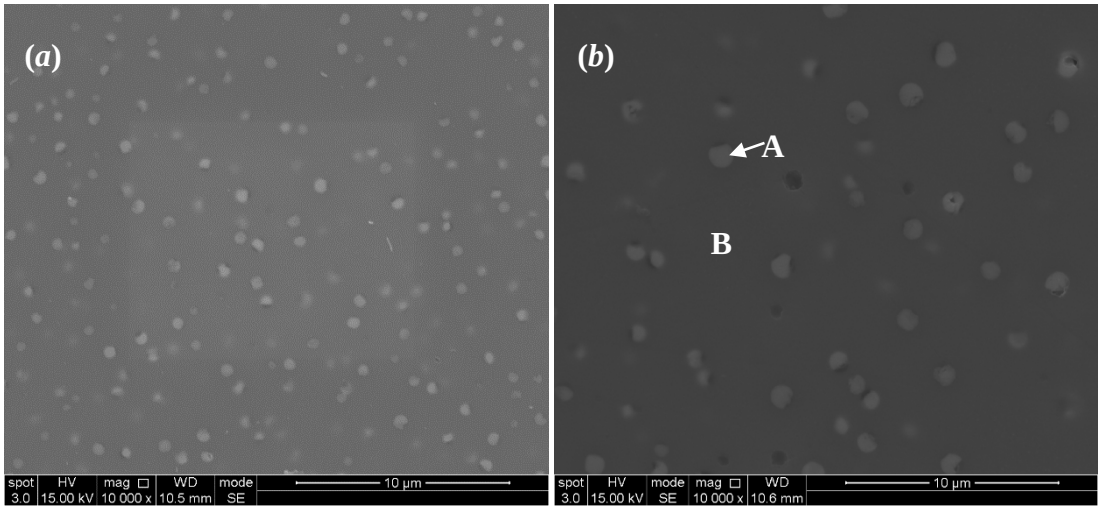

Figure 6-29 Secondary electron images of (*a*) CBS-3.5M and (*b*) CBS-4M glasses. Spots A and B in CBS-4M glass are selected for compositional comparison.

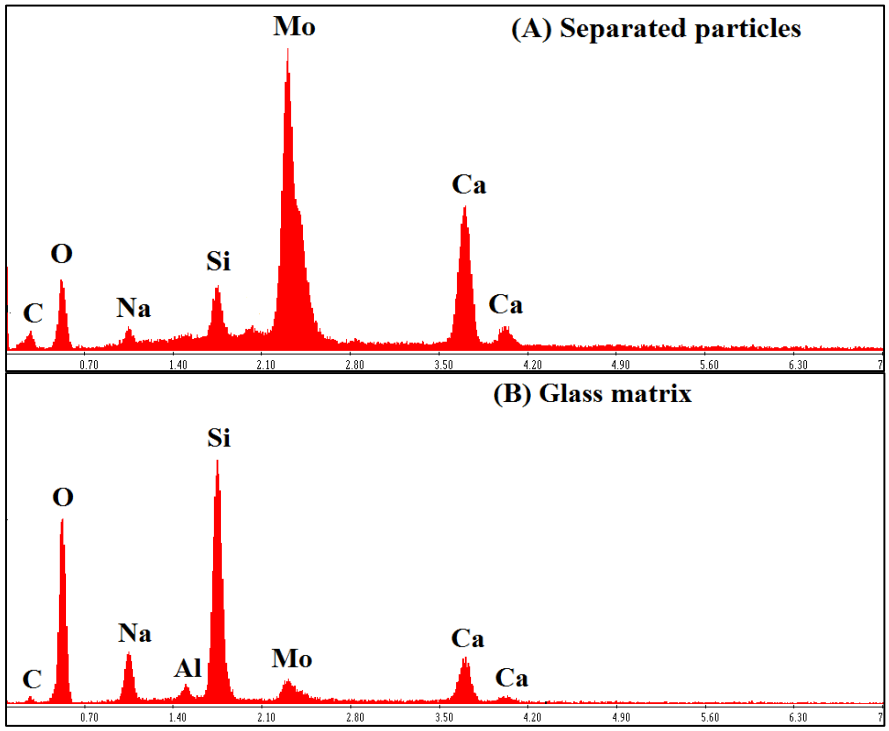

Figure 6-30 EDX spectra of selected areas in CBS-4M glass shown in Figure 6-29. (A) Separated particles and (B) Glass matrix.

In CBS-4M glass there are also some “crystal waves” observed with SEM observation. The waves are composed of large crystals which have a variety of sizes showing more severe crystallisation (Figure 6-31). Many large precipitated particles trapped in the

holes of glass matrix have been removed, probably during the sample preparation process. EDX analysis for the remaining crystals also shows that they are much more enriched in Ca and Mo, indicating that the precipitates are most likely to be $CaMoO_4$.

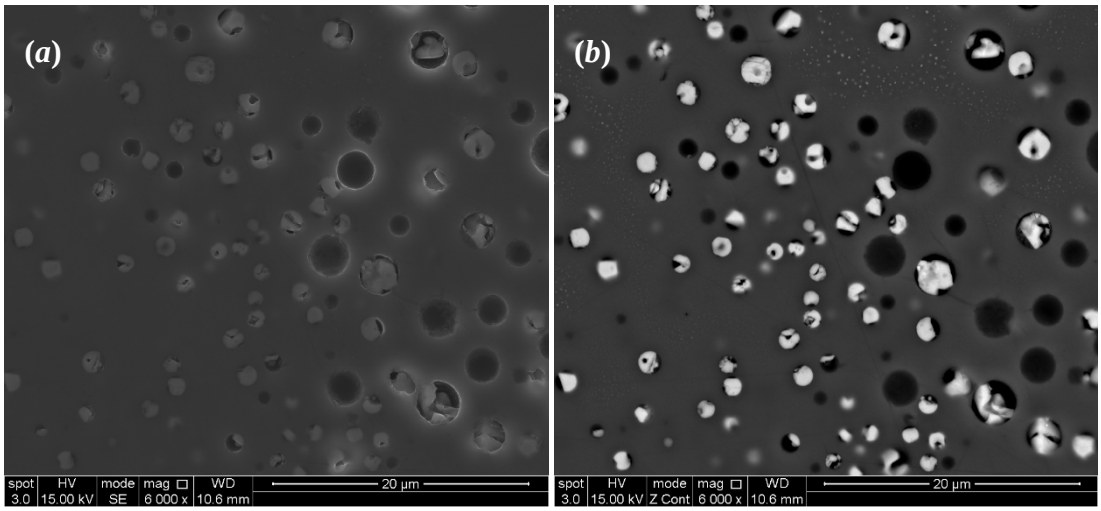

Figure 6-31 SE and BSE image of "crystal waves" in CBS-4M glass, respectively.

Separated phases in SBBS3-2.5M and SBBS3-3M glasses were also observed with SEM, as displayed in Figure 6-32 (*a*)-(*d*). The separated particles in SBBS3-3M glass are randomly dispersed within glass matrix (Figure 6-32(*a*)) and about 100 nm in diameter according to Figure 6-32(*b*). EDX analysis of these particles was not performed as they are smaller than the resolution of the measurement, but XRD and Raman results suggest they are likely to be molybdates. Figure 6-32 (*c*) and (*d*) compare the separated phases in SBBS3-2.5M and SBBS3-3M glasses at the same magnification (160,000×). Only at this magnification can the separated particles in SBBS-2.5M glass be seen, but still not clearly. They are much smaller (less than 50 nm in diameter) than the separated particles in SBBS3-3M glass; however, apart from the size, they are both spherical and randomly distributed.

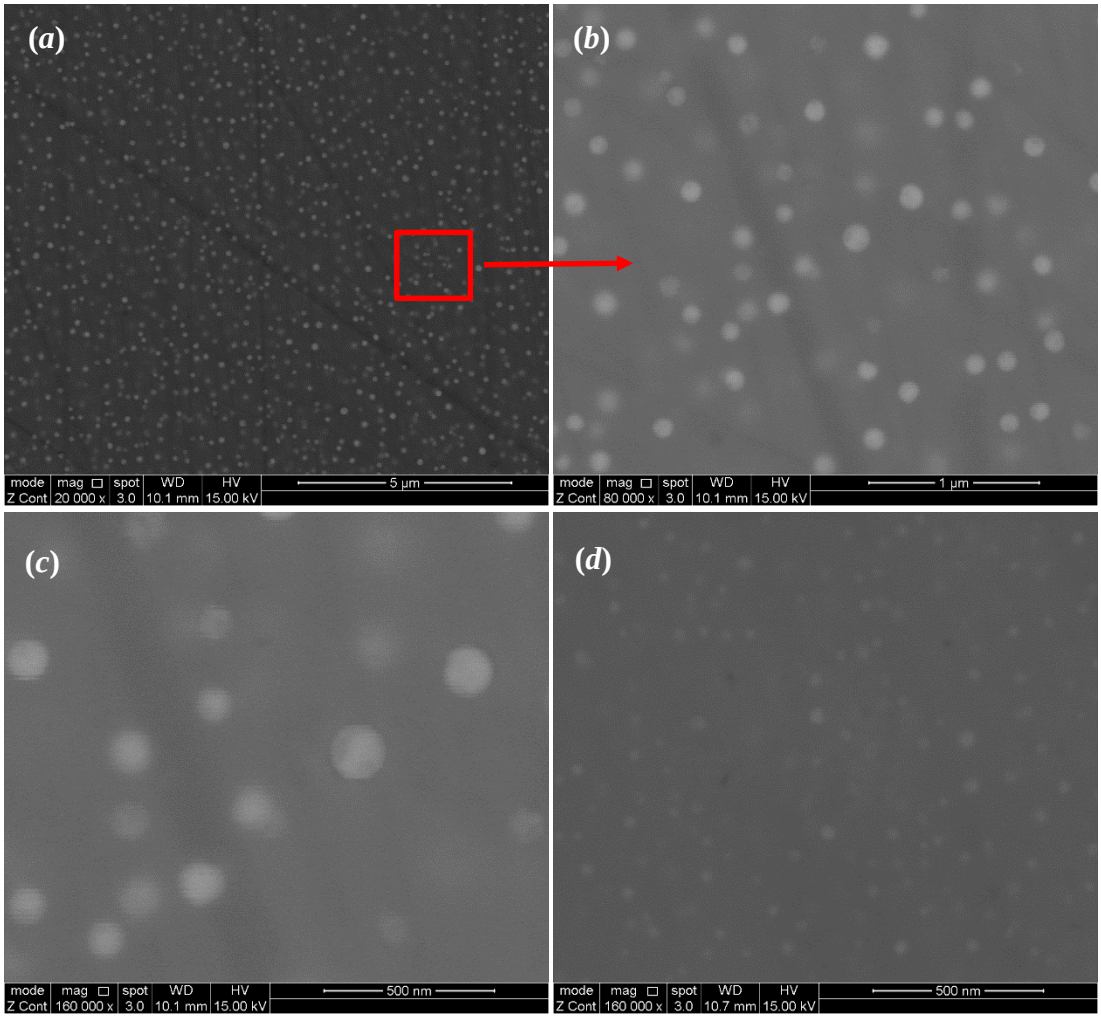

Figure 6-32 Backscattered electron images of separated particles in SBBS3-3M glass (*a*) 20,000×, (*b*) 80,000× and (*c*) 160,000× and in SBBS3-2.5M glass (*d*) 160,000×.

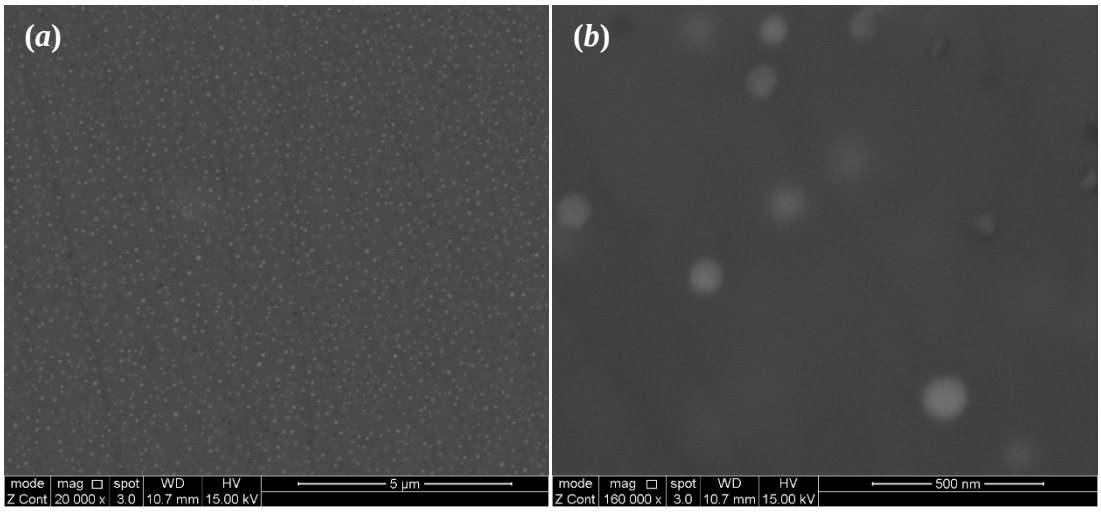

Figure 6-33 Backscattered electron images of BBS-2.5M glass at (*a*) 20,000× and (*b*) 160,000× magnifications.

The BBS-2.5M sample is partially crystallised and its crystallised region shows similar features to SBBS-3M, as shown in Figure 6-33 (*a*) and (*b*). The separated particles are randomly dispersed in the crystallised region in BBS-2.5M, but with a less intense distribution compared with the particles in SBBS-3M glass. This makes the crystallised region of BBS-2.5M glass less opaque than SBBS3-3M glass. In addition, the particles are also spherical and less than 100 nm in diameter.

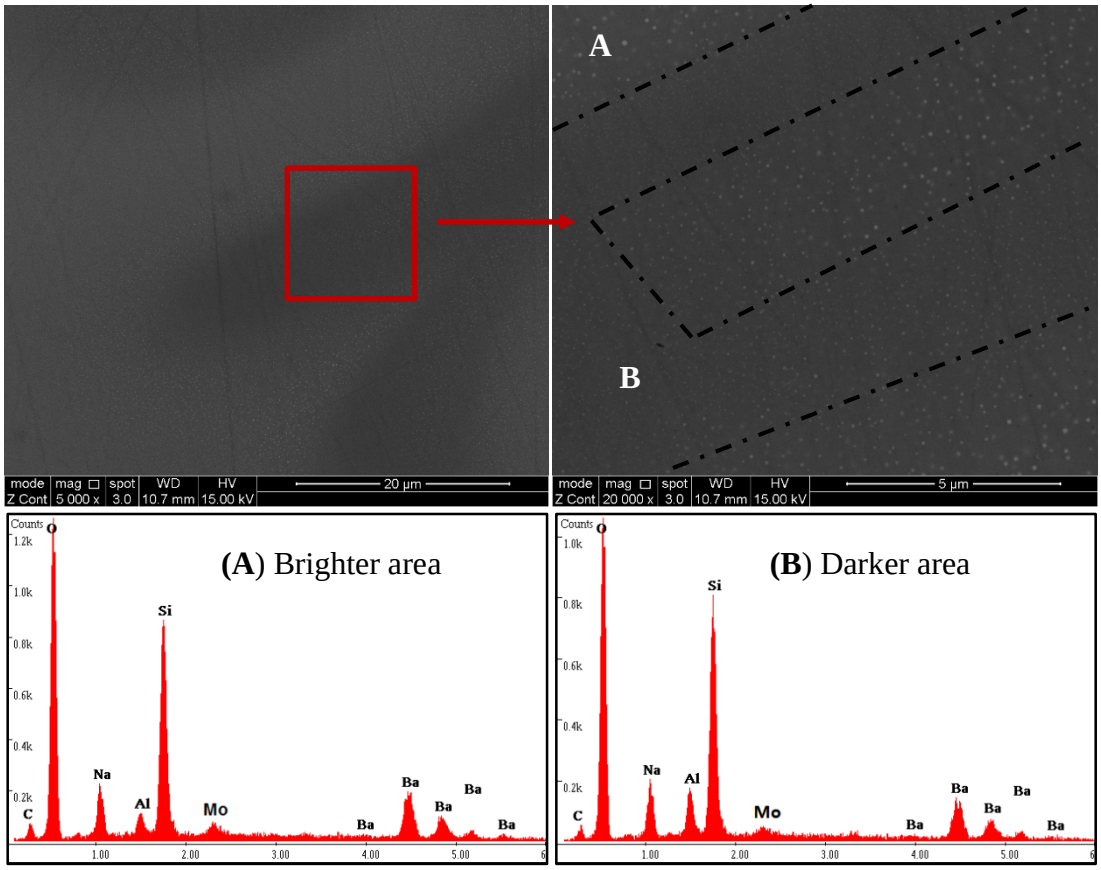

Figure 6-34 Backscattered electron images and EDX spectra of brighter and darker areas in the crystallised region of BBS-2.5M glass. The dash-dot line has been added to show the boundary.

Nevertheless, on the edge of crystallised region of BBS-2.5M glass, there are some compositional differences among the areas as shown in Figure 6-34. The brighter area, which indicates that it contains more heavy elements, contains a number of larger separated particles within glass matrix while the darker area, which contains less heavy elements, shows fewer particles with a smaller size. According to the EDX analysis on each respective area, the main compositional difference between them is the

enrichment of Al in the darker area which suffers less molybdate crystallisation. Given the amounts of other components are not apparently different between the two areas, the separation and crystallisation of molybdate in borosilicate glasses is likely related to the Al_2O_3 content.

6.2.10.2. Aluminosilicate glasses

MAS-0M to MAS-7M glasses are visibly homogeneous. Figure 6-35(*a*) indicates the backscattered electron image of MAS-4M glass, showing no feature within the limit of resolution and indicating the micro-homogeneity of glass. Element distribution has been scanned over an area of 1600 μm^2 on MAS-4M glass with Si Kα, Al Kα, Mg Kα and Mo Lα X-rays, as shown in Figure 6-35(*b*)-(*f*), suggesting that all elements are distributed homogeneously within the glass matrix. Sample MAS-8M is phase separated and the backscattered electron images of sample MAS-8M are presented in Figure 6-36. Figure 6-36(*a*) shows an area inside the crystallised part of the MAS-8M sample and Figure 6-36(*b*) is Figure 6-36(*a*) at a higher magnification. The crystallised particles are spherical (droplet-like) and are randomly dispersed in this region. The diameters of these spheres are not constant, varying from 200 to 400 nm. EDX analysis (Table 6-2) indicates that the crystallised region of MAS-8M sample contains more Mg and Mo than the glassy part does; however, due to the resolution limit of EDS (1 μm), the exact composition of these spheres cannot be obtained. Figure 6-36(*c*) and (*d*) show boundary areas between the two distinct parts of MAS-8M sample: a part which remains completely homogeneous, which is assumed to be glass, and a crystallised part as observed in Figure 6-36(*a*) and (*b*) that contains crystals within the glass matrix. These two parts are separated by a boundary region made up of even smaller particles.

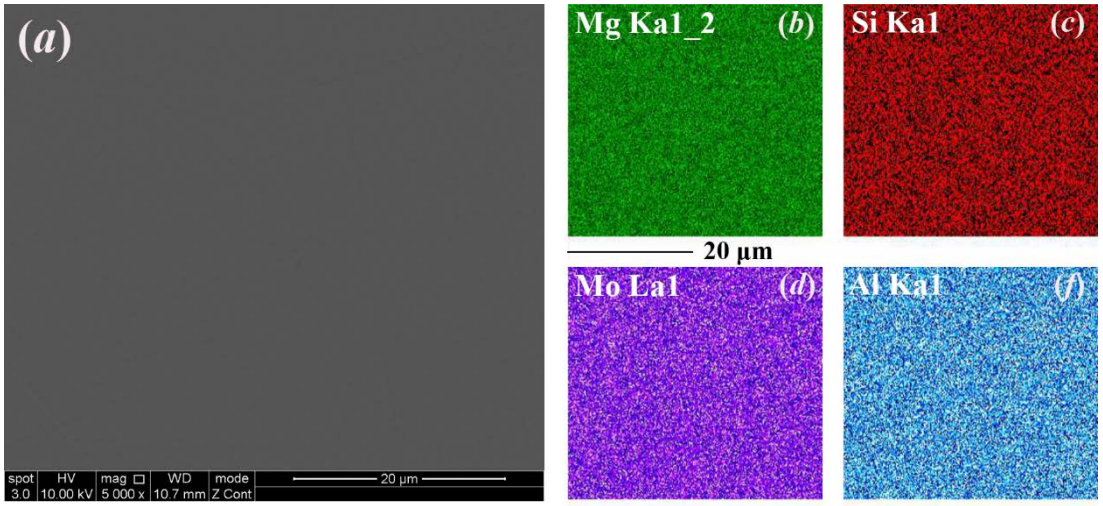

Figure 6-35 (*a*) Backscattered electron image of MAS-4M glass and (*b-f*) dot mapped elemental distribution within glass obtained by EDX.

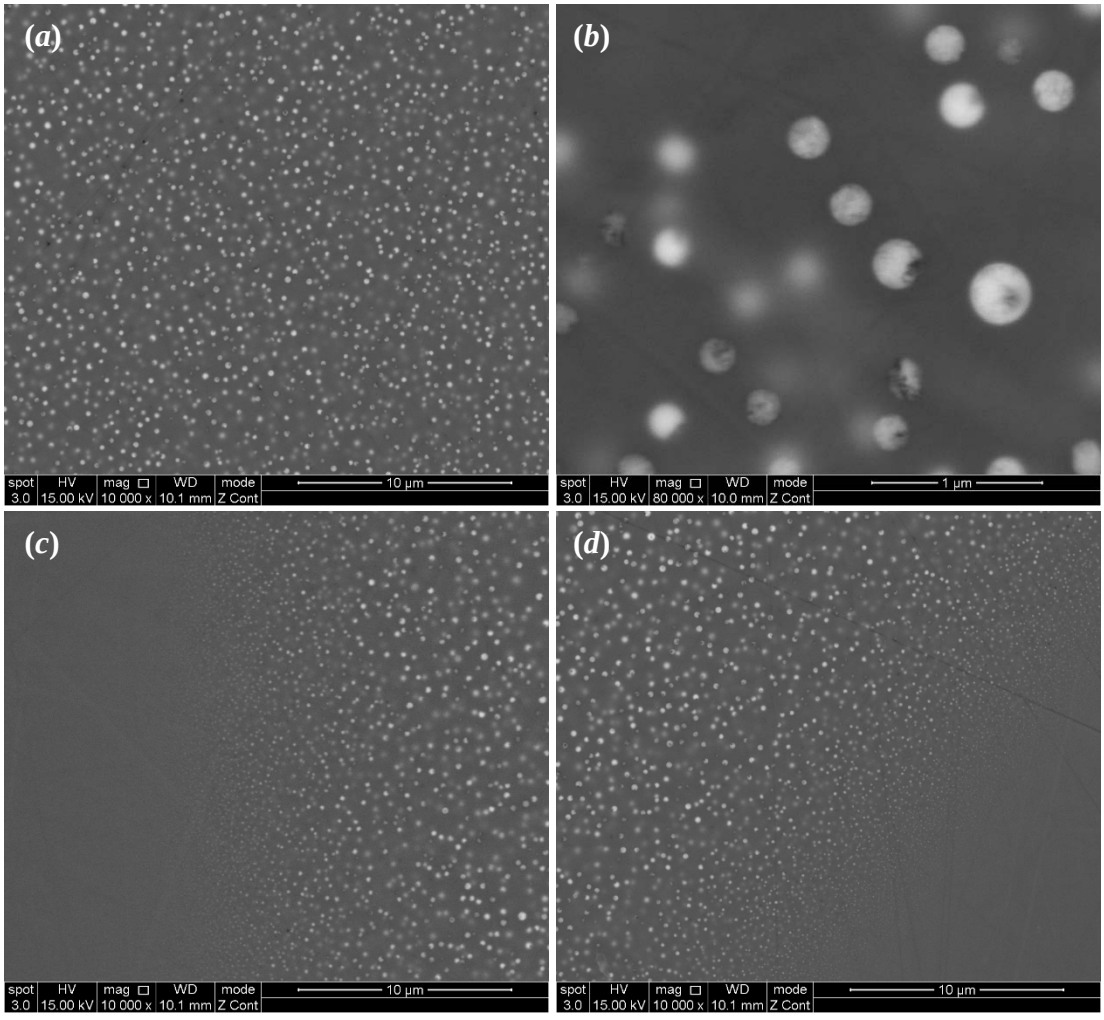

Figure 6-36 Backscattered electron images of MAS-8M glass. (*a*) and (*b*): crystallised region; (*c*) and (*d*): boundary areas between crystallised and glassy regions.

The crystallisation in CAS-4M and CMAS-4M samples is less apparent than that in MAS-8M glass, as seen in Figure 6-37. Only particles smaller than 100 nm have been observed in both glasses, but due to the resolution limit of the SEM used the morphologies of these particles are not clear. It appears that these particles are widely dispersed in the crystalline region and varying in diameter from 50 to 100 nm. These features are akin to the particles in SBBS3-2.5M glass where subtle crystallisation also occurs, indicating that molybdate separates from glass as a number of nanoparticles in the glasses with a slight excess of MoO_3.

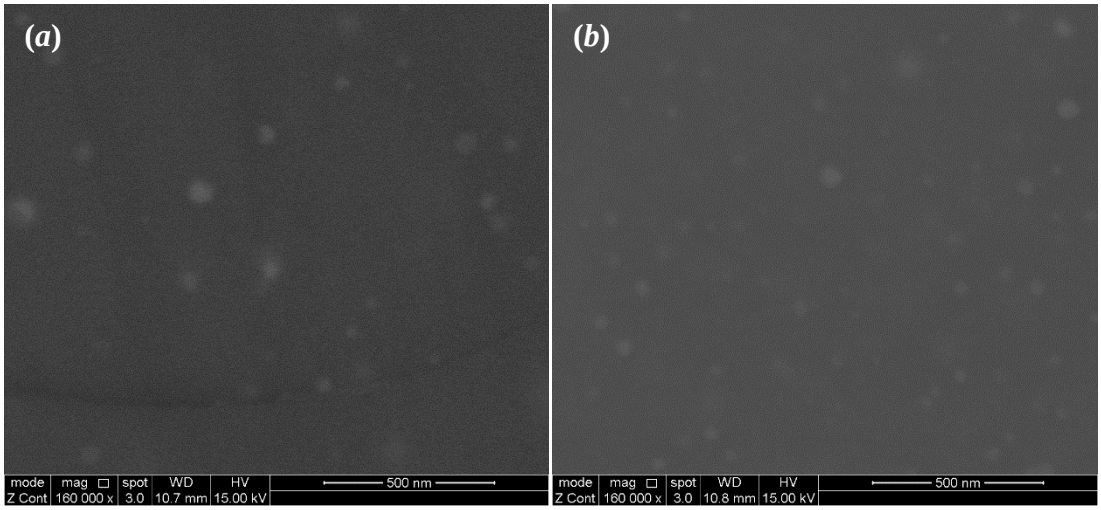

Figure 6-37 Backscattered electron images of separated particles in (*a*) CAS-4M glass and (*b*) CMAS-4M glass.

Backscattered electron images of SBAS-3M glass which is heavily crystallised and completely opaque are presented in Figure 6-38. Figure 6-38(*a*) shows the random and widespread distribution of precipitated particles within glass matrix while Figure 6-38(*b*) indicates that these particles are mostly spherical and are around 300 nm in diameter. There are also some large separated crystalline features observed in the sample, one of them shown in Figure 6-38(*c*). The feature is around 50 μm in width and more than 400 μm in length. It has straight and clear boundaries with the surrounding glass matrix and EDX analysis (Figure 6-38(*d*)) suggests that it is essentially composed of Mo, O, Sr and Ba (C is from carbon coating). Therefore the separated phase in these features is likely a strontium-barium molybdate solid solution.

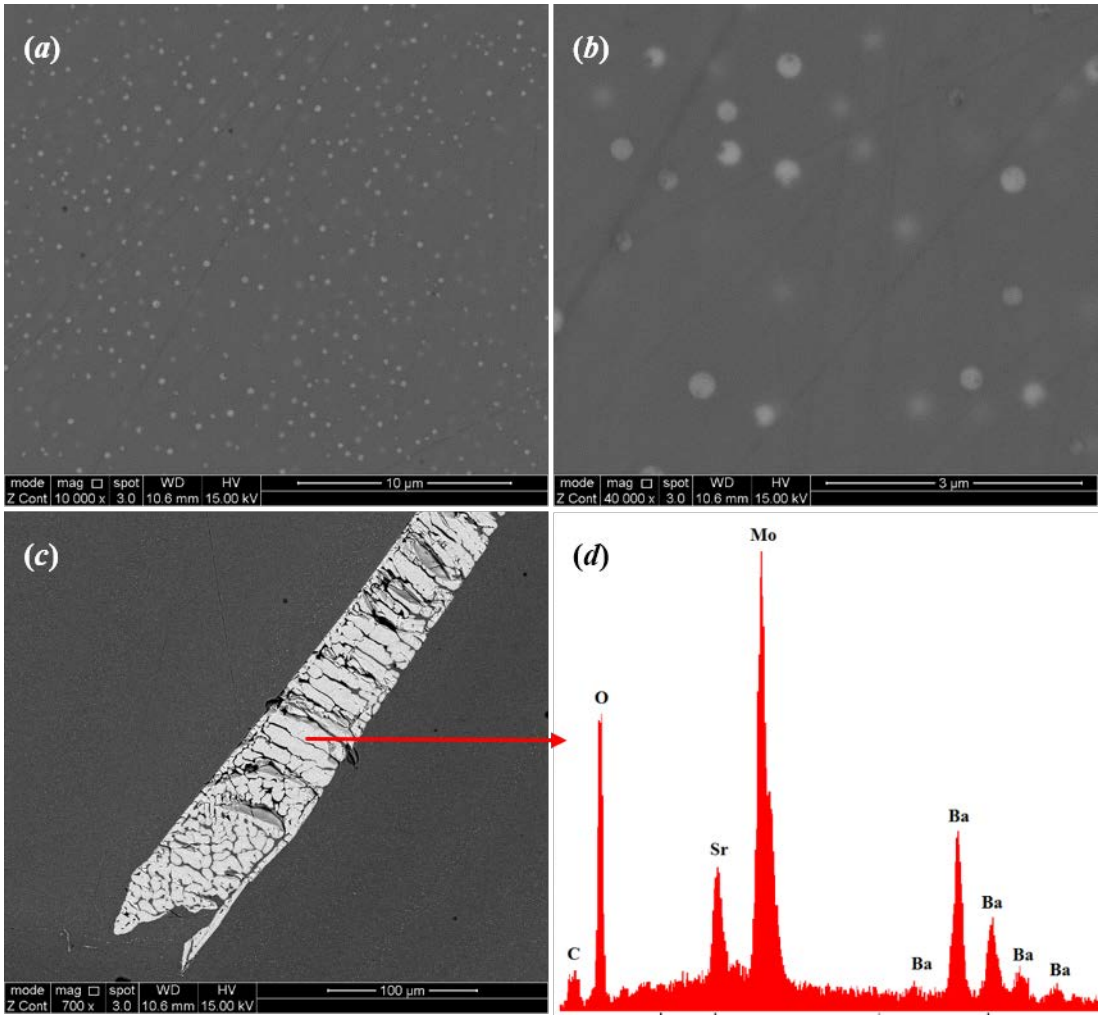

Figure 6-38 Separated particles in SBAS-3M glass at (*a*) 10,000× and (*b*) 40,000× magnifications. (*c*) and (*d*) is a trapped molybdate feature in the glass and its EDX spectrum, respectively.

Similarly, BAS-3M glass contains a large number of separated particles within its glass matrix, as shown in Figure 6-39. These spherical particles are around 400-500 nm in diameter, slightly larger than that of the particles observed in SBAS-3M glass. Comparative EDX analysis has been performed on a sphere and its surrounding glass matrix (Figure 6-39 (*c*) and (*d*)), showing that the sphere is more enriched in Ba and Mo and less enriched in Si and Al. Consequently, it is likely that the separated phase in BAS-3M glass is $BaMoO_4$. In addition, the ratio of vacant holes which are probably caused by the escape of separated particles during sample preparation is apparently higher in BAS-3M glass than in SBAS-3M and MAS-8M glasses.

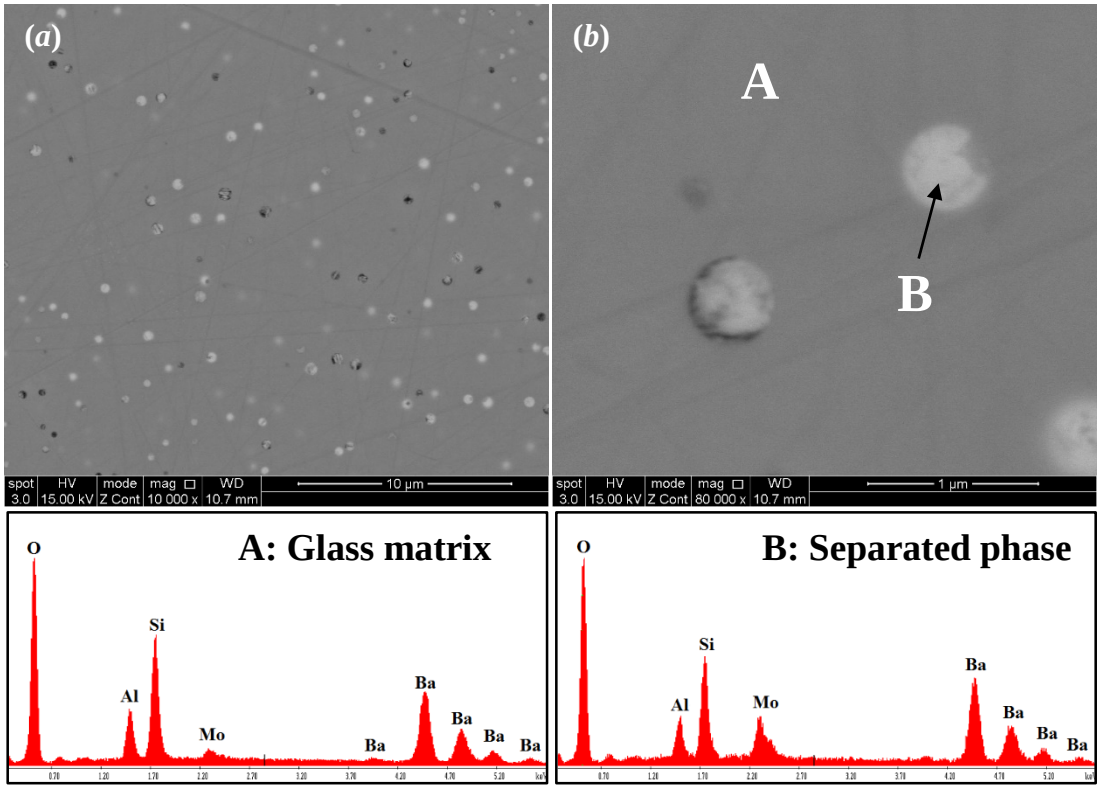

Figure 6-39 Separated particles in BAS-3M glass at (*a*) 10,000× and (*b*) 80,000× magnifications, respectively.

6.2.11. TEM

Some of the phase separated glasses were selected for TEM observations. Figure 6-40 presents TEM images and diffraction patterns for the separated particles in SBBS3-3M glass. According to Figure 6-40(*a*), there are many separated spheres 100-200 nm in diameter widely dispersed within glass matrix, as observed by SEM image Figure 6-32(*c*). However, apart from these "big" spheres, there are a number of tiny particles, which either surround the big spheres or are randomly distributed in other places (Figure 6-40(*b*)), that can be observed within the glass matrix. Some thin areas and remote particles were selected to perform TEM diffraction. Figure 6-40 (*c*) and (*e*) show diffraction patterns, which are probably from the [111] axis of cubic Na_2MoO_4 and the [112] axis of tetragonal Ba/$SrMoO_4$, respectively, Figure 6-40(*d*) shows a pattern of several dotted rings indicating the presence of multiple single crystals in the region. At least two molybdate phases exist in the sample.

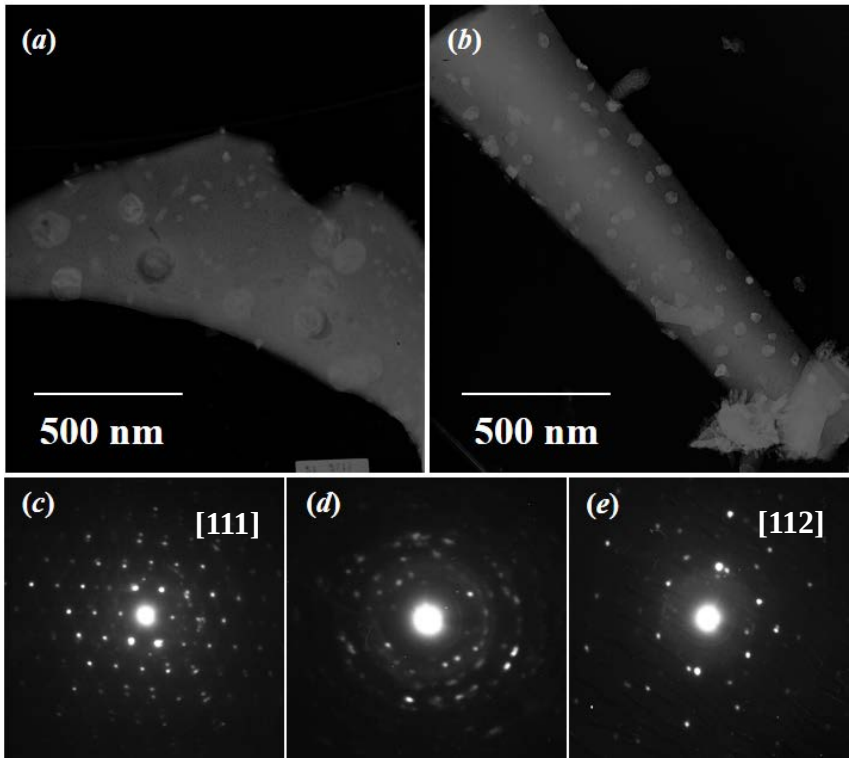

Figure 6-40 TEM images (*a* and *b*) and some diffraction patterns (*c*, *d*, and *e*) of separated particles in SBBS3-3M glass.

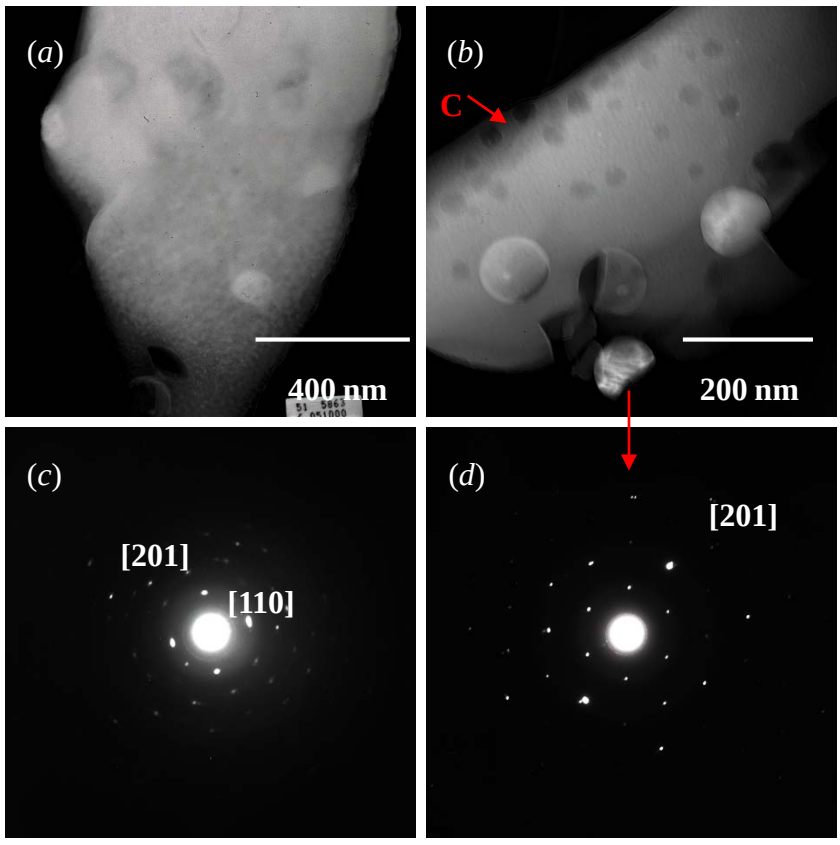

Figure 6-41 TEM images and electron diffraction patterns of CBS-4M glass.

Figure 6-41 (*a*) and (*b*) are two TEM images of the separated particles formed within the CBS-4M glass matrix. Similar to sample SBBS3-3M glass, the separated phase in CBS-4M also contains some larger spheres together with a large number of smaller particles. In the bottom of Figure 6-41(*a*) there is a vacant pore with a nearby particle, indicating the escape of the separated particles within glass matrix. The spheres are more apparent in Figure 6-41(*b*) showing a diameter of ~100 nm. Figure 6-41(*c*) and (*d*) are electron diffraction patterns of smaller particles (Area C) and larger spheres, respectively. It can be seen that the smaller particles are composed of several single crystals, the index of which is marked in Figure 6-41(*c*). The diffraction spots in Figure 6-41(*d*) are in accordance with the diffraction patterns from [201] axis of tetragonal $CaMoO_4$ crystals.

Figure 6-42 exhibits a TEM image of some pieces of the crystallised part of MAS-8M glass, along with electron diffraction patterns of selected areas. The separated crystals (Area C) have a distinctive morphology compared to the glass matrix (Areas A and B) under TEM; the electron diffraction patterns for Areas A and B are composed of scattered weak rings with a small amount of bright diffraction rings (Figure 6-42*A* and *B*), indicating the predominantly amorphous nature of these areas. Diffraction patterns for Area C consist of numerous bright diffraction rings and spots (Figure 6-42*C*), which means multiple crystals are dominant in Area C. Figure 6-42*D* primarily consists of two series of diffraction spots, indicative of the [101] and [201] diffraction axes of single monoclinic $MgMoO_4$ crystals, respectively.

Similarly, the separated crystals in CAS-4M glass also show a distinctive morphology compared to the glass matrix (Figure 6-43(*a*)). The electron diffraction pattern for the crystals (Figure 6-43(*b*)) consists of a number of diffraction dashed rings, suggesting there are multiple crystals in the observed area. An isolated piece of crystal is shown in Figure 6-43(*c*), with its diffraction pattern in Figure 6-43(*d*). It is clear that this piece is made up of one or two single crystals, probably $CaMoO_4$, from [211] and/or [311] diffraction axes.

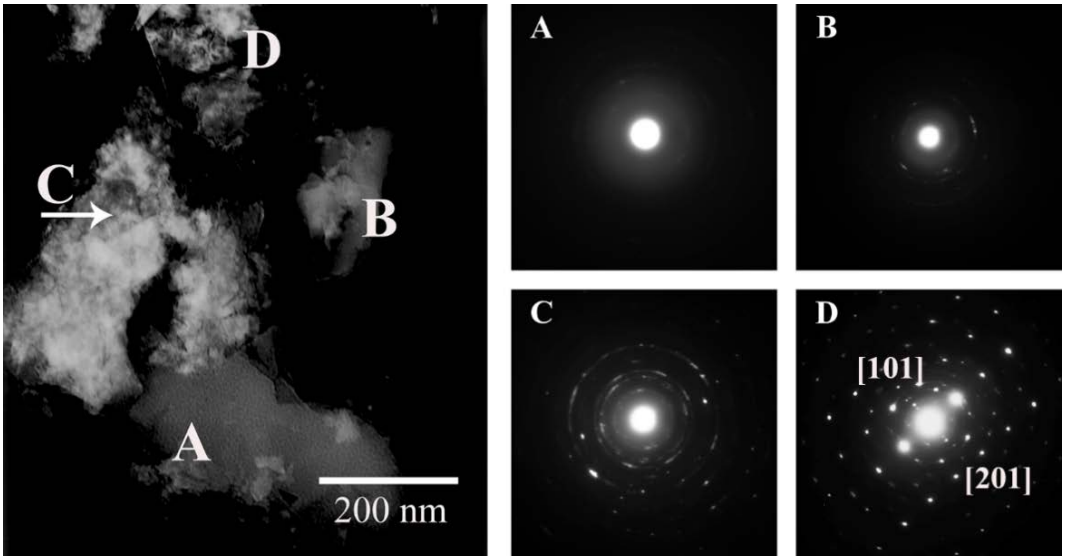

Figure 6-42 TEM image (left) and diffraction patterns (right) of MAS-8M sample.

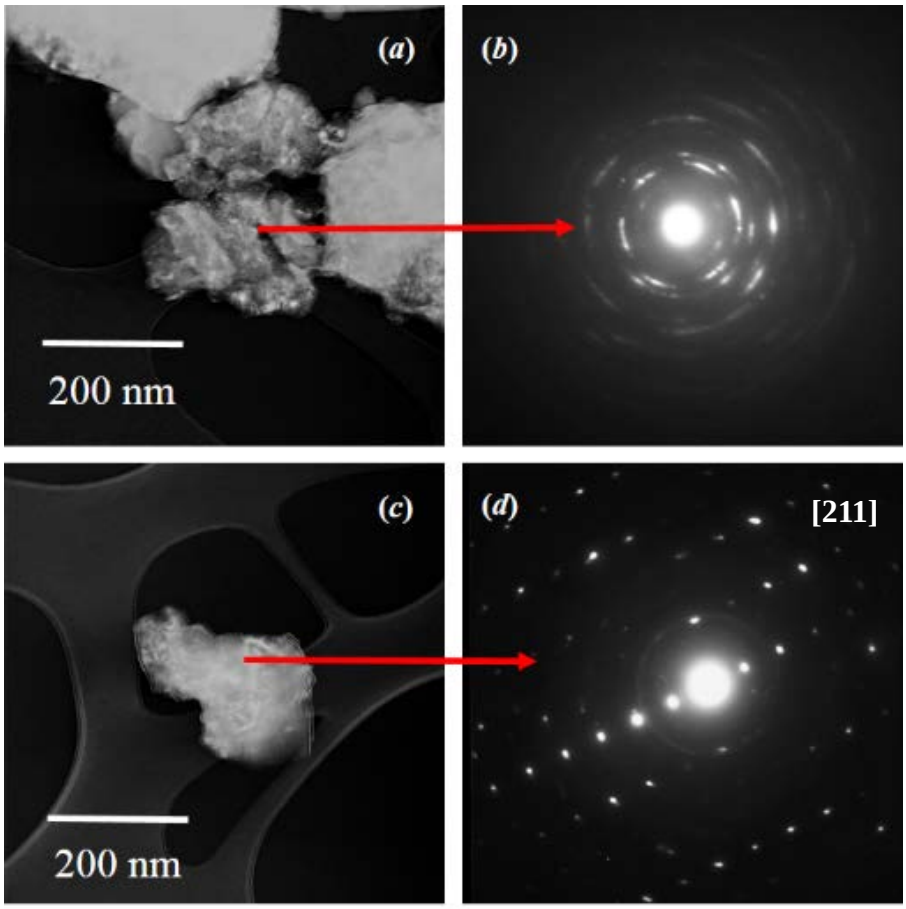

Figure 6-43 TEM images of separated phase in CAS-4M glass (*a* and *c*) with their corresponding electron diffraction patterns (*b* and *d*).

6.3. Discussion

6.3.1. MoO_3 loading limit, retention and solubility in glass

Given the high retention rate of MoO_3 in both glass series, the MoO_3 loading limit and MoO_3 solubility in glass are more or less the same except for MAS glass which has an unusually high MoO_3 loading limit of 6.54 mol% with a solubility of 5.34 mol%. In aluminosilicate glasses, MoO_3 solubility monotonically increases with the equimolar replacement of larger by smaller alkaline earths, from 1.85 mol% for BAS glass to 5.34 mol% for MAS glass. However, this increasing trend in borosilicate glasses only lasts from 1.92 mol% of BBS glass to 2.84 mol% of CBS glass whereas MoO_3 solubility in MBS glass becomes very low(<1 mol%). In addition, the MoO_3 solubility of glass with the mixed alkaline earths follows the lower MoO_3 solubility of glass obtained with the single alkaline earths.

MoO_3 content continues increasing in the glassy region of all phase separated glasses except MAS glass; excess MoO_3 addition results in phase separation and also greater MoO_3 incorporation in the glass. This suggests that the saturation of MoO_3 incorporation has not been reached in these glasses when phase separated, which means that MoO_3 solubility in glass is not controlled by the capability of glass network to accommodate MoO_3, but by the separation tendency of molybdates. Only in MAS glass MoO_3 content has stopped increasing before phase separation occurs in MAS-8M glass. MAS glass network is able to accommodate ~5.30 mol% MoO_3, at which level $MgMoO_4$ still does not tend to crystallise.

As the separated phase has been identified to be molybdates (discussed below), it can be deemed that the separation tendency of molybdates from glass network declines from $BaMoO_4$ to $SrMoO_4$ to $CaMoO_4$ to $MgMoO_4$; the associated alkaline earth ions are originally as network modifiers. Even in borosilicate glasses with the presence of Na_2O, the separated phase does not occur as Na_2MoO_4 firstly in CBS, SBS and BBS glasses. The only exception is MBS glass where MoO_4^{2-} can be associated with Mg^{2+} and Na^+ at the same time to form $Na_{2.4}Mg_{0.8}(MoO_4)_2$ a readily crystallised compound. This also results in a significantly reduced MoO_3 solubility in MBS glass. Therefore, the coexistence of Mg^{2+} and Na^{2+} with MoO_4^{2-} in glass network may not be suitable

to immobilise molybdate. In addition, with the comparison between MoO_3 solubility in glass with combined alkaline earths and with pure alkaline earth, it is observed that the glass with mixed alkaline earths exhibits a MoO_3 solubility close to that of the glass made with a single alkaline earth with a lower solubility (compare MAS, CMAS and CAS glasses). This means that MoO_3 solubility in glass is controlled by the factor that gives rise to the lowest solubility of each single molybdate.

The excellent MoO_3 retention in both glass series is probably linked to the miscibility of molten molybdate and silicate. It can be seen that the MoO_3 retention rate in MAS-6M to MAS-8M glasses is reduced as MoO_3 incorporation in MAS glass seems to have been saturated. Thus the remaining excess MoO_3 which cannot be dissolved in melt is expelled from the melt, gradually evaporating during melting. However, in most cases, as discussed above, MoO_3 incorporation is in reality not saturated when phase separation occurs and the excess MoO_3 is miscible with glass melt and consequently the loss of MoO_3 by evaporation will be limited.

6.3.2. Effects of MoO_3 incorporation on glass structure and properties

6.3.2.1. Density

MoO_3 incorporation leads to increased density of both borosilicate and aluminosilicate glasses until phase separation, after which the density change is not consistent. The higher density of glass arises from the greater mass of MoO_3 compared to other components such as SiO_2 and Na_2O. But with increasing MoO_3 additions, the density increase is gradually reduced, showing a generally quadratic increase in densities of CBS, CAS and MAS glass series, although MoO_3 content in them linearly increases with MoO_3 solubility. This may suggest an expansion in glass network with increasing MoO_3 incorporation.

6.3.2.2. T_g and T_c

As shown in Figure 6-12 to Figure 6-16, T_g is reduced by the incorporation of MoO_3 in all investigated glass compositions. This is in contradiction to the observation that MoO_4^{2-} is associated with modifying cations such as Ca^{2+} and Mg^{2+} to form molybdate clusters in glass network, in which case the ratio of non-bridging oxygens (NBOs) that are originally associated with modifying cations could be expected to decrease and thus result in a polymerised network. The reduction in T_g is also found in nuclear waste borosilicate glasses reported by Caurant *et al.* (2007), where the authors ascribed it to the increased size of depolymerised domains caused by the location of MoO_4^{2-} ions, which overrides the increased connectivity of the network. Another possibility is that network modifying cations are associated with MoO_4^{2-} ions and NBOs simultaneously. The interstices of glass network are occupied by MoO_4^{2-} units which have a strong association with modifying cations. However, the formed large molybdate clusters are still weakly functioned with nearby oxygens in the network, in which the nearby oxygens remain NBOs with a slight association with the modifiers. In this case, the connectivity between silicate tetrahedra is not increased and the energy required for structural relaxation upon heating is reduced because of the readily disassociation of NBOs with network modifiers. These two explanations are based on different connectivity results, but the heavy overlapping of molybdate bands with silicate bands in Raman spectra makes the deconvolution of Q_n species from Raman spectroscopy not realistic and hence further investigation using, for example, ^{29}Si MAS NMR, are

required to explain the reduction in T_g.

The decreasing trend of T_g continues in the phase separated glasses. The T_gs of subtly and slightly crystallised glass, such as CBS-3.5M, SBBS3-2.5M and CAS-4M glasses, are in accordance with the decreasing rate of T_g with increasing MoO_3 content, which suggests that at this stage T_g is still completely controlled by the MoO_3 content in glass. The slightly lower T_g in partially crystallised MAS-8M glass compared to homogeneous MAS-7M glass may be because of its crystallised region which contains more MoO_3. Moreover, the heavily crystallised CBS-4M and SBBS3-3M glasses have apparently lower T_gs than CBS-3.5M and SBBS3-2.5M glasses. This suggests that the severe crystallisation of molybdate may have significantly affected the glass structure and glass composition; one possibility is that the precipitation of molybdate from glass matrix makes the remaining composition greatly changed and as a result the obtained T_g deviates from the line.

The incorporation of MoO_3 does not make significant changes in T_c of borosilicate glasses except the heavily crystallised CBS-4M and SBBS3-3M glasses in which the crystallisation exothermic peak is less apparent. The large amount of crystals within glass matrix may be responsible for this apparent change as there is less material present that can undergo crystallisation. On the other hand, T_cs of aluminosilicate glasses generally linearly decrease with increasing MoO_3 additions, following a similar trend to T_g. However, an intense exothermic peak can be observed after the first crystallisation peak. The onset temperature of this peak linearly decreases from MAS-0M to MAS-6M glasses. The presence of this peak for MAS-0M glass (no-MoO_3) indicates that this peak should be related to the magnesium aluminosilicate glass network. According to the high temperature XRD results (Figure 6-17), the exothermic peak of MAS glasses probably arises from the phase transition between cordierite (hexagonal $Mg_2Al_2Si_5O_{18}$) and indialite (pseudo-hexagonal $Mg_2Al_2Si_5O_{18}$) at high temperatures. XRD patterns of these two phases are too close to differentiate; only the intensities of respective peaks are slightly changed. Indeed, the intensities of peaks assigned to $MgMoO_4$ are also increased in MAS-3M and MAS-6M glasses between 850 and 950 ºC, but the contribution of $MgMoO_4$ to DTA curves is limited due to its relatively low amount compared to the basic glass network. The second exothermic peak is not observed in MAS-7M and MAS-8M glasses, which suggests

that the transition has completed with the first crystallisation or the transition is much less intense at high MoO_3 contents. This agrees with the high temperature XRD result that the intensities of $MgMoO_4$ peaks for MAS-7M glass are not increased after 900 ºC; the second crystallisation is irrelevant to molybdate and is likely related to the phase transition between cordierite and indialite. CAS glasses also show a decreased onset of second exothermic peak although the peaks are not complete in the measured temperature range. Generally speaking, MoO_3 incorporation in aluminosilicate glasses reduces the characteristic temperatures for each thermal reaction upon heating.

6.3.2.3. Raman and FTIR spectroscopies

Similar to sulphate incorporation in glass (Chapter 4), molybdate incorporation in glass results in prominent changes in Raman spectra. The main band created by MoO_3 incorporation in glass (remain homogeneous) is located at 890-960 cm^{-1}, the central frequencies of which are dependent on glass composition, as plotted in Figure 6-44.

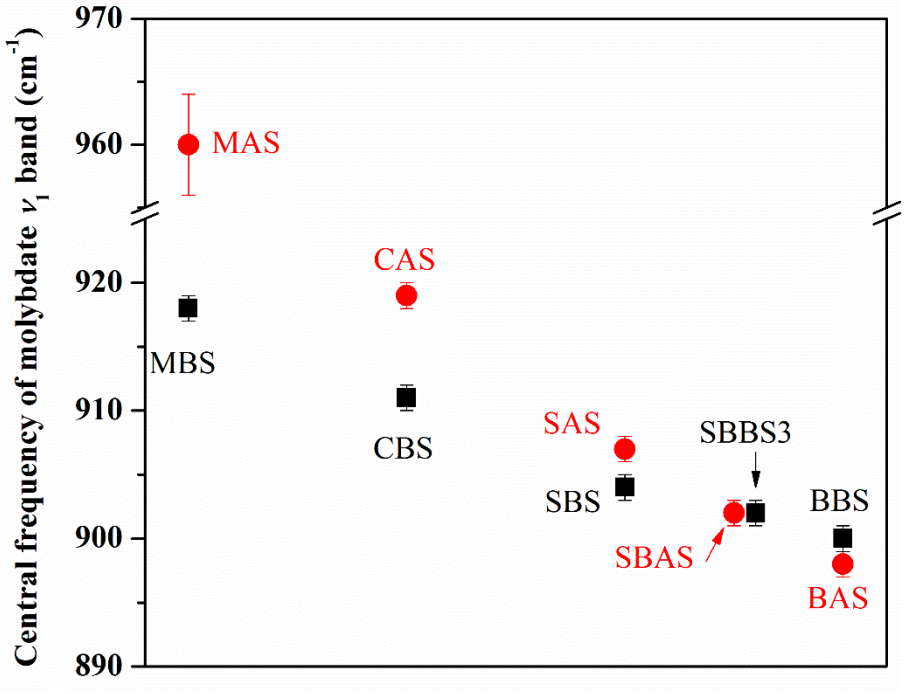

Figure 6-44 Central frequencies of Raman band assigned to symmetric stretching vibrations of MoO_4^{2-} in different glass compositions.

The lowered frequencies of molybdate band υ_1 alkaline earth size indicates that the

local environments of MoO_4^{2-} units are strongly related to the alkaline earth cations in the glass network. The larger cations, such as Ba^{2+} and Sr^{2+}, have a stronger distortion effect on the surrounding MoO_4^{2-} anions than the smaller cations such as Ca^{2+} and Mg^{2+} and thus result in a lower Raman shift of MoO_4^{2-} υ_1 band. Especially, the combination of strontium and barium in glass (SBAS and SBBS3) leads to the frequency lying between the ones of glass with strontium and barium solely, suggesting that MoO_4^{2-} units have no strong preference to associate with either Sr^{2+} or Ba^{2+} in glass network. Moreover, the apparently high frequency of this band for MAS glass (~965 cm^{-1}) indicates different local environments of MoO_4^{2-} in MAS glass from other glasses. It is possible this difference that enables MAS glass to have its unusually high MoO_3 solubility.

Meanwhile, the MoO_3 content in glass can also be reflected by the relative intensities of molybdate bands to silicate bands. According to Figure 6-18 to Figure 6-23, the MoO_4^{2-} υ_1 band is apparently increased with increasing MoO_3 addition until phase separation. The phase separated glasses are not compared because they are not micro-homogeneous. Figure 6-45 plots the relative areas of molybdate bands to silicate bands as a function of molybdate addition in MAS glasses.

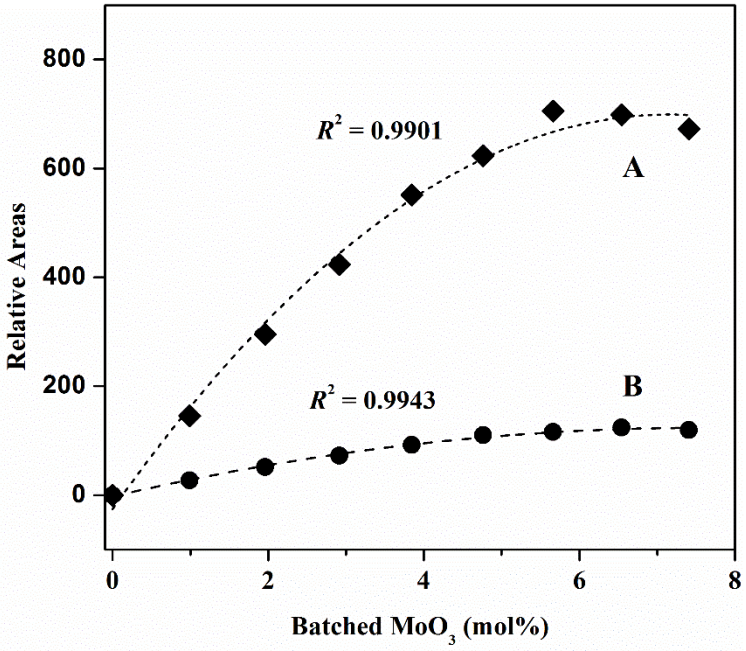

Figure 6-45 Relative areas of (A) molybdate 965 cm^{-1} band and (B) molybdate 320 cm^{-1} band to the normalised silicate 550 cm^{-1} band.

The significant overlap of the 965 cm^{-1} molybdate band and 980 cm^{-1} silicate band in MAS glass makes it difficult to directly compare their relative areas and as a result the areas of the molybdate bands are compared with the area of the silicate band at 550 cm^{-1} which does not overlap with any band assigned to MoO_4^{2-}. Assuming that the area ratio of the 980 cm^{-1} silicate band to the 550 cm^{-1} silicate band is constant among all of the MAS glasses, then the area of the silicate band at 980 cm^{-1} can be estimated from the area of the silicate band at 550 cm^{-1} if it can be assumed that there is no major change in glass polymerisation across the compositions studied. This assumption is reasonable for these glasses given that the [Al]/[Si] ratio and the [modifier]/([Al]+[Si]) ratios are essentially constant, unless Mo is acting as a modifier; previous work indicates that although Mo associates with modifiers it does not act as a modifier (Colomban and Paulsen 2005). Hence the area of the 965 cm^{-1} molybdate band can obtained by subtracting the area of the estimated 980 cm^{-1} silicate band from the whole area of this region. Meanwhile, the area of 320 cm^{-1} the molybdate band can be directly obtained by comparison with the area of 550 cm^{-1} silicate band. The relative values for these areas plotted in Figure 6-45 indicate that, as for both molybdate bands, the relative area increases linearly with molybdate additions, reaches maximum at MAS-6M glass and slightly reduces with further molybdate additions.

The changes in FTIR spectra of glass caused by the incorporation of MoO_3 are not as prominent as those in the Raman spectra. Only some shoulders can be observed due to the incorporation of MoO_3 in borosilicate glasses, being narrowed and intensified for the phase separated glasses. The increasing addition of MoO_3 results in notable changes in the 800-1200 cm^{-1} band assigned to silicate stretching vibrations, but deconvolution of this band cannot be obtained unless the contribution of molybdate in this region is removed. Meanwhile, MoO_3 incorporation in aluminosilicate glasses does not result in any notable change in the FTIR spectra except for the phase separated cases. Only the relatively higher intensity of the 800-1200 cm^{-1} band with higher MoO_3 content may suggest that the molybdate bands in this region have been completely merged with the silicate bands. Therefore, Raman spectroscopy is better than FTIR when investigating the evolution of structural characteristics of MoO_4^{2-} in glass.

6.3.3. Phase separation and microstructure

6.3.3.1. Borosilicate glasses

Phase separation of glasses occurs when the amount of MoO_3 content in glass exceeds the loading limit. The composition of separated phase also varies with different MoO_3 additions. According to XRD results for borosilicate glasses (Figure 6-6 to Figure 6-8), alkaline earth molybdates are the preferential phase at the beginning of crystallisation when MoO_3 content in glass reaches the critical solubility limit, except in MBS glass where the formed phase is a magnesium-sodium molybdate solid solution. However, evidence for the presence of Na_2MoO_4 crystals as a minor phase is also found in XRD patterns of MBS-2M and CBS-3.5M glasses and further MoO_3 additions give rise to an increased proportion of Na_2MoO_4 in the separated phases in MBS-3M and CBS-4M glasses. The hydrated Na_2MoO_4 (Na_2MoO_4•$2H_2O$) in CBS-4M glassy bulk could result from the absorption of water by separated phases during sample processing, *e.g.* sectioning. The segregated layer of CBS-4M glass, which is directly collected from sample surface, does not contain any hydrated phase. The presence of Na_2MoO_4 is not found in SBS, SBBS and BBS glasses, possibly because the amounts of MoO_3 in them are not that large.

Nevertheless, it is worth noting that the Raman spectra of phase separated glasses (not including the segregated layer and the aggregated separated phase trapped in glass) do not show any band assigned to Na_2MoO_4, which means that the separated phase within glass matrix is exclusively an alkaline earth molybdate (except in the MBS glasses). The presence of Na_2MoO_4 in XRD patterns probably originates from the excess molybdate in the melt. The excess molybdate, which is a mixture of Na_2MoO_4 and alkaline earth molybdate, is immiscible with the melt and as the melt cools down the excess molybdate remains outside the glass network. As the Raman measurement is performed on the surface of polished bulk glass, the trapped immiscible molybdates may not be detected and only the segregated layer of CBS-4M glass shows a majority of Na_2MoO_4 with a minority of $CaMoO_4$. But XRD analysis is carried out on the ground powders of bulk glass and hence any presence of trapped immiscible molybdates or residual segregated layer will give rise to peaks of Na_2MoO_4; similar are the FTIR results obtained from ground powders of glass. In summary, Na_2MoO_4

phase is from the segregated layer undissolved in the melt while the separated phase forming within glass matrix is mainly $CaMoO_4$.

This explanation also agrees with the EDX analysis (Figure 6-30) for the separated particles within CBS-4M glass matrix. Although the exact composition of the particles was not obtained, the comparison between the particles and the surrounding glass matrix indicates that the particles are much more enriched in Mo and Ca while the Na content is not enriched. Therefore, the separated particles should be $CaMoO_4$.

The microstructure of the separated particles is similar among borosilicate glasses: spherical (droplet-like) shape, randomly dispersed and <1 μm in diameter. However, the size of separated particles notably varies with the amount of MoO_3 added to the glass. Through the comparisons of CBS glasses (Figure 6-29) and SBBS3 glasses (Figure 6-32) it can be seen that the particles from glass with higher MoO_3 additions are about twice as big as those from glass with lower MoO_3 additions. The more excess MoO_3 is added, the greater the extent of phase separation occurring within glass during cooling. The droplet-like morphology of particles observed by SEM suggests that liquid-liquid phase separation occurs prior to the crystallisation of the separated phase during cooling. On the other hand, TEM results for SBBS3-3M glass (Figure 6-40) indicate that, apart from the spherical particles observed by SEM, there are a number of even smaller particles (<50 nm in diameter) widely dispersed within the glass matrix. It is possible that these particles are also formed through liquid-liquid phase separation during cooling, but there is not sufficient time for them to aggregate to form larger droplets and as a result they are trapped as nanoparticles within glass. Since evidence of Na_2MoO_4 crystals is neither observed in XRD nor in the Raman results of SBBS3-3M glass, such tiny particles could be Sr/$BaMoO_4$ crystals. According to the XRD patterns (Figure 6-8), the crystals in SBBS3-2.5M and -3M glasses are not exactly identical. It is obvious that the peaks for SBBS3-2.5M glass are in full accordance with the peaks for BBS-2.5M glass and for crystalline $BaMoO_4$, while the peaks for SBBS3-3M glass shift to higher angles indicating that some of the Ba^{2+} ions in $BaMoO_4$ crystals are probably replaced by Sr^{2+} ions. This indicates that MoO_4^{2-} ions are prone to separate with Ba^{2+} from the network, but Sr^{2+} ions are able to join the separated phase at higher MoO_4^{2-} concentrations. Thus the solubility of MoO_3 in glass is controlled by the network modifying cations with the largest crystallisation

tendency with MoO_4^{2-} ions.

In the partially crystallised BBS-2.5M sample, there are boundaries between the crystallised region and the glassy region (Figure 6-34). It is interesting that the main compositional difference between these two regions arises from the Al_2O_3 content which is from the dissolution of mullite crucible, with a small change in SiO_2 content. It seems that Al_2O_3 is not distributed homogeneously in melt and the region with more Al_2O_3 (darker area) less readily phase separates. Since MoO_4^{2-} ions are believed to be located in the alkali or alkaline earth enriched area, the area with higher Al_2O_3 content may contain less MoO_3 and therefore phase separation firstly occurs in the areas that contain less Al_2O_3 and SiO_2.

In summary, the crystallised molybdates within borosilicate glass matrices are formed through liquid-liquid phase separation and thereafter crystallisation. Alkaline earth molybdates are the preferential separated phase while Na_2MoO_4 is found as a minor phase in MBS and CBS glasses. The amount of Na_2MoO_4 increases as the MoO_3 addition increases. The separated particles show distinct morphology being mainly spherical and randomly dispersed. The size of the particles are less than 1 μm in diameter and dependent on the amount of MoO_3, although TEM images suggest that there are also a number of nanoparticles widely distributed or not surrounding the large spheres. Moreover, the region enriched in more network formers less readily suffers phase separation according to the compositional comparison between crystallised and glassy regions of the phase separated glass.

6.3.3.2. Aluminosilicate glasses

Unlike in borosilicate glasses, MoO_4^{2-} ions in aluminosilicate glasses only have one cation with which they are likely to associate upon phase separation and, as expected, the separated phases are alkaline earth molybdates in all glass compositions, according to the XRD and Raman results.

MAS glass has the highest MoO_3 solubility and when it comes to phase separation in MAS-8M glass the capacity for MoO_3 incorporation seems to have been reached. The excess molybdate which cannot enter the glass network separates from the melt during cooling, forming separated droplets as observed in the crystallised region of MAS-8M

sample (Figure 6-36). XRD patterns (Figure 6-9) indicate that the separated phase is most likely to be $MgMoO_4$, although the number of clearly corresponding peaks is limited. Raman spectra (Figure 6-21) also show the dominance of $MgMoO_4$ in the separated phase from the comparison with the spectrum of $MgMoO_4$ crystals. Similar to the separated particles in borosilicate glasses, these randomly distributed particles are also all spherical and have a clear interface with the glass matrix. Phase separation is more likely to have occurred through liquid-liquid separation in the melt rather than the direct nucleation from saturated melt during cooling. The separated phase exhibits a strong crystallisation tendency and eventually each particle is made up of numerous single $MgMoO_4$ crystals.

CAS-4M and CMAS-4M glasses are both slightly crystallised. The separated particles in CAS-4M glass are very small (<100 nm) and thus an EDX measurement could not be usefully performed. However, XRD patterns (Figure 6-10) and Raman spectra (Figure 6-22) suggest that the crystalline phase in CAS-4M glass is most likely to be $CaMoO_4$. Meanwhile, in CMAS-4M glass, where Ca^{2+} and Mg^{2+} ions are present simultaneously, the separated particles are similar to those in CAS-4M glass (Figure 6-37). This could also be because the MoO_3 addition in CMAS-4M glass is not as excessive as in MAS-8M glass and thus the separated particles are still tiny. EDX and XRD analysis cannot identify which molybdate species are in the separated phase, but the Raman spectrum of the crystallised region in CMAS-4M glass reveals a pattern very close to the spectrum of crystallised region of CAS-4M glass, which is very different from that of MAS-8M glass, as seen in Figure 6-46. This suggests that the separated phase in CMAS-4M glass should be mainly $CaMoO_4$; the slight shift to higher frequencies means that there may be a small amount of Ca^{2+} substituted by Mg^{2+} in $CaMoO_4$ crystals. In addition, the notable shift of the amorphous molybdate band centred at ~920 cm^{-1} (CAS-4M) and ~940 cm^{-1} (CMAS-4M) indicates that there are a significant number of MoO_4^{2-} anions in the glass network surrounded by Mg^{2+}.

According to the XRD patterns in Figure 6-11, the crystals in BAS-3M glass are $BaMoO_4$ while the crystals in SBAS-2.5M and -3M glasses are probably barium and strontium molybdate solid solutions as the diffraction angles slightly shift to higher angles. The EDX spectrum in Figure 6-38 suggests that in the separated phase the Ba level is higher than Sr level. This is in agreement with the XRD peaks of SBAS-3M

glass which are more closely located to the peaks of BAS-3M glass (assigned to $BaMoO_4$) and indicates that MoO_4^{2-} ions are preferably associated with Ba^{2+} than Sr^{2+} ions when separating out. However, there is no evidence that Ba^{2+} ions participate in crystallisation first as Ba^{2+} and Sr^{2+} ions are both present in the separated phase at the very beginning. In addition, the composition of the separated phase does not change with the amount of excess MoO_3 added.

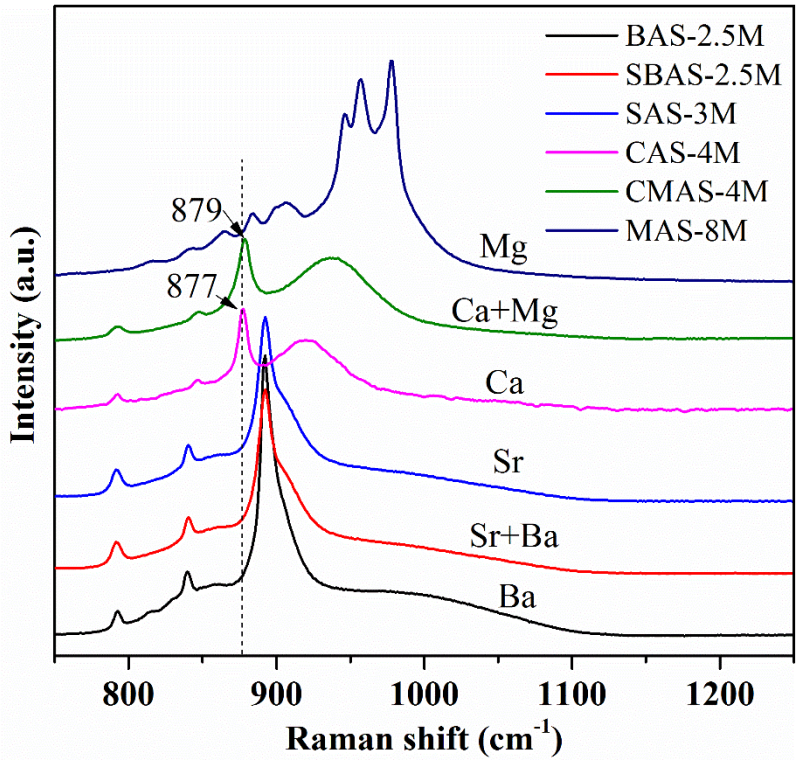

Figure 6-46 Raman spectra of separated phase/crystallisation region of different aluminosilicate glasses.

6.4. Conclusions

Based on the above results and discussion regarding molybdate incorporation in both borosilicate and aluminosilicate glasses, the following conclusions can be drawn:

- MoO_3 shows excellent retention rate (>95%) in glasses regardless of MoO_3 addition and glass composition; only MAS glass has a <90% retention rate when MoO_3 incorporation has been saturated.
- In aluminosilicate glasses, MoO_3 solubility increases in the order Ba<Sr<Ca<Mg; in borosilicate glasses, MoO_3 solubility increases in the order Mg<Ba<Sr<Ca. The highest MoO_3 solubilities achieved for the aluminosilicate and borosilicate glasses are 5.34 mol% in MAS-7M glass and 2.84 mol% in CBS-3M glass, respectively.
- MoO_3 incorporation results in decreased T_g and T_c of both glass series. MoO_3 incorporation in glass also yields two prominent Raman bands (890-960 cm^{-1} and 320-400 cm^{-1}) and the intensities of these bands increase with increasing MoO_3 content in glass. FTIR spectra are not sensitive to the structural changes caused by MoO_3 incorporation.
- The frequency of the MoO_4^{2-} Raman band at 960 cm^{-1} of MAS glass is apparently out of line, which is possibly linked with the structural features that account for the unusually high MoO_3 solubility in MAS glass.
- When separating out from borosilicate glass network, MoO_4^{2-} ions are prone to be associated with alkaline earth cations except in MBS glass where a sodium-magnesium molybdate solid solution can be formed. Na_2MoO_4 is only formed after the MoO_3 addition is apparently excessive and possibly originates from immiscible molybdates in melt.
- When separating out from aluminosilicate glass network, MoO_4^{2-} ions are associated with alkaline earth cations only.
- Under the coexistence of two alkaline earths, MoO_4^{2-} ions can associate either of them, but the proportion of association with the larger cation is larger.
- Phase separation of molybdates in glasses occurs via liquid-liquid separation and thereafter crystallisation. The separated particles are mostly spherical with

varying diameters and randomly dispersed within glass matrices. The size of the particles is largely dependent on the amount of excess MoO_3.

7. Incorporation of sulphur, chlorine and molybdenum in glass: similarities and differences

7.1. Introduction

In the previous three chapters, the incorporation of sulphate (SO_4^{2-}), chloride (Cl^-) and molybdate (MoO_4^{2-}) in borosilicate and aluminosilicate glasses has been investigated. Following the consideration of each anionic species separately, this chapter summarises the overall information about anionic incorporation in glass and provides the similarities and dissimilarities among different anionic species in varying glass compositions.

7.2. The effects of anionic incorporation on glass structure and properties

7.2.1. Corrosion from crucibles

According to Figure 7-1, the base glasses cause notable corrosion of the mullite crucibles during melting, given their introduced or increased Al_2O_3 content compared with the expected values. The corrosion is more significant in the borosilicate base glasses that contain BaO and SrO, whereas it is more significant in aluminosilicate glasses that contain CaO and MgO. The corrosion in borosilicate glasses is related to the viscosity of melts, as BaO and SrO lower the melt viscosity, which may allow the matters that come out from the crucible to diffuse further from the wall and thereby increasing the driving force for more corrosion. In comparison in the aluminosilicate glasses there is significant loss of MgO from the MAS base glass and CaO from the CAS base glass, which results in the relative amount of Al_2O_3 being increased. Therefore, the Al_2O_3 contents of the CAS and MAS glasses are much higher than those of the SAS and BAS glasses.

However, the crucible corrosion can be apparently reduced by the additions of MoO_3, Cl or SO_3, as seen in Figure 7-1. In borosilicate glasses, the additions of all the three components lead to sharp reduction in Al_2O_3 content initially and then a plateau or slow decline with further additions. There is little difference among the inhibitory function of molybdate, chloride and sulphate additions on borosilicate melt corrosivity, and the resultant corrosion with increasing anionic loadings is more related to the base glass compositions.

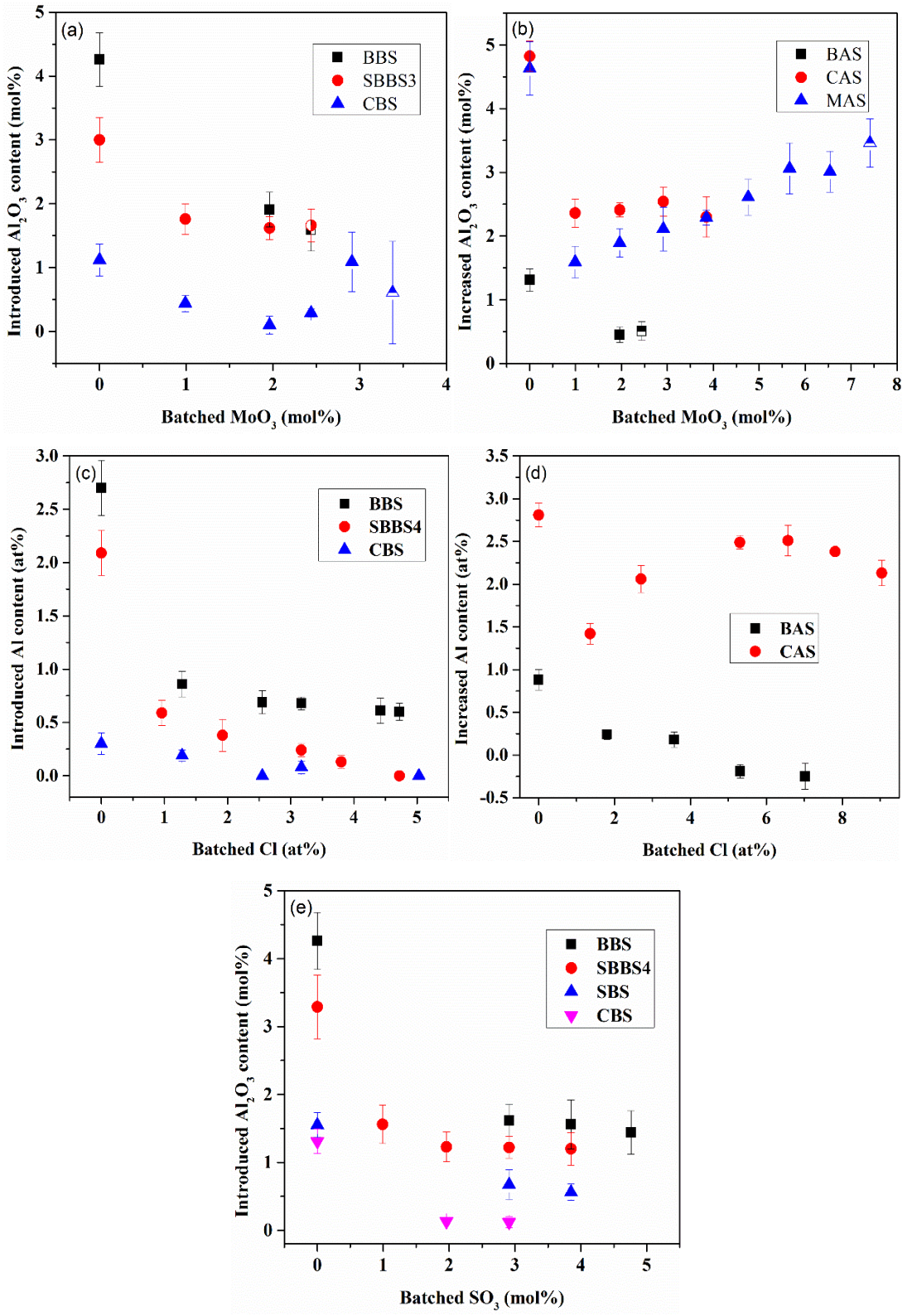

Figure 7-1 Alumina content change in the glasses studied versus increasing anionic additions: (*a*) MoO_3 to BS glasses; (*b*) MoO_3 to AS glasses; (*c*) Cl to BS glasses; (*d*) Cl to AS glasses and (*e*) SO_3 to BS glasses.

On the other hand, crucible corrosion with the aluminosilicate glasses is different with MoO_3 and Cl loadings (SO_3 retention in aluminosilicate glasses is very low and thus not discussed here). The same aspect between MoO_3 and Cl additions merely lies in the initial drop of Al_2O_3 content. Afterwards, Al_2O_3 content remains constant (CAS and BAS) or slightly increases (MAS) with increasing MoO_3 additions until phase separation. The effect of MoO_3 addition on melt corrosivity does not apparently vary with melt composition. In comparison, with increasing Cl additions, CAS glass shows a maximum of Al_2O_3 content while BAS glass shows a steadily downward Al_2O_3 content. The different trends seen with additions of MoO_3 and Cl to CAS glasses indicate that the function molybdates have on the melt properties are not same as those of chlorides. Considering their close anionic radii (MoO_4^{2-}: 1.77 Å; Cl^-: 1.81 Å), the difference in valency may be the reason for the difference. Meanwhile, the Al_2O_3 contents of BAS-15Cl and BAS-20Cl glasses are even lower than the batched values. This could be due to the formation of hexacelsian in glass that consumes much more aluminium and as a result the Al_2O_3 content in the glassy part is reduced.

Generally speaking, the additions of MoO_3, Cl and SO_3 in glasses all lead to reduced corrosion from the crucibles. In borosilicate glasses the additions of MoO_3, Cl and SO_3 function similarly, maintaining more or less unchanged low levels of corrosion with increasing anionic loadings. In aluminosilicate glasses the corrosion is different between MoO_3 and Cl additions and also varies with glass composition.

7.2.2. Retentions of SO_3, Cl and MoO_3 in glass

The retention of SO_3, Cl and MoO_3 in glass varies and is related to glass compositions and melting temperatures. The SO_3 retention rate in borosilicate glasses is normally higher than 95% at low loadings and around 90% at high loadings close to saturation. However, the SO_3 content is significantly reduced after the melting temperature increases to 1250 ºC and only a trace amount of SO_3 can be found in SBBS-3S prepared at 1300 ºC (Figure 4-3). It is also probably the increased melting temperature (1450 ºC) that makes the SO_3 retention in aluminosilicate glasses very limited.

Cl retention in borosilicate glasses ranges from 60-70% at low loadings (except for MBS glass, which has a poor Cl solubility) and when the Cl content approaches saturation this retention rate is gradually reduced to 55% or lower. At higher loadings,

Cl retention is improved by the equimolar substitution of larger to smaller alkaline earth cations. The temperature dependence of Cl retention in glass is not consistent when it comes to aluminosilicate glasses, some showing higher Cl retention rates (~80% in BAS glass) while some others showing pretty low rates (CAS and MAS glasses), as plotted in Figure 5-2. Cl retention is more dependent on the melt composition, probably via the cations with which Cl^- ions are associated in melts.

Among all the three anionic species MoO_3 shows the highest retention in glass, either borosilicate or aluminosilicate compositions. MoO_3 retention in borosilicate glasses is approximately 100%, regardless of glass composition and MoO_3 loadings as long as no molybdate segregation occurs. Melting temperature has limited influence on MoO_3 retention given the close-to-100% retention rate in aluminosilicate glasses, too. Only MAS glass shows a limiting in MoO_3 content when MoO_3 addition exceeds 5.66 mol%, indicating that molybdate saturation has been reached. Evaporation of excess molybdates which cannot be dissolved in melt occurs, resulting in some MoO_3 loss in MAS-7M and -8M glasses.

It is common among the three anionic species that retentions at initial loadings do not vary with alkaline earth substitution. At higher loadings, the SO_3, Cl or MoO_3 retention rate is slightly reduced with the substitution of smaller to larger alkaline earths, though the reduction is not significant. Under the same melting temperatures, melts with heavier components such as BaO and SrO are more fluid than melts with lighter components such as CaO and MgO and thus suffer greater weight loss during melting (Beerkens 2008). However, the retention results are opposite to this assumption, indicating that melt viscosity/fluidity is not the controlling factor for anionic evaporation. Glass networks with larger cations are more depolymerised (Brendebach *et al.* 2009) and hence can be tuned to accommodate more SO_4^{2-}, Cl^- and MoO_4^{2-} ions. There should be a balance between anionic dissolution and anionic evaporation.

The retentions of SO_3 and MoO_3 in borosilicate glasses are high, whereas Cl retention is much lower. In aluminosilicate glasses, the retention of MoO_3 is still high but the retention of SO_3 is zero, whereas Cl retention varies with composition. Only SO_3 retention shows strong and consistent dependence on melting temperature. This is explained in Section 4.3.1.1, by the accelerated decomposition of sulphate in melt at

high temperatures. This explanation could also be applicable to MoO_3 retention, but the influence is insignificant as observed, given MoO_3 has a much higher boiling point (1155 ºC) or decomposition point than SO_3. The evaporation of Cl^- is complex. Considering that alkali and alkaline earth contents are not apparently reduced with Cl content, it can be deemed that Cl content is not mainly lost through vaporisation of chloride. Chloride does not decompose directly in the melt, and Cl^- ions are oxidised by O_2 to form Cl_2 gas and then evaporated. In borosilicate glasses all chlorides are batched as NaCl, so the Cl^- evaporation is primarily based on the nature of NaCl and not significantly varied by melt composition. In aluminosilicate glasses, Cl^- is supplied by different alkaline earth chlorides which vary with glass composition. Chlorides in aluminosilicate glasses are batched as hydrated chlorides. Indeed, Schofield (2011) reported that batching of $CaCl_2$ as hydrated $CaCl_2 \cdot 2H_2O$ when preparing an analogous calcium aluminosilicate glass accelerates chloride loss *via* vaporisation of chloride during heating, but compared to the loss caused by Cl^- oxidisation this amount should not be dominant.

7.2.3. Anionic presence and locations

Although sulphur and molybdenum in the glasses prepared under oxidising and neutral atmosphere are predominantly present as S^{6+} and Mo^{6+}, respectively, they are actually surrounded by oxygens to form isolated SO_4^{2-} or MoO_4^{2-} units in the glass network. The dominance of SO_4^{2-} can be reflected by the Raman spectra shown in Figure 4-9, where the prominent 985 cm^{-1} band assigned to the υ_1 vibrational mode of SO_4^{2-} is created and intensified by SO_3 additions. Raman spectra (Figures 6-18 to 6-23) also indicate the dominance of MoO_4^{2-} in all glass compositions containing MoO_3 given the observation that the positions of bands induced by MoO_3 addition are in agreement with the positions of Raman peaks for crystalline molybdates. In addition, chlorine in glass is directly present as negative Cl^-. Therefore, despite of different valences showing in glass, these three elements are actually all negatively present (SO_4^{2-}, Cl^- and MoO_4^{2-}, respectively) in the investigated glasses. These results meet the expectation of this study, which is to investigate the incorporation of *anionic* species into the glass network, and facilitates further comparison among different anions.

There is no evidence of any SO_4^{2-}, Cl^- or MoO_4^{2-} joining the glass network. According

to Short *et al.* (2005) and Caurant *et al.* (2007), each MoO_4^{2-} unit is isolated in glass network and therefore it is likely to enter interstitial spaces associated with network modifiers. Such locations seem to be also applicable to SO_4^{2-} and Cl^- because neither Raman spectra nor FTIR spectra display the bands assigned to Si-O-S or Si-Cl vibrations. This agrees with previous observations in the literature (Siwadamrongpong *et al.* 2004, Brendebach *et al.* 2009, Bingham *et al.* 2010) and simplifies the investigations on the incorporation of SO_4^{2-}, Cl^- and MoO_4^{2-} in glass. SO_4^{2-} ions have the same valence (-2) of MoO_4^{2-} ions while Cl^- ions have a close anionic radius to MoO_4^{2-} ions; these three anions therefore have both common points and differences between them (Table 7-1). The influence of anionic geometry and anionic valence on glass structure thus can be compared.

Table 7-1 The charge and radius of SO_4^{2-}, Cl^- and MoO_4^{2-}.

Anion	Charge	Radius (Å)
SO_4^{2-}	-2	1.41
Cl^-	-1	1.81
MoO_4^{2-}	-2	1.77

7.2.4. The changes in Raman spectra along with increasing anionic loadings

The incorporation of SO_4^{2-} and MoO_4^{2-} into glass network results in significant changes in the Raman spectra, whereas the incorporation of Cl^- does not lead to any new Raman band. The deconvolution of Raman bands assigned to silicate stretching vibrations (800-1200 cm^{-1}) has been successfully undertaken for the sulphur- and chlorine-containing glasses; the severe overlapping of bands assigned to MoO_4^{2-} vibrations in this region makes accurate deconvolution for molybdenum containing glasses impossible.

Both SO_4^{2-} and MoO_4^{2-} units have symmetric stretching vibrational modes (Section 2.3.1.2 and 2.3.3.2) which are very sensitive to Raman scattering. The area ratio of SO_4^{2-} band centred at 990 cm^{-1} to the silicate band covering the range 800-1200 cm^{-1} in SBBS4 glass shows a quadratic increase with increasing SO_3 loadings until SBBS4-4S glass which is heavily crystallised, as plotted in Figure 7-2 (a combination of Figure 4-11 and Figure 6-45). Similarly, the relative areas of bands assigned to MoO_4^{2-}

vibrations increase quadratically in MAS glass. The quadratic increase to a maximum of relative areas agrees with the observation that high levels of loading leads to a decreased retention rate. These bands prove that the retained SO_4^{2-} or MoO_4^{2-} units have been incorporated into glass network. Nevertheless, Raman spectroscopy is not sensitive to the vibrations of ionic chloride bonds and thus does not record any new band assigned to chloride incorporation. Therefore, the abundance of Cl^- in glass cannot be reflected in the Raman spectra.

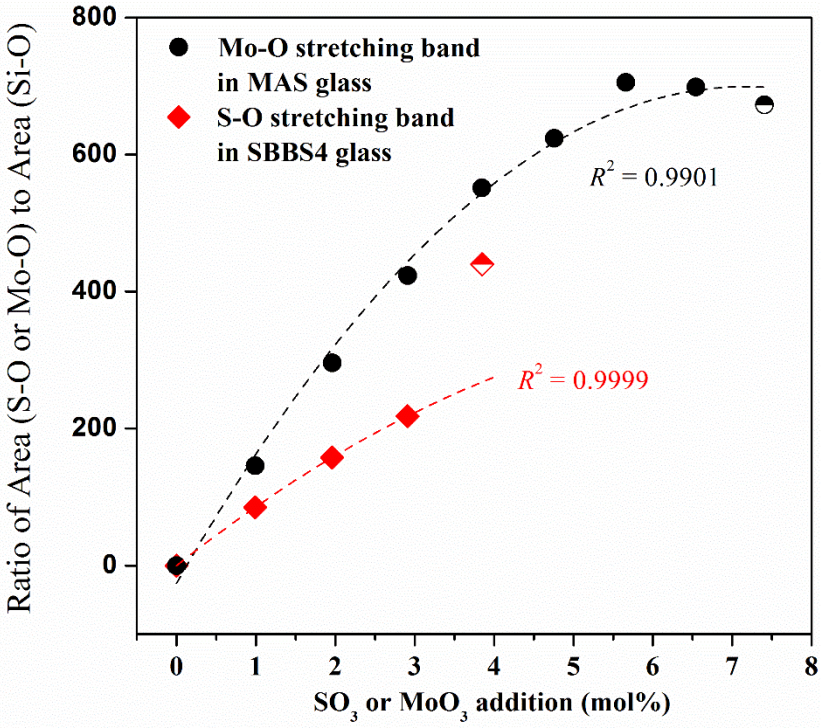

Figure 7-2 The relative areas of SO_4^{2-} stretching bands against SO_3 addition in SBBS4 glass and the relative area of MoO_4^{2-} stretching bands against MoO_3 addition in MAS glass, respectively. Half-filled symbols are for those glasses which are phase separated.

The associations of SO_4^{2-} and MoO_4^{2-} ions in glass network are also indicated by the Raman spectra. The results in Figure 4-12 for SO_4^{2-} and Figure 6-44 for MoO_4^{2-} are combined in Figure 7-3. It shows that the central frequency of SO_4^{2-} υ_1 band linearly shifts with the substitution of SrO by BaO in borosilicate glasses, indicating that the local environments of SO_4^{2-} are strongly related to the alkaline earth cations. A nearly linear correlation is also observed for the central frequency of MoO_4^{2-} υ_1 band with the substitution of alkaline earths in borosilicate glasses, which means that MoO_4^{2-} ions are also closely linked to M^{2+} ions in glass network. The abundance of different

alkaline earths may influence SO_3 and MoO_3 solubilities through changing their associations. However, there is also a major difference between SO_4^{2-} bands and MoO_4^{2-} bands in the Raman spectra of borosilicate glasses. The centre of the SO_4^{2-} υ_1 band is constant no matter whether the glass is homogeneous or not, implying that the amorphous and crystalline SO_4^{2-} units have a same central frequency. On the other hand, the centre of MoO_4^{2-} υ_1 band in critically and excessively loaded glasses can be shifted or split, which means that the local environments of MoO_4^{2-} in glass networks are very much different from the local environments in separated phases. Given the fact that such a shift or split can be observed for both borosilicate and aluminosilicate glasses, this feature is likely due to the nature of MoO_4^{2-} units and the structures of molybdates themselves. In other words, it may suggest that SO_4^{2-} ions adopt similar structural roles in amorphous and crystalline materials but that MoO_4^{2-} ions adopt distinct structures in amorphous and crystalline materials.

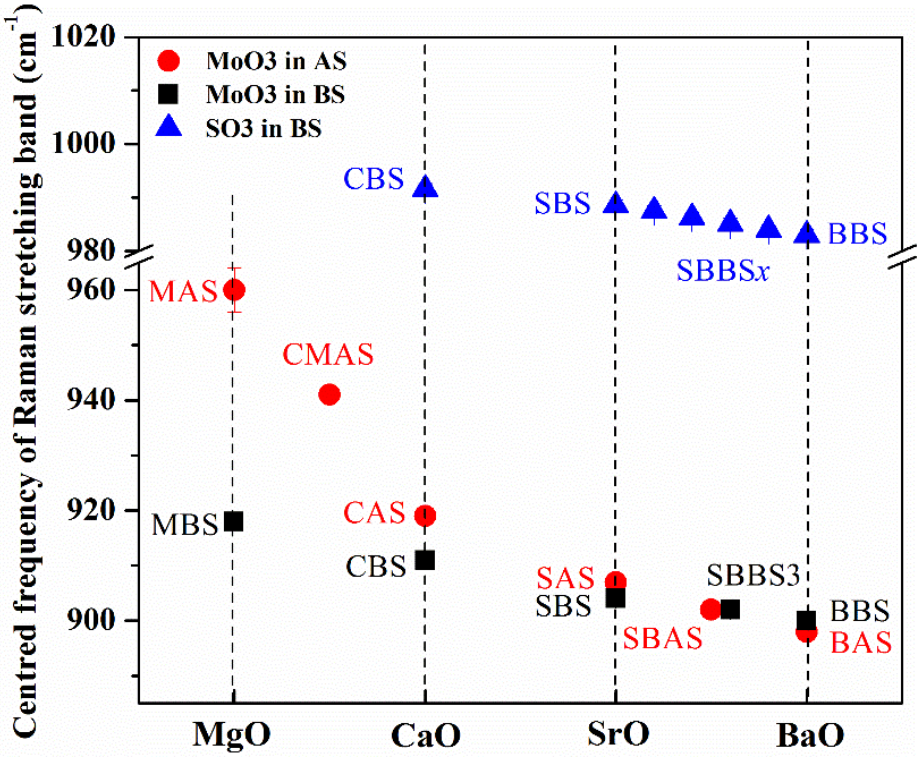

Figure 7-3 Central frequency of Raman bands assigned to SO_4^{2-} and MoO_4^{2-} stretching vibrations in glass compositions with varying alkaline earth content.

The deconvolution of 800-1200 cm^{-1} regions for Raman spectra of SBBS4-*x*S, BBS-*x*Cl, SBBS4-*x*Cl and BAS-*x*Cl glass series has been performed to assess the evolution

of polymerisation extent with SO_4^{2-} and Cl^- incorporation. With the same borosilicate glass composition (SBBS4, combined plots are shown in Figure 7-4), SO_4^{2-} and Cl^- ions reveal opposite functions on network connectivity. The ratio of Q_3 to Q_2 slightly increases with the initial SO_3 additions, an indication of increased polymerisation, and then rapidly decreases with further SO_3 additions until phase separation. However, with increasing chlorine contents, the Q_3/Q_2 ratio initially decreases and afterwards gradually increases until phase separation. Chlorine in BBS glass exhibits a similar behaviour to that in SBBS4 glass. This suggests that SO_4^{2-} and Cl^- ions have different mechanisms when incorporated into the glass network. This may arise from their geometric difference or valency difference that leads to different local arrangements in SO_4^{2-} or Cl^- enriched areas. This could also be a primary factor that influences their solubility dependences in glass. There are possibly four bands assigned to MoO_4^{2-} vibrations in 800-1200 cm^{-1} region, together with the silicate bands assigned to different Q_n species, making any deconvolution of this area less reliable.

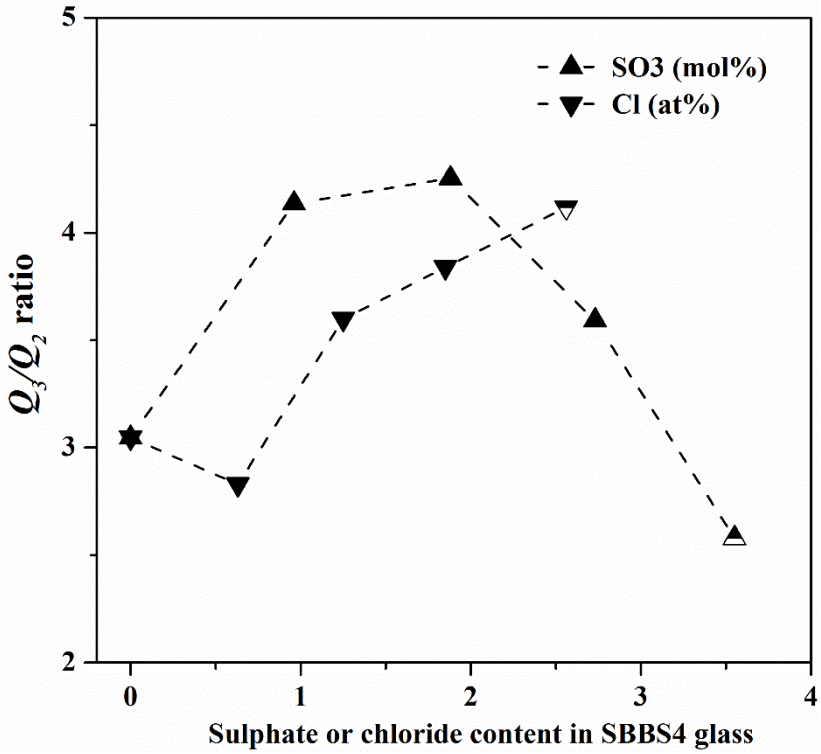

Figure 7-4 The Q_3/Q_2 ratios in SBBS4 glass with different SO_3 and Cl contents. The calculation of Q species is based on the deconvolution results in Sections 4.2.2 and 5.2.2. Dashed lines were added to guide the eyes.

7.2.5. FTIR changes with increasing SO_3, Cl and MoO_3 loadings

None of the SO_4^{2-}, Cl^- and MoO_4^{2-} ions led to significant changes in FTIR spectra unlike the corresponding Raman spectra. According to Figure 4-14, the presence of SO_4^{2-} in SBBS4 glass can be identified by the creation and intensification of ~620 cm^{-1} band. The presence of MoO_4^{2-} in SBBS4 glass can be identified by the emergence of bands between 800 and 900 cm^{-1}. Like the Raman spectra, in FTIR spectra there is no band created by Cl^- incorporation.

Figure 4-15 compares the FTIR spectra of sulphur-containing borosilicate glasses with different ratios of BaO to SrO, however, showing little difference in the 620 cm^{-1} band, the only one identified as being due to the presence of SO_4^{2-}. There are indeed some changes in the 800-1200 cm^{-1} bands among the compositions, but such changes are more likely to be due to structural differences caused by compositional variation rather than SO_4^{2-} associations. Figure 6-26 compares the FTIR spectra of Mo-containing borosilicate glasses. The shift in the centre of bands at 800-860 cm^{-1} (plotted as Figure 7-5) proves the correlation of MoO_4^{2-} ions and alkaline earth cations in glass network. There are also some changes in the shape of silicate main band at 800-1200 cm^{-1} observed, but as in the sulphur-containing glasses, these changes are more likely due to compositional variation.

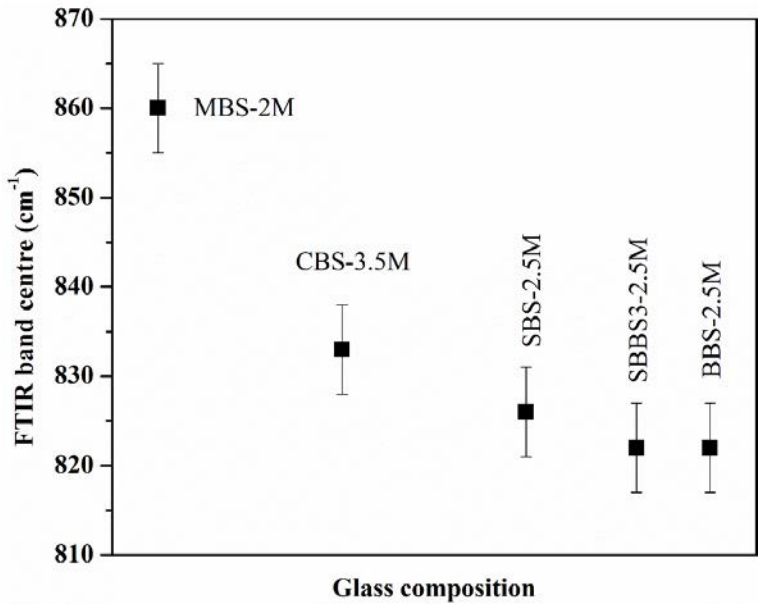

Figure 7-5 The shift of FTIR molybdate band centre with the change in alkaline earth species in borosilicate glasses.

In summary, the incorporation of SO_4^{2-} and MoO_4^{2-} leads to creation of some small bands in FTIR spectra, but the evolution of these bands are not as apparent as the bands in their Raman spectra. The incorporation of Cl^- is not reflected by FTIR. Therefore, compared with Raman spectroscopy, FTIR spectroscopy is less useful in the determination of structural change caused by SO_4^{2-}, Cl^- and MoO_4^{2-} incorporation.

7.2.6. The changes in DTA curves along with increasing anionic loadings

All the homogeneous glasses containing SO_4^{2-}, Cl^- or MoO_4^{2-} ions are thermally stable until glass transition temperature. For borosilicate glasses, a smooth crystallisation peak is observed soon after the glass transition peak. For aluminosilicate glasses, there is a second and sharp exothermic peak after the first and smooth one. These features are universal and are not significantly changed with anionic species incorporation.

Nevertheless, the temperatures at which glass transition and crystallisation occur are changed by incorporating SO_4^{2-}, Cl^- and MoO_4^{2-}. The T_gs of some typical glass series with increasing SO_3, Cl and MoO_3 additions are plotted in Figure 7-6. Initial additions of SO_3, Cl and MoO_3 all result in a notable decrease in T_g while at higher additions the variation depends on the anionic species.

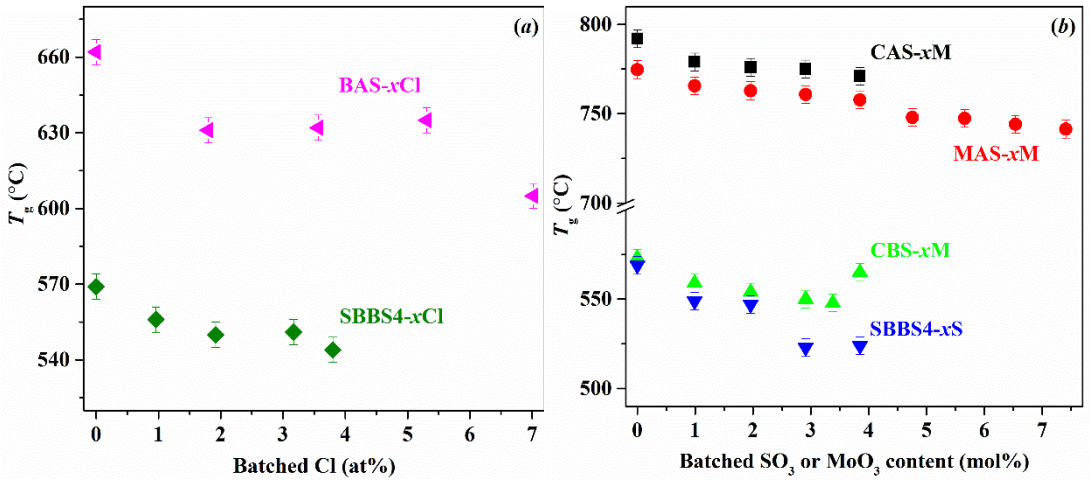

Figure 7-6 Changes in T_g of glasses with increasing (*a*) chlorine and (*b*) molybdate or sulphate additions.

After initial reduction, T_gs of glasses with further Cl addition generally keep constant

before another notable reduction occurring in the heavily phase separated glasses. This behaviour is observed in both borosilicate and aluminosilicate glasses. Meanwhile, the further addition of MoO_3 results in continuous reduction in T_g after the initial reduction regardless of glass composition. This downward tendency also continues for partly crystallised glasses except for CBS-4M glass which is a mixture of crystallised bulk glass and segregated molybdate layer. The T_g change with further SO_3 addition in borosilicate glasses is similar to that seen with Cl addition, but a sudden reduction in T_g occurs in SBBS-3S glass which is, however, still homogeneous.

The T_g reductions may arise from two aspects: the reduced corrosion from crucibles and the incorporated anionic species. The reduced corrosion means lower SiO_2 and Al_2O_3 contents and higher alkali and alkaline earth oxide contents. Such compositional changes can lead to either decreased or increased T_gs (Siwadamrongpong *et al.* 2004, Ehrt and Keding 2009, Tiegel *et al.* 2013), depending on the specific glass composition. Among the literature data Siwadamrongpong *et al.* (2004) has the closest compositions to the aluminosilicate glasses prepared here, in addition to the same tendency of changing T_g. The incorporation of anionic species also influences T_g. At higher anionic loadings, when corrosion from the crucible becomes limited, the T_g change is mainly due to the incorporated anions and different T_g trends may reflect different incorporation mechanisms.

Previous studies, *e.g.* Caurant *et al.* (2007), have shown that increasing MoO_3 content in borosilicate glasses leads to a more polymerised glass network *via* NMR study, in which it is hypothesised that network modifiers, such as Na^+ and Ca^{2+}, are attracted by MoO_4^{2-} in the more depolymerised region rather than create NBOs with silicate units to depolymerise network. However, polymerised glass network usually induces increased T_g and as a result there must be other reasons that contribute to T_g reduction with increasing MoO_3 addition.

7.2.7. Density changes caused by SO_4^{2-}, Cl^- and MoO_4^{2-} additions

Glass densities are also changed with the incorporation of SO_4^{2-}, Cl^- and MoO_4^{2-} ions into the glass network. Figure 7-7, which combines Figures 4-5, 5-4, 5-5, 6-4 and 6-5 together, shows that the density changes of glasses with increasing SO_4^{2-} and MoO_4^{2-} incorporations are similar to each other, but both distinct from Cl^- incorporation: glass densities are continuously increased by increasing SO_4^{2-} and MoO_4^{2-} incorporations while showing an initial maximum with increasing Cl^- incorporation.

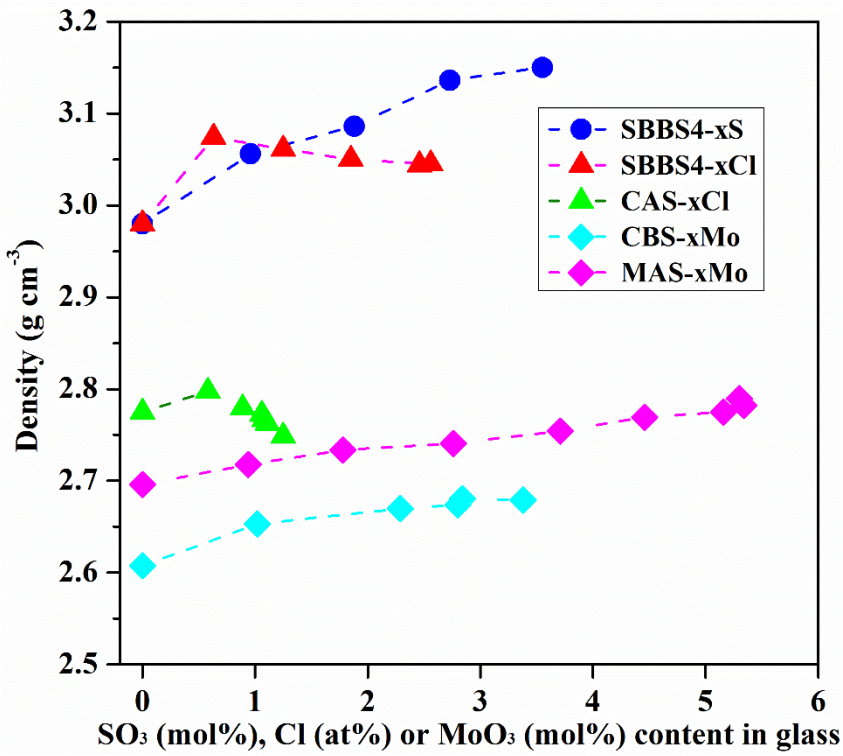

Figure 7-7 Density changes with different SO_3, Cl and MoO_3 content retained in glass.

Figure 7-8 shows the changes in molar volume of glasses with SO_4^{2-}, Cl^- and MoO_4^{2-} contents in the glasses plotted in Figure 7-7. The molar volume of a glass is calculated as its molar mass divided by density, which reflects the volume alteration of glass network caused by anionic incorporation. As can be seen in Figure 7-8, both Cl^- and MoO_4^{2-} incorporations result in an initial reduction in molar volume followed by a steady increase with further incorporations, while SO_4^{2-} incorporation monotonically decreases glass molar volumes regardless of SO_4^{2-} amount in glass. These features are in agreement with the normal changes in volume of solid and liquid solutions, which indicates the dissolution of these anions in glass network.

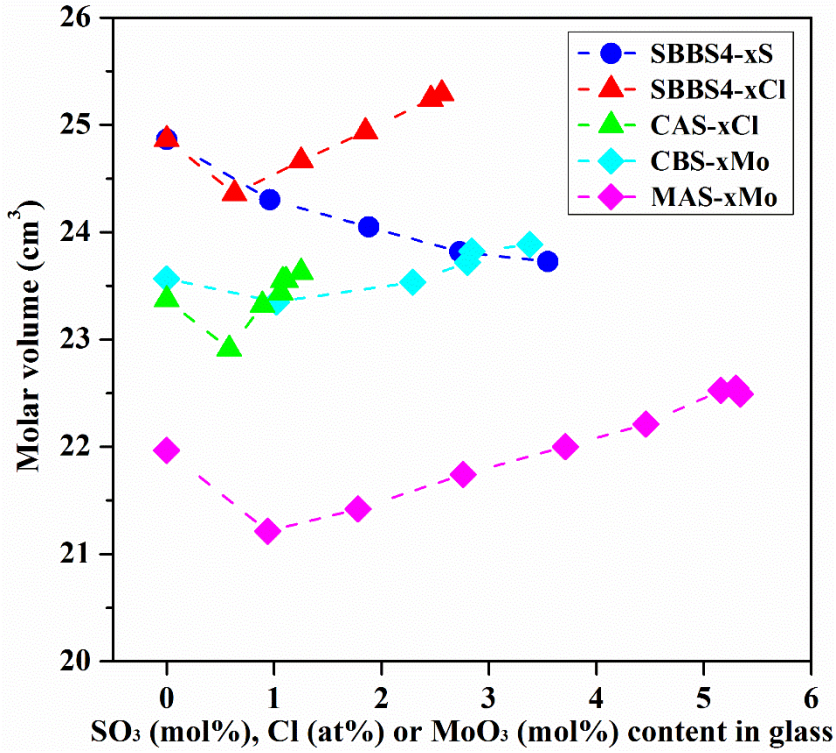

Figure 7-8 Changes in molar volume of glasses with different SO_3, Cl and MoO_3 content.

The changes in glass density and glass molar volume with SO_4^{2-}, Cl^- and MoO_4^{2-} incorporations are probably related to their anionic sizes and locations in glass network. Initially, there exists some interstitial space in glass network which allows a certain amount of SO_4^{2-}, Cl^- and MoO_4^{2-} ions to be directly accommodated. In this stage, glass network is densified and glass molar volume is decreased. However, as the amounts of SO_4^{2-}, Cl^- and MoO_4^{2-} ions increase, the tendencies in glass density and molar volume vary among species. As for SO_4^{2-}, the continued increase in density and decrease in molar volume with further SO_4^{2-} incorporation may imply that SO_4^{2-} ions are all located in the interstices while not causing network expansion. This is reasonable because SO_4^{2-} are the smallest among the three anions but with a high anionic density (see Table 7-2). Meanwhile, MoO_4^{2-} have a similar density to SO_4^{2-} (both are heavier than base glass), hence resulting in similar density increases with further MoO_4^{2-} incorporation in glass. However, unlike SO_4^{2-}, further MoO_4^{2-} incorporation in glass leads to increased glass molar volume, which is likely due to the original free space for MoO_4^{2-} incorporation having been saturated and further MoO_4^{2-} incorporation requiring network expansion (MoO_4^{2-} are much larger than

SO_4^{2-}). In contrast, Cl^- ions have a large volume but with a very light mass, making it least dense among the three anions and less dense than the original network. The further incorporation of Cl^- thus results in network expansion and as a result the glass density is reduced.

Table 7-2 Calculated densities of SO_4^{2-}, Cl^- and MoO_4^{2-} ions. Ionic radii refer to Shannon (1976) and $r(O^{2-})$ is assumed to be 1.40 Å.

Anions	Molecular weight	Volume (Å^3)	Density (g Å^{-3})
SO_4^{2-}	96.06	14.71	6.5
Cl^-	35.45	24.84	1.4
MoO_4^{2-}	159.93	23.23	6.9

7.2.8. Phase separation due to excess loadings of SO_4^{2-}, Cl^- and MoO_4^{2-}

Phase separation occurs in glass when the sulphate, chloride and molybdate additions exceed the loading limit (see Figure 7-9). This can be identified when the prepared glasses are not completely transparent, or identified by XRD patterns and/or Raman spectra if crystalline phases develop. Although SO_4^{2-}, Cl^- and MoO_4^{2-} ions are all readily separated from glass melts, the mechanisms of their separation are not the same.

According to the XRD patterns in Figure 4-6, the sulphate species at the beginning of phase separation in glass depends on glass compositions: for MBS glass the separated phase is Na_2SO_4, for CBS glass the separated phase is likely $(Ca_xNa_{1-2x})_2SO_4$ ($x \leq 0.5$) and for SBS, BBS and SBBS*x* glasses the separated phases are Sr/$BaSO_4$. The abundance of larger alkaline earth cations in glass facilitates the change from the formation of alkali sulphates to alkaline earth sulphates. The formation of alkaline earth sulphates such as $BaSO_4$ and $SrSO_4$ should more be advantageous for wasteform performance than the formation of Na_2SO_4 because $BaSO_4$ and $SrSO_4$ are more stable and less water soluble than Na_2SO_4. Meanwhile, it was also observed that a segregated Na_2SO_4 layer or aggregated Na_2SO_4 clusters can be formed, as reported in literature (Jantzen *et al.* 2004, Mishra *et al.* 2008), if SO_4^{2-} ions have already become excessive in the melt. Therefore, the abundance of larger alkaline earths in glass only changes the association of SO_4^{2-} ions dissolved in glass melt, but not the tendency that excess SO_4^{2-} ions in the melt will be expelled to melt surface to form Na_2SO_4 aggregates.

Crystallisation within critically sulphate-loaded glass arises from the reduced capacity of the glass network to accommodate sulphate caused by temperature reduction.

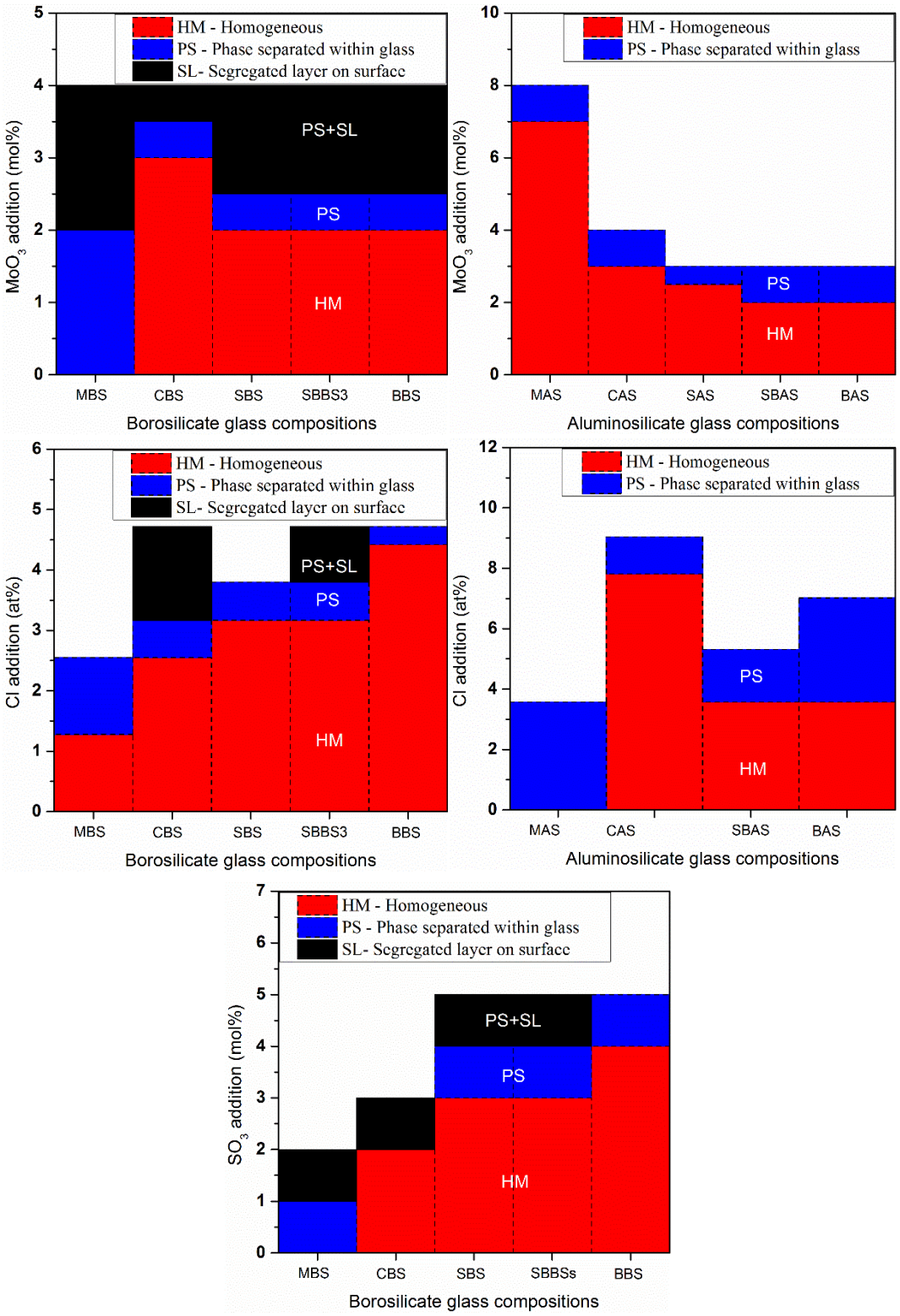

Figure 7-9 The homogeneity of glasses at different levels of molybdate, chloride and sulphate addition, respectively.

Excess chloride in glass also leads to the occurrence of phase separation; however, the separated phases formed at the beginning are not chloride phases. For borosilicate glasses, the separated phase is SiO_2 (mainly quartz but cristobalite may also coexist), irrespective of the glass composition. Based on the chlorine retention results in Figure 5-1, chlorine content may continue increasing even though the glass is phase separated. Cl solubility in borosilicate glass is controlled by the separation tendency of SiO_2. Given the fact that the incorporation of SO_4^{2-} and MoO_4^{2-} in the same compositions does not cause SiO_2 separation, it is believed that SiO_2 separation is triggered by Cl^- addition but is not due to glass network itself. A NaCl segregated layer is only formed on CBS-16Cl and SBBS4-15Cl glasses where Cl addition is apparently excessive. Meanwhile, the separated phases in aluminosilicate glasses such as BAS and MAS are corresponding alkaline earth aluminosilicates. While the Cl content in BAS glass linearly increases with increasing Cl addition regardless of phase separation, MAS glass actually does not contain any Cl at all. It is likely that the presence of chlorine in the melts causes instability of melt and thus phase separation during cooling.

Excess MoO_4^{2-} additions in both borosilicate and aluminosilicate glasses lead to phase separation. As can be seen in Figures 6-6 to 6-8, the separated phases in borosilicate glasses are primarily crystalline molybdates. Similar to sulphate separation in glass, the types of separated molybdates depend on glass composition and molybdate loading. At the beginning of phase separation, MoO_4^{2-} ions separate with Mg^{2+} and Na^+ ions together in MBS glass to form a $Na_{2.4}Mg_{0.8}(MoO_4)_2$ solid solution whereas MoO_4^{2-} separates solely with alkaline earth cations in CBS, SBS, SBBSs and BBS glasses. However, in MBS and CBS glasses, a small amount of Na_2MoO_4 crystals can also be observed and are enriched with increasing MoO_3 additions. Similar to sulphate separation from glass, the abundance of larger alkaline earths are helpful to form alkaline earth molybdates when MoO_4^{2-} ions separate out from borosilicate glass network although increasingly excessive MoO_3 addition results in formation of Na_2SO_4 on the surface of the melt. Meanwhile, the separated phases in alkaline earth aluminosilicate glasses are exclusively alkaline earth molybdates. Moreover, Raman spectra in Figure 6-46 indicate that the separated phase in CMAS-4M glass (mixed CaO and MgO) is very close to the separated phase in CAS-4M glass ($CaMoO_4$) but distinct from that in MAS-8M glass ($MgMoO_4$). Thus it can be concluded that MoO_3

solubility in aluminosilicate glasses is controlled by the molybdate that has the highest separation tendency in the glass network.

In comparison, phase separation within borosilicate glass with an excess SO_4^{2-} or MoO_4^{2-} ions is similar. The separated phases forming during the cooling of critically loaded melts are both related to the species of alkaline earths in glass. Larger alkaline earth cations are beneficial to the formation of alkaline earth salts while smaller alkaline earths are beneficial to the formation of alkali salts when phase separation occurs. This may arise from the geometric reason that larger cations are surrounded by more SO_4^{2-} and MoO_4^{2-} ions and consequently SO_4^{2-} or MoO_4^{2-} ions expelled from glass network tend to associate with Sr^{2+} and Ba^{2+} to form strontium/barium sulphates and molybdates (ionic radii: Ba^{2+} 1.42Å, Sr^{2+} 1.26Å, Ca^{2+} 1.00Å, Mg^{2+} 0.72Å and Na^{+} 1.02Å). Conversely, the separated phase of borosilicate glass with excess Cl^- is SiO_2, which is irrelevant to chloride phases. The excess addition of chloride has a function of destabilising the glass network and the stability of glass network is the controlling factor for chloride solubility in borosilicate glass. However, the destabilisation of glass network by Cl^- incorporation is not clearly understood and requires deeper investigation. On the other hand, it is commonly observed that the segregated layer formed on melt surface when SO_4^{2-}, Cl^- and MoO_4^{2-} ions in melts are apparently excessive is composed of sodium salts only (Na_2SO_4, NaCl or Na_2MoO_4). In this case, the SO_4^{2-}, Cl^- and MoO_4^{2-} additions have exceeded the capacity of glass network to incorporate them and excess anions are associated with Na^{+} ions outside of the melts. The formation of segregated layer and the crystallisation within glass matrix can occur simultaneously and these two stages of phase separation are independent of each other.

Similarly, phase separation in aluminosilicate glasses caused by excess additions of Cl and MoO_3 is very significant. The formation of barium aluminosilicate in BAS glass and magnesium aluminosilicate in MAS glass suggest that separation of glass network occurs prior to separation of chloride components. However, the lack of retention of Cl in MAS glass implies that the phase separation may not be triggered by Cl^- incorporation in glass network. MAS-5Cl and -10Cl glasses are compositionally close to MAS base glass and MAS glass with MoO_3 additions, thus this composition should be able to form glass. It is possible that the released Cl_2 gas destabilises glass network, making the glass readily crystallised. Phase separation of aluminosilicate glasses

caused by excess MoO_3 addition is similar to that of borosilicate glasses, but only alkaline earth molybdates are observed because there is no Na_2O content. When MoO_3 addition is supercritical (SBAS-3M glass), there exists a number of $Sr_xBa_{1-x}MoO_4$ aggregates inside glass.

In conclusion, each of SO_4^{2-}, Cl^- and MoO_4^{2-} species has its own features of glass phase separation if present in excess. Phase separation is much more characteristic of the specific anionic species than the glass composition.

7.2.9. Microstructure of separated phases

The microstructural features of separated phases forming during the cooling of melts with critical and excess SO_4^{2-}, Cl^- and MoO_4^{2-} levels were observed by SEM and TEM.

The morphologies of separated sulphate and molybdate phases in borosilicate glasses are similar. The separated particles within glass matrices are both spherical and randomly dispersed, which implies that they are formed through liquid-liquid phase separation during cooling and crystallisation thereafter. The size of these particles ranges between 50 to 1000 nm in diameter and is dependent on glass composition and the amount of SO_3 or MoO_3. For example, at the beginning of phase separation, molybdate particles in CBS glass are larger than those in SBS and BBS glasses; the particles in heavily crystallised SBBS3-3M glass are at least four times larger than those in slightly crystallised SBBS3-2.5M glass. The more MoO_3 is present in excess in the melt, the larger the separated particles observed within the final glasses. Meanwhile, separated phases in borosilicate glasses with excess chloride show diverse morphologies. The separated particles in MBS and CBS glasses are irregularly shaped, internally cracked, randomly trapped and are hundreds of microns in size. These features are distinct from the separated phases in the sulphate and molybdate glasses. The separated particles in SBS to BBS glasses are however rather small, showing a spherical shape which is akin to separated sulphate and molybdate particles. But the darker colour of particles in backscattered electron images of BBS-15Cl glass (Figure 5-19*b*) suggests that these particles have lower average atomic number than the glass matrix, which is opposite to the observations for separated particles in sulphate and molybdate loaded glasses. This can be explained by the relative light mass of SiO_2 (as identified by XRD patterns in Figure 5-7) compared with the barium borosilicate glass

network. $BaSO_4$ and $BaMoO_4$, the separated phases in BBS-5S and BBS-2.5M glass, respectively, have higher densities than BBS glass and as a result the separated particles are brighter in backscattered electron images.

The morphologies of the separated phases in aluminosilicate glasses with excess Cl and MoO_3 contents are distinct from each other. In BAS-15Cl and BAS-20Cl glasses, the separated particles are needle-like or plate-like, showing strong evidence of nucleation and growth regarding crystallisation process. Flower-shaped separated phases are observed in MAS-5Cl and MAS-10Cl glasses. As the compositional analysis indicates, these phases do not originate from excess Cl^- ions in glass and therefore they are likely formed because of reduced glass stability caused by chloride addition. Meanwhile, in the phase separated MoO_3-containing aluminosilicate glasses, the observed molybdates particles resemble those observed in borosilicate glasses except in SBAS-3M glass where some aggregated Sr/$BaMoO_4$ rods are found as well. The EDX results suggest that separated particles are more enriched in Mo and alkaline earths while less in Si and Al, in agreement with XRD/Raman results that they are alkaline earth molybdates. The similarity between the separated molybdates in borosilicate and aluminosilicate glasses is probably due to their similar formation mechanisms and the fact that they are all alkaline earth molybdates (Na_2MoO_4 and/or $Na_{2.4}Mg_{0.8}(MoO_4)_2$. They are mostly found in segregated layer or aggregates trapped in glass.

In conclusion, sulphate and molybdate phase separation occurs through liquid-liquid phase separation and subsequent crystallisation during cooling, whereas phase separation in glasses containing excess Cl occurs through crystal nucleation and growth. The separated sulphates and molybdates within glasses are both spherical and randomly dispersed. The size of these spheres ranges from 50 nm to 1 μm, both depending on alkaline earth species and loading levels but regardless of glass types (for MoO_3). The separated phases in Cl excessive glasses vary with both glass types and alkaline earth species. They are micron sized at least (except in BBS-15Cl glass) and are all non-chlorine components.

7.3. Conclusions

There are many similarities among the incorporation of SO_3, Cl and MoO_3 in glass. The initial addition of SO_3, Cl and MoO_3 results in notably reduced corrosions from mullite crucibles. As expected, these species are all present as anions in the glass network (SO_4^{2-}, Cl^- and MoO_4^{2-}, respectively). These anions do not act as network formers and are incorporated into the interstitial space in the glass network. A small amount of SO_4^{2-}, Cl^- and MoO_4^{2-} ions in glass leads to decreased T_g and increased glass density, while excess SO_4^{2-}, Cl^- and MoO_4^{2-} ions in glass leads to phase separation within glass matrices.

With respect to dissimilarities among the incorporation of SO_4^{2-}, Cl^- and MoO_4^{2-} in glass, SO_4^{2-} and MoO_4^{2-} incorporations are still similar to each other in many cases but distinct from Cl^- incorporation. The retention rate of SO_3 and MoO_3 contents are both extremely high in borosilicate glasses; however, SO_3 content is vulnerable to increasing melting temperature and thus aluminosilicate glasses only contain trace amount of SO_3. The retention rate of Cl in prepared glasses are relatively low and are strongly dependent on alkaline earth species in aluminosilicate glasses.

8. The solubilities of SO_3, Cl and MoO_3 in glass

8.1. Introduction

One of the major aims in this thesis is to seek the solubility dependence of the three components on glass compositions. In this chapter, three compositional parameters which represent different features of glass compositions will be investigated to determine whether they correlate or not with S, Cl and Mo solubilities in glass.

8.2. Compositional factors

Non-bridging oxygens (NBOs) in a glass network are key to a variety of glass properties including the capacity of incorporating the target anions. Traditionally the calculation of NBO fraction (f_{NBO}) is based on the assumptions that each mole of alkali oxide (*e.g.* Na_2O) and alkaline earth oxide (*e.g.* CaO) creates two moles NBOs and that one mole B_2O_3 or Al_2O_3 at low levels consumes one mole alkali or alkaline earth oxide to compensate the negative charge of BO_4^- or AlO_4^- units. Currently, most calculations of f_{NBO}, *e.g.* Li *et al.* (2001) and Jantzen *et al.* (2004), are based on the assumptions. However, these assumptions do not consider the difference among alkali or alkaline earth species and thus deviation from the calculation may occur when there are large cations, *e.g.* Ba^{2+}, present in glass network (Harding 1972, Zhao *et al.* 2000). Hence, the utilisation of other factors to represent glass composition is of interest, particularly for the present study where alkaline earth species are substituted equivalently.

In the following sections, cation field strength, cation electronegativity and cation surface area will be introduced to explore their contributions to solubilities of SO_3, Cl and MoO_3 in glass.

8.2.1. Cation field strength

Cation field strength (CFS) was proposed by Dietzel in 1948 and first applied to study sulphate solubility dependence in glass by Bingham and Hand (2008). It is defined as Z/a^2, where Z is the cationic charge divided by the square of the M-O bond length a in Å. The normalised CFS (NCFS) of glass is then defined as the sum of CFS in glass normalised to 1 mole cations:

$$\sum (Z/a^2) = \frac{\sum_i m_i x_i \mathrm{CFS}_i}{\sum_i m_i x_i} \qquad \text{Equation 8-1}$$

where m_i is the molar fraction of oxide i and x_i is the number of cations in oxide i. The values of each M-O bond length were obtained from Shannon and Prewitt (1969) and Shannon (1976). The coordination number and calculated CFS value of each cation

are assumed to be in accordance with Bingham and Hand (2008) and Ojovan *et al.* (2005); details are listed in Table 8-1. The field strengths of S^{6+} and Mo^{6+} are not calculated and not taken into account when calculating NCFS of glass as their incorporations are assumed not to significantly affect the capacity of glass to incorporate themselves.

Table 8-1 Calculated values of field strength, electronegativity and surface area of each cation in prepared glasses (CN = coordination number).

Element	Charge	CN	CFS	Electronegativity	Surface area (r^2/Å^2)
Si	4	4	1.57	1.94	0.068
B	3	4	1.34	1.77	0.012
Al	3	4	0.96	1.64	0.152
Na	1	6	0.19	1.11	1.040
Mg	2	6	0.45	1.32	0.518
Ca	2	6	0.33	1.24	1.254
Sr	2	8	0.28	1.16	1.588
Ba	2	8	0.25	1.11	2.016

Bingham and Hand (2008) reported a general trend of increasing SO_3 solubility with decreasing NCFS of glass. However, the trend is primarily based on phosphate glasses and in fact the investigated borosilicate glasses do not strictly follow the same fit. Given the significant difference between phosphate and borosilicate glass systems, it is desirable to approach an independent correlation of SO_3 solubility with borosilicate glasses only. It is also worthwhile to investigate the contribution of NCFS to Cl and MoO_3 solubilities in glass.

8.2.2. Cation electronegativity

Electronegativity is a parameter related to the charge and the ionic size of a cation. It was introduced by Duffy (1986) to characterise silicate melt composition and based on predicting the electronegativity behaviour of various cations in glass melt. In this study, we use the electronegativity value calculated according to Duffy (2010) using the following empirical formula:

$$X = 0.274Z - 0.15Zr - 0.01r + 1 \qquad \text{Equation 8-2}$$

where X, Z and r are electronegativity, valence and ionic radius of a cation, respectively. The calculated values for each cation in glass are listed in Table 8-1.

Hence, X_R, which means the ratio of X due to the modifiers to X arising from all cations in glass is used to characterise glass composition:

$$X_R = \frac{\sum m_i x_i X_i (\text{modifiers})}{\sum m_i x_i X_i} \qquad \text{Equation 8-3}$$

Although electronegativity is related to cationic valence, radius and field strength, it places greater emphasis on the valence. Therefore, it provides a possible method to investigate the contribution of cationic charge on the incorporation of SO_4^{2-}, Cl^- and MoO_4^{2-} ions in the glass network.

8.2.3. Cation surface area

Cation surface area (SA) provides a measure of the capability of a cation to be coordinated with anions. It is a geometrical factor that ignores the charge of cations and is simply dependent on cationic radius. The introduction of SA to characterise glass composition arises from the observation that Cl^- ions do not show preferential association with either Na^+ or Ca^{2+} in aluminosilicate glasses if they coexist (Sandland *et al.* 2004). Since the cationic sizes of Na^+ and Ca^{2+} are very close, it implies that the network modifiers with similar size have equivalent chance to bond with target anions even if the cationic charges are different. Therefore, it is possible that the capability of glass to accommodate target anions primarily rely on the surface area of modifiers in network.

In this study, S_R, the proportion of the sum of surface areas of network modifiers to sum of the surface areas of all the cations in glass network is calculated to evaluate its correlation with anionic solubility, as expressed in Equation 8-4.

$$S_R = \frac{\sum_i m_i x_i \mathrm{SA}_i (\text{Modifiers})}{\sum_i m_i x_i \mathrm{SA}_i} \qquad \text{Equation 8-4}$$

where m_i is the molar fraction of oxide *i* and x_i is the number of cation in oxide *i*.

The SA of each cation in glass is calculated in accordance with the assumptions when calculating CFS and the results are present in Table 8-1. Unlike the CFS and electronegativity, the SA of a cation is only related to the cationic radius and assesses the packing ability of cations.

8.2.4. Summary

Cation field strength, electronegativity and surface area are utilised in this study to investigate their relations to the solubilities of SO_3, Cl and MoO_3 in glass. These three compositional parameters are relevant to cationic charge and size, however, differing from each other in the contributions of each aspect. The dependence of SO_3, Cl and MoO_3 solubilities on these parameters is established in the following section using both the data obtained here and relevant data from literature.

8.3. Empirical modelling

The calculations of NCFS, X_R and S_M of glasses are based on measured compositions excluding the amounts of SO_3, Cl and MoO_3. In agreement with the previous chapters, SO_3 and MoO_3 solubilities in glass are expressed as mol% whereas Cl solubility is expressed as at%. In the comparison with literature data, only those having comparable experimental conditions and measured solubilities are chosen. The solubility data from loaded values are separately indicated in the modelling results.

8.3.1. SO_3 solubility

As mentioned in Chapter 4, SO_3 content in glass is vulnerable to melting temperature and thus the loss of SO_3 is significantly increased in glasses prepared at temperatures higher than 1200 ºC. Therefore, in this chapter, only the literature data from glasses prepared at ≤1200 ºC are considered as comparable during the empirical modelling.

8.3.1.1. NCFS

The correlation of SO_3 solubility with NCFS of glasses prepared in this study is shown in Figure 8-1. Similar to the results of Bingham and Hand (2008) (mainly based on phosphate glasses but with some data from borosilicate glasses), SO_3 solubility shows an exponential increase ($R^2 = 0.918$) with decreasing NCFS value of glasses. However, this increasing trend does not agree well with overall literature data although a roughly monotonic increase of SO_3 solubility in them has also been obtained in Figure 8-2. In the literature data, the increasing trend is relatively smooth within a wide NCFS range whereas, in this study, a limited NCFS decrease results in a significant improvement of SO_3 solubility. This means that the NCFS change by replacement of alkaline earth species may play a much more important role than the NCFS change realised by other compositional variations in determining SO_3 solubility in glass. Therefore, NCFS is not an ideal measure for the universal prediction of SO_3 solubility in silicate glasses.

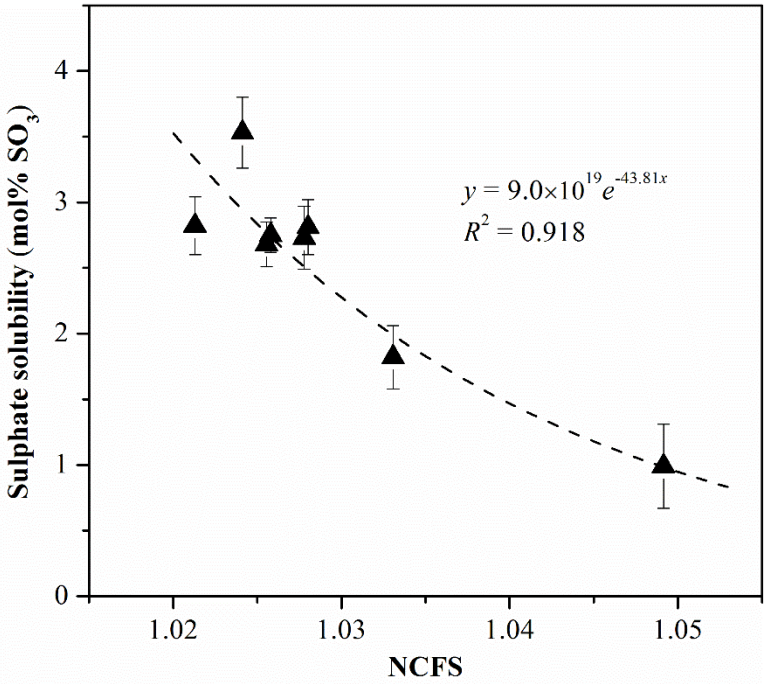

Figure 8-1 Sulphate solubility (mol%SO_3) versus NCFS values of different glasses.

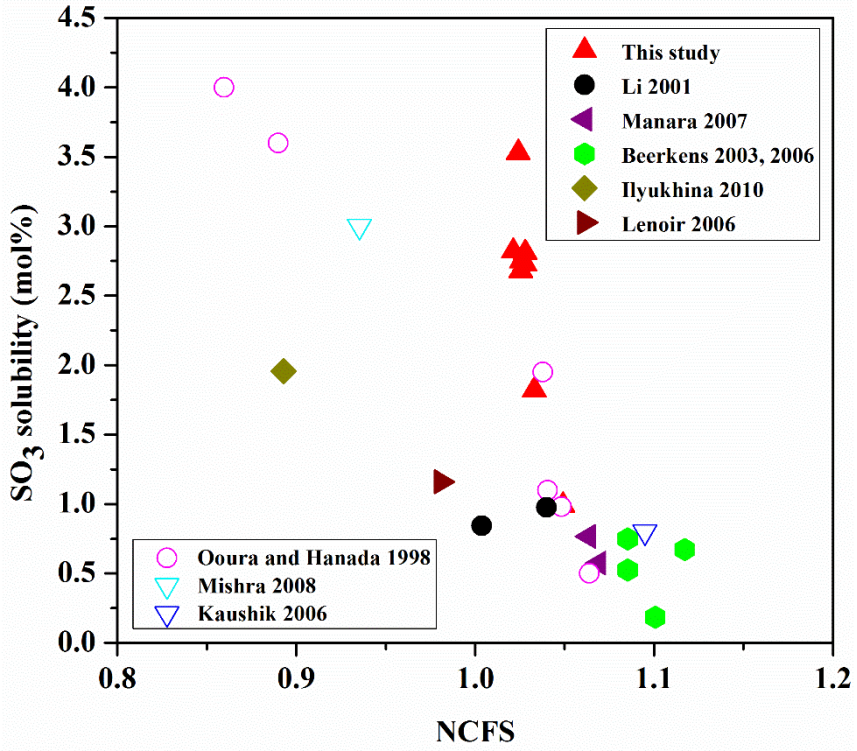

Figure 8-2 SO_3 solubility versus NCFS of glass, combined with literature data (Ooura and Hanada 1998, Li *et al.* 2001, Beerkens 2003, Kaushik *et al.* 2006, Manara *et al.* 2007, Mishra *et al.* 2008, Lenoir *et al.* 2009, Ilyukhina *et al.* 2010). Solid symbols referred to measured SO_3 contents and hollow symbols referred to batched amounts.

However, the deviation between the functions of NCFS changes caused by alkaline earth replacement and overall composition change does not affect the increasing trends of SO_3 solubility with decreasing NCFS values in individual glass series. Hence, if other glass components are held constant, it is still the case that an abundance of network modifying cations with lower field strength results in higher SO_3 solubility.

8.3.1.2. X_R

By fitting literature data, a general trend of increasing SO_3 solubility with increasing X_R can be obtained, as plotted as circles in Figure 8-3. According to the definition of electronegativity of a cation, X_R places emphasis more on the cationic charge than cationic size and glasses with a higher content of larger network modifiers are supposed to have higher X_R values.

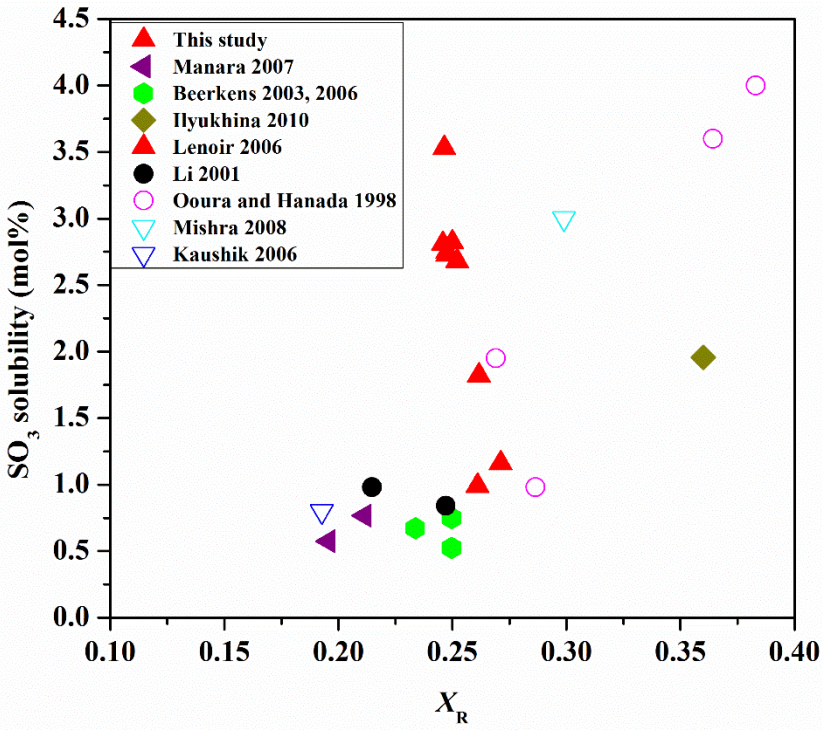

Figure 8-3 SO_3 solubility versus X_R, combined with literature data (Oura and Hanada 1998, Li *et al.* 2001, Beerkens 2003, Kaushik *et al.* 2006, Manara *et al.* 2007, Mishra *et al.* 2008, Lenoir *et al.* 2009, Ilyukhina *et al.* 2010). Solid symbols referred to measured SO_3 contents and hollow symbols referred to batched amounts.

However, the data from the current experiments gives rise to a different behaviour

such that within a very limited X_R range, SO_3 solubility varies significantly (red triangles in Figure 8-3). The contradiction in results between literature and this study suggest that X_R cannot be used to characterise the capacity of the glass network to incorporate SO_4^{2-} at all.

8.3.1.3. S_R

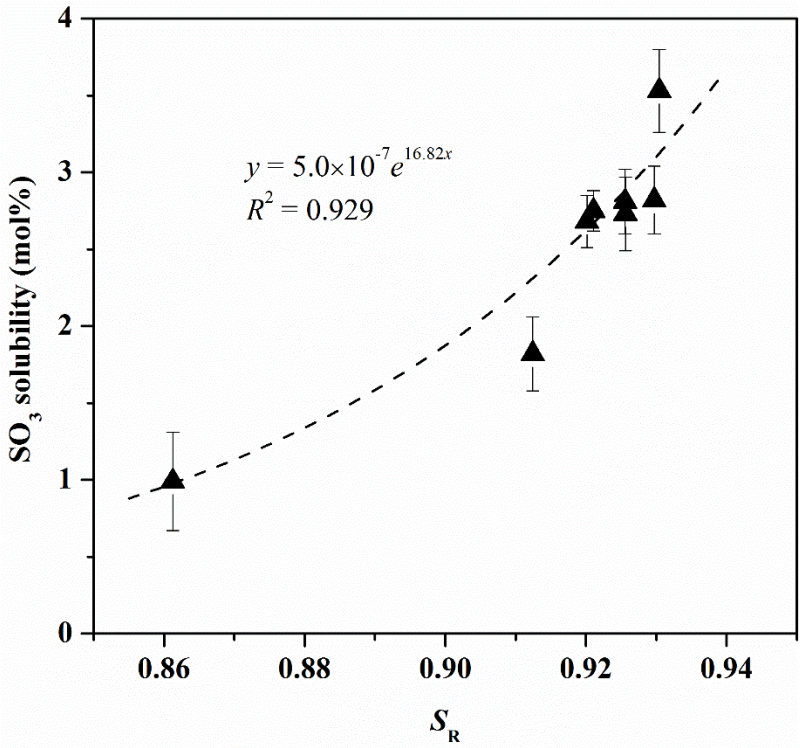

Figure 8-4 SO_3 solubility (mol%) versus S_R of glasses prepared in this study.

As plotted in Figure 8-4, SO_3 solubility shows an exponential increase with increasing S_R of glasses prepared in this study (R^2 = 0.929). This result agrees with the hypothesis that larger network modifying cations and higher content of modifiers help to improve sulphate capacity. Moreover, this trend is consistent with literature data where a rough exponential dependence can also be fitted (combined in Figure 8-5). The overall fitting has R^2 = 0.925 (excluding Li *et al.* (2001) which are out of range) and the S_R ranges are similar between the glasses in this study and in literature, indicating that the use of S_R of glass to model and predict SO_3 solubility in borosilicate glass is promising.

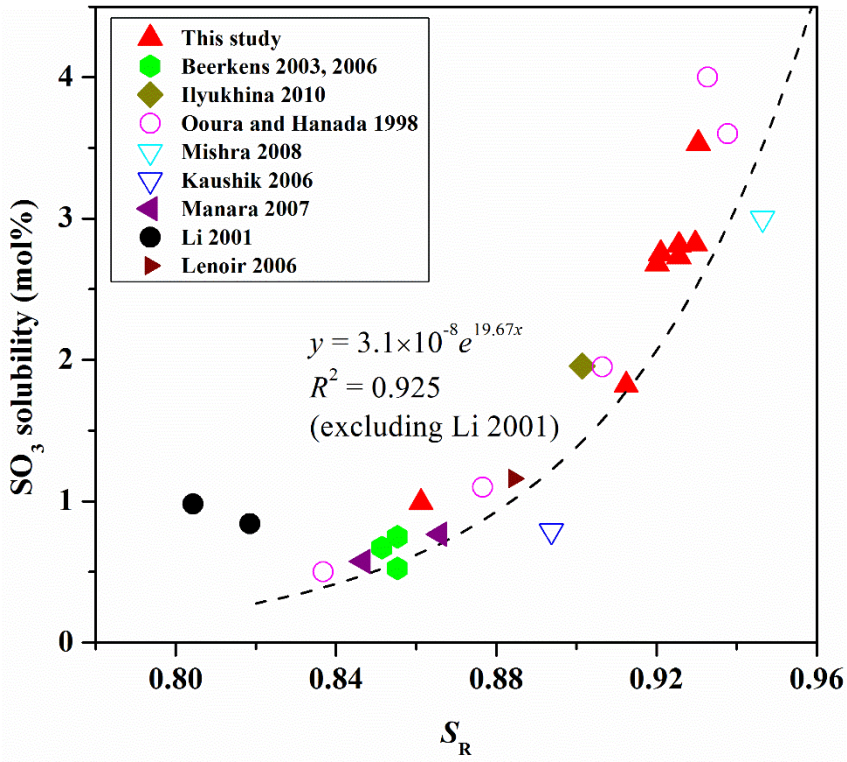

Figure 8-5 SO_3 solubility versus S_R, combined with literature data as in Figure 8-2. Solid symbols referred to measured SO_3 content and hollow symbols referred to the batched.

8.3.1.4. Summary

Among all the three proposed compositional parameters for sulphate solubility, S_R shows the best ability to express SO_3 solubility dependence on glass compositions based on combined results, achieving an overall empirical formula with R^2 = 0.925. This result suggests that S_R may be used for the universal prediction of SO_3 solubility in glass when the melting temperature is below 1200 ºC. Since S_R is a parameter that only relates to the size of cations, it implies that the packing ability of cations in the glass network may be a critical feature in determining SO_3 solubility, given the amount of network modifiers are the same.

8.3.2. Cl solubility

As indicated in Chapter 5, the evaporation of chloride from glass melt during melting is more dependent on glass composition than melting temperature and as a result the Cl solubilities in the glasses prepared at a wider range of temperatures (1100-1500 ºC) are considered as comparable. In addition, the glasses analysed in Webster and De Vivo (2002) and Siwadamrongpong *et al.* (2004) were prepared under reducing or inert atmospheres, which is believed to result in slightly higher Cl^- dissolution in glass. Glasses containing combinations of halogens (Cl^-, F^- and I^-) are excluded from data collection. For consistency, glass compositions from literature have been all converted from mole or weight percentage to atomic percentage as used in this study.

8.3.2.1. NCFS

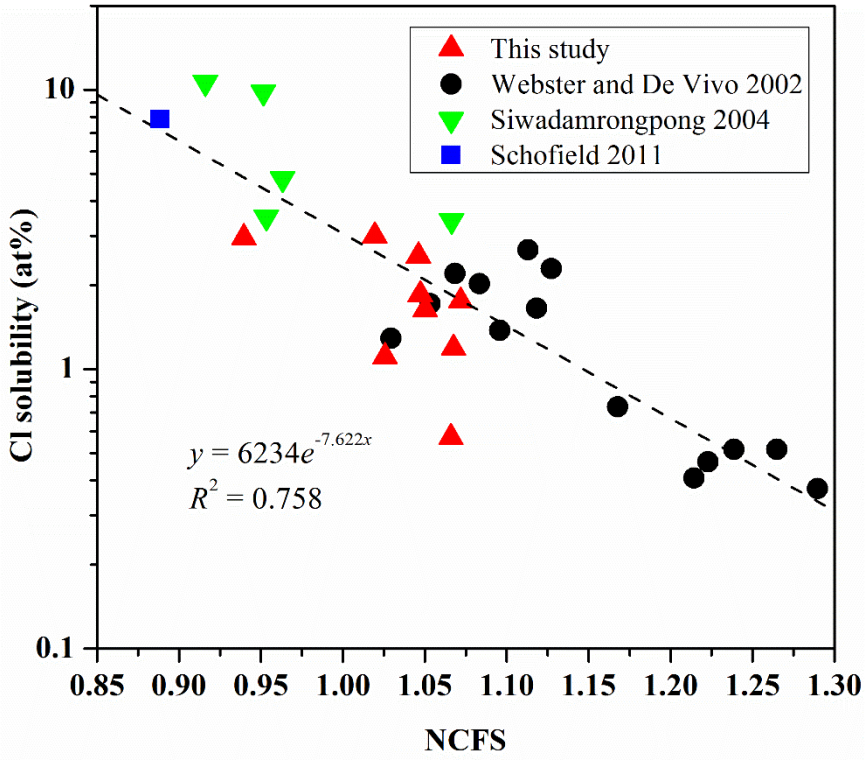

Figure 8-6 Cl solubility versus NCFS of glasses prepared in this study and from Webster and De Vivo (2002), Siwadamrongpong *et al.* (2004) and Schofield (2011).

It has been shown in Figure 8-6 that Cl solubility exhibits a decreasing exponential trend with increasing NCFS values of glasses, with a R^2 of 0.76 for the overall dataset. Unlike SO_3 solubility which shows different dependences for the exponential fitting,

Cl solubility dependence on NCFS shows good agreement between the literature data and this study. It suggests that, although the overall coefficient of determination is not that high, NCFS value of glass indeed provides a possible way to predict Cl solubility within a wide compositional range.

8.3.2.2. X_R

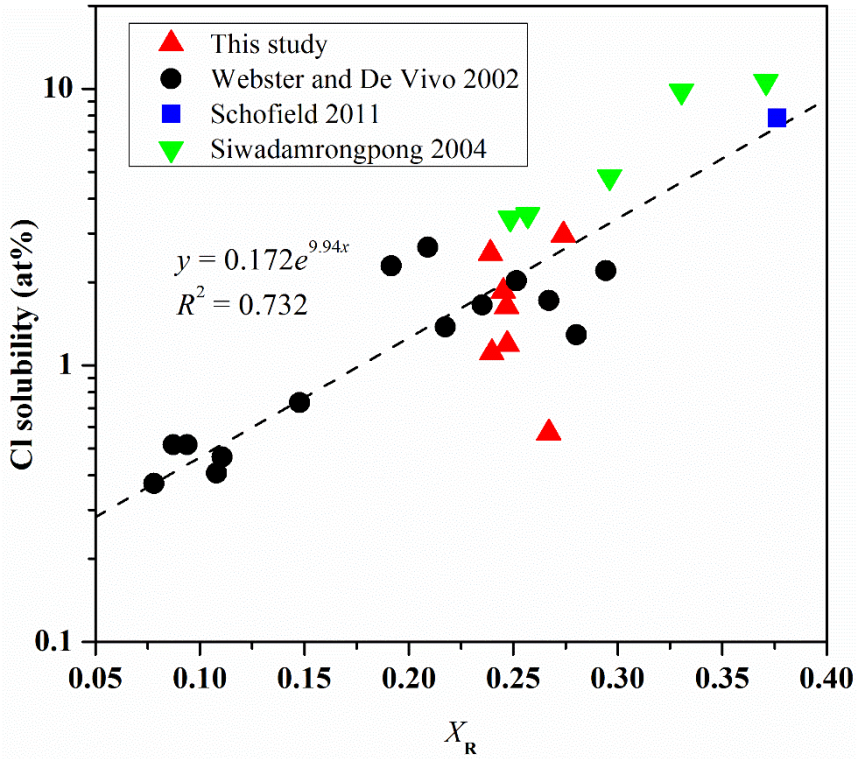

Figure 8-7 Cl solubility versus X_R of glasses prepared in this study and from Webster and De Vivo (2002), Siwadamrongpong *et al.* (2004) and Schofield (2011)

The plots in Figure 8-7 suggest that there is a general correlation between increasing Cl solubility and increasing X_R of glass, in which the glass compositions of high Cl solubility are all of high X_R values. Although the Cl solubilities obtained in this study do not show any strong dependence on X_R, they are all located close to the fitted line except for MBS glass which exhibits severe phase separation. The deviation of MBS glass also occurs when fitting with NCFS (Figure 8-6) and it is likely that the structure of MBS glass may differ significantly from other investigated glasses. Generally speaking, the X_R values to a large extent may determine Cl solubility in glass, with a slightly lower correlation coefficient compared to NCFS values of glass, while for

specific glasses its indication becomes much less reliable. Therefore, like NCFS, X_R is able to indicate Cl solubility trend of general glass compositions, but is not applicable to compare the changes caused by controlled compositional variations.

8.3.2.3. S_R

There seems to be a general correlation between Cl solubility and S_R of glasses, similar to the fittings with NCFS and X_R, showing the best function to be increasing exponential with R^2 of 0.690. The relative low R^2 value here compared to NCFS and X_R suggests that the reliance on S_R is less strong and thus S_R is less applicable for indication of Cl solubility. Nevertheless, the results of borosilicate glasses prepared in this study (red and up triangles in Figure 8-8) indicate that, within these glasses, the increasing exponential function works very well, with R^2 of 0.987. The data for aluminosilicate glasses in this study are insufficient to conclude anything, but the two points similarly follow the trend to borosilicate glass series.

The divergence between the results in literature studies and present study suggests that, although S_R, a measure of the cationic size of network modifiers, is able to provide a general prediction of Cl solubility in glass, it confronts difficulties in combining those glasses with largely various compositions together. Its contribution appears vulnerable by the detailed glass compositions. Thus, S_R only applies to those glasses with certain molar compositions and varying cation species: larger ones are favourable.

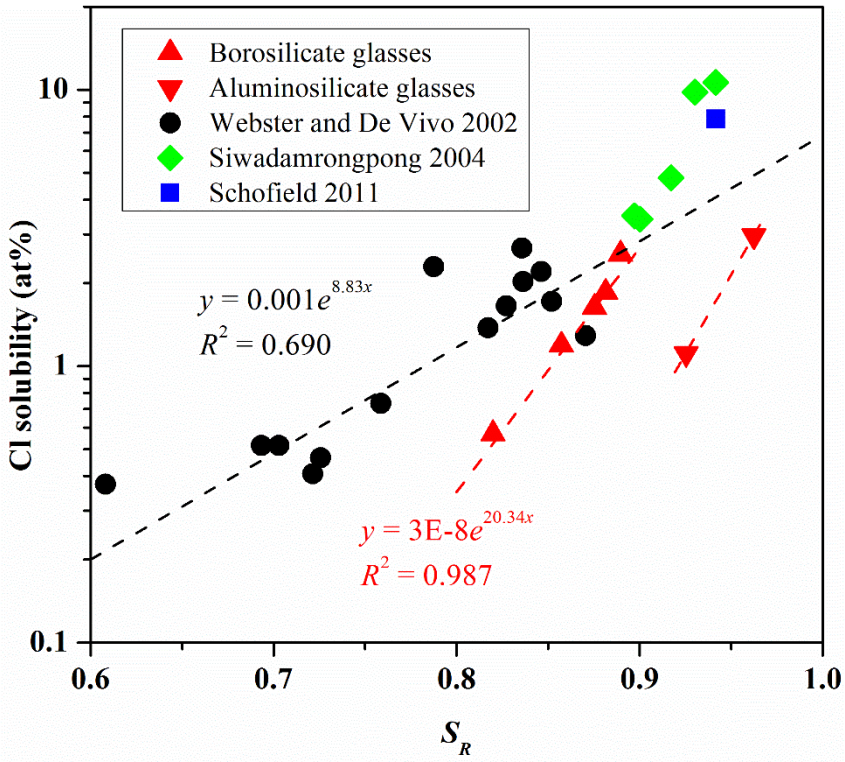

Figure 8-8 Cl solubility versus S_R of glasses prepared in this study and from Webster and De Vivo (2002), Siwadamrongpong *et al.* (2004) and Schofield (2011).

8.3.2.4. Summary

All the three compositional parameters exhibit a general exponential indication to Cl solubility in glass. NCFS shows the highest correlation and applies to both individual and combined data from literature and present study, and thus it is recommended for the prediction of Cl solubility. The correlations of X_R and S_R are relatively low, and especially for S_R the dependence on different glass composition series are apparently deviated. Therefore, according to the definition of NCFS, it suggests that the charge and size of network modifiers are both the key to determination of Cl solubility in glass.

8.3.3. Molybdenum

The results in Chapter 6 indicate that there is little MoO_3 loss during the melting of borosilicate glasses at 1100 ºC and aluminosilicate glasses at 1450 ºC, thus the melting temperature here is considered not to significantly influence MoO_3 solubility. Besides, since the references regarding MoO_3 solubility in glass without crystallisation are very limited, empirical modelling of MoO_3 solubility dependence is in fact mainly based on the data from this study. Although molybdate components themselves can be glass-forming (*e.g.* with Ag_2O and/or SeO_2 (Dimitriev and Iordanova 2009, Deb and Ghosh 2014)), the molybdate-based glass systems are not included in the comparison as these are very different glasses from a structural perspective.

8.3.3.1. NCFS

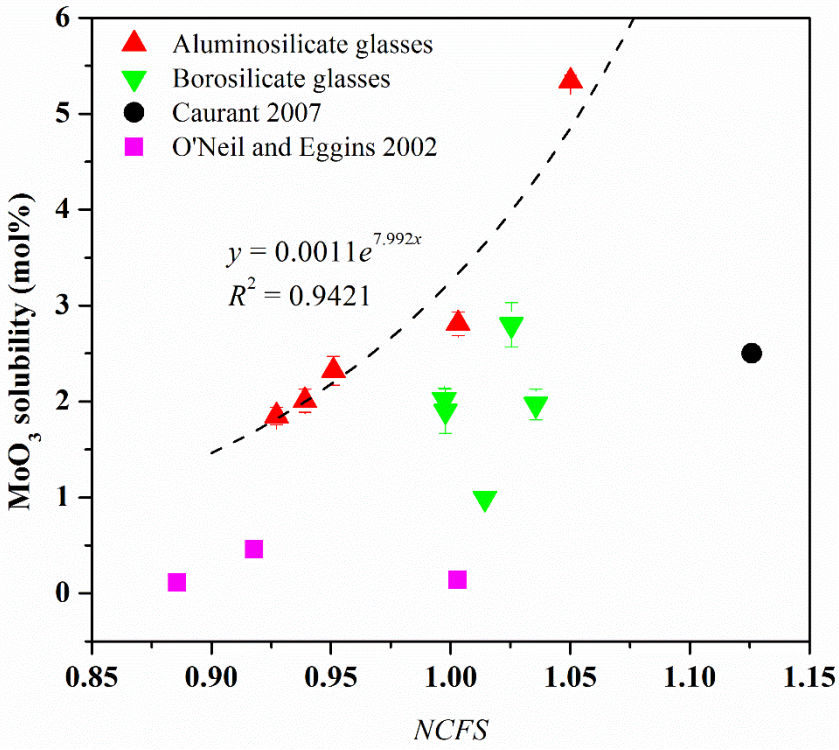

Figure 8-9 MoO_3 solubility versus NCFS of glasses prepared in this study and from O'Neill and Eggins (2002) and Caurant *et al.* (2007).

The MoO_3 solubility dependence on NCFS of glasses is distinctive from SO_3 and Cl solubilities. As plotted in Figure 8-9, there is no indicative dependence showing the correlation between MoO_3 solubility and NCFS value of glasses when the data from

borosilicate and aluminosilicate glasses in the present work are combined together. For individual glass series, MoO_3 solubility in aluminosilicate glasses seems to obey an increasing exponential tendency with increasing NCFS, which is opposite in sign to the tendencies for SO_3 and Cl solubilities, while MoO_3 solubility in borosilicate glasses is completely random, showing no dependence at all. In combination the data from the current work and the literature does not show any predictable dependence of MoO_3 solubility on NCFS. This suggests that NCFS is not a quality parameter to be used to predict MoO_3 solubility in glass.

8.3.3.2. X_R

Figure 8-10 indicates that a clear dependence of MoO_3 solubility on X_R of individual glass series cannot be achieved; however, by combining all the data together, a general linear trend of increasing MoO_3 solubility with decreasing X_R is observed, with the exception of the extraordinary high solubility in MAS glass prepared in the present study. The resultant increased MoO_3 solubility by decreasing X_R goes against the assumption that the addition of network modifiers facilitates MoO_4^{2-} dissolution as network formers are usually of higher electronegativity than network modifiers. It then may imply that, as discussed in Section 2.3, MoO_3 solubility is controlled not only by the incorporation capacity of glass network but also by the stability of silicate-molybdate melts during cooling. It is possible that the nature of network modifiers associated with MoO_4^{2-}, rather than the nature of network modifiers functioning to depolymerise the glass network, determines MoO_3 solubility in glass. In this case, MoO_3 solubility will be restricted by the molybdate phase that crystallises most readily and hence the modifier species will be the major determinant. This is partly verified by the fact in this study that CAS and CMAS (mixed Ca and Mg) have a very similar MoO_3 loading limit, which is much lower than that of MAS glass. The association of MoO_4^{2-} with Ca^{2+} determines MoO_3 solubility in CAS and CMAS glasses.

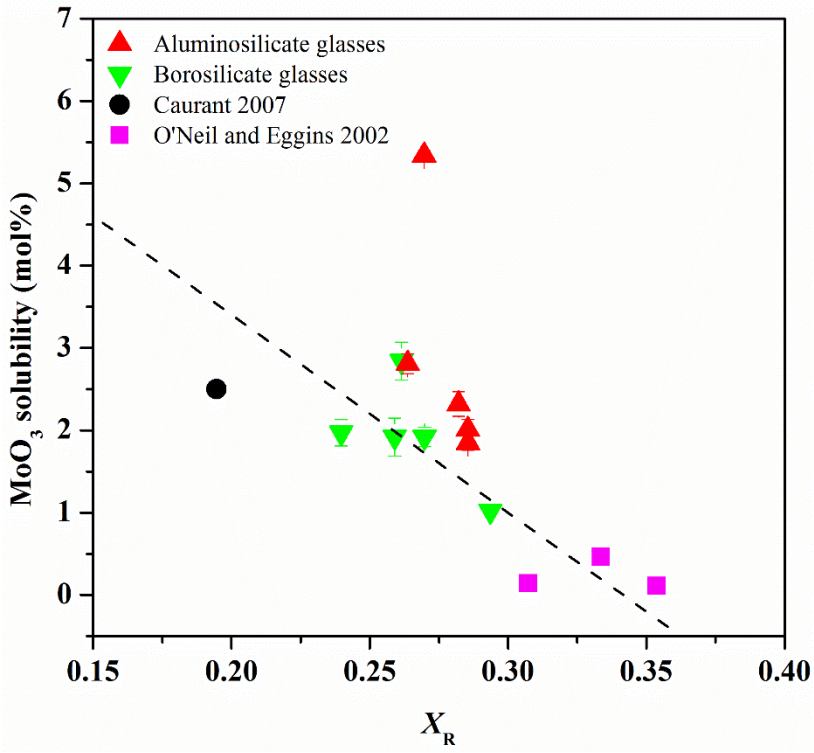

Figure 8-10 MoO_3 solubility versus X_R of glasses prepared in this study and from O'Neill and Eggins (2002) and Caurant *et al.* (2007).

8.3.3.3. S_R

The dependence of MoO_3 solubility on S_R of glass is not consistent at all, as can be seen in Figure 8-11. This is very different from SO_3 and Cl solubilities in glass, suggesting that the contribution of glass composition to MoO_3 dissolution may differ from them. Nevertheless, it is interesting that the dependence on S_R of aluminosilicate glasses prepared in this study is apparent and consistent. Considering their relatively simple compositions, this result may suggest that S_R is indeed able to reflect MoO_3 solubility of given glass compositions but its applicability will disappear as the compositions become complicated. Therefore, it is not possible to use S_R for prediction of MoO_3 solubility in a wider range of glasses.

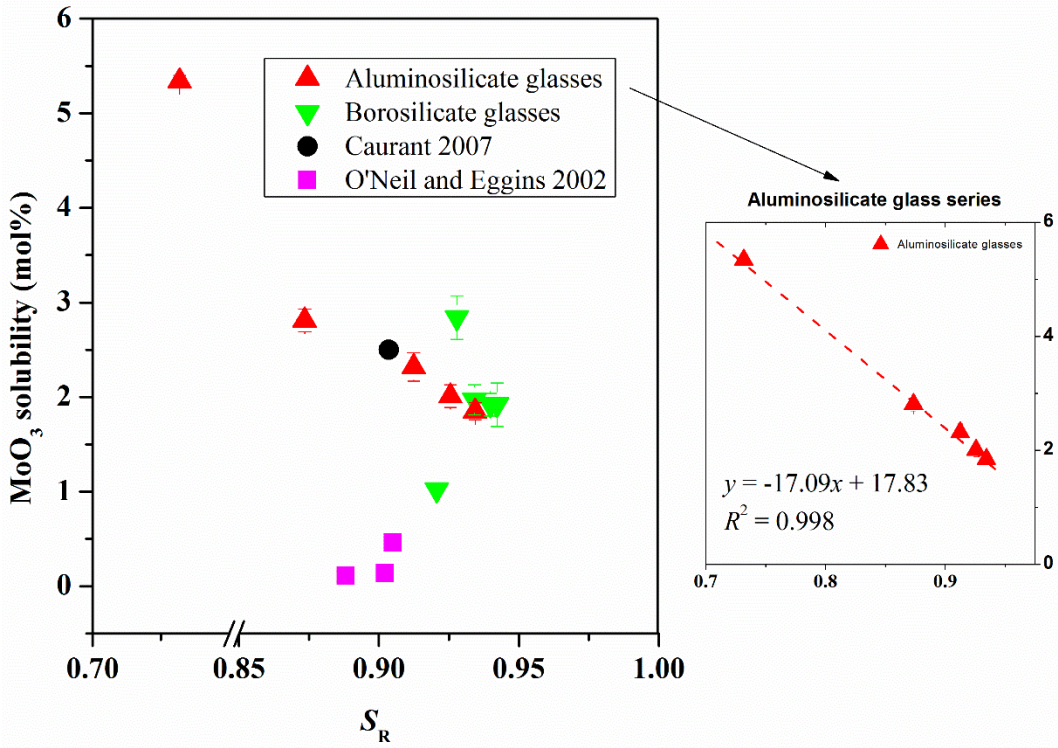

Figure 8-11 MoO_3 solubility versus S_R of glasses prepared in this study and from O'Neill and Eggins (2002) and Caurant *et al.* (2007).

8.3.3.4. Summary

The above fittings suggest that only X_R is able to establish a reliable formula to predict MoO_3 solubility in glass (although even then not all data fitted the line), while the other two parameters do not work at all. It is interesting that the MoO_3 solubility dependence on S_R of aluminosilicate glasses studied here demonstrates complete consistency, although the dependence on overall glass compositions is rather random. It would therefore seem that the size of network modifiers is readily overcome by other compositional variations. In conclusion, the electronegativity of network modifiers is likely to be the most important factor to influence MoO_3 solubility in glass.

8.4. Conclusions

In this chapter, NCFS, X_R and S_R have been assessed to evaluate their correlations with the solubilities of S, Cl and Mo in glass, respectively. The empirical modelling results suggest that, although these elements are all present as anions in the glasses of interest, their solubility dependences vary largely from each other:

- SO_3 solubility shows the highest (increasing exponential) dependence on S_R of glass, which indicates that the size of network modifiers may dominate the determination of SO_3 solubility in glass.
- Cl solubility shows increasing exponential dependence on all the parameters, with NCFS having the highest correlation. It indicates that the field strength of network modifiers contributes most to the determination of Cl solubility in glass.
- MoO_3 solubility only shows a generally decreasing linear dependence on X_R of glass while the other two parameters are not applicable at all. This suggests that the electronegativity of network modifiers can mostly reflect the ability of glass network to dissolve MoO_4^{2-}.

All of these conclusions are drawn from empirical modelling. Although these dependences are indeed able to correlate the solubilities well with compositional features, the rationales behind these correlations are still not clear and require further investigation.

9. Conclusions and recommendations for future work

9.1. The solubility of anionic species in glass

This study evaluates the incorporation behaviour and solubility dependence of three anionic species (SO_4^{2-}, Cl^- and MoO_4^{2-}) in both borosilicate and aluminosilicate glass compositions. Glasses with varying alkaline earth species were loaded with different levels of anionic species to obtain the loading limits and solubilities of each species in different glasses thereby exploring their solubility dependence on glass composition. Three composition parameters NCFS, X_R and S_R, which are relevant to cationic charge and size, however, differing from each other in the contributions of each aspect, were used to express the compositional solubility dependence. In combination with literature data, several empirical models have shown potential to universally predict the solubility of such anions in silicate glass systems. These models may therefore provide helpful approaches to designing new nuclear waste glass compositions with enhanced anionic solubilities. However, the different dependences found among anionic species also suggest that the factors that influence anionic solubilities in glass vary from each other and thus developing a composition that suits to immobilise all of them is difficult.

Moreover, the solubility results of glasses investigated in this work are encouraging. Magnesium aluminosilicate (MAS) glass shows a 5.34 mol%MoO_3 solubility, which is much higher than that in previously studied glasses. The highest sulphate solubility is 3.53 mol%SO_3 found in barium borosilicate (BBS) glass. Although this value is not the highest among literature, it does reveal the ability of BBS glass to incorporate a high level of SO_4^{2-}. In addition, the highest chloride retention (~80%) and solubility (2.96 at%Cl) are observed in barium aluminosilicate (BAS) glass. Particularly and interestingly, this retention rate in BAS glass is much higher than that in those borosilicate glasses which were processed at a much lower temperature.

The detailed retention and solubility behaviours of each species are summarised in the following sections.

9.1.1. Sulphate

Among the three anionic species sulphate shows the highest retention dependence on melting temperature. All borosilicate glasses processed at 1100 ºC reveal the ability to retain higher than 90% sulphate from the batches whereas all aluminosilicate glasses processed at 1450 ºC do not retain sulphate at all. In addition, a glass composition (SBBS4-3S) processed at different temperatures suggests that sulphate retention begins to considerably decrease after melting temperature exceeds 1200 ºC. Therefore, any composition that requires a melting temperature higher than 1200 ºC is believed not suitable as the vitreous host to immobilise sulphate bearing waste.

Based on the results of sulphate dissolution in borosilicate glass series, the equimolar substitution of larger to smaller alkaline earths (*e.g.* Ba to Ca) results in monotonically increased sulphate solubility, with the highest solubility of 3.53 mol%SO_3 found in BBS glass and the lowest of <0.99 mol%SO_3 in magnesium borosilicate (MBS) glass. Regarding the compositional dependence of sulphate solubility, both NCFS (a measure of cation field strength in glass) and S_R (a measure of cationic size in glass) demonstrate strong correlations within the data in this study; however, when combined with data from literature, only S_R remains applicable. An exponential formula for S_R was finally established with $R^2 = 0.925$:

$$Sol(mol\%SO_3) = 3.1\times10^{-8}e^{19.67S_R} \qquad \text{Equation 9-1}$$

Since S_R is a parameter that only relates to the size of cations, it may suggest that the packing ability of cations in the glass network may be a critical feature in determining SO_3 solubility, given the amount of network modifiers are the same. Therefore, glasses containing larger network modifiers are expected to have higher capacity for sulphate incorporation.

In addition, one critically loaded melt (SBBS4-4S) was cooled through annealing and splat quenching, respectively. The annealed sample is opaque whereas the quenched sample remains transparent. XRD results suggest the quenched sample is completely amorphous, indicating that sulphate solubility of a glass melt can be increased by rapid cooling which disallows the occurrence of crystallisation within glass melt. However, with this method the sulphate capacity of glass does not increase and no bulk glass is

obtained.

9.1.2. Chloride

Chloride is the most volatile among the three anion species in borosilicate glass series, showing a retention rate range of 50-67% with initial additions (<1.28 at%Cl). Yet it is still much higher than the average value 33% of borosilicate nuclear waste glasses prepared at laboratory scale. Chloride retention in aluminosilicate glasses seems to be sensitive to glass composition. BAS is the most capable of incorporating and retaining chloride among all the compositions studied, remaining homogeneous until 2.96 at%Cl incorporation with an 80% retention rate, while MAS glass does not retain Cl at all even though phase separation occurred because of chloride addition. At the same time, calcium aluminosilicate (CAS) glass shows a lower retention rate than BAS glass but with a higher loading limit. The cations with which Cl^- ions are associated in melt determine the Cl^- retention in glass.

Despite the many uncertainties in determining chloride solubility, larger alkaline earths are observed to contribute higher chloride solubilities than smaller ones in both glass series. For example, BBS glass has the highest Cl solubility of 2.54 at% while MBS has the lowest Cl solubility of 0.57 at%. This enhancement applies to the glasses with two combined alkaline earths. Partial replacement of SrO by BaO results in higher Cl solubility in SBBS4 glass than in SBS glass: the loading limit does not increase, but the higher Cl retention leads to higher Cl solubility.

Among the compositional parameters NCFS demonstrates the best ability to combine the data from this study with literature in a wide range of glass compositions together. The best fitting of solubility dependence is established as an exponential formula with R^2 of 0.758:

$$Sol(at\%Cl) = 6.23\times10^{3} e^{-7.62\,NCFS} \qquad \text{Equation 9-2}$$

Since NCFS is a measure of cation field strength, the result indicates that the field strength of network modifiers contributes most to the determination of Cl solubility in glass, given other components remain constant. Therefore, glasses containing cations with lower field strengths are beneficial to achieve a higher chloride solubility.

It is worth noting here that, unlike in sulphate- and molybdate-containing glasses, the separated phases that initially occurred in chloride-containing glasses are non-chlorine components. Therefore, the factor that controls chlorine solubility in glass is not the capacity of glass network to accommodate Cl^-, but the ability to form a homogeneous glass with the presence of Cl^-. Particularly, MAS-5Cl and MAS-10Cl glasses are phase separated in spite of no chlorine being retained. Given the MAS base glass and with MoO_3 additions are homogeneous, it is likely the presence of chlorine in melts triggers the phase separation. However, the mechanism of how it takes place is still unknown.

9.1.3. Molybdate

Molybdate shows the best retention among the three anionic species in glass regardless of glass types. Essentially all molybdate have been retained in the prepared glasses except MAS-7M and -8M glasses which have close molybdate contents. It is probably that the incorporation of MoO_4^{2-} has been saturated in these two glasses and the excess molybdate cannot enter the glass anymore, which results in a decreased retention rate. The evaporation of molybdate can be of secondary consideration when designing glass compositions for molybdate immobilisation.

The features between molybdate solubility in borosilicate and aluminosilicate glasses are different. For aluminosilicate glasses, molybdate solubility steadily increases from BAS to MAS glass, reaching the highest 5.34 mol%MoO_3. When two alkaline earths are combined in glass, the solubility follows the lower one, which is different from when chloride is added. As the phase separation in overloaded glasses all occurs as crystalline molybdates, it suggests that molybdate solubility of glass is determined by the cations which separate most readily from glass network. The favoured contribution of smaller alkaline earths to molybdate solubility remains true from Ba to Ca in borosilicate glasses; MBS glass, however, has a very poor molybdate solubility. Such a poor solubility probably arises from the ready formation of $Na_{2.4}Mg_{0.8}(MoO_4)_2$ from the melt according to XRD results.

Excluding those Mg-containing glasses, molybdate solubility actually monotonically increases with larger to smaller alkaline earths in glass. This differs from sulphate and chloride solubility dependence in which larger alkaline earths are favourable. This also suggests that the factors determining their solubilities in glass may be adversely

different from each other. It is therefore difficult to develop glass compositions with decent ability to immobilise all of them; glass compositions for nuclear waste immobilisation have to cater for specific waste compositions.

All the three compositional parameters demonstrate strong correlation with molybdate solubility in aluminosilicate glasses; however, when combined with the solubilities in borosilicate glasses or further in literature, the dependence becomes less reliable. The best overall fitting is achieved with X_R with a decreasing linear dependence; however, the highest value in MAS glass apparently deviates from the line. This suggests that, even if X_R can be used as a measure of prediction for molybdate solubility, it can be overridden by other compositional factors. And because the literature data regarding molybdate solubility in glass are quite limited, it is necessary to investigate more compositions prior to establishing a universal model for the prediction of molybdate solubility in glass.

9.2. The effects of anionic incorporation on glass structure and properties.

The incorporation of SO_4^{2-}, Cl^- and MoO_4^{2-} results in significant changes in glass network. Having similarities and differences among themselves, these three anions therefore have diverse and distinct effects on glass structure and properties.

9.2.1. Sulphate

A small amount of sulphate addition leads to reduced corrosions from mullite crucibles compared with base glasses while further addition does not change the corrosion very much. Sulphate is present as SO_4^{2-} in prepared glasses, as expected, proven by Raman spectra. The increasing amount of SO_4^{2-} dissolved in glass is also reflected by Raman spectra, in which the contribution of bands assigned to SO_4^{2-} vibrations increases with sulphate addition, in agreement with the EDX analysis. The deconvolution results of Raman bands assigned to silicate vibrations indicate that SO_4^{2-} incorporation initially polymerises while subsequently depolymerises glass network. The linear shift in the centre of SO_4^{2-} υ_1 band with gradual substitution of SrO to BaO indicates that SO_4^{2-} ion are more likely associated with or related to alkaline earth cations in the glass network. FTIR spectra do not show significant changes with SO_4^{2-} incorporation. Moreover, SO_4^{2-} incorporation does not affect the thermal stability of glass, but is conducive to decreasing the T_g of the glass. Glass densities are increased by sulphate incorporation, best fitted with a quadratic manner.

Some glasses loaded with critical amount of sulphate are able to keep homogeneous as melts, but these melts will become phase separated and opaque after cooling to form inhomogeneous products. Crystallisation occurs within glass matrices during cooling to form a large number of randomly dispersed submicron separated spheres which are identified to be crystalline (alkaline earth) sulphates. Further addition of sulphate in excess results in a segregated layer forming on the melt surface, which is identified to be crystalline Na_2SO_4. It suggests that the undissolved sulphate in the melt remains as Na_2SO_4 while alkaline earth sulphates are more readily expelled from glass during cooling.

9.2.2. Chloride

Similar to sulphate addition, initial chloride addition also results in reduced corrosions from mullite crucibles compared with base glasses. But further addition may increase or further decrease the corrosion depending on glass compositions. The presence of Cl in glass is revealed by EDX analysis while neither Raman nor FTIR shows evidence of Cl^- in glass network. However, the deconvolution results of Raman bands assigned to silicate vibrations reveal changes in the extent of glass polymerisation. The average n in Q_n firstly decreases and then increases with increasing chlorine content, suggesting a depolymerisation process followed by polymerisation until phase separation. Distinct from the other anions, Cl^- incorporation exhibits a maximal density in all compositions. The initial density increase may arise from Cl^- entering the voids of network while the subsequent decrease is probably due to the relatively large volume and low weight of Cl^-. The T_g tendencies with increasing chlorine additions are similar between borosilicate and aluminosilicate glasses; both show an initial drop and little change afterwards until phase separation.

The phase separation occurring in Cl-containing glasses are very different from that in SO_3- and MoO_3-containing glasses. XRD results indicate the separated phases are non-Cl containing components: the separated phase in borosilicate glasses is mainly SiO_2 (quartz and/or cristobalite) while the separated phase in aluminosilicate glasses is crystalline alkaline earth aluminosilicates. Only if the Cl addition is apparently excessive can a layer of NaCl form on the surface of borosilicate melt like excess sulphate does. The separated SiO_2 are mostly in large size (hundreds of microns in diameter) and are probably from the undissolved batches). The crystalline aluminosilicates show a flower-, needle- or plate-like shape, indicating that these crystals are formed within glass matrices through nucleation and growth, rather than liquid-liquid separation and crystallisation as in SO_3- and MoO_3-containing glasses. Moreover, the absence of Cl in these separated phases indicates that the dissolved Cl^- is still entrapped in glass network.

9.2.3. Molybdate

A small amount of MoO_3 added to the melts significantly reduces corrosion from mullite crucibles either in the borosilicate or in the aluminosilicate glass series.

However, at higher MoO_3 additions, the corrosion increases in aluminosilicate glasses while it remains or decreases in borosilicate glasses. The dominant presence of MoO_4^{2-} as molybdenum species is proven by Raman spectra where two prominent bands are created at 890-960 cm^{-1} and 320-400 cm^{-1}, assigned to stretching vibrations and bending vibrations of MoO_4^{2-}, respectively. The increasing amount of MoO_4^{2-} in glass is reflected by the increasing contribution of molybdate bands in comparison to silicate bands in Raman spectra. The central frequencies of molybdate bands regularly shift with the variation in alkaline earth species in glass, which suggests that the environment of MoO_4^{2-} ions is strongly affected by alkaline earth cations, irrespective to the presence of Na^+. Like sulphate addition, molybdate addition does not make apparent changes in FTIR spectra.

MoO_3 incorporation results in linearly decreased T_g and T_c of both glass series. In particular, there is a second and intense exothermic peak after the first crystallisation peak for aluminosilicate glasses. High temperature XRD results indicate this may be due to the phase transitions between alkaline earth aluminosilicate components, while molybdate phases are not involved. MoO_3 incorporation also results in increased glass densities. Results of some complete glass series suggest that the increasing functions of densities are generally quadratic, excluding those phase separated compositions.

Similar to sulphate separation in glass, the types of separated molybdates depend on glass composition and molybdate loading. Except for the phase separation in MBS glass where $Na_{2.4}Mg_{0.8}(MoO_4)_2$ occurs, MoO_4^{2-} separates solely with alkaline earth cations in all other borosilicate glasses at the beginning of phase separation. Further molybdate in excess leads to the formation of Na_2MoO_4 in borosilicate glass, primarily as trapped aggregates or a surface layer. The separated particles are formed within glass matrices through liquid-liquid separation and thereafter crystallisation, and are mostly spherical and randomly distributed. These particles are sub-micron in diameter, with varying sizes depending on the loading levels: the greater the excess of MoO_3, the larger separated particles in glass. In addition, there are some boundary areas, which can be found in both glass types, composed of a large quantity of even tiny molybdate particles dividing the samples to be a glassy region and a crystallised region.

9.3. Drawbacks and some recommendations for future work

9.3.1. Larger batches melted in platinum crucibles with stirring

Most glasses in this work were prepared in a small scale (~50 g products in target) in mullite crucibles without stirring. This does not cause problems as the experimental conditions are kept consistent throughout the thesis; however, in order to reduce the corrosions from crucibles and to improve the homogeneity of glasses, it is worth trying to prepare some of the most interesting glasses, *e.g.* those with enhanced anionic solubilities, in a larger scale in platinum crucibles with stirring. The use of platinum crucibles will hopefully eliminate the contaminants from the walls of mullite crucibles to the melts thereby minimising the discrepancy between batched and obtained glass compositions. This may be of importance because all base glasses have suffered severe attacks from mullite crucibles and if platinum crucibles are used the compositions between base glass and anion-loaded glasses will become more consistent. Another way to keep the glass compositions consistent is to modify the batch compositions by considering the corrosions. This allows to continue using mullite crucibles which are favourable for cost and convenience reasons, but the calculation and prediction of the corrosion for each composition may vary from each other and hence become difficult. In addition, the persistent stirring of melt will facilitate the homogenisation of melt and accelerate the dissolution of anionic species into melt.

9.3.2. Durability test on loaded glasses

Chemical durability is one of the most important parameters concerning the selection of suitable host in nuclear waste immobilisation. This work has shown some promising glass compositions which are capable of incorporating such difficult anionic species, and the next stage, if applicable, will be performing durability tests on these glasses loaded with abundant difficult anions or simulant wastes. This is to ensure whether the candidate compositions are qualified to be vitrification hosts, as well as to investigate the effects of anionic incorporation on glass durability. It is also interesting to evaluate the durability of some phase separated MoO_3-containing glasses, *e.g.* MAS-8M and CAS-4M glasses. The formation of molybdate crystals in nuclear glasses is reportedly acceptable in vitrification (Henry *et al.* 2004, Schuller *et al.* 2008), but this judgement

may not apply to all compositions.

Given the crystallisation and heterogeneity in some glasses, it may be better to investigate their chemical durability with the MCC method which uses polished glass slices rather than with the PCT method which uses ground sample powders.

9.3.3. Phase separation due to Cl presence in glass melts

This work has observed the deteriorating effect of Cl presence on the stability of glass network. Even though Cl is not present in the separated phase, it is believed that phase separation is due to Cl in melt. We have noticed that, if not considering Cl content, the crystallised particles in BAS glass and the remaining glass matrix are compositionally very different. It is possible that the residual composition is the most stable one for Cl^- immobilisation and the crystallisation of celsian is a self-adjustment of the glass melt to reach this stability. Therefore, it may be of interest to prepare batches towards the measured residual composition including Cl and melt them in platinum crucibles to minimise the composition discrepancy. If crystallisation occurs too, then it means Cl causes separation of glass network regardless of glass composition; if crystallisation does not occur, the compositions with higher Cl solubility and stability are achieved.

9.3.4. Cl loss in aluminosilicate glasses

The evaporation of Cl in glass, especially CAS and MAS glasses, is significant. In this work hydrated alkaline earth chlorides were directly used as the chlorine source in aluminosilicate batches; however Schofield (2011) suggests that heating the hydrated chlorides in batches to obtain anhydrous chlorides prior to a second heating to melting temperature helps to reduce the evaporation. It would also be worthwhile to do so in this study to improve Cl retention in glass.

9.3.5. Structural information of MAS-*x*M glasses

Although XAS measurements have been made for several MAS glasses containing MoO_3, analysed data have not been obtained before submission of this thesis. XAS data will provide insight into the local environment and valence of Mo so as to better understand how Mo is dissolved in MAS glass which has a very high MoO_3 solubility.

Other structural studies, such as Mg NMR, may also be helpful to understand the specific structural characteristics of MAS glass compared with other aluminosilicate glasses. The abnormally high MoO_3 solubility in MAS glass may be related to these features.

9.3.6. Poor MoO_3 solubility in MBS glass

It is believed in this work that MoO_3 is poorly soluble in MBS glass because of the formation of $Na_{2.4}Mg_{0.8}(MoO_4)_2$ phase, whereas MoO_3 is highly soluble in MAS glass. It is worth investigating whether MoO_3 solubility will increase or not if Na_2O content in glass is partly or completely replaced by other components such as MgO itself or Li_2O (the replacement is to avoid the formation of Na-Mg molybdate phase). Another proposal is to add some boron oxide to the MAS glass to reduce the processing temperature and to see if the MoO_3 solubility changes.

9.3.7. Empirical modelling for MoO_3 solubility dependence

To a certain extent MoO_3 solubility shows evident dependence on those compositional parameters within some glasses in this study; however, when it comes to the overall fittings, these tendencies do not work anymore. It is necessary to employ some new compositional parameters to describe the contribution of glass composition to MoO_3 solubility. In addition, more glass compositions need to be investigated as the literature data are quite limited and not adequate to establish models for universal prediction of MoO_3 solubility in glass.

References

Advocat, T., Jollivet, P., Crovisier, J. L. and del Nero, M. (2001). "Long-term alteration mechanisms in water for SON68 radioactive borosilicate glass." *J Nucl Mater* **298**: 55-62.

Ahmed, A. A., Sharaf, N. A. and Condrate, R. A. (1997). "Raman microprobe investigation of sulphur-doped alkali borate glasses." *J Non-Cryst Solids* **210**: 59-69.

Allen, J. A. and Clark, A. J. (1966). "The reaction of oxygen with metallic chlorides." *J Appl Chem* **16**: 327-332.

Ansari, A., Alam, M. and Parchur, A. K. (2014). "Nd-doped calcium molybdate core and particles: synthesis, optical and photoluminescence studies." *Appl Phys A* **116**: 1719-1728.

Aronne, A., Esposito, S., Ferone, C., Pansini, M. and Pernice, P. (2002). "FTIR study of the thermal transformation of barium- exchanged zeolite A to celsian." *J Mater Chem* **12**: 3039-3045.

Baker, D. R. (1993). "The Effect of F and Cl on the Interdiffusion of Peralkaline Intermediate and Silicic Melts." *Am Mineral* **78**: 316-324.

Balazs, G. B. and Rüssel, C. (1988). "Electrochemical studies of the corrosion of molybdenum electrodes in soda-lime glass metls." *J Non-Cryst Solids* **105**: 1-6.

Ball, M. C. (1977). "The reaction of oxygen with magnesium chloride." *Thermochim Acta* **21**: 349-354.

Bancroft (1960). "The incorporation of fission products into glass for disposal." *Can J Chem Eng* **38**: 19-24.

Bart, F., Cau-dit-Coumes, C., Frizon, F. and Lorente, S. (2013). Cement-based materials for nuclear waste storage. London, Springer.

Beerkens, R. (2003). "Sulphate decomposition and sodium oxide activity in Soda–Lime–Silica Glass Melts." *J Am Ceram Soc* **86**: 1893-1899.

Beerkens, R. (2007). "Sulphur chemistry and sulphate fining and foaming of glass melts." *Glass Technol-Part A* **48**: 41-52.

Beerkens, R. (2008). "Analysis of elementary process steps in industrial glass melting tanks - some ideas on innovations in industrial glass melting." *Ceram* **52**: 206-217.

Behrens, H. and Webster, J. D. (2011). Sulfur in Magmas and Melts - Its Importance for Natural and Technical Processes. Virginia, Reviews in Mineralogy and Geochemistry.

Bendersky, L. A. and Gayle, F. W. (2001). "Electron diffraction using transmission electron microscopy." *J Res Natl Inst Stand Technol* **106**: 997-1012.

Billings, A. L. and Fox, K. M. (2010). "Retention of Sulfate in Savannah River Site High-Level Radioactive Waste Glass." *Int J Appl Glass Sci* **1**: 388-400.

Bingham, P. A. and Hand, R. J. (2008). "Sulphate incorporation and glass formation in phosphate systems for nuclear and toxic waste immobilization." *Mater Res Bull* **43**: 1679-1693.

Bingham, P. A., Connelly, A. J., Hand, R. J., Hyatt, N. C., Northrup, P. A., Mori, R. A., Glatzel, P., Kavcic, M., Zitnik, M., Bucar, K. and Edge, R. (2010). "A multi-spectroscopic investigation of sulphur speciation in silicate glasses and slags." *Glass Technol-Part A* **51**: 63-80.

Brendebach, B., Denecke, M. A., Roth, G. and Weisenburger, S. (2009). "Sulfur incorporation in high level nuclear waste glass: a S K-edge XAFS investigation." *J Phys Conf Ser* **190**: 012186.

Bye, G. C. (1999). Portland Cement. London, Thomas Telford Limited.

Calas, G., Le Grand, M., Galoisy, L. and Ghaleb, D. (2003). "Structural role of molybdenum in nuclear glasses: an EXAFS study." *J Nucl Mater* **322**: 15-20.

Caurant, D., Majérus, O., Fadel, E., Lenoir, M., Gervais, C. and Pinet, O. (2007). "Effect of Molybdenum on the Structure and on the Crystallization of SiO_2-Na_2O-CaO-B_2O_3 Glasses." *J Am Ceram Soc* **90**: 774-783.

Caurant, D. (2009). Glasses, Glass-ceramics and Ceramics for Immobilization of Highly Radioactive Nuclear Wastes, Nova Science Publishers.

Caurant, D., Majerus, O., Fadel, E., Quintas, A., Gervais, C., Charpentier, T. and Neuville, D. (2010). "Structural investigations of borosilicate glasses containing MoO3 by MAS NMR and Raman spectroscopies." *J Nucl Mater* **396**: 94-101.

Chae, B., Jung, Y. M., Wu, X. L. and Kim, S. B. (2003). "Characterization of a series of sodium molybdate structures by two-dimensional Raman correlation analysis." *J Raman Spectrosc* **34**: 451-458.

Chmel, A. and Svetlov, V. N. (1996). "Si-Cl groups in chlorine-impregnated silica." *J Non-Cryst Solids* **195**: 176-179.

Choppin, G. R. and Khankhasayev, M. K. (1999). Chemical Separation Technologies and Related Methods of Nuclear Waste Management, NATO Science Series.

Chouard, N., Caurant, D., Majerus, O., Dussossoy, J. L., Ledieu, A., Peuget, S., Baddour-Hadjean, R. and Pereira-Ramos, J. P. (2011). "Effect of neodymium oxide on the solubility of MoO3 in an aluminoborosilicate glass." *J Non-Cryst Solids* **357**: 2752-2762.

Colomban, P. and Paulsen, O. (2005). "Non-destructive determination of the structure and composition of glazes by Raman spectroscopy." *J Am Ceram Soc* **88**: 390-395.

Crovisier, J. L., Advocat, T. and Dussossoy, J. L. (2003). "Nature and role of natural

alteration gels formed on the surface of ancient volcanic glasses (Natural analogs of waste containment glasses)." *J Nucl Mater* **321**: 91-109.

Darwish, H. and Gomaa, M. M. (2006). "Effect of compositional changes on the structure and properties of alkali-alumino borosilicate glasses." *J Mater Sci: Mater Electron* **17**: 35-42.

Deb, B. and Ghosh, A. (2014). "Kinetics of crystallization in selenium molybdate glass." *J Non-Cryst Solids* **385**: 30-33.

Dell, W. J., Bray, P. J. and Xiao, S. Z. (1983). "^{11}B NMR studies and structural modeling of Na_2O-B_2O_3-SiO_2 glasses of high soda content." *J Non-Cryst Solids* **58**: 1-16.

Dimitriev, Y. and Iordanova, R. (2009). "Non-traditional molybdate glasses." *Phys Chem Glasses-B* **50**: 123-132.

Dingwell, D. B. and Hess, K. U. (1998). "Melt viscosities in the system Na-Fe-Si-O-F-Cl: Contrasting effects of F and Cl in alkaline melts." *Am Mineral* **83**: 1016-1021.

Do Quang, R., Petitjean, V., Hollebecque, F., Pinet, O., Flament, O. and Prod'homme, A. (2003). Vitrification of HLW produced by uranium-molybdenum fuel reprocessing in COGEMA's cold crucible melter. WM'03 Conference, Tucson, AZ.

Donald, I. W., Metcalfe, B. L. and Taylor, R. N. J. (1997). "Review: The immobilization of high level radioactive wastes using ceramics and glasses." *J Mater Sci* **32**: 5851-5887.

Donald, I. W., Metcalfe, B. L., Fong, S. K., Gerrard, L. A., Strachan, D. M. and Scheele, R. D. (2007). "A glass-encapsulated calcium phosphate wasteform for the immobilization of actinide-, fluoride-, and chloride-containing radioactive wastes from the pyrochemical reprocessing of plutonium metal." *J Nucl Mater* **361**: 78-93.

Donald, I. W. (2010). Waste immobilisation in glass and ceramic based hosts: radioactive, toxic and hazardous wastes, Wiley-Blackwell.

Duffy, J. A. (1986). "Chemical Bonding in the Oxides of the Elements - a New Appraisal." *J Solid State Chem* **62**: 145-157.

Duffy, J. A. (2010). "Optical basicity of fluorides and mixed oxide-fluoride glasses and melts." *Phys Chem Glasses-B* **52**: 107-114.

Dunnett, B. F., Gribble, N. R., Short, R., Turner, E., Steele, C. J. and Riley, A. D. (2012). "Vitrification of high molybdenum waste." *Glass Technol-Part A* **53**: 166-171.

Ehrt, D. and Keding, R. (2009). "Electrical conductivity and viscosity of borosilicate glasses and melts." *Phys Chem Glasses-B* **50**: 165-171.

Evans, K. A., Mavrogenes, J. A., O'Neill, H. S., Keller, N. S. and Jang, L. Y. (2008). "A preliminary investigation of chlorine XANES in silicate glasses." *Geochem Geophy Geosy* **9**: 15.

Ewing, R. C., Weber, W. J. and Clinard Jr, F. W. (1995). "Radiation effects in nuclear waste forms for high-level radioactive waste." *Prog Nucl Energy* **29**: 63-127.

Ewing, R. C. (1999). "Nuclear waste forms for actinides." *Proc Natl Acad Sci USA* **96**: 3432-3439.

Ewing, R. C., Weber, W. J. and Lian, J. (2004). "Nuclear waste disposal—pyrochlore (A2B2O7): Nuclear waste form for the immobilization of plutonium and "minor" actinides." *J Appl Phys* **95**: 5949-5971.

Fábián, M., Sváb, E., Mészáros, G., Révay, Z. and Veress, E. (2007). "Neutron diffraction study of sodium borosilicate waste glasses containing uranium." *J Non-Cryst Solids* **353**: 1941-1945.

Farges, F., Siewert, R., Brown, G. E., Guesdon, A. and Morin, G. (2006). "Structural environments around molybdenum in silicate glasses and melts. I. Influence of composition and oxygen fugacity on the local structure of molybdenum." *Can Mineral* **44**: 731-753.

Feng, X., Schweiger, M. J., Li, H. and Gong, M. (1996). Retention of sulphur, phosphorus, chlorine and fluorine in Hanford phase II vendor LLW glasses. Proceedings of the International Topical Meeting on Nuclear and Hazardous Waste Management Spectrum, La Gland Park, Illinois, American Nuclear Society.

Fincham, C. J. B. and Richardson, F. D. (1954). "The Behaviour of Sulphur in Silicate and Aluminate Melts." *Proc R Soc Lon Ser-A* **223**: 40-62.

Frugier, P., Gin, S., Minet, Y., Chave, T., Bonin, B., Godon, N., Lartigue, J. E., Jollivet, P., Ayral, A., De Windt, L. and Santarini, G. (2008). "SON68 nuclear glass dissolution kinetics: Current state of knowledge and basis of the new GRAAL model." *J Nucl Mater* **380**: 8-21.

Furukawa, T. and White, W. (1981). "Raman spectroscopic investigation of sodium borosilicate glass structure." *J Mater Sci* **16**: 2689-2700.

Galoisy, L., Cormier, L., Rossano, S., Ramos, A., Calas, G., Gaskell, P. and Le Grand, M. (2000). "Cationic ordering in oxide glasses: the example of transition elements." *Mineral Mag* **64**: 409-424.

Gautam, C., Yadav, A. K. and Singh, A. K. (2012). "A Review on Infrared Spectroscopy of Borate Glasses with Effects of Different Additives." *Ceram* **2012**: 1-17.

Gin, S., Jollivet, P., Mestre, J. P., Jullien, M. and Pozo, C. (2001). "French SON 68 nuclear glass alteration mechanisms on contact with clay media." *Appl Geochem* **16**: 861-881.

Goles, R. W. and Nakaoka, R. K. (1990). Hanford waste vitrification program pilot-scale ceramic melter test 23. Richland, Washington, Pacific Northwest Laboratory.

Griffiths, J. E. (1967). "Performance of a New Photoelectric Detection Method for

Optical Spectroscopy. II. Application to Laser Raman Spectroscopy." *J Chem Phys* **46**: 1679.

Gwinner, B., Sercombe, J., Tiffreau, C., Simondi-Teisseire, B., Felines, I. and Adenot, F. (2006). "Modelling of bituminized radioactive waste leaching. Part II: Experimental validation." *J Nucl Mater* **349**: 107-118.

Halle, J. C. and Stern, K. H. (1980). "Vaporization and decomposition of sodium sulfate. Thermodynamics and kinetics." *J Phys Chem* **84**: 1699-1704.

Hamodi, N. (2012). "Thermal Analysis and Immobilisation of Spent Ion Exchange Resin in Borosilicate Glass." *New J Glass Ceram* **02**: 111-120.

Hamodi, N. H. and Iqbal, Y. (2009). "Immobilisation of spent ion exchange resin arising from nuclear power plants: an introduction." *J Pak Mater Soc* **3**: 7-19.

Harding, F. L. (1972). "Dependence of Melt Oxygen Activity and Water Retention on Composition of Amber Glass." *J Am Ceram Soc* **55**: 368-373.

Henry, N., Deniard, P., Jobic, S., Brec, R., Fillet, C., Bart, F., Grandjean, A. and Pinet, O. (2004). "Heat treatments versus microstructure in a molybdenum-rich borosilicate." *J Non-Cryst Solids* **333**: 199-205.

Hoell, A., Kranold, R., Lembke, U. and Aures, J. (1996). "Effect of fining with sodium chloride on the phase separation of a soda lime silica glass." *J Non-Cryst Solids* **208**: 294-302.

Holmquist, S. (1966). "Oxygen activities and the solubility of sulfur trioxide in sodium silicate melts." *J Am Ceram Soc* **49**: 467-473.

Hrma, P. (2010). Retention of halogens in waste glass. Richland, Washington, Pacific Northwest National Laboratory.

Hwang, J. H., Kim, C. Y., Kwon, J. G. and Kim, K. D. (2005). "Corrosion of molybdenum electrodes in alkali–alkaline earth–silica glass melts doped with antimony." *Glass Technol-Part A* **46**: 142-145.

Hyatt, N. C., Short, R. J., Hand, R. J., Lee, W. E., Livens, F., Charnock, J. M. and Bilsborrow, R. L. (2012). "The strucural chemistry of molybdenum in model high level nuclear waste glasses, investigated by Mo K-edge X-ray absorption spectroscopy." *Environ Issues Waste Manage Technol Ceram Nucl Ind* **X**: 179-185.

IAEA (2002). Application of ion exchange processes for the treatment of radioactive waste and management of spent ion exchangers. Vienna, Austria, International Atomic Energy Agency.

IAEA (2007). New developments and improvements in processing of 'problematic' radioactive waste. Vienna, Austria, International Atomic Energy Agency.

IAEA (2007). Spent Fuel and High Level Waste: Chemical durability and performance under simulated repository conditions. Vienna, Austria, International Atomic Energy

Agency.

IAEA. (2014). "Operational & Long-Term Shutdown Reactors." Retrieved April 15th, 2014,.

Ilyukhina, N. S., Panomaryova, I. Y. and Lashchenova, T. N. (2010). Solubility of Sulfate and Chloride Ions in Borosilicate Melts at Vitrification of Intermediate-Level Radioactive Wastes. WM2010 Conference. Phoenix. **March 7-11**.

Inagaki, Y., Furuya, H., Idemitsu, K. and Yonezawa, S. (1994). "Corrosion behavior of a powdered simulated nuclear waste glass: A corrosion model including diffusion process." *J Nucl Mater* **208**: 27-34.

Jahagirdar, P. B. and Wattal, P. K. (1998). "Vitrification of sulphate bearing high level wastes in borosilicate matrix." *Waste Manage* **18**: 265-273.

Jantzen, C. M. (1986). "Systems-Approach to Nuclear Waste Glass Development." *J Non-Cryst Solids* **84**: 215-225.

Jantzen, C. M., Smith, M. E. and Peeler, D. Y. (2004). "Dependency of sulphate solubility on melt composition and melt polymerisation." *Environ Issues Waste Manage Technol Ceram Nucl Ind **X***: 141-153.

Jantzen, C. M., Brown, K. G. and Pickett, J. B. (2010). "Durable Glass for Thousands of Years." *Int J Appl Glass Sci* **1**: 38-62.

Jantzen, C. M. (2011). Development of glass matrices for high level radioactive wastes. Handbook of advanced radioactive waste conditioning technologies. M. I. Ojovan. Philadelphia, Woodhead**:** 230-292.

Jantzen, C. M. (2011). Historic development of glass and ceramic waste forms for high level radioactive waste. Handbook of advanced radioactive waste conditioning technologies. M. I. Ojovan. Philadelphia, Woodhead**:** 159-172.

Jantzen, C. M., Lee, W. E. and Ojovan, M. I. (2013). Radioactive waste conditioning, immobilisation and encapsulation process and technologies: Overview and advances. Radioactive waste management and contaminated site clean-up: Processes, technologies and international experience. W. E. Lee, M. I. Ojovan and C. M. Jantzen. Cambridge, Woodhead**:** 171-272.

Jiang, J., May, I., Sarsfield, M. J., Ogden, M., Fox, D. O., Jones, C. J. and Mayhew, P. (2005). "A spectroscopic study of the dissolution of cesium phosphomolybdate and zirconium molybdate by ammonium carbamate." *J Solution Chem* **34**: 443-468.

Jollivet, P., Den Auwer, C. and Simoni, E. (2002). "Evolution of the uranium local environment during alteration of SON68 glass." *J Nucl Mater* **301**: 142-152.

Jugo, P. J. (2009). "Sulfur content at sulfide saturation in oxidized magmas." *Geology* **37**: 415-418.

Kaushik, C. P., Mishra, R. K., Sengupta, P., Kumar, A., Das, D., Kale, G. B. and Raj,

K. (2006). "Barium borosilicate glass – a potential matrix for immobilization of sulfate bearing high-level radioactive liquid waste." *J Nucl Mater* **358**: 129-138.

Kiprianov, A. A., Karpukhina, N. G. and Molodozhen, V. A. (2004). "Investigation into the Influence of Chloride Additives on the Properties of Alkali Silicate Glasses." *Glass Phys Chem* **30**: 325-332.

Kiprianov, A. A. and Karpukhina, N. G. (2006). "Oxyhalide silicate glasses." *Glass Phys Chem* **32**: 1-27.

Klimm, K. and Botcharnikov, R. E. (2010). "The determination of sulfate and sulfide species in hydrous silicate glasses using Raman spectroscopy." *Am Mineral* **95**: 1574-1579.

Koroleva, O. N., Shabunina, L. A. and Bykov, V. N. (2011). "Structure of borosilicate glass according to raman spectroscopy data." *Glass Ceram* **67**: 340-342.

Kranold, R., Kammel, M. and Hoell, A. (2001). "Effect of the Cl− content on the formation and dissolution of precipitates in a soda–lime–silica glass." *J Non-Cryst Solids* **293–295**: 642-648.

Kremenovic, A., Colomban, P., Piriou, B., Massiot, D. and Florian, P. (2003). "Structural and spectroscopic characterization of the quenched hexacelsian." *J Phys Chem Solids* **64**: 2253-2268.

Lenoir, M., Grandjean, A., Poissonnet, S. and Neuville, D. R. (2009). "Quantitation of sulfate solubility in borosilicate glasses using Raman spectroscopy." *J Non-Cryst Solids* **355**: 1468-1473.

Lenoir, M., Neuville, D. R., Malki, M. and Grandjean, A. (2010). "Volatilization kinetics of sulphur from borosilicate melts A correlation between sulphur diffusion and melt viscosity." *J Non-Cryst Solids* **356**: 2722-2727.

Leturcq, G., Berger, G., Advocat, T. and Vernaz, E. (1999). "Initial and long-term dissolution rates of aluminosilicate glasses enriched with Ti, Zr and Nd." *Chem Geol* **160**: 39-62.

Li, C. S. and Ripley, E. M. (2005). "Empirical equations to predict the sulfur content of mafic magmas at sulfide saturation and applications to magmatic sulfide deposits." *Miner Deposita* **40**: 218-230.

Li, H., Hrma, P. R. and Vienna, J. D. (2001). Sulfate retention and segregation in simulated radioactive waste borosilicate glasses. Environmental Issues and Waste Management Technology. D. R. Spearing. Westerville, OH, American Ceramic Society. **VI:** 237-245.

Lima, M. M. and Monteiro, R. (2001). "Characterisation and thermal behaviour of a borosilicate glass." *Thermochim Acta* **373**: 69-74.

Liu, Y. N., Samaha, N. T. and Baker, D. R. (2007). "Sulfur concentration at sulfide saturation (SCSS) in magmatic silicate melts." *Geochim Cosmochim Ac* **71**: 1783-

1799.

Long, D. A. (1977). Raman spectroscopy. London, McGraw-Hill Inc.

Lorier, T. H., Reamer, I. A. and Workman, R. J. (2005). Initial sulfate solubility study for sludge batch 4 (SB4). U. S. Department of Energy. Aiken, SC, SRNL.

Lutze, W. and Ewing, R. C. (1988). Radioactive Wasteforms for the Future. Amsterdam, North Holland.

Magnin, M., Schuller, S., Mercier, C., Trébosc, J., Caurant, D., Majérus, O., Angéli, F., Charpentier, T. and Jantzen, C. (2011). "Modification of Molybdenum Structural Environment in Borosilicate Glasses with Increasing Content of Boron and Calcium Oxide by 95Mo MAS NMR." *J Am Ceram Soc* **94**: 4274-4282.

Mahadevan Pillai, V. P., Pradeep, T., Bushiri, M. J., Jayasree, R. S. and Nayar, V. U. (1997). "Vibrational spectroscopic studies of $FeClMoO_4$, Na_2MoO_4 and $Na_2MoO_4 \cdot 2H_2O/D_2O$." *Spectrochim Acta A* **53**: 867-876.

Manara, D., Grandjean, A., Pinet, O., Dussossoy, J. L. and Neuville, D. R. (2007). "Sulfur behavior in silicate glasses and melts: Implications for sulfate incorporation in nuclear waste glasses as a function of alkali cation and V2O5 content." *J Non-Cryst Solids* **353**: 12-23.

Manara, D., Grandjean, A. and Neuville, D. R. (2009). "Structure of borosilicate glasses and melts: A revision of the Yun, Bray and Dell model." *J Non-Cryst Solids* **355**: 2528-2531.

Manara, D., Grandjean, A. and Neuville, D. R. (2009). "Advances in understanding the structure of borosilicate glasses: A Raman spectroscopy study." *Am Mineral* **94**: 777-784.

Marr, R. A., Baker, D. R., Vreugdenhil, A. J. and Williams-Jones, A. E. (1999). "The effects of Cl on structure of Zr and Ti alkali alunimosilicate glasses." *J Non-Cryst Solids* **243**: 175-184.

Marra, J. C., Andrews, M. K. and Schumacher, R. F. (1994). vitrification in the presence of salts (U). American Ceramic Society. Indianapolis, IN.

Matyas, J. and Hrma, P. (2005). Sulfate Fining Chemistry in Oxidized and Reduced Soda-Lime-Silica Glasses. U. S. Department of Energy, PNNL. **15175**.

Mckeown, D. A., Galeener, F. L. and Brown, G. E. (1984). "Raman Studies of Al Coordination in Silica-Rich Sodium Aluminosilicate Glasses and Some Related Minerals." *J Non-Cryst Solids* **68**: 361-378.

McKeown, D. A., Muller, I. S., Gan, H., Pegg, I. L. and Kendziora, C. A. (2001). "Raman studies of sulfur in borosilicate waste glasses: sulfate environments." *J Non-Cryst Solids* **288**: 191-199.

McKeown, D. A., Muller, I. S., Gan, H., Pegg, I. L. and Stolte, W. C. (2004).

"Determination of sulfur environments in borosilicate waste glasses using X-ray absorption near-edge spectroscopy." *J Non-Cryst Solids* **333**: 74-84.

McKeown, D. A., Gan, H., Pegg, I. L., Stolte, W. C. and Demchenko, I. N. (2011). "X-ray absorption studies of chlorine valence and local environments in borosilicate waste glasses." *J Nucl Mater* **408**: 236-245.

McMillan, P. F. (1984). "Structural study of silicate glasses and melts - applications and limitations of Raman spectroscopy." *Am Mineral* **69**: 622-644.

McMillan, P. F. (1989). "Raman-Spectroscopy in Mineralogy and Geochemistry." *Annu Rev Earth Pl Sc* **17**: 255-283.

Melnyk, T. W., Walton, F. B. and Johnson, L. H. (1984). "High-Level Waste Glass Field Burial Test - Leaching and Migration of Fission-Products." *Nucl Chem Waste Man* **5**: 49-62.

Metcalfe, B. L. and Donald, I. W. (2004). "Candidate wasteforms for the immobilization of chloride-containing radioactive waste." *J Non-Cryst Solids* **348**: 225-229.

Miller, F. A. and Wilkins, C. H. (1952). "Infrared Spectra and Characteristic Frequencies of Inorganic Ions - Their Use in Qualitative Analysis." *Anal Chem* **24**: 1253-1294.

Mishra, R. K., Sudarsan, V., Kaushik, C. P., Raj, K., Kulshreshtha, S. K. and Tyagi, A. K. (2006). "Structural aspects of barium borosilicate glasses containing thorium and uranium oxides." *J Nucl Mater* **359**: 132-138.

Mishra, R. K., Sengupta, P., Kaushik, C. P., Tyagi, A. K., Kale, G. B. and Raj, K. (2007). "Studies on immobilization of thorium in barium borosilicate glass." *J Nucl Mater* **360**: 143-150.

Mishra, R. K., Kumar, S., Tomar, B. S., Tyagi, A. K., Kaushik, C. P., Raj, K. and Manchanda, V. K. (2008). "Effect of barium on diffusion of sodium in borosilicate glass." *J Hazard Mater* **156**: 129-134.

Mishra, R. K., Sudarsan, K. V., Sengupta, P., Vatsa, R. K., Tyagi, A. K., Kaushik, C. P., Das, D. and Raj, K. (2008). "Role of Sulfate in Structural Modifications of Sodium Barium Borosilicate Glasses Developed for Nuclear Waste Immobilization." *J Am Ceram Soc* **91**: 3903-3907.

Mohazzabi, P. and Searcy, A. W. (1976). "Kinetics and Thermodynamics of Decomposition of Barium Sulfate." *J Chem Soc Farad T 1* **72**: 290-295.

Morizet, Y., Paris, M., Di Carlo, I. and Scaillet, B. (2013). "Effect of sulphur on the structure of silicate melts under oxidizing conditions." *Chem Geol* **358**: 131-147.

Müller-Simon, H. (2011). "Fining of Glass Melts." *Rev Mineral Geochem* **73**: 337-361.

Nagashima, S. and Katsura, T. (1973). "The solubility of sulfur in Na_2O-SiO_2 melts

under various oxygen partial pressures at 1100 ºC, 1250 ºC and 1300 ºC." *Bull Chem Soc Jpn* **46**: 3099-3103.

NDA (2014). Radioactive Wastes in the UK: A Summary of the 2013 Inventory. Nuclear Decommissioning Authority, Department of Energy & Climate Change.

Neuville, D. R. and Mysen, B. O. (1996). "Role of aluminium in the silicate network: In situ, high-temperature study of glasses and melts on the join SiO_2-$NaAlO_2$." *Geochim Cosmochim Ac* **60**: 1727-1737.

O'Neill, H. S. C. and Eggins, S. M. (2002). "The effect of melt composition on trace element partitioning: an experimental investigation of the activity coefficients of FeO, NiO, CoO, MoO2 and MoO3 in silicate melts." *Chem Geol* **186**: 151-181.

Ojovan, M. I., Ojovan, N. V., Startceva, I. V., Tchuikova, G. N., Golubeva, Z. I. and Barinov, A. S. (2001). "Waste glass behavior in a loamy soil of a wet repository site." *J Nucl Mater* **298**: 174-179.

Ojovan, M. I., Lee, W. E., Barinov, A. S., Ojovan, N. V., Startceva, I. V., Bacon, D. H., McGrail, B. P. and Vienna, J. D. (2004). Corrosion mechanisms of low level vitrified radioactive waste in a loamy soil. Materials Research Society Symposium Proceedings, Boston.

Ojovan, M. I., Hand, R. J., Ojovan, N. V. and Lee, W. E. (2005). "Corrosion of alkali–borosilicate waste glass K-26 in non-saturated conditions." *J Nucl Mater* **340**: 12-24.

Ojovan, M. I. and Lee, W. E. (2005). An Introduction to Nuclear Waste Immobilisation. Amsterdam, Elsevier.

Ojovan, M. I., Pankov, A. and Lee, W. E. (2006). "The ion exchange phase in corrosion of nuclear waste glasses." *J Nucl Mater* **358**: 57-68.

Ojovan, M. I. and Batyukhnova, O. G. (2007). Glasses for nuclear waste immobilisation. WM'07 Conference. Tucson AZ.

Ojovan, M. I. and Lee, W. E. (2007). New developments in glassy nuclear wasteforms. New York, Nova Science Publishers.

Ojovan, M. I. and Lee, W. E. (2010). "Glassy Wasteforms for Nuclear Waste Immobilization." *Metall Mater Trans A* **42**: 837-851.

Ooura, M. and Hanada, T. (1998). "Compositional dependence of solubility of sulphate in silicate glasses." *Glass Technol* **39**: 68-73.

Osipov, A. A., Osipova, L. M. and Eremyashev, V. E. (2013). "Structure of alkali borosilicate glasses and melts according to Raman spectroscopy data." *Glass Phys Chem* **39**: 105-112.

Ozeki, T., Murata, K., Kihara, H. and Hikime, S. (1987). "Studies on the interaction of molybdate ion and magnesium ion observed in the Raman spectra of the mixture solutions." *Bull. Chem. Soc. Jpn.* **1987**: 3585-3589.

Papadoloulos, K. (1973). "The solubility of SO_3 in soda-lime-silica melts." *Phys Chem Glasses* **14**: 60-65.

Paraguassu, W., Saraiva, G. D., Guerini, S., Freire, P. T. C., Abagaro, B. T. O. and Mendes, J. (2012). "Pressure-induced phase transition on K2MoO4: A Raman scattering study and ab initio calculations." *J Solid State Chem* **196**: 197-202.

Petr, G. Z., Aleksandr Ya, K., Tasoltan, T. B., Lyudmila, I. I. and Vyacheslav, V. O. (2003). "Stimulated Raman scattering of picosecond pulses in SrMoO 4 and Ca 3 (VO 4) 2 crystals." *Quantum Electron* **33**: 331.

Phuruangrat, A., Thongtem, T. and Thongtem, S. (2009). "Barium molybdate and barium tungstate nanocrystals synthesized by a cyclic microwave irradiation." *J Phys Chem Solids* **70**: 955-959.

Plodinec, M. J. (1982). An assessment of Savannah River borosilicate glass in the repository environment. Aiken, SC, Savannah River Laboratory Publisher.

Polyakova, I. G. (2000). "Alkali borosilicate systems: phase diagrams and properties of glasses." *Phys Chem Glasses* **41**: 247-258.

Pope, S. J. A. and West, Y. D. (1995). "Use of the FT Raman spectrum of Na2MoO4 to study sample heating by the laser." *Spectrochim Acta A* **51**: 2011-2017.

Potuzak, M., Mauro, J. C., Kiczenski, T. J., Ellison, A. J. and Allan, D. C. (2010). "Communication: Resolving the vibrational and configurational contributions to thermal expansion in isobaric glass-forming systems." *J Chem Phys* **133**: 091102.

Pye, L. D., Montenero, A. and Joseph, I. (2005). Properties of Glass-forming Melts. Boca Raton, France, CRC Press.

Ramkumar, J., Chandramouleeswaran, S., Sudarsan, V., Mishra, R. K., Kaushik, C. P., Raj, K. and Tyagi, A. K. (2009). "Barium borosilicate glass as a matrix for the uptake of dyes." *J Hazard Mater* **172**: 457-464.

Ringwood, A. E. (1979). "The SYNROC process: A geochemical approach to nuclear waste immobilization." *Geochim J* **13**: 141-165.

Ringwood, A. E., Kesson, S. E., Ware, N. G., Hibberson, W. and Major, A. (1979). "Immobilization of High-Level Nuclear-Reactor Wastes in Synroc." *Nat* **278**: 219-223.

Roffey, R. and Norqvist, A. (1991). "Biodegradation of bitumen used for nuclear waste disposal." *Experientia* **47**: 539-542.

Sandland, T. O., Du, L. S., Stebbins, J. F. and Webster, J. D. (2004). "Structure of Cl-containing silicate and aluminosilicate glasses: A 35Cl MAS-NMR study." *Geochim Cosmochim Ac* **68**: 5059-5069.

Saraiva, G. D., Paraguassu, W., Maczka, M., Freire, P. T. C., Lima, J. A., Paschoal, C. W. A., Mendes Filho, J. and Souza Filho, A. G. (2008). "Temperature ‐ dependent Raman scattering studies of Na2MoO4." *J Raman Spectrosc* **39**: 937-941.

Schofield, J. (2011). Vitrification of a chloride containing actinide waste surrogate. PhD Thesis, the University of Sheffield.

Schuller, S., Pinet, O., Grandjean, A. and Blisson, T. (2008). "Phase separation and crystallization of borosilicate glass enriched in MoO_3, P_2O_5, ZrO_2, CaO." *J Non-Cryst Solids* **354**: 296-300.

Sercombe, J., Gwinner, B., Tiffreau, C., Simondi-Teisseire, B. and Adenot, F. (2006). "Modelling of bituminized radioactive waste leaching. Part I: Constitutive equations." *J Nucl Mater* **349**: 96-106.

Shannon, R. D. and Prewitt, C. T. (1969). "Effective ionic radii in oxides and fluorides." *Acta Crystall B-Stru* **25**: 925-946.

Shannon, R. D. (1976). "Revised Effective Ionic Radii and Systematic Studies of Interatomie Distances in Halides and Chaleogenides." *Acta Crystallogr* **A32**: 751-768.

Sharp, J. H., Hill, J., Milestone, N. B. and Miller, E. W. (2003). Cementitious systems for encapsulation of intermediate level waste. The 9th International Conference on Radioactive Waste Management and Environmental Remediation, Oxford.

Sheng, J. W., Luo, S. G. and Tang, B. L. (1999). "The leaching behavior of borate waste glass SL-1." *Waste Manage* **19**: 401-407.

Short, R., Turner, E., Dunnett, B. and Riley, A. (2008). Devitrified and Phase Separated Material Found in Simulated High Level Nuclear Waste Glasses Containing Ca and Zn Additions. MRS Online Proceedings Library, Cambridge Journals Online.

Short, R. J. (2004). Incorporation of molybdenum in nuclear waste glasses. PhD Thesis, the University of Sheffield.

Short, R. J., Hand, R. J., Hyatt, N. C. and Mobus, G. (2005). "Environment and oxidation state of molybdenum in simulated high level nuclear waste glass compositions." *J Nucl Mater* **340**: 179-186.

Singh, S., Kumar, A., Singh, D., Thind, K. S. and Mudahar, G. S. (2008). "Barium–borate–flyash glasses: As radiation shielding materials." *Nucl Instru Methods Phys Res B* **266**: 140-146.

Siwadamrongpong, S., Koide, M. and Matusita, K. (2004). "Prediction of chloride solubility in $CaO–Al_2O_3–SiO_2$ glass systems." *J. Non-Cryst. Solids* **347**: 114-120.

Sobolev, I. A., Lifanov, F. A., Stefanovskii, S. V., Dmitriev, S. A., Musatov, N. D., Kobelev, A. P. and Zakharenko, N. V. (1990). "Handling nuclear power station wastes in a pilot plant fitted with an electrical bath oven." *Atomic Energy* **69**: 233-236.

Sobolev, I. A., Barinov, A. S. and Ojovan, M. I. (2000). LILW bituminization programme at SIA "Radon": Waste form performance. WM'00 Conference. Tucson AZ.

Sokolov, I. A., Valova, N. A., Tarlakov, Y. P. and Pronkin, A. A. (2003). "Electrical

Properties and the Structure of Glasses in the Li2SO4–LiPO3 System." *Glass Phys Chem* **29**: 548-554.

Stebbins, J. F. and Xu, Z. (1997). "NMR evidence for excess non-bridging oxygen in an aluminosilciate glass." *Nat* **390**: 60-62.

Stebbins, J. F. and Du, L. S. (2002). "Chloride ion sites in silicate and aluminosilicate glasses A preliminary study by 35Cl solid-state NMR." *Am Mineral* **87**: 359-363.

Stern, K. H. and Weise, E. L. (1966). High temperature properties and decomposition of inorganic salts. Part I: Sulphates. Washington, United States Department of Commerce.

Stevenson, P. (2012). Foam Engineering: Fundamentals and Applications. Chichester, United Kingdom, John Wiley & Sons Ltd.

Sun, Q. (2012). "Raman spectroscopic study of the effects of dissolved NaCl on water structure." *Vib Spectrosc* **62**: 110-114.

Tandia, A., Vargheese, K. D. and Mauro, J. C. (2012). "Elasticity of ion stuffing in chemically strengthened glass." *J Non-Cryst Solids* **358**: 1569-1574.

Taurines, T. and Boizot, B. (2011). "Synthesis of powellite-rich glasses for high level waste immobilization." *J Non-Cryst Solids* **357**: 2723-2725.

Techer, I., Advocat, T., Lancelot, J. and Liotard, J. M. (2000). "Basaltic glass: alteration mechanisms and analogy with nuclear waste glasses." *J Nucl Mater* **282**: 40-46.

Tiegel, M., Herrmann, A., Russel, C., Korner, J., Klopfel, D., Hein, J. and Kaluza, M. C. (2013). "Magnesium aluminosilicate glasses as potential laser host material for ultrahigh power laser systems." *J. Mater. Chem. C* **1**: 5031-5039.

Tomilin, S. V., Lukinykh, A. N., Lizin, A. A., Bychkov, A. V., Yakovlev, V. V. and Konovalov, V. I. (2007). "Investigation of the incorporation of spent alkali chloride melt in ceramic." *Atom Energy* **102**: 217-222.

Tronche, E., Lacombe, J., Ledoux, A., Boen, R. and Ladirat, C. (2009). Vitrification of HLLW surrogate solutions containing sulfate in a Direct-Induction cold crucible melter - 9136. WM2009 Conference. Phoneix AZ.

Tsujimura, T., Xue, X. Y., Kanzaki, M. and Walter, M. J. (2004). "Sulfur speciation and network structural changes in sodium silicate glasses: Constraints from NMR and Raman spectroscopy." *Geochim Cosmochim Ac* **68**: 5081-5101.

Tuscharoen, S., Kaewkhao, J., Limsuwan, P. and Chewpraditkul, W. (2012). "Structural, Optical and Radiation Shielding Properties of BaO-B2O3-Rice Husk Ash Glasses." *Proc Eng* **32**: 734-739.

Uchino, T., Sakka, T., Hotta, K. and Iwasaki, M. (1989). "Attenuated Toatal Reflectance Fourier-Transform Infrared Spectra of a Hydrated Sodium Soilicate

Glass." *J Am Ceram Soc* **72**: 2173-2175.

Uruga, K., Sawada, K., Enokida, Y. and Yamamoto, I. (2008). "Liquid Metal Extraction for Removal of Molybdenum from Molten Glass Containing Simulated Nuclear Waste Elements." *J Nucl Sci Technol* **45**: 1063-1071.

Vance, E. R., Davis, J., Olufson, K., Chironi, I., Karatchevtseva, I. and Farnan, I. (2012). "Candidate waste forms for immobilisation of waste chloride salt from pyroprocessing of spent nuclear fuel." *J Nucl Mater* **420**: 396-404.

Vanmoortel, I., De Strycker, J., Temmerman, E. and Adriaens, A. (2007). "The influence of polyvalent metal cations on the corrosion rate of molybdenum in molten glass." *J Non-Cryst Solids* **353**: 2179-2185.

Varshneya, A. K. (1994). Fundamentals of inorganic glasses. London, Academic Press Ltd.

Veksler, I. V., Dorfman, A. M., Dulski, P., Kamenetsky, V. S., Danyushevsky, L. V., Jeffries, T. and Dingwell, D. B. (2012). "Partitioning of elements between silicate melt and immiscible fluoride, chloride, carbonate, phosphate and sulfate melts, with implications to the origin of natrocarbonatite." *Geochim Cosmochim Ac* **79**: 20-40.

Vinod, P., Nandini, G. and Surinder, M. S. (2006). "Raman and X-ray diffraction investigations on $BaMoO_4$ under high pressures." *J Phys Condens Matter* **18**: 3917.

Volkovicha, V. A., Griffiths, T. R., Thied, R. C. and Lewin, B. (2003). "Behavior of molybdenum in pyrochemical reprocessing: A spectroscopic study of the chlorination of molybdenum and its oxides in chloride melts." *J Nucl Mater* **323**: 93-100.

Webster, J. D., Kinzler, R. J. and Mathez, E. A. (1999). "Chloride and water solubility in basalt and andesite melts and implications for magmatic degassing." *Geochim Cosmochim Ac* **63**: 729-738.

Webster, J. D. and De Vivo, B. (2002). "Experimental and modeled solubilities of chlorine in aluminosilicate melts, consequences of magma evolution, and implications for exsolution of hydrous chloride melt at Mt. Somma-Vesuvius." *Am Mineral* **87**: 1046-1061.

Werme, L., Bjorner, I. K., Bart, G., Zwicky, H. U., Grambow, B., Lutze, W., Ewing, R. C. and Magrabi, C. (1990). "Chemical Corrosion of Highly Radioactive Borosilicate Nuclear Waste Glass under Simulated Repository Conditions." *J Mater Res* **5**: 1130-1146.

Wilson, P. D. (1996). The nuclear fuel cycle: from ore to waste. Oxford, Oxford University Press.

Xiang, Y., Du, J., Smedskjaer, M. M. and Mauro, J. C. (2013). "Structure and properties of sodium aluminosilicate glasses from molecular dynamics simulations." *J Chem Phys* **139**: 044507.

Xu, Z. K., Shull, J. L. and Kriven, W. M. (2002). "Hot-stage transmission electron

microscopy study of phase transformations in hexacelsian ($BaAl_2Si_2O_8$)." *J Mater Res* **17**: 1287-1297.

Yun, Y. H. and Bray, P. J. (1978). "Nuclear magnetic resonance studies of the glasses in the system Na2O B2O3 SiO2." *J Non-Cryst Solids* **27**: 363-380.

Zhao, P. D., Kroeker, S. and Stebbins, J. F. (2000). "Non-bridging oxygen sites in barium borosilicate glasses: results from B-11 and O-17 NMR." *J Non-Cryst Solids* **276**: 122-131.

Zhu, Y. (2006). The characterisation and measurement techniques of nanomaterials (in Chinese). Beijing, Chemical Engineering Press.

Zimova, M. and Webb, S. (2006). "The effect of chlorine on the viscosity of Na_2O-Fe_2O_3-Al_2O_3-SiO_2 melts." *Am Mineral* **91**: 344-352.

Appendix I

The melting and boiling points of possible chloride compounds in the batches or melts are listed below:

Compound	Melting/decomposition point (ºC)	Boiling point (ºC)
NaCl	800.7	1465
$MgCl_2$	714	1412
$MgCl_2 \cdot 6H_2O$	~100 (dec)	
$CaCl_2$	775	1935.5
$CaCl_2 \cdot 2H_2O$	175 (dec)	
$SrCl_2$	874	1250
$SrCl_2 \cdot 6H_2O$	100 (dec)	
$BaCl_2$	962	1560
$BaCl_2 \cdot 2H_2O$	~120 (dec)	

Appendix II

The estimated (from DTA curves) glass transition temperature T_g and crystallisation temperatures T_{c1} and T_{c2} (if applicable) of strontium and/or barium aluminosilicate glasses (SAS, SBAS and BAS series) with molybdate additions are listed below:

Sample	T_g (±5 ºC)	T_c (T_{c1}) (±5 ºC)	T_{c2} (±2 ºC)
SAS-0M	727	-	-
SAS-2.5M	659	798	963
SBAS-0M	685	-	-
SBAS-2M	633	809	970
SBAS-2.5M*	630	806	971
SBAS-3M*	618	791	953
BAS-0M	662	828	-
BAS-2M	645	812	-
BAS-2.5M*	639	807	-

* Samples marked with "*" are phase separated.